MAX-PLANCK-INSTITUT FÜR PLASMAPHYSIK
GARCHING BEI MÜNCHEN

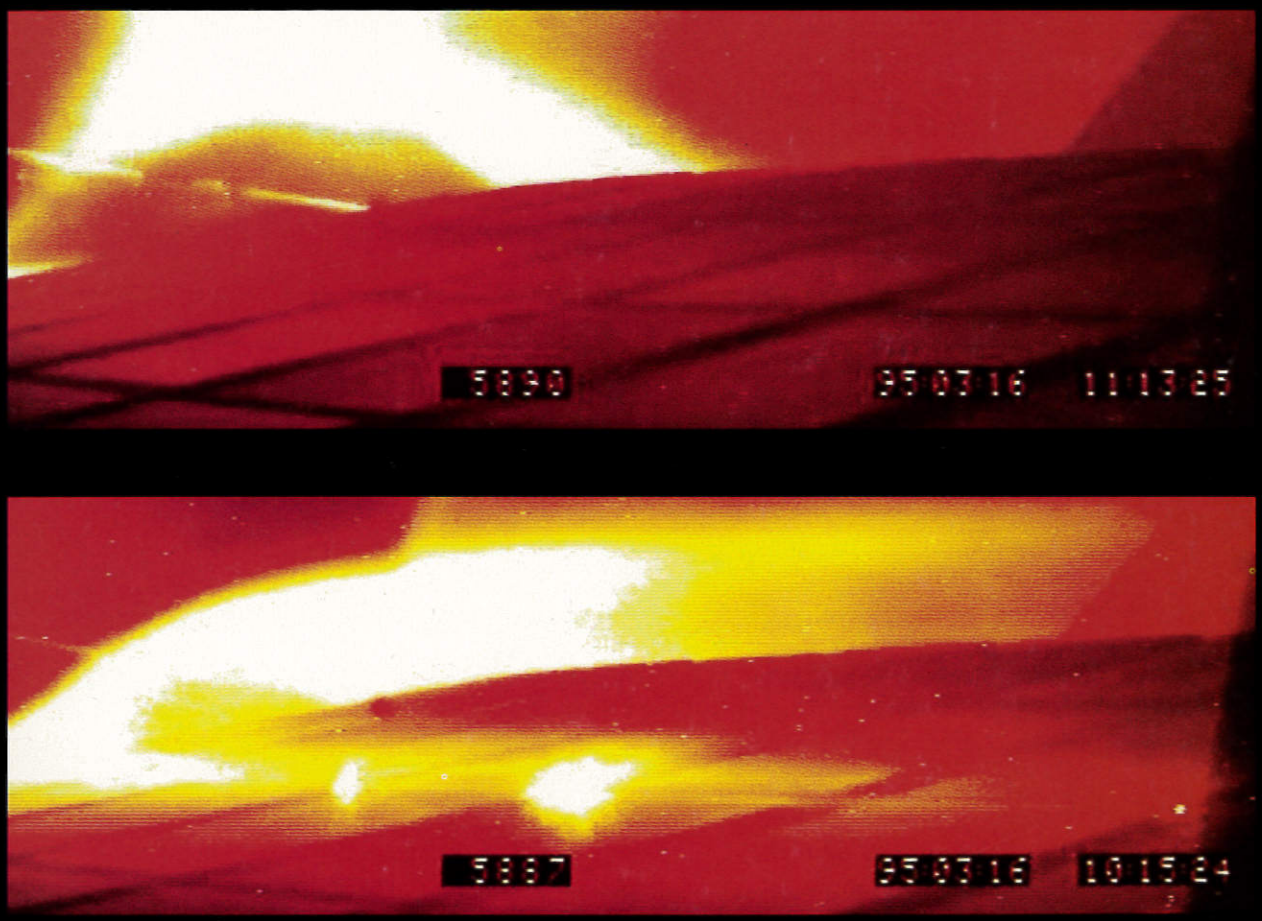

IPP

ANNUAL REPORT 1994

COVER ILLUSTRATION

The CDH-mode of plasma discharges in ASDEX Upgrade is characterized by detachment of the plasma from the divertor. Two artificially coloured pictures of the outer divertor plates in normal ELM'y H-mode and in CDH-mode are shown. The plasma in the H-mode (lower picture) is attached to the outer divertor plates, causing heavy erosion of the graphite tiles, mostly at the edges. The plasma in the CDH-mode (upper picture) is detached from the outer divertor plates, thus strongly reducing erosion.
(Pictures by kind courtesy of K. Büchl and J. Wolff)

MAX-PLANCK-INSTITUT FÜR PLASMAPHYSIK
GARCHING BEI MÜNCHEN

Annual Report 1994

CONTENTS

PREFACE

Two types of fusion experiments are being investigated at Max-Planck-Institut für Plasmaphysik (IPP): the tokamak and the stellarator. The aim of the ASDEX Upgrade divertor tokamak is to realize a reactor-compatible, open divertor and study reactor-relevant plasma edge physics. In 1994 a new plasma regime, the so-called CDH-mode (Completely Detached H-mode), was discovered. The CDH-mode combines the good confinement properties of the H-regime with a "detached" plasma, i.e. a very small energy flow to the divertor plates. Further investigations with higher heating power will be conducted to determine the significance of the CDH-regime for ITER. To optimize the radiation from the plasma boundary and divertor region, reconstruction of the divertor was prepared and an application for preferential support approved by Euratom.

At the WENDELSTEIN 7-AS stellarator the plasma experiments concentrated on investigations of the edge physics, the H-regime and the natural divertor in stellarators. A new limiter system adapted to the fivefold periodicity of the magnetic configuration now allows the island divertor concept to be studied with greater accuracy - this being one of the exhaust principles envisaged for WENDELSTEIN 7-X. In the cooperation between the Russian and German research institutes - IAP Nizhny Novgorod and IPF Stuttgart - and the ECRH team of WENDELSTEIN 7-AS, it could be demonstrated that a gyrotron can be used to measure the ion energy distribution by collective Thomson scattering. This diagnostic method has a high potential to explore the alpha-particle dynamics in future fusion reactors.

The follow-up experiment for demonstrating the reactor relevance of the Advanced Stellarator principle, WENDELSTEIN 7-X, will be a 5-period Helias configuration with a helical divertor and a superconducting coil assembly. In 1994 increased attention was paid to the divertor and plasma boundary physics. The contract for a demonstration coil was awarded, the demonstration cryostat designed, and the call for tender issued. The Phase II proposal for Euratom concerning the technical design was completed.

Work in the Berlin Division of IPP is largely oriented to the fusion experiments at IPP, concentrating on investigation of the plasma edge by experimental as well as theoretical methods. In 1994 a large probe manipulator as part of the diagnostic of the scrape-off layer in ASDEX Upgrade was completed and put into operation. A boundary layer spectrometer for observation of the boundary and divertor regions was also installed. In Berlin the Division runs a linear plasma generator to study the plasma behaviour near material surfaces and plasma-wall interaction and to develop diagnostics.

On the national level, IPP coordinates its research effort with Forschungszentrum Karlsruhe within the "Entwicklungsgemeinschaft Kernfusion" and also with Forschungszentrum Jülich and other National Research Centres involved in fusion research. IPP also closely cooperates with a number of German universities, the collaboration with the University of Stuttgart being particularly intensive.
The research conducted at IPP is part of the European fusion programme: IPP is involved in JET, the joint European experiment. The ASDEX Upgrade tokamak and the alternative stellarator concept as embodied in the WENDELSTEIN experiments provide essential information for preparing the next steps in the overall European programme. Furthermore, IPP acts as host to NET, the European reactor study group, which has been working at Garching since 1983.

Coordination of research activities also extends to the worldwide level. IPP is party to two Implementing Agreements: the one with the USA covering cooperation on the ASDEX Upgrade divertor tokamak; the other - with the USA, Japan, Australia and Russia - regulating cooperation in the joint stellarator programme, to which the WENDELSTEIN experiments make a major contribution. From April 1988 IPP provided the technical site for the American-European-Japanese-Soviet group responsible for the conceptual design activities of ITER, the International Thermonuclear Experimental Reactor. After completion of the conceptual design, IPP was also chosen in 1992 - together with the fusion laboratories in Naka and San Diego - as site for the ITER Engineering Design Phase.

Klaus Pinkau

Projects

TOKAMAKS

A large part of the capacity at IPP is devoted to investigating confinement in the tokamak configuration. IPP have concentrated their tokamak research with the ASDEX Upgrade experiment on the divertor principle. Experimental results and theoretical studies of plasma boundary problems in a tokamak reactor showed the divertor to be the candidate for the ITER experimental fusion reactor for solving problems such as energy transfer to the wall, erosion, pumping of hydrogen and helium, and limitation of impurity production.

The divertor promises solutions for the plasma boundary because:

- the temperature at the plasma edge can be decoupled from the temperature at the target plates;
- a dense and cold plasma forming in front of the target plates limits erosion and impurity flow into the bulk plasma;
- this dense plasma facilitates pumping of hydrogen and helium;
- ultimately, the energy flow to the target plates can be drastically reduced by converting it to radiation or redistributing it through charge exchange ("detached divertor").

Already before the ITER activities IPP had designed and constructed ASDEX Upgrade with magnetic field and divertor configurations very similar to those of ITER. Besides the divertor investigations, ASDEX Upgrade affords the possibility of investigating a reactor-compatible poloidal field configuration in general. Plasma control of the unstable position, strategies to prevent disruptions, and details of the disruptions themselves can be most realistically tested in ASDEX Upgrade.

The main results in operating ASDEX Upgrade and physical results in 1994 can be summarized as follows:

The focal point of investigations and a remarkable success were experiments with a combination of divertor detachment and the H-mode. The boundary can be loaded with suitable impurities up to a radiated fraction of 90 % of the heating power without reducing the bulk plasma confinement. This is especially successful in combination with deuterium gas puffing. The H-mode persists as long as the power crossing the separatrix exceeds the H-L-mode back-transition threshold. The large bursts of type-I ELMs degenerate to smaller, more frequent type-III ELMs for large radiated power fractions. The divertor detaches even during the ELMs under these conditions. Long-lasting nearly stationary discharges were obtained.

Further investigations dealt with the power threshold for the transition from L-mode to H-mode confinement and for the back transition; L-mode and H-mode confinement and steady-state properties; effects depending on the direction of the toroidal field, the plasma boundary in L-mode and H-mode and the characteristic of ELMs; vertical instabilities and disruptions; forces on structures and the vessel caused by disruptions; tungsten in the bulk plasma with regard to distribution and drifting; sputtering and redistribution of tungsten as a divertor target material; and helium transport and pumping through the divertor.

Neutral injection heating has proved to be a reliable workhorse. The heating power with deuterium injection was extended to 10 MW. The heating in ASDEX Upgrade will be continually extended in the coming years. After installation of the 140 GHz ECRH system with 2 MW in 1995, a second injector box will extend the heating capacity to 24 MW.

The extended heating power and especially the need to simulate the ITER divertor will require redesign of the divertor. The concept of the new divertor II was fixed in mid-1994 and presented to EURATOM as an application for priority support. After the anticipated approval the divertor II will be constructed in 1995 and 1996 and is to go into operation in 1997.

Simulation of the plasma boundary (SOL) was a major task. The experimental data of ASDEX Upgrade were used for validation of the code calculations. Application to ITER resulted in a considerable contribution to the ITER divertor concept evolution and guaranteed the ITER relevance of the divertor II concept as well.

Cooperation is playing a growing role in the field of fusion research in order to fully exploit the capacity of experimental devices. An IEA Implementing Agreement between EURATOM and the US Department of Energy focuses on investigation of the poloidal divertor. In particular, the problem of plasma shape and position control, plasma disruptions, and vertical displacement effects (VDE) in ITER will be dealt with in ASDEX Upgrade. The plasma dynamics and forces on structures involved in VDEs and current disruptions have been extensively simulated with Princeton's Tokamak Simulation Code.

Further fruitful cooperation on ASDEX Upgrade is maintained with the University of Cork, Ireland, Institute of Applied Physics, Nizhni Novgorod, Russia, Kurchatov Institute, Moscow, Russia, Technical University, St. Petersburg, Russia, Ioffe Institute, St. Petersburg, Russia, KFKI, Budapest, Hungary, Centro de Fusao Nuclear, Lisbon, Portugal, AEA Culham, United Kingdom, Institut für Allgemeine Physik, TU Vienna, Austria, University of Augsburg, Germany, University of Bayreuth, Germany, and University of Stuttgart, Germany.

Besides operating their own ASDEX Upgrade tokamak, IPP have been involved in JET, the joint European large-scale project at Culham (UK) for many years. IPP constructed and put into operation a large fraction of the JET diagnostics and also participate in exploitation of the JET experiment. In January 1994, JET completed a shutdown which lasted almost two years. The most important changes to the machine were the installation of four in-vessel divertor coils, a new divertor target structure, and a cryopump. In addition, new antennae for ion cyclotron resonance heating, a new launcher for lower-frequency current drive, and various new plasma diagnostic systems were installed. With this new configuration a plasma current of 5 MA, a heating power of 26 MW, and a plasma-stored energy of 11.3 MJ were obtained. The JET experiment is devoted mainly to investigating plasma conditions relevant to ITER with reduced power flow to the divertor target. In H-mode discharges partially detached plasmas were produced by puffing a mixture of nitrogen and deuterium gases. IPP have intensified the scientific cooperation through informal meetings and contributed directly in different areas to the programme.

The results of JET, the IPP divertor programme, and the other associations form the groundwork for planning an experimental reactor as a next step, for which IPP are hosting the NET ("Next European Torus") Team. Meanwhile, the European Union, Japan, the USA, and Russia have agreed to prepare a possible next step as a joint venture. An engineering design study (EDA) of the ITER experimental reactor is being carried out by a joint team of the four partners, one of the three groups being stationed at Garching. IPP are contributing to this work through three major channels: (i) direct participation of IPP scientists in the numerous expert meetings called together by ITER to deal with special subjects, (ii) handling of special tasks in support of NET/ITER, and (iii) participating in various NET/ITER committees. Important contributions included the analysis of the confinement data base and the contribution to the development of a divertor model.

ASDEX UPGRADE PROJECT

(Head of Project: Dr. Walter Köppendörfer)

1. OVERVIEW

1.1 Introduction

The programme on ASDEX Upgrade was mainly devoted to the problem of controlling the plasma energy loss and particle exhaust with respect to ITER requirements. Only a small fraction of the α-particle power in ITER can be transferred to the target plates. Energy flow to the target plates has to be limited to solve the technical problems: the plasma has to "detach". This necessity has to be combined with the H-mode to guarantee sufficiently good confinement. It was now demonstrated on ASDEX Upgrade that both requirements can be fulfilled at the same time. In the so-called CDH-mode (Completely Detached H-mode) good H-mode confinement was observed at the same time, even during ELMs as the plasma remained detached in front of the target plates. These results were obtained on the basis of reliable machine operation, a high-performance heating system, a sophisticated plasma control scheme and improved diagnostics. In combination with analytical and numerical studies of the plasma boundary, understanding of the SOL was considerably improved. This constitutes a very important contribution to ITER.

Further exploration of the CDH-mode and extension of these investigations to higher heating power will form an essential part of the ASDEX Upgrade programme in the coming years. The new heating systems will provide the necessary power (ECRH: 2 MW, 2nd NI injector: $\leq$ 10 MW). To optimize the radiation from the SOL and divertor region, reconstruction of the divertor had to be prepared. An application for "preferential support" for the construction of the so-called "Divertor II" was submitted to EURATOM. The intended reconstruction will enable ASDEX Upgrade to investigate both ITER divertor options for the time being: the gas-bag and an inclined target plate configuration called "Lyre".

In 1994 the ASDEX Upgrade experiments proceeded on the technical side as scheduled. The preferred plasma configuration was a single-null divertor (SN) with an elongation of κ = 1.6 and low triangularity $\delta \leq 0.1$ which fits the outer plasma boundary to the ICRH antenna contour. Plasma currents were run from 0.6 to 1.2 MA, with $B_t = \pm 1.1 - 3.0$ T, allowing densities of up to $1.2 \cdot 10^{20}$ m^{-3}. The arcing during disruptions across the insulation gaps in the passively stabilizing loop (PSL) did not greatly hamper the programme. However, further steps (replacing the gap insulation, rounding edges, and shunting with resistors) were taken during the autumn shutdown to finally prevent arcing. The bolts of the PSL support rods were replaced by new ones of higher-strength steel. At the end of the year the vessel and internal structure were reinforced to withstand 1.6 MA plasma current disruptions.

1.2 Technical Improvements of ASDEX Upgrade

In order to approach this goal, the following technical provisions were made:

1. Technically, the full 1st-step heating powers of 10 MW (D) neutral injection (design value 9 MW) and 4 MW ion cyclotron resonance heating (ICRH) were available. The plasma was heated with up to 12 MW combined heating.
2. The fast plasma control computer (feed-forward) was equipped with a new safety system for controlling all electric supply systems and control computers. Depending on the specific fault condition, pulse stop or controlled ramp-down provides machine safety. It was an improvement to be able to record the specific fault events, which allows the error to be quickly found.
3. The feedback control computer for plasma position and shape (R2) was supplemented by improved software, especially by recording the online magnetic input data. For the next discharge period the whole R2 system software was rewritten for better transparency and to allow interaction with the R4 plasma parameter control computer later on.
4. A second feedback control computer (R4) for plasma parameter control was put into operation. Feedback-controlled gas puffing using the D_2 filling gas and impurities (Ne, Ar) for controlling the detachment was the first application. Control input was provided by the divertor neutral gas flux and the power radiated from the plasma.

The diagnostic systems were supplemented mainly with regard to plasma edge and divertor investigations: by a midplane manipulator for SOL investigations, an edge Thomson scattering

system, a lithium beam probe, a wide angle UV and visible spectrometer system, additional bolometer cameras, and an extended ECE radiometer system.

1.3 Main Tasks and Results of the 1994 Discharge Programme

The experimental programme carried out can be divided into the following areas:

1. Exploitation of the operating regime of the SN divertor configuration in the range of available heating powers with regard to:
   a. loading of the plasma boundary with deuterium gas puffing and radiation-controlled impurity puffing, loading to detachment of the divertor area, MARFES and the density limit;
   b. power threshold for the transition from L-mode to H-mode confinement and for the back transition;
   c. L-mode and H-mode confinement and steady-state properties, ELM properties;
   d. effects depending on the direction of the toroidal field;
   e. vertical instabilities and disruptions; forces on structures and vessel caused by disruptions.
2. Investigation of plasma parameters for the different operating regimes with emphasis on:
   a. the plasma boundary in L-mode and H-mode and the characteristics of ELMs;
   b. the possibility of plasma profile control by gas puffing and multiple pellet injection;
   c. the behaviour of intrinsic and added (by gas puffing and laser blow-off) impurities and the question of accumulation and attainability of steady-state conditions;
   d. the diagnosis of added tungsten in the bulk plasma with regard to distribution and drifting;
   e. feedback control of the impurity-loaded plasma boundary under ELMy H-mode conditions.
3. Divertor operation and plasma power handling with the following more specific tasks:
   a. radiative boundary and the variation of power losses through the different loss channels: bulk radiation, plasma boundary and SOL radiation and loss through the divertor;
   b. divertor properties and detachment in conjunction with the confinement mode with emphasis on steady-state H-mode confinement;
   c. power load distribution on the divertor plates as a function of heating powers and operational regimes including disruptions;
   d. divertor density and main chamber recycling;
   e. MARFEs and divertor detachment;
   f. sputtering and redistribution of tungsten as a divertor target material;
   g. helium transport and pumping through the divertor.

All these tasks could be essentially covered. The most important results can be briefly summarized as follows:

1. ASDEX Upgrade can realize steady-state H-mode discharges with ELMing boundary.
2. The boundary can be loaded with suitable impurities (neon) up to a radiated fraction of 90 % of the heating power without reducing the plasma bulk parameters.
3. The H-mode persists as long as the power crossing the separatrix exceeds the H-L-mode back-transition threshold.
4. The large bursts of type-I ELMs degenerate to smaller, more frequent type-III ELMs for large radiated power fractions in the boundary.
5. The divertor can detach and the widening of the SOL diminish during ELMs under these conditions.

These investigations will be continued with improved diagnostics, increased plasma current, and heating powers of up to 16 MW until 1996. In autumn 1995 the graphite divertor target plates will be replaced with tungsten-clad tiles in order to investigate high-Z materials with regard to heat load capability and sputtering.

The programme which will then follow is to fully exploit the divertor capability of ASDEX Upgrade (Divertor II). A second neutral injector supplements the heating power to 24 MW. The divertor surface contour will be optimized to take maximum power flux density with extensive backscattering of neutrals into the hot plasma fan. The graphite material will be selected to take the maximum possible heat load. The pumping of the divertor will be improved by installation of a helium cryopump with 100 m^3/s.

In the following sections the achievements of the Technical Systems (Sect. 2), the experimental findings with regard to the operational regimes, the plasma configuration and control, and the bulk plasma (Sect. 3), the investigations regarding the plasma boundary and divertor (Sect. 4) and the development of new diagnostics (Sect. 5) are described.

2. TECHNICAL SYSTEMS

During the summer shutdown, the coaxial bridge of the passively stabilizing conductor (PSL) was shunted by two parallel 0.3 mΩ resistors. The PSL is a saddle loop increasing the feedback time constant for controlling the vertical plasma position. During hard plasma disruptions without shunt loop voltages of up to 180 V were measured across the coaxial bridge, causing arcing. After an arcing event there were generally no conditioning discharges required for regaining normal discharge conditions. The impact of arcing on the machine availability was therefore negligible. However, the onset of arcing dropped with time towards lower disruption-induced voltages and finally occurred already at about 80 V due to increasing deterioration of the Vespel insulation inside the bridge. Measurements in combination with computations predicted that the resulting shunt resistor of 0.15 mΩ would limit the bridge voltage to below 60 V, even for the worst-case disruption at 1.6 MA to

be expected. The new pair of resistors are now in operation and reduced the bridge voltage during first hard disruptions by more than a factor of 5.

During the 1995 summer shutdown, the strike point tiles of the lower inner and outer target plates will be replaced by tungsten-coated graphite tiles (Fig. 2.1). Therefore, in 1994 the most favourable manufacturing methods for tungsten coating on graphite were tested. Screening tests up to 15 MW/m^2 and 2 s (typical surface temperature 2000 C) as well as cyclic tests (N = 1000, 10 MW/m^2, 2 s, typical surface temperature 1450 C), performed in the electron and hydrogen beam facilities of KFA Jülich, have shown that plasma-sprayed (PS) coatings can withstand higher heat loads without damage than coatings manufactured by physical vapour deposition. Two of three tested qualities of PS coatings survived the full range of tests without disabling damage. Leading edges cannot be tolerated with tungsten-coated tiles. Plasma discharges depositing sizeable energy in the divertor would cause carbon evaporation from the substrate and in turn cracking, detachment from the substrate and melting of the tungsten layer. During the 1994 summer shutdown, 8 PS specimens were installed with hidden edges for final in vessel testing. The roof-shaped specimens are placed on the inner and outer divertor plates at positions where observation by CCD cameras and spectroscopy is feasible. In summer 1995, tilted edge-shadowing tungsten-coated tiles, which offer a higher safety margin against overheating than roof tiles, will be installed.

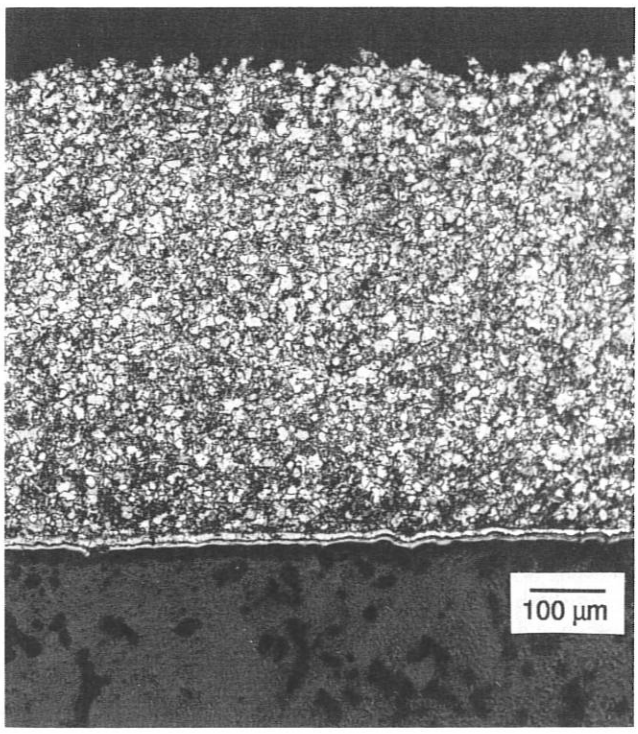

FIG. 2.1: Plasma-sprayed tungsten coating on EK graphite.

The first neutral beam injector (NI) reached 10 MW (deuterium), more than the nominal design value. Together with ion cyclotron heating (ICRH) the maximum auxiliary heating power during a discharge was 12 MW. ICRH could successfully develop a feed-back system for operation during H-mode discharges with strong type-I ELMs. In addition, a system was implemented for automatic pre-setting of optimum parameters for the next discharge by relying on data of the preceding discharge. ECRH has commissioned the first gyratron with 0.5 MW of power and will start plasma operation in early 1995.

2.1 Machine

The installation of the PSL bridge resistor (Fig. 2.2) was combined with rigorous improvements of the insulation system for the complete bridge. All the Vespel of the coaxial bridge was removed and replaced by inorganically bonded mica plates. Tests have shown that the latter is much less carbonized by arcs than Vespel. The electrode distances of the coax part were increased wherever possible and all corners rounded. The bridge therefore had to be removed from the vacuum vessel. This required the routine summer shut-down to be extended to early December. As a consequence there were only 47 experimenting days with 1,055 counted shots in 1994.

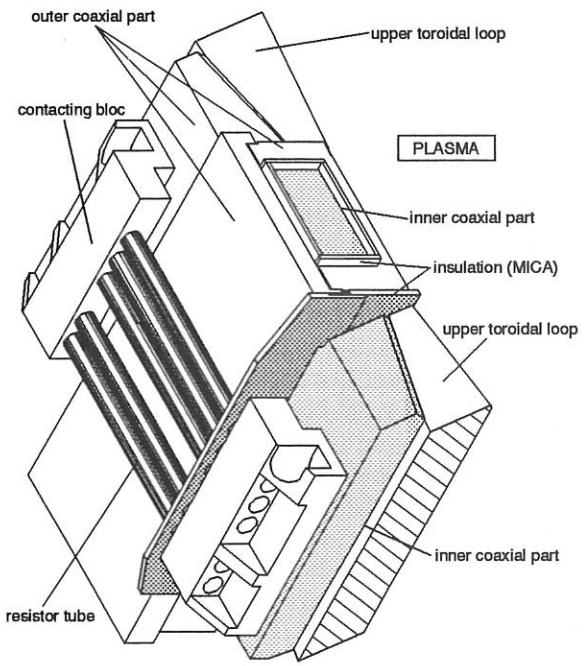

FIG. 2.2: Coaxial bridge of PSL with new shunt resistor

The prolonged shutdown period was also used for cabling work required to energize the coils OH2o, OH2u of the OH-coil system by additional thyristors. After plasma breakdown the additional OH2o, OH2u currents to be superimposed on the main current of the OH-coil system permit one to control the lower separatrix strike point (OH2u) with more precision and achieve a larger triangularity of the plasma cross-section. For plasma currents above 1 MA the coil set of the AUG experiment requires three generators as supply. The loading and unloading of their flywheels is now completely controlled via the AUG timer. This saves grid energy and keeps the heating of the generator bearings at a minimum. The changed Q3 closing switch

(without ignitrons [449]) of the OH-breaker system proved its reliability in 1994. Also the available ASDEX inductance used for reducing the Q3 arcing coulombs by a factor of about 50 could be commissioned under restricted breakdown conditions. To eliminate these restrictions, a new inductance with larger permissible voltage will be procured. Voltage and current transducers, installed during this year, now permit a precise monitoring of the transient behaviour in all switching circuits. The measurements are in good agreement with computations.

The in-vessel components were further reinforced to increase the disruption safety for plasma discharges up to 1.6 MA. The suspension of the PSL was equipped with stronger hinge bolts. Also the heat shield fixtures on the vacuum vessel were reinforced by elements of higher-grade steel. The inner target plates received CFC tiles where diagnostic paths perforate the steel support. To prevent arcs from penetrating the region behind the PSL, where many diagnostics are installed, the last aperture open to the plasma was closed for field lines by carbon limiter blocks of appropriate spacing. Energetic particles of the neutral beam, lost in banana orbits, had caused hot spots on the ICRH limiters. To reduce the danger of carbon bloom at these locations, the total limiter area was increased by additional protection limiters, fixed at two pillars linking the lower and upper rings of the PSL.

2.2 Control Systems and Information Technology

The **control** group's activities focussed on three fields : commissioning of the R4 plasma parameter controller, upgrading of the R2 shape controller and rejuvenation of host computers for standardization of operating systems.

A significant contribution to the physics programme was the commissioning and first operation of the R4 plasma parameter controller. It was designed as a universal device to optimize discharges. A number of independent feedback processes, collecting information from various diagnostics, are available to control heating and refuelling systems. Subsets of processes are activated to form recipes for controlling specific scenarios. Physicists assemble a time-varying list of such recipes to tune various plasma parameters simultaneously throughout the evolution of a discharge.

Basic density control and radiated power fraction control were performed for the start of operation and performance evaluation. Dynamic behaviour was tested with a transition from bulk density control to divertor neutral gas flux control. The recipe concept proved its power with the radiative boundary scenario, which requires parallel feedback control of the radiated power fraction and divertor neutral gas flux (see Section 4.3).

As a result of extensive simulation, system-inherent coordination mechanisms and built-in protocol functions the commissioning could be drastically speeded up. The R4 plasma parameter controller project will be further pursued to offer physicists a valuable tool to produce better plasmas.

The prerequisite for all plasma control is dependable position and shape control. The experience of years of reliable operation and continuous enhancements went into the redesign of the position and shape controller R2. Its functions were modularized and tidied up to give a sound basis for the introduction of extended shape control. Throughout the code new data objects were introduced for structuring characteristic signal descriptions and values. Modifications to the coil system required adaptations of the control algorithm and upgraded I/O capabilities.

In parallel, conceptual work was carried out for identification of optimal sets of shape control parameters, interactive tuning of controller gains and evaluation of function parametrization performance. The MATLAB package greatly facilitated this task and provided powerful tools for troubleshooting during experiment operation.

Considerable personnel and financial effort was put into the overdue rejuvenation of the system infrastructure. Most urgent was the replacement of obsolete host computers by modern workstations. This allows the long-planned unification of the operating system and development environments throughout the control network.

A further measure was the upgrading of the simulation environment, which is a mirror image of the experiment control environment. The benefit is a clear-cut separation of tokamak operation and system development and easy migration between the two platforms. These improvements resulted in a clearer structure of the control system, reduced costs for maintenance and software development, and increased availabiliy of the tokamak for the physics programme.

The main task of the Information Technology group at ASDEX Upgrade is to maintain the data acquisition software and equipment and the office workstations of the scientific staff at the project.

Modifications to the access routines now allow transparent access to shotfiles residing in the old mainframe-based AMOS system as well as in the Andrew File System (AFS). Finally, the complete replacement of AMOS by AFS is planned for the end of 1995 if the operation of AFS in the meantime is stable and satisfactory. (Since the replacement of AMOS and the introduction of AFS and multi-resident AFS were activities, which have been carried out in close collaboration with the development departments of the Computer Centre and the Computer Science Division; see also the relevant section of this report.)

Development, started last year, of a new programmable pulse generator for triggering CAMAC transient recorders and an SBus card to attach CAMAC crates direct to Sun workstations was finished. The first charge of these devices is now in operation and especially the SBus card will make it possible to replace our eight years old VMEbus workstations with cheap and powerful new machines.

Some effort was made to move our Sun systems from Solaris 1.1 to Solaris 2.3. This involved the port of the data acquisition software as well as modification of a couple of servers and clients. However, up till now the Solaris performance and the operation of some commercial software does not seem to be satisfactory. So before moving the bulk of stations we will

have to wait for the Solaris 2.4 release and new releases of some commercial packages.

2.3 Neutral Injection into ASDEX Upgrade

In 1994 operation of the first injector was successfully extended. Power levels exceeding the nominal neutral power were achieved routinely and reliably. Progress was also made with the second injector: the regulated RF supply was delivered and successfully put into operation; the performance of the RF source was advanced to a level such that its application on the second injector can now be considered with confidence.

In the first year of neutral beam **injector operation** on ASDEX Upgrade H^0 beams of up to 7 MW (55 kV, $t_p \approx 2$ s) and D^0 beams of up to 10 MW (60 kV, $t_p \approx 2.7$ s) were injected into the torus, exceeding their respective design values by 1 MW. The present limitation is imposed by the capability of HV power supplies and modulators. For internal shots onto the calorimeter the pulse length was extended up to the design value of 5 s without any indication of thermal overloading. The overall efficiency – defined as the power injected into the vessel / $U_{ex} \times I_{ex}$ – was found to be 36 % for 55 kV H^0 beams and 53 % for 60 kV D^0 beams. Since completion of the commissioning the injector was ready to inject with all four ion sources on every day of ASDEX Upgrade operation, with only two exceptions, and approximately 80 % of the injection shots were run at the required power and pulse length.

Neutral beam transmission through the 2 m long duct which connects the injector box with the ASDEX Upgrade vessel was monitored by various diagnostics. Thermal loading due to direct interception of the neutral beam with different protection plates was found to increase roughly linearly with the energy transmitted through the duct. However, reionized particles hitting unprotected duct areas led under some circumstances to local heating-up and therefore longer pulse intervals than otherwise required. During the summer shutdown of ASDEX Upgrade melting traces were found on the surface of the entrance port, which most likely occurred due to extreme focussing of reionized particles in one specific magnetic field configuration. Consequently, additional wall protection and improved diagnostics were installed and commissioned after the start of tokamak operation.

A special feature of the HV modulator control is that it allows the extraction voltage to be repeatedly switched off and on during one shot. Measurements of the neutral beam power onto the calorimeter as a function of the beam-on fraction for a periodically modulated beam (H^0 at 54.5 kV) show a linear relation between the power and beam-on fraction (Fig. 2.3). Beam modulation therefore allows one to vary the injected power averaged over a time period smaller than the plasma energy confinement time in arbitrary steps, and it was extensively used to determine, among other things, the power threshold for L-to-H and H-to-L transitions of ASDEX Upgrade plasmas. This method is envisaged for feedback regulation of the injected power by controlling the beam modulation from the fast ASDEX Upgrade control computer.

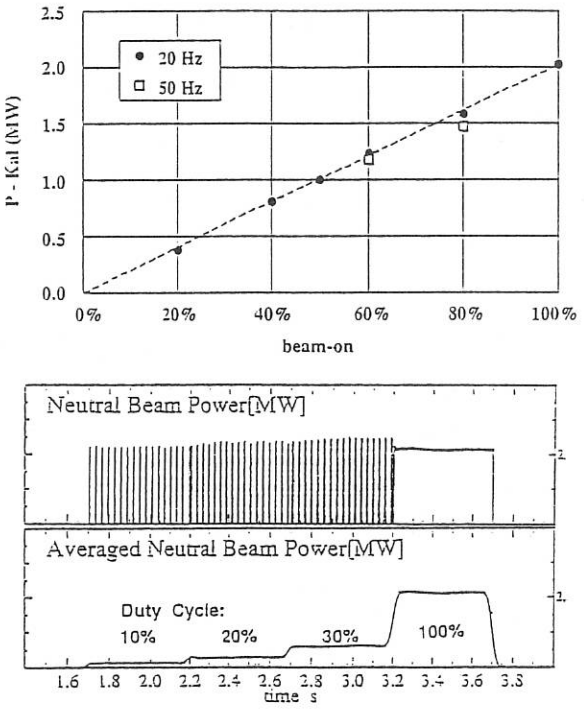

FIG. 2.3: Measured calorimetric power versus beam-on fraction for modulation frequencies of 20 Hz and 50 Hz.

The work at the **teststand** was devoted entirely to the RF source development for the second injector (see also Technology Division). Twelve different source configurations (RF coil immersed in or external to the plasma, various arrangements of magnets, protection of quartz surfaces with a Faraday screen) were tested with more than 9,000 pulses in order to improve beam quality, power efficiency and long-time reliability. In particular, the latter was not satisfactory with the previous configuration, decribed in 1992/93, because apparently Si sputtered by the plasma was deposited on the HV grids. The present version gave almost the same results as the standard bucket source. It is the original "external coil" version, but with a water-cooled copper Faraday screen with vertical slits every 2 cm mounted close to the quartz walls. The Faraday shield decreased the number of breakdowns and the extraction reliability was considerably improved, so that a series of 5 s/75 A pulses at 50 kV could be successfully carried out.

Furthermore, the heat load on the quartz walls is reduced, so that RF breakdowns at the coil no longer occur because of the reduced pressure rise outside the plasma volume during the pulses. Also the beam transmission increased and, after addition of permanent magnets to the side-walls, the required values were almost reached.

These results led to the decision to use the RF source on the second injector of ASDEX Upgrade. It is considered as an attractive low-cost alternative compared with the bucket source. The next work will be the final reliability tests with long pulses

at 55 kV and 90 A using a fresh, clean extraction system (because of the residual Si layers on the present grids).

Concerning the **second injector**, a contract for the delivery and installation of the cooling system was placed, and calls for tenders for the vacuum box and the titanium power supplies were sent out. Both components were recently ordered. The design of the injector environment in the torus hall (piping, access) was advanced to the extent that fabrication and installation can start soon. For the control systems most of the hardware components are in-house and programming of the software is under way.

2.4 Ion Cyclotron Resonance Heating (ICRH)

After ICRH at ASDEX Upgrade had been successfully started in 1992, further development of the technical system proved to be needed for reliable high-power operation. These efforts, described in the Annual Report 1993, resulted in improvements at the antennas and at the safety protection of the generators, in methods to improve the generator stability to load variations and in a new and faster matching method. These devices and methods were implemented and tested in the experimental phase of 1994, and allowed us to achieve reliably about 1 MW per system, peaking in a total of 4 MW for minority heating at 30 MHz.

The experiments in 1994 showed new limitations due to strong variations of the antenna coupling, especially at type-I ELMs during the H-mode with high heating power. Such coupling variations result in power reflections causing output power reductions at the generator. For too large reflections (as during ELMs) the power is cut off by the protection circuit. Variations slow enough (>ms), e.g. in the case of L-H transitions, can in principle be compensated by feedback measures (not yet available in 1994). Type-I ELMs are too fast (a few 10 μs) for feedback methods. Furthermore, it is difficult for the RF system to distinguish between the similar reactions to ELMs and arcs, the safety cut-off being triggered in both cases.

The available matching equipment allowed pre-adjustment of the matching elements (stub tuners) for the expected coupling conditions of the next shot (see Technology Division). In case of coupling variations during shots, compromise values were preadjusted (between L and H or ELM and ELM-free) allowing stable operation to be achieved in the case of L-H transitions and ELMs for generator powers of up to about 1 MW, the reflection remaining below its limit in both phases.

This experimental experience resulted in the following development efforts to overcome such coupling variations:
For slower variations (> ms, e.g. increasing density or L-H transitions) feedback measures were prepared: The stub tuners can be automatically reset (> about 2 s, to be tested in early 1995), and a coupling feedback, keeping the antenna resistance constant by shifting the plasma position, is prepared for implementation in April 1995. For fast, but not too large variations an additional matching feedback has been developed, shifting the generator frequency. This is limited by the generator's bandwidth, and by the voltage standoff in the transmission lines, and works only in the case of adequately preadjusted stub tuners. It can be tested, too, in early 1995.

The coupling variations during ELMs can be overcome by fast power reductions triggered by the ELM peaks on the ring voltage signal. Such an electronic device fast enough to avoid high reflection peaks was successfully tested (see Technology Division).

2.5 Electron Cyclotron Resonance Heating (ECRH)

The ECRH system is under construction. Its parameters are f = 140 GHz, P = 2 MW (generated by 4 gyrotrons), T = 2 sec. The gyrotrons will also allow operation at slightly higher power of 4 $\times$ 0.7 MW, but then only for a pulse length of 1 sec. The power will be launched from the low-field side, mainly in the second harmonic X-mode because of its high optical depth, which assures single-pass absorption and thus very localized power deposition. This is essential for the planned experimental programme. However, O-mode operation is also possible.

The present status of construction is as follows:
One high-voltage unit, consisting of high-voltage line, crowbar and series tube modulator, is ready to feed two gyrotrons in parallel. Construction of the second unit will start this year. The cooling system for all four gyrotrons is ready, as well as a fast timer and the SIMATIC system control. The combined quasioptical and waveguide transmission line for the power of one gyrotron is partly installed, and also a first set of mirrors inside the torus. These mirrors allow a focused microwave beam to be launched from the low-field side midplane in variable toroidal and poloidal directions. The beam waist is w_o = 22 mm. It is located at r/a = -0.5 (on the high-field side). Pickup waveguides are installed on the high-field side in order to allow checks of the mirror positioning.

The first two gyrotrons and cryomagnets are expected for October 1995, the next two for July 1996. In the meantime we have installed, in cooperation with IAP Nizhni Novgorod, a gyrotron with 0.5 MW/0.5 sec in order to start first experiments. This gyrotron is now in test operation with a high power dummy load. It has been used to test the compatibility of gyrotron operation with the stray magnetic field of the tokamak. We found that the gyrotron can be operated both at the beginning of the discharge and at its end, i.e. with a stray magnetic field of opposite directions. These tests were restricted to the present performance of ASDEX Upgrade with $I_p \approx$ I MA. However, from the deformation of the electron beam deposition in the collector we estimate that operation at full performance should still be possible. Otherwise some compensation would be needed (see Technology Division).

The first transmission line will be completed soon and we expect first shots into the plasma in March 1995. We will then aim at experimental determination of the power deposition profile, studies of electron heat transport by means of heat wave propagation, and the power transport through the H-mode transport barrier.

3. OPERATIONAL REGIMES AND BULK PLASMA PHYSICS

3.1 Operational Regimes

The operational regime was further consolidated in 1994 and significantly expanded. The particle fuelling methods were refined by increasing the number of gas valves and varying the pellet injection parameters and the heating power was enlarged (see Sect. 2.3). The experiments concentrated on the H-mode as the most promising regime. It was extended to higher P_{heat} power levels (i.e. leading deep into the type-I ELM regime) and, especially, to radiative mantle scenarios with cold divertor characteristics and radiated power levels P_{rad}^{total}/P_{heat} above 90 %. Complete detachment of both strike zones between and even during ELMs was demonstrated (CDH mode). Such high performance discharges could only be realized in steady state since a real-time multi-transputer feedback computer system (R4) came into operation. It includes at present algorithms controlling the line-averaged electron density $\bar{n}_e$, the neutral particle flux density in the outer divertor Γ_0^{div} and the radiated power fraction P_{rad}^{total}/P_{heat} separately or in combination.

To reach high density and cold divertor discharges, extensive deuterium and/or noble gas puffing and multiple pellet injection was performed. We injected deuterium pellets with 1.7 • 10^{20} or 2.8 • 10^{20} particles per pellet and velocities of 240 m/s or 560 m/s into ELMy H-modes. The experiments, however, showed that $\bar{n}_e$ could only be increased by about 30 %. The achieved density $\bar{n}_e$ did not exceed the Greenwald limit, which can also be reached under purely ohmic conditions. In parallel, the pellet fuelling efficiency, defined as the increase of the plasma particle inventory divided by the injected pellet particles degrades with rising heating power down to about 20 % or less (in contrast, the efficiency approaches 100 % in ohmic discharges).

Moreover, the increased auxiliary heating power and its enlarged duration can lead to detrimental temperature rise of the carbon target tiles. To reduce the local strong concentration of the heat load on the divertor plates, especially the leading edges of the tiles, the vertical position of the plasma was sinusoidally swept $\pm$1.5 cm with frequencies of up to 5 Hz, resulting in a roughly $\pm$1 cm variation of the strike point intersection on the divertor.

Maximum poloidal $\beta_\perp$ values of up to 2 and corresponding normalized β values $\beta_N = \beta_t/(I_p/\alpha B_t)$ {%, MA, m, T} $\leq$ 3.5 were achieved. During I_p ramp-down this value could be transiently improved to about 3.8.

Furthermore, first experiments were undertaken (I_p = 0.8 MA, B_T = -2.5 T) to explore the potential of the enhanced H-mode (VH-mode) characterized by enlarged triangularity. Since, however, the OH2 coils could not be run as an independent pair of PF coils, the triangularity $\delta_R = < (R - R_{geo})^3 > /a^3_{min}$ is only moderately increased by about 40 %, from 0.11 to 0.15. The first attempts show an increased ELM-free period of $\approx$ 150 ms compared to $\approx$ 30 ms in the standard configuration at a comparable heating power of about 2.5 MW. However, due to the onset of ELMs after one confinement time, a VH-mode does not develop. The experiments will be continued in 1995.

3.1.1 ICR-heated H-mode and ELMs

The H-mode had been achieved on ASDEX Upgrade with ICRF alone very early on. Periods of ELM-free H-modes as well as discharges with type-I ELMs have subsequently been achieved in combination with NI. Now, with the increased power coupled to the plasma, those regimes were also achieved with ICRF alone. The frequency of the type-I ELM with ICRF is not different from this frequency for NI alone or for the combination.

3.1.2 Second-harmonic heating of H at low H concentrations

It was possible to operate at the second harmonic of H even with low H concentrations. While at these low concentrations the second harmonic heating at low power is less efficient than the minority heating, at high power (1 MW) the plasma energy content (from equilibrium) obtained with heating at the second harmonic was the same as that obtained with minority heating indicating that at high power the second harmonic is able to "bootstrap" itself by creating its high-energy tail, to which it can then efficiently couple. A similar effect can be obtained by combining minority heating and second harmonic.

3.2 H-mode Operation and Power Thresholds

The operational window was further analyzed by extending the toroidal magnetic field range, in particular to positive values, for which the ion ∇B drift, a key parameter in the H-mode, is directed away from the X-point. Figure 3.1 also shows the power necessary to reach the β limit for $\bar{n}_e$ = 0.5 •10^{20} m^{-3} and for the global confinement time routinely achieved in the H-mode as given in the next section. Note that some discharges reached the β limit.

The resulting diagram of Fig. 3.1 represents the L-to-H power threshold and the windows of different confinement regimes (L-mode, dithering, H-mode with both type-I and III ELMs). This diagram contains data from discharges under "standard conditions", i.e. without strong gas puffing, and therefore with $\bar{n}_e \leq 0.5 \cdot 10^{20}$ m^{-3} in the L-mode before the L-to-H transition. In the right part of the diagram (ion ∇B drift towards X-point, standard configuration), the threshold linearly increases with toroidal field times density, independently of the heating method (ohmic, NBI, ICRH), is low and comparable with the results from other tokamaks (see section on ITER threshold database). In this region, all the H-mode types are observed as the heating power is increased: dithering just above the threshold, type-III ELMs, ELM-free and finally type-I ELMs, which are obtained in the major part of this region. For the ion ∇B drift direction away from the X-point, the threshold power is at least 1.8 times higher than for the other direction. For B_T above 2 T the magnetic field dependence becomes stronger than linear, for reasons not yet identified. In the left part of Fig. 3.1 only type-I ELMs occur in the H-mode region under the standard conditions considered here. However, in discharges with Ne puffing for the cold radiative edge mantle (see section on divertor physics) type-III ELMs were observed just above

the threshold power for the H-to-L transition, showing that type-III ELMs are not essentially forbidden for this ion ∇B drift direction but are probably related to the edge temperature. Some discharges performed in hydrogen show that for both ion ∇B drift directions the threshold for this isotope is 1.8 times higher than for deuterium. The threshold in helium lies in between. The H-mode hysteresis is the well-known property of the H-mode in this confinement regime being sustained with less power than is necessary to reach it. The experimental campaign of this year demonstrated that the threshold power for the H-to-L back- transition is independent of the ion ∇B drift direction. So far limited results suggest that, under the conditions for the radiative mantle, the threshold is higher than the results of Fig. 3.1 and becomes more symmetric.

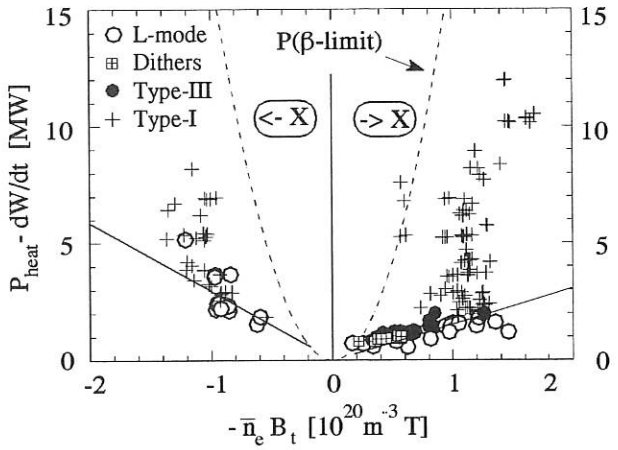

FIG. 3.1: H-mode operational diagramme. The solid lines represent the L→H mode transition for both ion ∇B drift directions. The corresponding H→L mode back transitions happen at lower hating powers.

3.3 Confinement Studies

The global confinement time was studied in the different regimes described above and compared with the widely used ITER89-P L-mode scaling law. The high-power discharges performed under the standard conditions are stationary with type-I ELMing H-mode. The global confinement time in these discharges shows the usual behaviour $\tau_e \propto I_p P_{heat}^{-0.5}$, as well as a not yet quantized but finite isotope effect. The enhancement factor H above the L-mode scaling is almost 2 at q_{95} = 3 and slightly decreases with q_{95} reaching 1.6 at q_{95} = 4. This yields for the "ITER quality factor" $H/q_{95} \approx 0.65$ at q_{95} = 3. The global confinement time with radiative cooling mantle also reaches H $\approx$ 1.6 during the CDH phases (q_{95} = 4). This good result is only partly due to the reduction of the ELM activity ($\leq$15 %), but also possibly to the slight electron density profile peaking and the peaking of the temperature profile, which leads to a higher value of the internal inductance, known to be a factor of improved confinement.

Furthermore, an additional transient improvement of the energy confinement is often observed at the beginning of the NBI pulse. Combination of NBI with ICRF (minority heating) might extend this transient improvement for longer times. Some explanations, such as changes in the sawtooth behaviour, could be excluded.

3.4 Behaviour of Laser-Ablated Materials

Different metals, ranging from aluminum to tungsten, were injected by means of laser blow-off. The number of ablated particles, which was evaluated by automatic image processing of the probe, ranges from $0.4 \cdot 10^{17}$ to $7 \cdot 10^{17}$ particles. The decay time of spectral lines was measured with SPRED, the grazing-incidence and the Bragg spectrometers. In the case of strong radiation the temporal evolution of bolometer and soft X-ray profiles could also be recorded.

Up to now, only the light elements were injected into ohmic discharges. The modelling of the decay time of the line radiation with the ZEDIFF impurity transport code yields diffusion coefficients of 0.5 - 0.6 m^2/s for intermediate plasma radii.

The main part of the investigations was dedicated to the behaviour of high-Z materials in the plasma. Here especially tungsten played a major role, since it will be used as divertor target material in ASDEX Upgrade in the near future.

The measured radiated power induced by tungsten laser blow-off, was a factor of 10 larger than with titanium under identical experimental discharge conditions. The fuelling efficiency for laser-ablated W ranges from 20 to 50 %, depending on the discharge conditions. Transport analyses for the high-Z elements are much more ambiguous due to uncertainties in the ionization and excitation rates. Nevertheless, distinct differences in the decay time of a tungsten line array at 5 nm could be found. They varied from 60 ms in L-mode discharges to 200 ms in H-mode discharges. Using the equation $P_W = n_e n_W L_W$, where n_e is the electron density and L_W the radiation loss parameter, the approximate W density n_W could be calculated from the radiation profile P_W. Figure 3.2 shows the radiation profile for discharge # 4542 80 ms after laser ablation and the extracted W concentration profile. Central W concentrations of the order of a few 10^{-5} were typical.

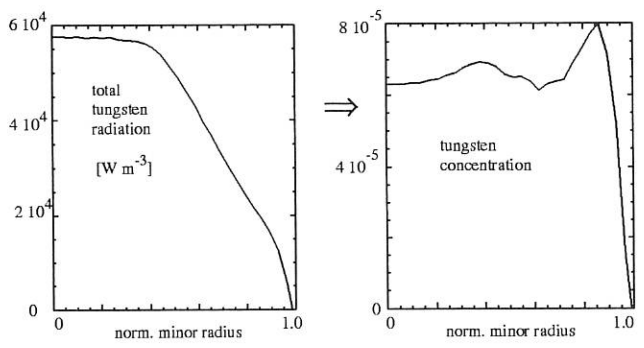

FIG. 3.2: Bolometer radiation profile (background subtracted) and extracted W concentration for discharge # 4542 80 ms after injection.

In some discharges accumulation of tungsten could be observed. Here the bolometer and SXR profiles show a marked radiation maximum in the centre and a very long decay time (up to 500 ms). For these discharges the good spatial and temporal resolution of the SXR diagnostic allows identification of the rotating islands of a strong m = 1, n = 1 mode (Fig. 3.3) with a rotation frequency of about 10 kHz and spatial extension of a few centimetres in radial direction.

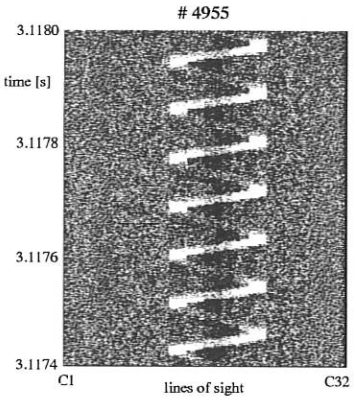

FIG. 3.3: "Snake-like" soft X-radiation in discharge # 4955. Tungsten laser blow-off occurred at 3.00 s.

3.4.1 Impurity confinement with ICRF

It was also observed on ASDEX Upgrade that metal impurities injected by laser blow-off disappear more quicky from the centre when ICRF is added on top of NI, as compared with similar discharges without NI. This extends work of TEXTOR where the impurity content of the plasma, using a W limiter, was smaller with ICRF than without ICRF. Two possible explantations could not be distinguished there: either less impurities would come into the plasma because of the changes at the edge due to the ICRF or the confinement time of the impurities was reduced because of the ICRF. The experiments on ASDEX Upgrade now tend to indicate that the confinement of the impurities is reduced.

3.5 ICRF Power Modulation Experiments

Modulation of the external heating power is an experimental technique to study dynamic plasma behaviour. One objective is to measure the power deposition profile and the absorption efficiency. Another aspect is that the time delay in the heat conduction allows to extract local heat conduction coefficients. Furthermore, the dynamic response may be qualitatively different from the stationary plasma and may thus give additional clues to anomalous transport.

A series of discharges (B = -2 T, I_p = 0.8 MA) was conducted where ≥1 MW heating power was switched on and off with a frequency of 18 and 38 Hz. The heating scenario was minority heating on ≈15 % H in D. The pulse train was 1 s in duration. The switching of the generators caused no problems (up to 3 generators were synchronously switched). Relevant diagnostics were electron cyclotron emission radiation (ECE), Thomson scattering of laser light with a YAG laser, the detection of charge exchange results of H and D and neutrons. The time signals were Fourier analyzed. From ECE and YAG, radial profiles of the spectral components were extracted. That spectral component of the temperature signal $T_\omega^e(r)$, with the fundamental frequency ω of the modulation and which lags $-\pi/2$ behind the imposed power gives an upper limit of the width of the deposition profile, $P^{lim}(r) = (3/2) \cdot n(r) \cdot \omega \cdot T_\omega^e(r)$. Due to heat transport the true deposition profile is narrower. Since the determination of the heat conductivity in the instationary case has sufficient incertainties we present here P^{lim}, see Fig. 3.4. We conclude that the half width of the deposition profile is ≤ 0.2 · a. The absorption efficiency is approximately $\alpha = (\tilde{P}_{Plasma}/\tilde{P}_{Gen}) = (\tilde{W}/\tilde{P}_{Gen}) \cdot \sqrt{1/\tau_E^2 + \omega^2}$. The oscillating part of the plasma energy $\tilde{W}$ was taken from the equilibrium reconstruction (W_{MHD}). We found α = 95 ± 5 %. The amplitude of $\tilde{W}$ was about 5 kJ in comparison to 120 kJ average plasma energy.

From ECE measurements in the outer third of the plasma column, well outside the deposition region, the electron heat conductivity was calculated. We found a value of $\chi_e^{dynamic}$ = 10 m²/s.

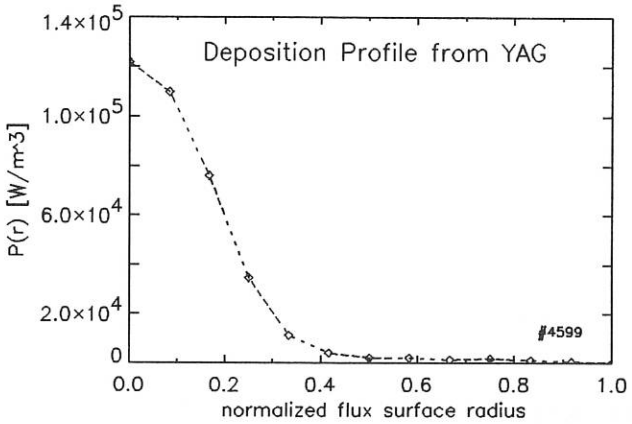

FIG. 3.4: Upper limit P^{lim} of the width of the ICRH power deposition profile derived from the temperature measurement of the YAG diagnostic.

3.6 Disruption Phase Investigation

The investigation of the disruption phase on ASDEX Upgrade consists of several activities: development and use of fast diagnostics to measure the thermal and mechanical loads on the vessel internal components, study of disruption dynamics and modelling, development of strategies for the mitigation of the disruptions impact on the machine.

In 1994 a fast bolometer system and a fast ECE diagnostic allowed us to record in detail the time histories of the power radiated during the whole disruption duration and the plasma energy loss during the thermal quench.

The time history of the radiated power, recorded with 1 ms time resolution, is shown in Fig. 3.5. It shows two phases of intense radiation. The first phase, which lasts typically 5 ms, starts with the voltage spike and the thermal quench. The second phase coincides with the phase of fastest current decay, stronger interaction between plasma and divertors and higher halo currents. During the first phase, the radiation is relatively in-out symmetric and chords intersecting the divertor plates show higher radiation. During the second phase, the radiation profile is clearly in-out asymmetric, the asymmetry depending on the direction of B: with B > 0 T (i.e. ion ∇ B drift away from the X-point) the outer part of the plasma radiates more, and vice versa when B < 0 T. This is consistent with the presence of electric arcs on the divertor tiles (cause of impurity influx) which are observed on the ion-target side, that is the outer (inner) divertor for B > 0 T (B < 0 T). We find that the energy radiated in the first phase is consistent with a change of magnetic energy due to current flattening and a final value of $l_i \simeq 0.5$.

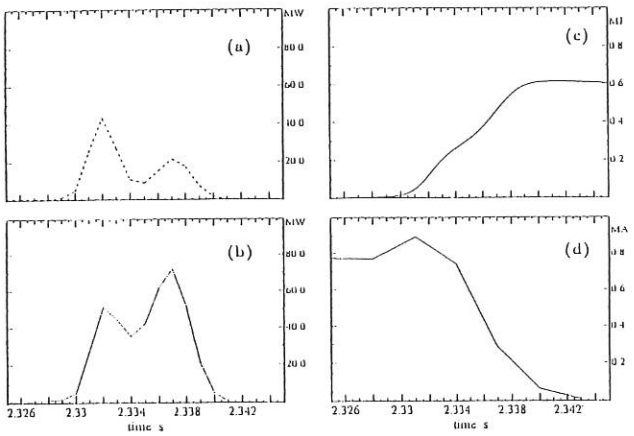

FIG. 3.5: Time histories of radiated power from the outer (a) and inner (b) divertor and plasma region, of the radiated energy (c) and plsama current (d) during disruption.

For the ten shots analyzed in detail, the total radiated energy amounts typically to 50 % of the total plasma energy before disruption; the energy deposited onto the divertor amounts to 30 % of the pre-disruption plasma magnetic energy. The remaining 20 % can be attributed mostly to the magnetic energy dissipated (as induced mirror and eddy currents) in the machine structures.

Measurements of electron temperature in the plasma bulk during the thermal quench of low q disruptions and of density limit disruptions showed that the plasma loses its thermal energy in two steps. In the first step the temperature drops to 50-200 eV, remains about this value for typically 0.5 ms and then drops to values below the diagnostic sensitivity threshold (a few eV). The second temperature drop is also accompanied by the appearance of the voltage spike and by enhanced particle flux to the divertor plates. The whole thermal quench duration is of the order of 1 ms. The two-phase evolution of the thermal quench has hitherto been observed on few other machines; its duration is strongly machine-dependent. Exploratory simulations were started to reproduce the time-scale of the quench in terms of enhanced energy diffusion coefficients.

Compilation of the Disruption Database is in progress. It already contains information on the rate of current decay, and the magnitudes of forces and halo currents during disruption for approximately 1.000 shots. Figure 3.6 shows the maximum and minimum vertical forces on the vessel support during flat-top disruptions and their parabolic dependence on plasma current, as expected from theoretical considerations. In the coming year the database will contain a collection of parameters allowing a complete analysis of the parametric dependence of the thermal and mechanical effects of disruptions on the machine.

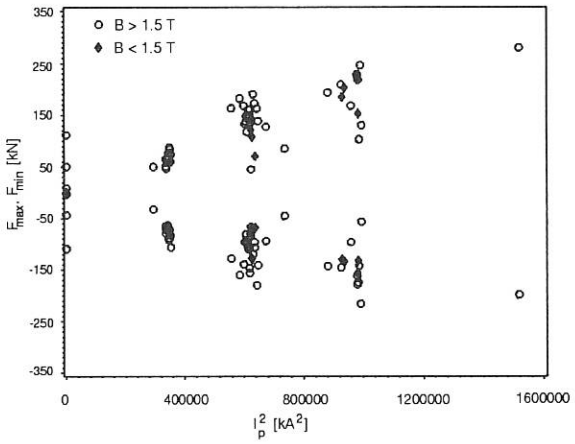

FIG. 3.6: Maximum (>0) and minimum (<0) vertical forces at the vessel supports during current quench (shot range: 4000 - 5000).

Among the strategies aimed at protecting the divertor plates in case of unavoidable disruptions, injection of impurity pellets has been considered. Such impurities, injected in a plasma which is going to disrupt, should radiate most of the plasma thermal energy, preventing the high heat load onto plates typical of the thermal quench. Studies done with simple plasma models show that krypton is a favourable candidate because of its high radiating power at high temperatures. For an AUG plasma with a typical central temperature of 2000 eV, a krypton pellet 1 mm in diameter would cool down the plasma to approx. 100 eV in a few ms.

3.7 MHD Equilibrium Identification

A new version (version 2) of FP was implemented. The database for this version 2 is based on 8.000 equilibria and contains the OH current and separate currents in the upper and lower arms of the passive stabilizer. In addition, the class of plasma current profiles used for equilibrium generation was extended to a family having 7 free parameters.

For the new FP algorithms 36 magnetic measurements are used. The number of principal components (PCs) is increased to 16 for FPC, FPG, FPP. (The online version in R2 is still operating with 12 PCs, but an upgrade to 16 PCs is planned.)

The generalization of the current family made it obvious that the regression of the poloidal flux function (FPP) in the core of the plasma (inside the 50 % surface) is not reliable. The shape

of the flux surfaces is recoverable, however, and it is hoped that the use of the volume as a flux surface label instead of the poloidal flux will allow the accurate determination of the topology of the inner flux surfaces.

To determine the current profile (or, equivalently, q(ψ)), the incorporation of additional non-magnetic diagnostic measurements into FP is essential. A promising candidate appears to be the location of the q = 1 surface from the observation of rotating (m = 1, n = 1) modes by soft X-ray pinhole cameras. A sensitivity study to quantify the benefit of this information for the recovery of the q profile is under way.

4. EDGE AND DIVERTOR PHYSICS

4.1 Hydrogene Plasma Properties

4.1.1 T_E from ECE heterodyne radiometer

As of May 1994, a 16-channel heterodyne radiometer has been used to measure electron cyclotron resonance (ECE) emission from the plasma edge of ASDEX Upgrade near the midplane (z = +4.5 cm). The system is calibrated to evaluate absolute electron temperatures from the second harmonic of extraordinary mode emission, which is optically thick inside the separatrix under most operating conditions of ASDEX Upgrade.

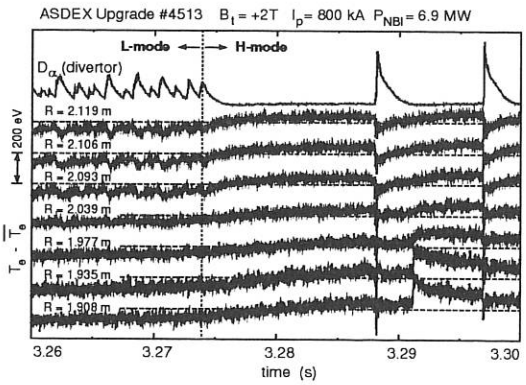

FIG. 4.1: ECE heterodyne radiometer traces (measured near midplane) and D_α radiation from the divertor during a L → H transition and subsequent H-mode phase. T_e traces are plotted with zeros suppressed.

Figure 4.1 shows traces of the ECE heterodyne radiometer system measured during the L→H transition in a NBI-heated ASDEX Upgrade discharge in single-null configuration with unfavourable magnetic field direction (ion grad B drift away from the X point). A spatial channel width of 6 mm and a time resolution of 16 μs are employed. The L→H transition is recognized in the ECE signals by an increase of T_e and a steepening of the edge T_e profile setting in shortly before the drop of the D_α signal. For the selected magnetic field direction, no "dithering cycles" (i.e. repeated L→ H → L transitions) occur.

During the L-mode, the particle flux as shown by the D_α signal fluctuates. These fluctuations are correlated to electron temperature variations at R > 2.093 m, i.e. in a region extending from the separatrix to ≈4 cm inside the main plasma.

After a short quiescent H phase (duration 14 ms) type-I ELM activity begins. The particle outflux during each ELM is accompanied by a reduction of T_e in a radial range of 15 cm. T_e recovers until the following ELM occurs. During the ELM proper, the local electron density at the edge fluctuates with peak densities exceeding the critical density (n_e^{crit} = 7.5 × 10^{19} m^{-3}) for cyclotron wave cut-off ($\omega_{uh} > 2\omega_c$). These density fluctuations are consequently detected by a loss of the ECE signal as the cyclotron radiation is reflected back into the plasma whenever a cut-off layer forms. In between the two ELMs, the ECE traces show the outgoing heat wave induced by a sawtooth crash.

The influence of the L→H transition and ELM's on local energy confinement has been discussed only qualitatively so far. The ECE radiometer, however, provides quantitative diagnostics of T_e. Relevant time-dependent transport parameters (heat transport coefficients, drift velocity) have yet to be evaluated from these measurements.

4.1.2 n_e from Lithium Beam

The lithium beam diagnostic system for measuring midplane electron densities (Li-IXS) in the scrape-off layer of ASDEX Upgrade started operation in summer 1994. Electron density profiles were reconstructed from measured Li(2p-2s) emission profiles in a radial range of -4 to +10 cm relative to the separatrix position R_{sep} with spatial and time resolutions of 0.6 cm and 200 μs, respectively. (Li-IXS) has proven to deliver accurate plasma edge densities and thus contributes to the understanding of dynamic effects in the plasma edge, such as L-H transition and ELMs.

Typical e-folding lengths λ of the density profiles in the vicinity of the separatrix of 4.0 - 5.5 cm and 2.1 - 2.8 cm were determined for OH and H-mode discharges, respectively. Density profiles of the CDH mode show not as steep gradients as corresponding ones of an ordninary H-mode. In addition, significantly higher densities arise in the outermost radial range during a CDH-mode.

Studies on type-I ELMs showed an increase in the electron density by a factor of 4 - 6 in the outermost radial range accompanied by a dramatic increase of the e-folding length and a decrease of the separatrix density during an ELM. Between type-I ELMs a continual slow increase of the separatrix density was observed. However, in the case of CDH ELMs much smaller changes of the density profile in comparison with type-I ELMs were detected. A method which allows density profiles on flux surfaces to be determined from the measured DCN line densities, was improved by including Li-IXS plasma edge data in the unfolding algorithm in order to obtain more reliable density profiles within the complete radial range. This demonstrated peaking of central CDH mode densitiy profiles.

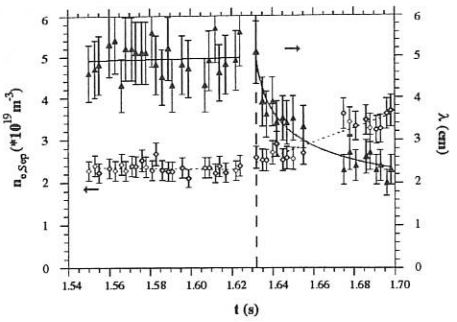

FIG. 4.2: Electron density on the separatrix $n_{e,Sep}$ and e-folding length λ for discharge #4878 during L-H transition. The vertical line indicates the time where the H_α signal starts to decrease.

4.1.3 T_i from low energy neutral spectra

The LENA (Low–Energy Neutral Particle Analyzer) started operation at ASDEX Upgrade in April 1994. It is a time-of-flight spectrometer for measuring the velocity disribution of neutral particles. For deuterium it covers the energy range from 30 eV to 1000 eV. The active period during a shot is 4.5 s with a time resolution of 150 μs. Since counts are very few, averaging over 50 ms up to 500 ms is necessary, depending on the neutral gas pressure and desired statistical relevance. The apparatus is essentially the same as that operated at W7–AS (cit.). Additional software for the separation of H and D contributions to the spectra was developed, but the interpretation for cases with roughly equal amounts has still to be improved. The high intrinsic time resolution of 1 μs (when the slit of the spectrometer is open) can be used to analyze ELMs occurring with high frequency. Assuming stationary conditions during a given time interval, the ELMs can be projected onto each other, thereby compressing all the information on an interval with the length of the ELM period. By such a procedure a time resolution of 100 μs can be achieved with LENA (see Fig. 4.3).

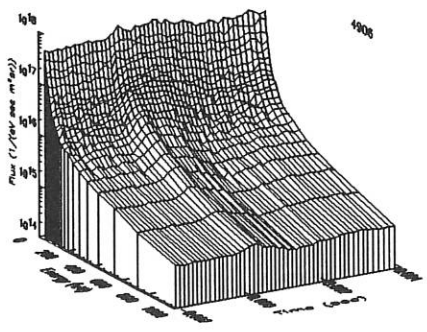

FIG. 4.3: Energy distribution of deuterium fluxes (#4906, ≈4 sec), type-I ELM, time relative to D_α raise.

The data contain information on the ion temperature profile at the plasma edge, which can be extracted with a complex code developed for ASDEX and W7-AS (cit.). This code is based on the EIRENE neutral particle code developed at KFA-Jülich and was adapted for the geometry and data acquisition at ASDEX Upgrade. As far as sufficiently accurate profiles of electron temperature and density are available, ion temperature profiles can be calculated, which is still time-consuming. Therefore, a fast procedure using a database was installed, which proved useful for the ASDEX data (cit.). The Upgrade database is not yet large enough, but will grow with the increasing number of calculated ion temperature profiles.

4.1.4 Electric Fields during L-to-H Transition and ELMs

The flux of neutral particles from charge exchange with ripple-trapped slowing-down ions is quite different during the different modes of the plasma ($L, H, H^\star$) and drastically changes during ELMs. This can be explained by the assumption of radial electric fields. Calculations show that the ripple loss of deuterons can be stopped if radial fields are larger than about 12 kV/m per 10 keV energy of the deuteron. There is no indication of a jump in the electric field larger than 10 kV/m at the L-to- H transition for negative B_t. There is a sudden (ms timescale) increase after the H-to-$H^\star$ transition. For $B_t > 0$, when type–III ELMs are absent, the jump occurs at the L-to-$H^\star$ transition. The electric field seems to build up with increasing plasma energy to 30 and more kV/m. During type–I ELMs the field disappears on a 100 μs scale and builds up again on a ms scale. The measurements suggest that the electric fields during ELMs fall back to L-mode level.

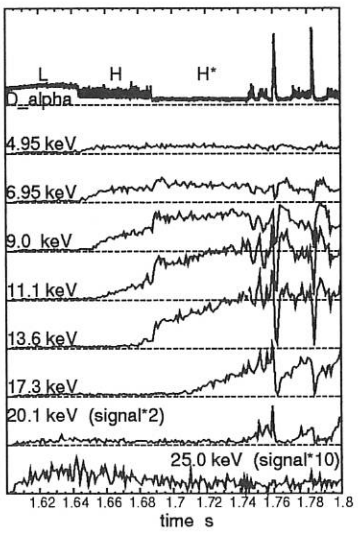

FIG. 4.4: D_α and neutral fluxes for eight energies during $L, H, H^\star$ mode and type–I ELMs. The fluxes increase slowly after L-to-H transition, the later the higher the energy is. A few energies show the jump at the H-to-$H^\star$ transition. Also after type-I ELMs the electric field builds up slowly.

4.1.5 Divertor detachment

During 1994 numerous studies were performed in conjunction with a number of divertor diagnostics, including the Boundary Layer and Divertor Spectrometers, the In-Vessel and Plate

Langmuir probes and the Plate Infrared Thermography System. The results of one such study with the In-Vessel Probes (IVP) and the Thermography System (IR) appear in Fig. 4.5 for the outer divertor. These results compare the divertor conditions at two values of line-average density under high power neutral beam heating (7.5 MW) between ELMs with a plasma current of 1 MA and a magnetic field of 2.1 T with the grad-B drift towards the X-Point. The two densities used in this comparison, ie $\bar{n}_e$ = 7.5 × 10^{19} m^{-3} and $\bar{n}_e$ = 1.0 × 10^{20} m^{-3}, correspond to 'attached' and 'detached' conditions, respectively.

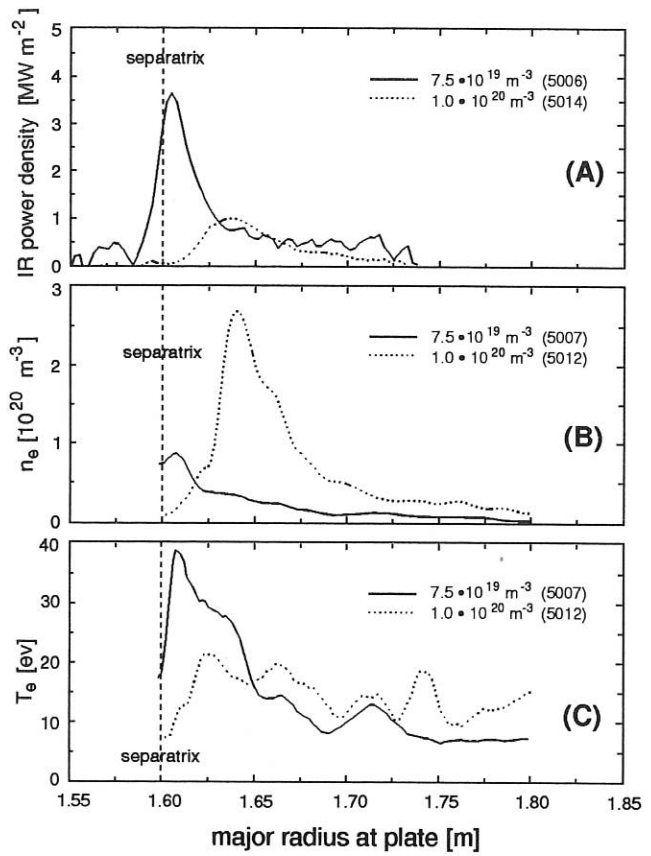

FIG. 4.5: Conditions at the outer divertor plate for attached ($\bar{n}_e$ = 7.5 × 10^{19} m^{-3}) and partially detached conditions ($\bar{n}_e$ = 10^{20} m^{-3}). (A) Infrared power density on the plate, (B) electron density above the plate as measured by the IVP, (C) electron temperature.

The deposited power density as determined by the Thermography System is very peaked in the vicinity of the separatrix in the 'attached' discharge. This contrasts with the situation in the 'detached' discharge, where the power density near the original separatrix peak is virtually eliminated, with the power now peaking some distance, ~ 5 cm, away from the separatrix.

Qualitatively similarly behaviour is found for the plasma density and temperature, ie the profiles shift outward. The peak density as measured by the IVP increases strongly, by approximately a factor of ~ 3 to a value of 3 × 10^{20} m^{-3}, nearly three times the line-average density, although the density on the separatrix drops by a large factor during detachment. The electron temperature in the vicinity of the separatrix drops from approximately 40 eV in the attached discharge to ~ 10 eV in the detached discharge.

From these findings, it thus appears that detachment occurs only in the immediate vicinity of the separatrix, since further out in the scrape-off layer the power, density and temperature stay the same or actually increase. This is a fortuitous situation, in that the region of intense power flux near the separatrix disappears during detachment, yet recycling still occurs further out in the scrape-off layer. Both features are desirable from the point of view of a reactor; the first since the heat removal becomes easier and the second since it facilitates helium removal from the system.

4.1.6 *Sheath transmission factor*

Power density profiles measured thermographically can be compared with the energy flux to the target calculated from the ion saturation current j_{sat} and electron energy kT_e, as measured by Langmuir triple probes: $P_{target} = \gamma kT_e \frac{j^{ion}_{sat}}{e}$, whereas the sheath transmission factor γ reflects the contribution of ions and secondary electrons to the power deposition. Consequently, the ratio of thermographically measured power density to the product $kT_e \frac{j^{ion}_{sat}}{e}$ from the probes represents the sheath transmission factor γ.

The sheath transmission factor calculated by combining thermography and Langmuir probe profiles across the outer target plate measured between type-I ELMs (I_p = 1.2 MA, B_t = 2 T, P_{NBI} = 5.5 MW, n_e = 1.1 × 10^{20} m^{-3}) (Fig. 4.6) varies, but no pronounced change is observed near the separatrix. The contribution of the ionization energy, the energy reflection at the target plates and the energy deposition due to neutrals influence the absolute value of γ. A more detailed calculation will be made in 1995.

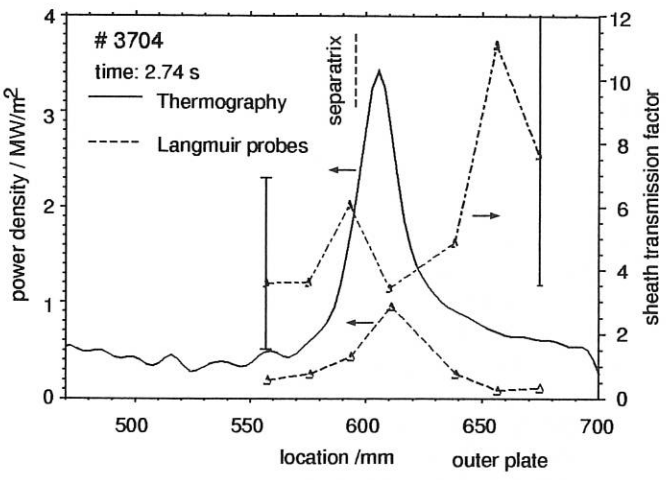

FIG. 4.6: Power density profile and electron energy flux to the target calculated from data of Langmuir triple probes (# 3704; between ELMs) and the corresponding sheath transmission factor.

4.1.7 Return currents from Langmuir probes

If current could not flow across the magnetic field, a Langmuir probe in the SOL would exhibit the I-V characteristic of a symmetric double probe. Measurements on ASDEX Upgrade and other machines, however, show electron saturation currents several times higher than the ion saturation current. This indicates that currents do flow across the field, raising the question of what force balances jXB. The forces acting on the plasma in the SOL are interesting for a number of reasons, not the least of which is to improve confidence in Langmuir probe measurements.

To approach this question experimentally, measurements were made of the 3-D pattern of the return current from a Langmuir probe. With one electrode being actively driven, the other electrodes in the same or an opposing 3X10 array in the divertor plates were grounded to measure the return current density. By averaging the signal over several periods of the driving voltage, the sensitivity could be improved to about 2 % of the driving current. It was discovered that only a small fraction of the current reached the opposing divertor plate, and essentially all of it returned to the surrounding divertor plate within about 3 mm measured perpendicular to the field. This is consistent with the interpretation of the observed value of the electron saturation current as being due to the ion saturation current limit on a virtual double probe. The small value of current at the opposing plate puts a lower limit on the force which opposes the rotation of the plasma column around the potential perturbation. Further experimental and theoretical investigations are planned to clarify the nature of this force.

4.1.8 Langmuir characteristics in the ion cyclotron frequency range

Six Langmuir probes were flush mounted in the ASDEX Upgrade lower outer divertor and specially equipped to allow 200 MHz bandwidth measurements with two probes simultaneously. They are being used to study the diagnostic possibilities of probes in the ion cyclotron frequency range. The hardware setup is described in the Technology Division chapter of this annual report.

As predicted by numerical simulation with Chodura's Particle-in-Cell code, a capacitive component of the Langmuir current has been measured on the ion saturation side of the characteristic. At 100 kHz, the associated capacitance value lies in the range of a few nF. It decreases with frequency, such that the Langmuir current hysteresis loops saturate at a few MHz. The hypothesis, that it is determined by the non-linear ion magnetic sheath capacitance, is being investigated. The confirmation of this model demands experimental evidence for the proportionality of this sheath capacitance with the (square root) of the ion temperature, which would be attractive from the point of view of developing a new diagnostic.

Other new aspects of Langmuir probe physics at frequencies from 10 kHz to 20 MHz, have also been studied. Below 1 MHz, one can observe hysteresis loops on the electron saturation side, which may suggest polarization current into the probe's flux tube, and thus contain information on the length of the current path along the magnetic field. The loops on the electron side disappear above 1 MHz. There is further evidence for the rise of the electron to ion saturation current ratio with frequency, which may shed light on the mechanisms which limit the perpendicular flow of electron current.

4.1.9 ELM simulation and model validation

The effects of ELMs (Edge Localized Modes) on ASDEX Upgrade plasmas have been simulated using B2-EIRENE (a 2D plasma fluid code coupled to a time dependent Monte Carlo neutrals code). Perpendicular transport coefficients in the edge region were increased for the duration of the ELM event, and experimental measurements were then compared to the equivalent simulated signals. Good agreement was obtained in comparing the power fluxes to the divertor plates with the measurements (see Fig. 4.7) and with Langmuir probe measurements in the target plates, as well as in comparison with the divertor H_α measurements, and ECE and reflectometry measurements in the midplane. In addition, when the ELM modelling results were analyzed using an ICRH coupling code, good agreement was obtained with the measured antenna resistance.

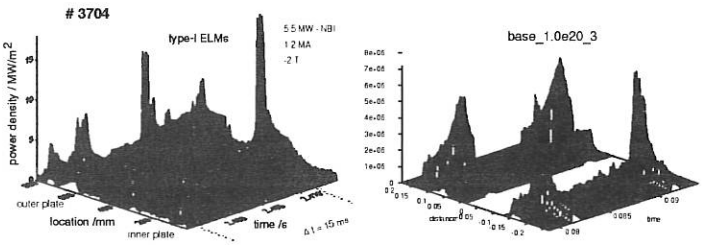

FIG. 4.7: Total power loading to the divertor plates, respectively, experimentally measured and predicted from the code.

4.2 Impurity Erosion and Transport

4.2.1 Erosion of different divertor materials

Erosion studies were continued on the divertor plates of ASDEX Upgrade, using evaporated marker layers on the graphite tiles. The erosion per discharge was evaluated from the decrease in marker thickness after entire discharge periods of several hundred discharges. Marker materials employed were Si, V, Mo and W. The markers were deposited along a radial line across the outer lower divertor plate and the resulting erosion clearly showed the variation with the divertor plasma parameters, the largest erosion being located at the separatrix position. Maximum erosion rates varied from 10 A/discharge for Si to 1 A/discharge for W. These values are in good agreement with computer simulations (ERO code) calculating the sputtering due to plasma and impurity ion bombardment for the actual plasma parameters as measured by Langmuir probes (Fig. 4.8). The values are also well comparable to recently published erosion rates for DIII-D, viz. 15 A/s for carbon and 0.5 A/s for W.

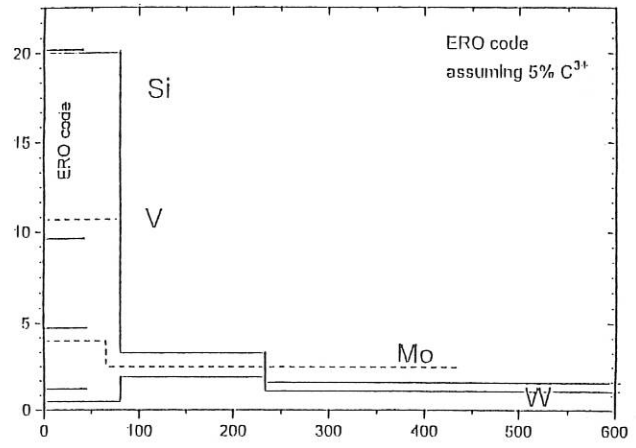

FIG. 4.8: Dependence of the erosion yield for Si V, Mo and W on the number of discharges. FRO code calculations assuming 5 % C^{3+} are shown for comparison.

Besides the decrease in layer thickness, the ion beam analysis showed increasing contamination of the marker layers with carbon atoms. After analysis the same marker tiles were installed for another discharge period. Figure 4.8 shows the decrease of the erosion rate as the layers are increasingly intermixed with carbon atoms deposited from the divertor plasma. This underlines the finding that erosion rates are critically dependent on impurity concentrations in the plasma, changing from net erosion for low carbon concentration to net deposition for carbon concentrations larger than about 5 %.

4.2.2 Chemical erosion of carbon

The investigation of the role of gaseous molecular impurities produced by chemical surface reactions, already started 1993 in collaboration with the PWW group, was continued. Results so far obtained were reported in an invited paper presented at the PSI in Mito, Japan, This task mainly focussed on hydrogenic chemical erosion of carbon via production of hydrocarbons. Mass spectrometric data obtained on the divertor were complemented by results from three optical spectrometers, two observing the divertor region and one scanning the inner heat shield. Hydrocarbon influxes were essentially deduced from the brightness of CH and CD bands based on the S/XB values as given by Behringer, and correlated with the resulting carbon fluxes. Central plasma concentrations of C, as well as O, were routinely measured with the ASDEX Upgrade C+O monitor. The impact of chemical erosion, in a qualitative though very obvious manner, showed up in the flux profiles seen by the divertor spectrometers, which, in contrast to those obtained in He discharges, could not be explained by physical sputtering alone. Moreover, together with the measured outflux of hydrogen and deuterium, erosion yields of typically 4 % were obtained from optical and mass spectrometric data.

In a more detailed study, correlating C and O fluxes originating from the inboard graphite heat shield in a numnber of ohmic discharges, the coherence between the measured carbon and oxygen concentrations and C^{2+} influxes was investigated. Variations in plasma density and wall conditions allowed different production channels to be separated. With aged and now only weakly effective boronization, oxygen recycling via CO not only is responsible for the central oxygen concentration, but also significantly contributed to the central carbon concentration. The concentration ratio of the two can be used to subtract that fraction of the C^{2+} influx attributable to CO recycling. The remaining part of the measured C^{2+} flux exhibits a closely linear relationship to the hydrogen wall flux with an effective yield $\Gamma_{C2+}/\Gamma_D \approx 0.45$ (see Fig. 4.9), which is compatible with the yield Γ_{CD}/Γ_D = 0.2–0.5 obtained from molecular spectroscopy of CD band emission. These results not only support the assumption that chemical erosion via hydrocarbon formation is in fact the origin of the part of C^{2+} flux not due to CO recycling, but also they leave little room for any significant contribution from physical sputtering. Chemical erosion by a high hydrogen flux at low energy seems to dominate here.

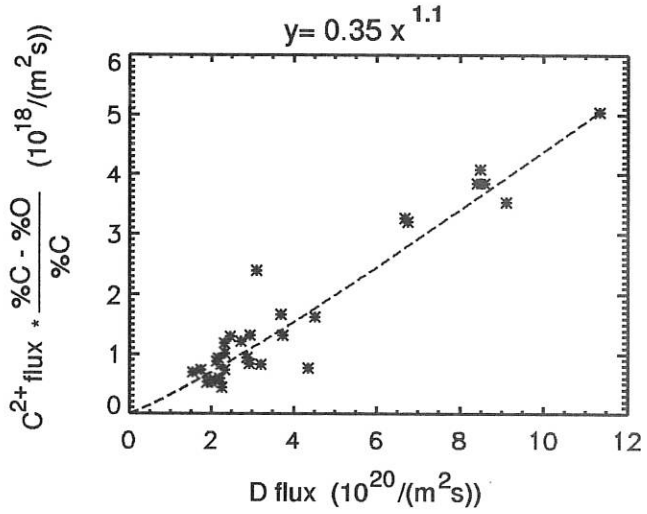

FIG. 4.9: Measured midplane carbon flux, reduced by the fraction owing to CO recycling, versus D_0 flux.

Such findings are in some conflict with past literature, where the problem of hydrogenic chemical erosion in fusion experiments in gross has been discussed away. Discrepancies concerning proper appreciation of the phenomenon arose mostly from the interpretation of spectroscopically observed C^+ fluxes near carbon limiters, which is seriously hampered by an obviously very high shielding action of the SOL for thermal hydrocarbon influx. While the resulting C^{2+} influxes are certainly more relevant concerning plasma purity, the erosion via the underlying hydrocarbon fluxes constitutes a serious problem in itself. Even in the case of strong redeposition of carbon, codedeposition of tritium can lead to unacceptably high inventories. The possible impact on Z_{eff} dilution, transport in SOL and final redeposition, also in extrapolation to ITER, requires further investigation.

4.2.3 Impurity transport studies with DIVIMP

The DIVIMP two-dimensional Monte Carlo impurity transport code is used as an interpretative tool for investigating impurity generation and transport processes in the ASDEX Upgrade di-

vertor and scrape-off layer. The code was installed and adapted for ASDEX Upgrade in collaboration with the University of Toronto. First studies were made to investigate the basic processes leading to the carbon contamination of the ASDEX Upgrade plasma. Analysis of spectroscopic measurements by DIVIMP simulations showed that carbon production by physical sputtering is not sufficient to explain the observed signals. A postulated further source of low-energy carbon atoms leads to more satisfactory results. This supports chemical erosion processes as an additional source of carbon in deuterium discharges.

A new version of the code was implemented in autumn 1994. A support code was developed to prepare data from the in-vessel Langmuir probe system for use in the edge plasma modelling part of the code. Work was started to establish a coupling scheme to the EIRENE neutral gas Monte Carlo code which will improve the modelling of the background plasma with respect to neutral ionization sources.

4.2.4 *Impurity transport during ELMs*

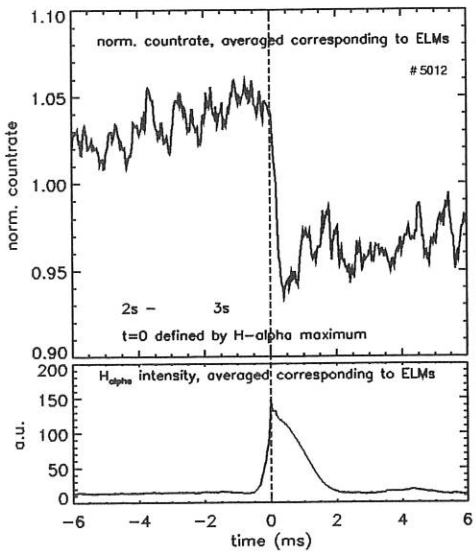

FIG. 4.10: The effect of an ELM on the emissivity of F IX Lyman$_\alpha$. The scatter before and after the ELM is within the statistical error bars. Bottom: averaged H_α signal.

The temporal evolution of impurity radiation during ELMs was measured by a fast Bragg spectrometer. The signal-to-noise ratio was increased by averaging over many ELMs with a fast H_α signal as temporal reference. As seen in Fig. 4.10 the result is a 5 - 15 % decrease of emissivity during ELMs within a period of 0.2 - 0.3 ms and a constant increase in between the ELMs. Modelling of impurity radiation in the ELMy H-mode was performed with the ZEDIFF 1-D transport code. Measured n_e and T_e profiles were used as input parameters. Calculations with two different ansatzes were discussed critically, the first assuming an outward drift velocity at the plasma edge during the ELM time period, the other applying a much higher value of the diffusion coefficient during the ELM. The consequence of the latter is an immediate increase of emissivity followed by a later decrease. The former assumption of a strong outward drift during the ELM better represents the measured behaviour.

4.3 H-mode Discharges with feedback controlled radiative boundary

4.3.1 *Main characteristics*

Radiative boundary discharges with high-power neutral beam injection were investigated, mainly neon being used as radiating species. Such scenarios are now being discussed as a tool to reduce the power flow onto the target plates required for future reactors. The total radiated power P_{rad}^{tot} could be increased to over 90 % of the total heating power, while the usual radiation level due to the intrinsic impurities is ≈50 % . The increase of P_{rad}^{tot} had the same effect on the H-mode behaviour as a decrease of heating power. In contrast to the strong X-point peaking of the intrinsic impurity radiation, the emission profile due to neon develops a more uniform layer around the boundary region of the plasma (see Fig. 4.11).

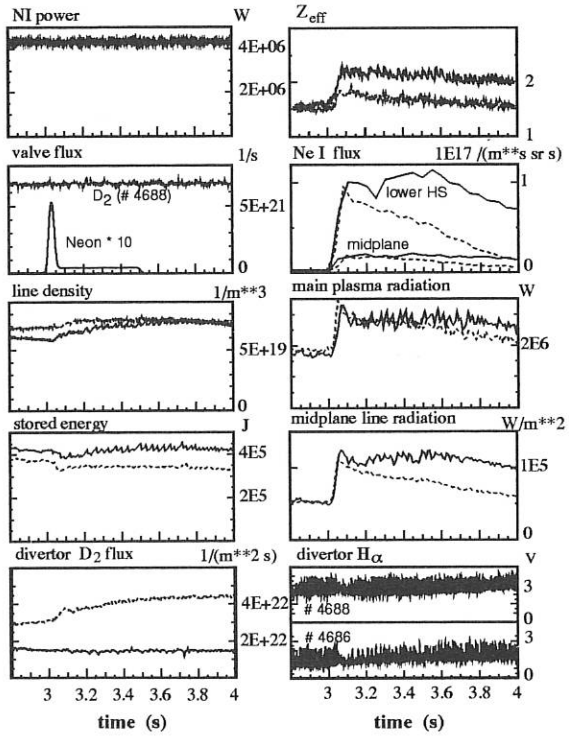

FIG. 4.11: Comparison of discharges with preprogrammed neon injection with (#4688, dotted lines) and without (#4686, solid lines) additional D_2 puffing and otherwise identical external parameters. Shown are the neutral beam power, gas valve fluxes, line-averaged electron density from DCN interferometry, total stored energy from magnetic equilibrium, divertor D_2 flux measured by the fast ionization gauge, line-averaged Z_{eff} derived from bremsstrahlung measurements, NeI photon fluxes in the midplane and lower divertor region, total main plasma radiation and line-averaged midplane radiation and H_α emission from the outer divertor. I_p = 0.8 MA.

Deuterium puffing in the main plasma strongly influences the behaviour of radiative boundary discharges. Figure 4.11 shows a comparison of two discharges with and without additional D_2 puffing and otherwise identical external parameters. The experimental parameter which is most affected by the deuterium puff is the neutral D_2 flux in the divertor. It increases almost offset-linearly with the magnitude of the applied gas puff. The decay rates of the neon recycling flux, radiation and Z_{eff} are faster by a factor of more than 3 for the discharge with the higher divertor neutral flux density Γ_{D_2}, and the increase of Z_{eff} is much smaller for the discharge with higher Γ_{D_2}, despite the fact that the injected amount of neon is the same. However, the power radiated by neon is the same in both cases, indicating that it is related to the neon influx rather than the neon content. The additional radiated power per unit Z_{eff} increase, a quantity which may be thought of as the radiation capability, shows an almost linear increase with the D_2 puff rate. This behaviour can be attributed to the higher electron density / lower temperature conditions at the plasma edge leading to improved impurity screening and stronger line radiation of the lower ionization stages. Accompanying these beneficial effects is a slight reduction in the energy confinement time with D_2 puffing.

4.3.2 Pumping and particle balance

A prerequiste for feedback control of a radiative plasma mantle is the ability to pump the injected species. The pumping behaviour can be described with a chamber model of the particle balance. In this model the particle fluxes between the scrape-off layer and divertor are treated by the simplified ansatz of empirical losses. Particles entering the SOL are lost to the divertor with a decay time $\tau_{SOL \rightarrow div}$. Particles in the divertor either escape to the main chamber with the time constant $\tau_{div \rightarrow SOL}$ or are pumped out within the pumping time τ_{pump}. The pumping time and pumping speed are connected via the pumped divertor volume $V^{div} = S \cdot \tau_{pump}$. The pumping speed S of the 14 turbomolecular pumps situated near the outer divertor was obtained from *in situ* calibration in the case of D_2. From the deuterium value S_{Ne} = 6.9 m^3/s can be calculated from the atomic mass ratio in the limiting case of molecular flow. With increasing gas density the pumping speed was estimated to increase somewhat more strongly than the deuterium value owing to the onset of laminar flow. At the highest divertor densities S_{Ne}= 11 m^3/s is used.

With complete recycling at the wall being assumed, the effective particle confinement time τ_p^* only depends on the pumping time and the relative populations in the main plasma volume N^{main} and divertor volume N^{div}:

$$\tau_p^* = \frac{V^{div}}{S} \cdot \left(1 + \frac{N^{main}}{N^{div}}\right)$$

Measurements of the 1/e-decay time $\tau^{1/e}$ of the recycling flux after the injection phase give a reasonable estimate of τ_p^* and allow one to determine the partition of neon between the main and divertor volumes from Eq. (1). With the volume V^{main} known the compression factor $C = n^{0,div}/n^{ion,main}$ (ratio of divertor neutral density and bulk plasma ion density) can be determined. Thus, the analysis of the decay time of the recycling flux as shown in 4.11 yields information about the effective particle confinement time τ_p^* and the neon compression C.

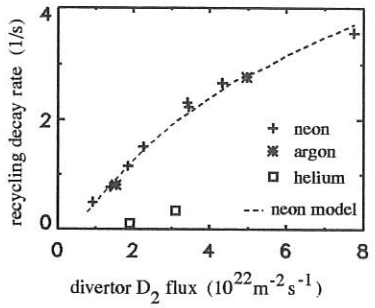

FIG. 4.12: Recycling 1/e-decay rates (inverse effective particle confinement times) from several discharges after Ne or Ar puffing versus divertor D_2 flux. The dashed line shows the prediction of the chamber model for neon for the offset-linear increase of the neon pumping speed and the assumption of a quadratic lengthening of divertor retention with $\Gamma_{D_2}^{div} \cdot P_{heat}$ = 4-6 MW, ion ∇B drift towards the X-point.

The variation of a number of experimental parameters revealed that the divertor neutral D_2 flux is the leading parameter to determine the exhaust rate (atoms/s) of neon in deuterium plasmas. Figure 4.12 shows recycling decay rates $1/\tau^{1/e}$ for neon and argon versus the divertor D_2 flux. The exhaust rate increases with the divertor D_2 flux but the slope decreases with higher values of the D_2 flux when the majority of neon atoms is already situated in the divertor volume. Not much difference is seen in the decay rates of neon and argon, but helium shows a strongly reduced decay rate. The large variation of the effective particle confinement time by a factor of 7 shown in Fig. 4.12 cannot be explained by the increase of the pumping speed, which changes by a factor of 1.5 to 2 at most. It is mainly determined by the large variation of the impurity distribution between the main plasma and the divertor volume (second factor in Eq. (1)). With a further simplified chamber model that handles the transport between the core and SOL volume in the same manner as has previously been explained for the transport to and from the divertor the measured 1/e-times and the connected change of the divertor population can readily be understood by a variation of the ratio of the time constants $\tau_{SOL \rightarrow div}/\tau_{div \rightarrow SOL}$. A decrease of this ratio causes a decrease of the ratio N^{main}/N^{div} leading to a faster decay rate. The dashed curve in Fig. 4.12 shows the result from such a model calculation where the assumption was used that the divertor retention time $\tau_{div \rightarrow SOL}$ increases with the square of the divertor D_2 flux density, while the other time constants are kept constant. An effective divertor volume V^{div} = 3 m^3 is used in approximate accordance with the real geometrical situation in the torus. In principle, the observed experimental behaviour could also be explained by a reduction of $\tau_{SOL \rightarrow div}$ with increasing Γ_{D_2}. The comparison with other experimental observations, like the early increase of the neon density in the main plasma after the opening of the valve, revealed that the retention time is indeed the parameter which predominantly varies with Γ_{D_2}.

4.3.3 *Modelling of impurity transport and radiation*

Impurity profiles and emission characteristics are modelled with the STRAHL radial impurity transport code using 1-d geometry and an ansatz of anomalous diffusivities and radial drift velocities. An essential feature of the modelling is the empirical description of the recycling and pumping using the simple chamber model for recycling and pumping, thus providing a self-consistent description of the particle content and its temporal development on the basis of the calibrated valve flux and the pumping speed of the turbomolecular pumps. Somewhat problematic in the modelling of the emission characteristics is the treatment of the neutral neon source function. The neutral neon influx is not spatially homogeneous, but peaked around the X-point region, as can be seen from the comparison of the emission along the midplane and lower viewing lines as shown in Fig. 4.11. However, the ionization stages which mainly contribute to the neon radiated power are expected to have a spatially homogeneous distribution owing to the rapid parallel transport. Therefore, the total neutral neon influx as derived from the simple chamber recycling model should result in a proper estimate of the radiation of these higher ionized states. The total neutral neon influx from the transport model divided by the total plasma surface is also compared with the neutral flux density derived from visible spectroscopy in the midplane and lower divertor region. As can be seen in Fig.4.13, the measured midplane recycling flux is an order of magnitude below the calculated averaged flux. The flux density above the X-point appears to be much higher, but the effective surface is only a fraction of the total plasma surface. Therefore, the apparent total neon influx is only partly established by the spectroscopic influx measurements. A possible explanation for this fact may be found in 'hidden' recycling regions, like limiter or baffling structures on the low-field side, the presence of a very high neutral influx just around the X-point, or the significant contribution of neon ions backstreaming from the divertor.

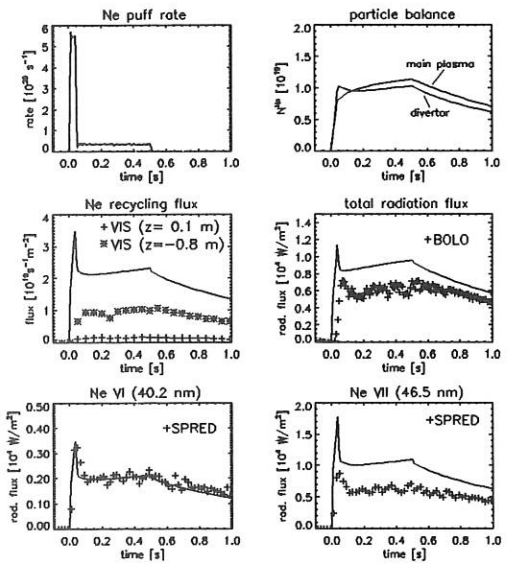

FIG. 4.13: STRAHL modelling of the H-mode discharge without the additional D_2 puffing (#4686) shown in Fig. 4.11

The deconvoluted emissivity profiles from bolometry are typically not accurate enough to determine, for example, the exact fraction of power emitted inside the separatrix. This quantity, which is thought to be essential for the H-mode behaviour, is better represented by the prediction of the 1-D radial impurity transport calculations. For the experimental conditions typical of this report, about 2/3 of the main chamber radiation is emitted inside the separatrix.

4.3.4 *Completely detached H-mode*

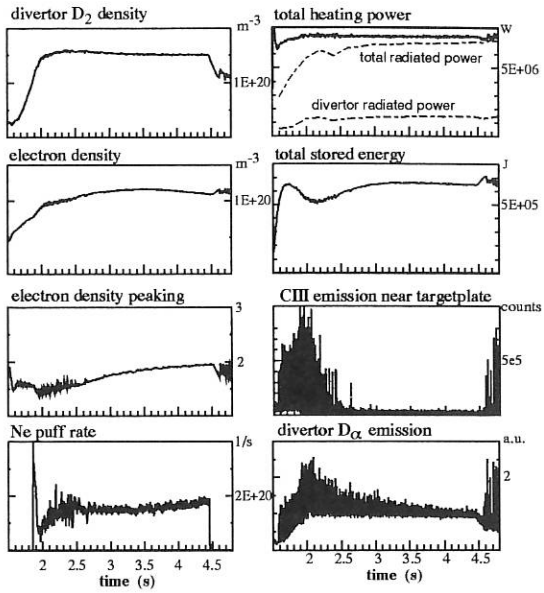

FIG. 4.14: Time traces of a discharge with simultaneous control of the radiated power fraction and the divertor neutral flux density. The electron density peaking factor is taken from the ratio of a central and a more peripheral ($\rho_{tang} \approx 0.5$) DCN interferometer chord integral, with a length ratio $l_{central}/l_{peripheral} = 1.2$. The CDH-mode is achieved in the time interval from 2.7-4.5, see # 5028, I_p = 1 MA.

Figure 4.14 shows the temporal development of various experimental parameters for a discharge with radiated power and divertor neutral flux feedback control exhibiting the completely detached high confinement (CDH-) mode with more than 90 % radiated power fraction. The small, high-frequency CDH-ELMs are buffered by the divertor plasma, as can be seen from the CIII emission, which vanishes in front of the target plate. Langmuir probe measurements indicate almost complete detachment at the strike point, while further outside partial attachment is observed at low power flux levels. Thermographic measurements of the power density at the outer target plate reveal no burnthrough of ELMs and a power level below 1 MW/m^2 during the CDH-phase. During the type-I ELMy H-mode before neon injection, a narrow energy deposition layer is seen in between ELMs, while the type-I ELMs exhibit a broad deposition profile. The global signature of the CDH-ELMs, in particular the power dependence, is type-III like. Such complete detachment preserving high H-mode confinement as obtained with neon injection could not be achieved with deuterium puffing alone. The most unambiguous characterization of the CDH-ELMs is given by the analysis of CII emission in front of

the target plates. The CII radiation in the CDH-phase exhibits a broad and nearly uniform emission characteristic over about 80 mm above the target plate. The type-I ELMs, in contrast, show intense emission localized just in front of the target plate.

The temporal development of the CDH-phase is accompanied by moderate peaking of the electron density profile, by the disappearance of the sawteeth and by the emergence of a strong m=1 mode in the plasma centre. It is speculated that this m = 1 mode stops the further evolution of density peaking in the centre and therefore prevents impurity accumulation, which is often observed in connection with electron density peaking

4.4 Divertor II

A modification of the ASDEX Upgrade divertor was planned and the application for EURATOM preferential support was submitted in October 1994. The present time schedule foresees the start of operation in 1997.

The main purpose of the new divertor II, which was designed to withstand the increased heating power available in 1997, is the test of divertor scenarios planned for ITER. Especially the influence of geometry on the hydrogen flow and hence on detachment and radiation losses will have to be studied experimentally. Therefore, different configurations will be investigated and the design allows a quick change of these configurations.

4.4.1 Predictive modelling of Divertor II

Comparable pure plasma density scans were done using B2 EIRENE for the actual ASDEX Upgrade divertor and the two basic geometry concepts of the new divertor (a GAS BAG geometry and the so-called LYRE geometry) for an input power of 7 MW, see Fig.4.15.

The same tendency as for the ITER cases is observed in the results for the momentum loss: the most symmetric results are obtained for the LYRE geometry, where due to the strong inclination very localized recycling is created, directing the neutrals towards the high-energy zone close to the separatrix. The GAS BAG is much less symmetric, whereas the actual ASDEX Upgrade divertor, because the outer target plate even reflects the neutrals away from the separatrix, in a sense prevents the detachment of the outer plate. The experimental test of different divertor geometries with respect to detachment is a crucial issue for the design of the ITER divertor.

4.4.2 Divertor II design

The design of Divertor II is based on the experience from Divertor I. It provides high flexibility for configuration variations. The density control will be improved by arranging a cryopump behind the passively stabilising conductor (PSL). The particle flux to the cryopump is conductance limited by the pumping channel of the LYRE configuration (Fig. 4.16). A reasonable compromise results for the design pumping speed of 100 m^3/s. It permits to remove the gas flux of two neutral injectors at divertor parameters typical for Divertor I discharges.

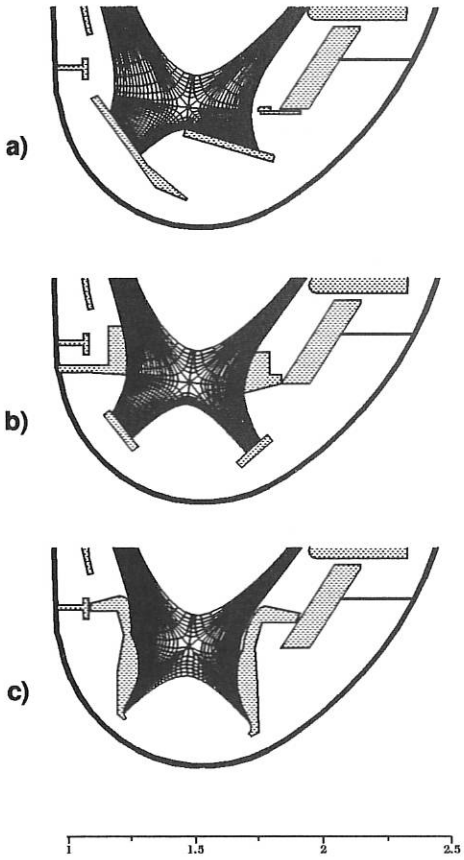

FIG. 4.15: Computational grids and configuration of target plates and in-vessel components for different ASDEX Upgrade versions a) Divertor I, b) GAS BAG, c) LYRA

The three envisaged Divertor II configurations LYRE (Fig. 4.16), GAS BAG 1 (Fig. 4.17) and GAS BAG 2, with target plates perpendicular to the Divertor fan (similar to Fig. 4.15b), can be equipped either with a roof baffle structure or a septum. The first configuration to be studied will be the LYRE (eventually with a roof baffle). All Divertor II configurations use the same base structure for supporting the tile modules. The target tile material will be carbon fibre composite (CFC) for the strike point zone and fine grain graphite for the remaining modules. All tiles are actively cooled via water pipes welded to the tile holder plates. The heat deposited during a pulse is taken up adiabatically and removed during the pulse interval. Access for vertical laser diagnostics (density interferometer) had to be reduced to an effective beam diameter of 20 mm. Vertical diagnostic slits, 20 mm wide, serve for horizontal diagnostic arrays in the case of the LYRE.

The LYRE was designed to provide the largest correspondence to Divertor I. The angle of power incidence and the pumping conditions have been kept identical for both. For full Divertor II additional heating power of 25 MW, the maximum power flux density, extrapolated for the LYRE from the thermography measurements of Divertor I, about 15 MW/m^2, is well within the capabilities of available CFC materials. The LYRE strike point tiles are steeply inwards inclined to scatter the cold gas formed there most effectively towards the high heat flux zone of the separatrix. Despite this steep inclination the tile shape could

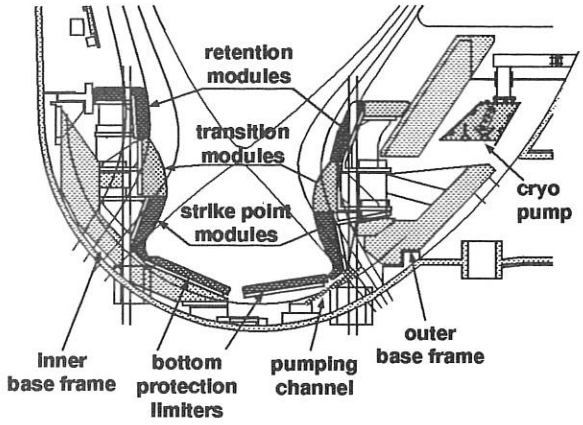

FIG. 4.16: The Divertor II LYRE configuration

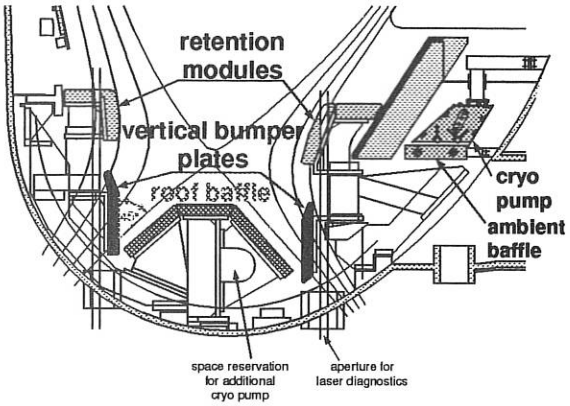

FIG. 4.17: The Divertor II GAS BAG 1 configuration

be formed in a way, which permits a large vertical tolerance of the strike point position without increasing the heat flux density. This in turn permits to satisfy the feed back power demands with the available power supplies. To improve the impurity retention compared to Divertor I, the separatrix strike point was arranged at the lowest possible location permitted by the constraints from the vessel shape and the vertical diagnostic access. In addition the retention modules, shaped to follow flux lines for functioning as a baffle, were added above the X-point region. In between the retention and strikepoint module, the transition module is inserted to smoothly link the shape of the two. Figure 4.18 shows a complete sector of the LYRE target plates.

For the GAS BAG configurations the LYRE transition module will be removed and the strikepoint module exchanged. This exchange can be achieved during a routine summer shut down of the experiment. The larger poloidal angles between separatrix and strike point tiles, 45° for GAS BAG 1 compared to 12.5° for the LYRE, entail for the GAS BAG configurations under conservative assumptions (only 50 % of the heating power is lost by radiation, no relevant power transport by charge exchange particles) heat flux densities which are not manageable. For the start up of the GAS BAG configurations a stepwise increase of the heating power is thus required in combination with an elaborate safety system. The time schedule permits to rely on more advanced CFC materials for the GAS BAG configu-

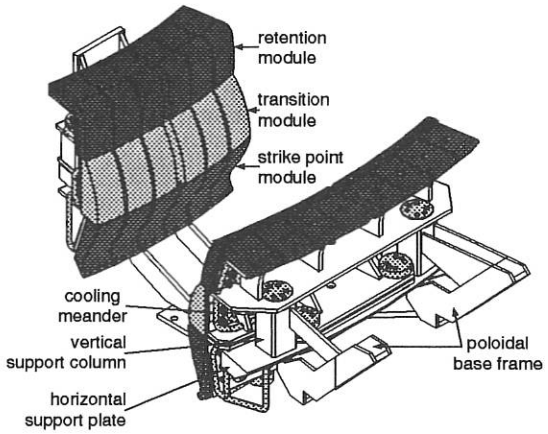

FIG. 4.18: Complete sector of the LYRE configuration

rations following only after the LYRE. A promising 3 D CFC candidate has been developed by industry due to initiatives of the NET team and we have initiated a comprehensive Divertor II tile test programme. For the GAS BAG options therefore a maximum heat flux density of 25 MW/m^2 seems feasible. With such a carbon material the GAS BAG 1 configuration can then be established from a heating power of 12 MW onwards with about 1 s tile overheating response time of the safety system.

Each tile of the strike point module is subdivided into 4 carbon pieces of 40 mm width, stacked in toroidal position. The stack is tied together by 3 rods. Like for Divertor I, the individual carbon pieces are pressed towards their cooling plate via T-shaped clamps located in toroidal grooves. The small carbon pieces are favourable for manufacturing and for small toroidal warping displacements. Between carbon pieces and cooling plate there is a thin wedge foreseen for tilting the tile in toroidal direction, such that the edges of adjacent tiles are shadowed. The wedge concept permits to decide upon the toroidal direction of the field line incidence (ion grad B drift) at a late state and also to reverse the tilting direction later on within short time.

The cryo pump (CP), arranged behind the PSL, has to give way for vertical diagnostic paths. It is therefore subdivided into 7 modules with a net pumping aperture of 1.4 m^2. Cryogenically the modules are series connected. The interconnecting cooling pipes of the LN_2 shield and the LHe cryo panel spare out the diagnostic paths.

Due to claims by DIIID that non-accommodated (energetic) plasma particles release water vapour from the LN2 surfaces in sufficient quantities to cause plasma disruption, an additional ambient baffle was foreseen for the GAS BAG configurations (Fig. 4.17). Recent experimental evidence from the JET in vessel cryo pump does not support the DIIID concerns. Therefore the ambient baffle of Fig. 4.17 will be dispensed with and the LN2 line of sight baffle (in green) changed into a chevron. Cryo pump and cryo supply will be tested by means of a prototypical CP module pair. Since the Joule Thompson current of the WVII refrigerator, available in mid 1995, can not be used, the LHe will be circulated by means of a cold centrifugal pump. Boiling LHe will feed the cryo panel. In case the test arrangement shows difficulties during refilling of

the cryo panel after He discharge-glowing there is also the possibility foreseen to switch to super critical (1 phase) helium.

4.4.3 *Divertor II diagnostics*

The installation of the new divertor requires the modification of a number of existing diagnostics. Some of them are needed for machine control and safety:

1. magnetic flux measurements to control the X-point position,
2. thermographic measurements of the strike point positions as check and back-up for the magnetic measurements,
3. conversion of two vertical legs of the DCN interferometer into a vibration compensated CO_2 interferometer to cope with the reduced aperture of the ports and to ensure reliable electron line density measurements without fringe losses during the strong m = 1 mode occurring at q < 3 operation with high NBI heating power,
4. pyrometric measurements of the inner wall temperature at the location of the NBI shine-through footprints as an additional interlock signal.

Other diagnostics are needed to evaluate how the new divertor performs. Practically all existing optical divertor diagnostics have to be modified since the lines of sight are blocked by the new target plate structure. However, the 20 mm wide poloidal slits in the target plates at the toroidal position of the pump ports will enable viewing of the strike point regions of both the inner and the outer target plates and of the divertor plasma in front of them. Conceptual designs for the required modifications exist and work on detailed designs will start in 95.

5. DIAGNOSTICS

The installation of nearly all diagnostics mentioned in the table of the Annual Report 1993 is completed. Here we describe only those diagnostics which were not yet mentioned in earlier reports.

5.1 Magnetic Diagnostics

A prototype of a new coil measuring magnetic fluctuations was installed. It consists of a printed circuit on which the windings form a spiral. Thus, the integration length is on the order of μm compared to $\approx$ 20 cm for a usual Mirnov coil. The printed circuit coil is installed very close to the plasma ($R - R_{sep}$ = 14 cm) to measure $\dot{B}_r$, whereas the usual Mirnov coils are located at $R - R_{sep}$ = 36 cm and detect $\dot{B}_\Theta$. This yields a much higher sensitivity to high (m, n) modes. With this coil it is possible to detect the typical precursor oscillation prio to type III ELMs which was not seen on ASDEX Upgrade using the normal Mirnov coils.

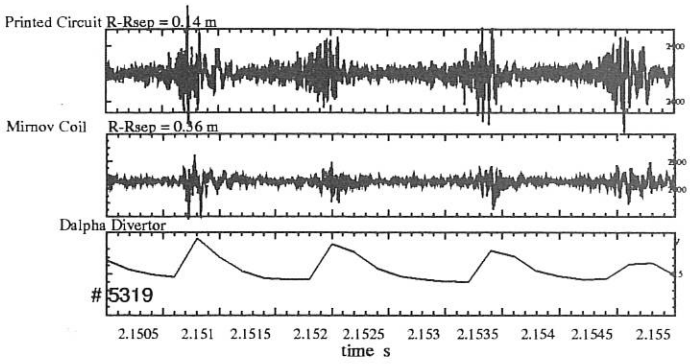

FIG. 5.1: Type III ELM with magnetic precursor seen on the printed circuit coil, but not on the usual Mornov coils. Both coils are located midplane outside.

5.2 Boundary Layer Spectrometer

During the Summer '94 vessel opening the full boundary layer spectrometer, which replaces the provisional system used until now, was installed on ASDEX-Upgrade. This system was conceptually designed by the E1 spectroscopy group and manufactured by BESTEC GmbH of Berlin, this contract being financed through the IPP's Berlin Division. A figure of the instrument in place on the tokamak is shown in the Berlin division's section of this report.

This system allows flexible observation of about 2/3 of the plasma in both vacuum-ultraviolet (VUV) and visible spectral ranges via plane, platinum coated swivel mirrors at the entrance to a horizontal port (see Fig. 1). The plane mirrors can be rotated about the port axis and a mutual perpendicular axis thus permitting observation of an almost full poloidal plasma cross-section and toroidally about 2/3 of the vessel including 3 of the 4 ICRH antennae.

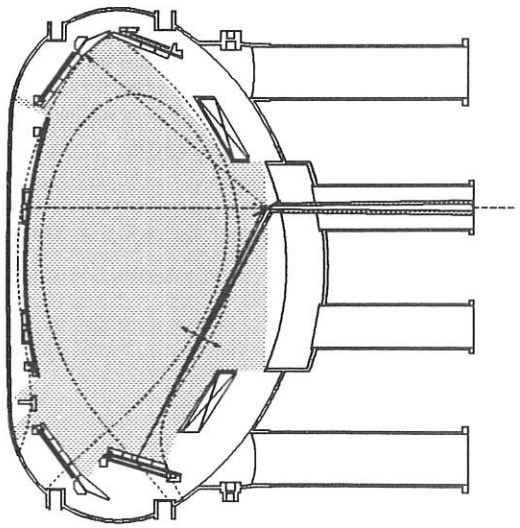

FIG. 5.2: Poloidal section showing possible lines of sight of the boundary layer spectrometer in Sect. 16. The light shaded region indicates the observable region of the vessel.

Light from concentric lines of sight is collimated into the VUV range (30–200 nm) 1 m normal incidence spectrometer by means of a Pt coated ellipsoidal mirror and into the visible range (200–800 nm) 1 m Czerny-Turner spectrometer using two mirrors in a Cassegrain configuration. The observation of almost equal plasma volumes greatly facilitates absolute calibration of the VUV instrument using the 'branching-ratios' technique.

The spectrometers are both fitted with intensified photodiode array cameras (2048 25 μm x 2.5 mm pixels) with $\geq$ 6 ms integration time. The visible detector utilises a closed micro-channel-plate intensifier (S20 cathode) and the VUV system an open CuI coated MCP. With 1200l/mm gratings the dispersion ($\approx$0.8 nm/mm) and resolution ($\approx$0.1 nm) of the two instruments are similar.

The rotatable plane mirrors can either be positioned, rotated or oscillated during the shot; the position being protocolled by absolute encoders at 10 ms intervals. The latter two modes allow spatial profiles of the measured intensities to be reconstructed from a series of frames. The spatial resolution is not limited by the optics (< 1 cm radial resolution viewing poloidally) but by the frame rate. As an example, scanning the outer target plate (amplitude $\Delta\theta$ = 6°), a maximum oscillation frequency of 5 Hz is achievable resulting in a spatial resolution of $\approx$2 cm at 6 Hz frame rate. Larger amplitudes are possible at lower frequencies ($\Delta\theta_{max} \propto 1/f^2$).

Fig. 2 shows spatial profiles of C II and O V line intensities measured during a single-null divertor discharge by sweeping the line-of-sight at 1 Hz across the lower part of the poloidal section ($-70° \leq \theta_b \leq -20°$). The C II emission is well localised to the separatrix strike-zones, the location of the dominant source of sputtered C ions. In contrast, the O V emission is distributed throughout the SOL due to parallel transport, peaking, however, in the x-point region where a maximum in the emissivity is usually observed by the bolometry.

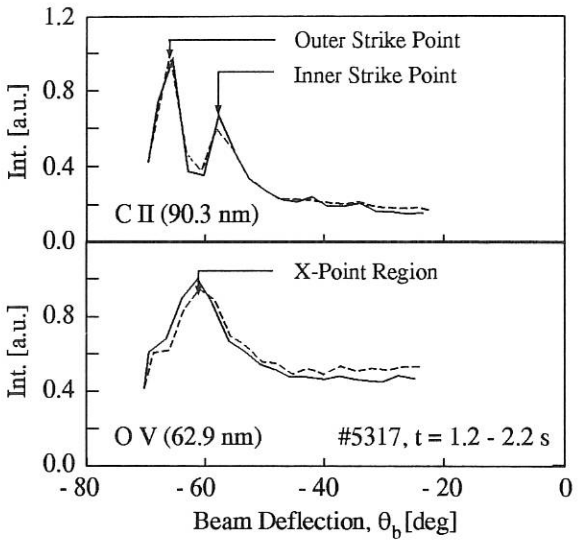

FIG. 5.3: Spatial profiles of line intensities of C II (90.3 nm) and O V (62.9 nm) measured during the flat-top phase of a discharge with I_p = 800kA, B_t = −2T, $\overline{n}_e = 4.5x10^{19}$ m^{-19} in D_2 with single-null configuration.

5.3 High Resolution Divertor Spectrometer

(see Section IPF Universität Stuttgart)

5.4 The Midplane Manipulator at ASDEX Upgrade

The midplane manipulator system for ASDEX Upgrade had been installed during spring 1994. This manipulator can be used for inserting different kinds of probes into the plasma boundary. Details of this system are described in the Annual Report 1993.

First measurements using a fast-moving Langmuir probe had been performed in July 1994. During the service time of ASDEX Upgrade the manipulator had been modified to take the experiences of these investigations into account. Especially, the pneumatic probe system was rebuilt, because the old control system failed some times in the presence of the magnetic field. A new controller using a one-chip computer, was designed, built up and installed. This system performs a stroke of 100 mm within 100 msec for and back. Additional a fast 6-channel data collection system for Langmuir probe measurements had been installed. This system records single probe characteristics within 0.3 msec or triple probe measurements within 2 μsec.

The probe head used is made full of graphite. It consists of two triple probes separated by a carbon wall. This design enables a direction sensitive measurement and comparison of single, double and triple probe measurements. Radial profiles of plasma density, electron temperature and floating potential are discussed in section Berlin!!!

INTERNATIONAL COOPERATION

1. DOE – ASDEX Upgrade

The main activities in this IEA Implementing Agreement for the joint work on the investigation of toroidal physics and plasma technologies in ASDEX Upgrade were personnel exchanges US ⟷ IPP and exchange of codes and a technical workshop on "Disruptions in Divertor Tokamaks" in connection with the annual (9th) IEA ASDEX Upgrade Executive Committee (EC) meeting on March 15, 1994, at MIT, Cambridge, Massachusetts, USA. ITER-related activities as well as extension of the present Agreement were major items.

1.1 Plasma Control

The problem of plasma shape and position control, plasma disruptions, and vertical displacement events (VDE) in ITER can be dealt with in ASDEX Upgrade, as already stated in the Annual Report 1993. The dynamics and forces involved during VDE's and current disruptions were extensively simulated with PPPL's **T**okamak **S**imulation **C**ode (TSC). Results were presented at the workshop mentioned above, at the 21st EPS Conference and at the 15th IAEA Conference. Design of a disruption data bank for ASDEX Upgrade was started to obtain – together with results from other experiments – scalings for extrapolations towards ITER.

1.2 Edge Physics

There is an ongoing joint activity in the field of tokamak edge modelling which is based on the B2 tokamak edge multifluid code, the EIRENE Monte Carlo neutral gas code, and the SONNET grid generator.
In 1994, among many smaller activities, emphasis was put on the implementation of a neutral fluid model in the IPP version of B2. In addition, preparatory work on B3, successor to the B2 code, now used, was done.

Two moving Langmuir probes for divertor profile measurements (IVP 1 and IVP 2, developed by S. Pitcher, Toronto/PPPL) were installed in ASDEX Upgrade. Precise edge profiles were taken in practically all relevant operation regimes. During the summer opening, both probes were brought back to Canada for maintenance work and re-installed in ASDEX Upgrade in November.
A magnetic field introduces for a Langmuir probe not only a preferential direction but also a number of new effects at frequencies related to the ion cyclotron frequency: methods to measure the Langmuir characteristics at these ICRF frequencies (tens of MHz) in the ASDEX Upgrade divertor were developed. The theoretical analysis and the experimental methods were compared with those at TEXT. Their goal is to obtain, with fast (a few MHz) switching of a single probe, measurements equivalent to those of a triple probe.

Within the framework of plasma-wall interaction the MOLDY-CASK molecular dynamics program for radiation damage in solids (developed at LLNL) was extended to problems at IPP, such as calculations of reflection coefficients, sputtering yields, and implantation profiles.

A new version of the DIVIMP code (developed by P.C. Stangeby and D. Elder) was adapted to the ASDEX Upgrade environment. Modifications of the previous IPP version of the code were incorporated. A program was developed by K. Krieger to provide input data for DIVIMP (electron density and temperature in the plasma edge region) from measurements of the divertor Langmuir probes (IVP1 and IVP2). The DIVIMP code will be extended to incorporate carbon production by chemical erosion and model the subsequent penetration of the resulting carbohydrates into the plasma. In addition, it will be modified to treat metastable states of ions as distinct species separate from the ground state. This is necessary because many important spectral lines used for diagnostics are excited from metastable states.

1.3 Transport, Heating and Refuelling Issues

Collaboration for the bulk plasma issues concentrated on transport and confinement studies and heating and refuelling issues.

Plasma transport analysis and simulation work for both ASDEX Upgrade and ITER predictions were done at IPP using PPPL's TRANSP and BALDUR codes. A set of ASDEX Upgrade discharges designed to study the transport of the intrinsic impurity boron in the divertor and scrape-off layer was analyzed. The focus was on applying edge transport models to analysis of the spectroscopic data using the NEWT 1D code, a one-dimensional fluid model of the divertor and SOL plasma that includes impurities.

Collaborative work on pellet ablation and vapour shield modelling studies is being pursued with several discussions.

RF heating and applications: IPP helped with the installation of two new RF transmitters bought by GA. They are from the same company and of the same type as those used for ASDEX Upgrade. A formal cooperation in the field of development of ICRF antennas for ASDEX Upgrade and development of arc detection systems was set up with ORNL. As a first step, the spare ASDEX Upgrade antenna was shipped to ORNL for measurements of the antenna impedance and RF field distributions.

2. DEMOKRITOS, Greece

There is ongoing cooperation between IPP and Demokritos in the field of divertor physics and especially divertor plasma diagnostics by movable Langmuir probes.

After a few design iterations between IPP and Demokritos, the construction of LPS by Demokritos was completed in 1994 and, after some remaining tests, LPS was shipped to IPP and mounted on ASDEX Upgrade at the end of 1994.

3. University of Cork, Ireland

The collaboration with the University of Cork concerning the MHD equilibrium identification using magnetic measurements and function parametrization of an equilibrium data base was continued. This method is the central part of our diagnostic data evaluation procedures and the results are in good agreement with those of other diagnostics. Function parametrization technique is now being tested to determine current density profiles from polarimetric and interferometric measurements.

4. Collaboration with Universities

For details see Chapter UNIVERSITY CONTRIBUTIONS TO IPP PROGRAMME.

5. Cooperation with Russian Institutes

Most of the collaborations are organized in the framework of WTZ, the Agreement between the Federal Ministry of Research and Technology of the FRG and the State Committee for the Use of Atomic Energy of the USSR on Scientific-Technological Cooperation for the Peaceful Use of Nuclear Energy.

1. Pellet injection – Technical University of St. Petersburg (SPU): *Experiment:* A diagnostic pellet injector for different solid pellets built at SPU is in operation. At present a microwave system for pellet mass measurements and a CCD camera system for observation of the ablation cloud are being developed at SPU. SPU is engaged in the analysis of experiments performed at ASDEX Upgrade with the diagnostic pellet injector. *Theory* a) A model was developed for the electrostatic shielding field at a solid surface exposed to energetic plasma particles. b) Scenario calculations were performed with the help of SPU for expansion of high-density low-temperature carbon clouds in hot plasmas, and scaling laws were established.
2. ECRH — Institute of Applied Physics, Nizhni Novgorod (IAP): In order to prepare the ECRH experiments, we installed a 0.5 MW/0.5 s gyrotron together with a cryomagnet, both on loan from IAP, and studied the impact of the poloidal stray magnetic field from ASDEX Upgrade on the gyrotron performance.
3. Neutral particle analysis — Kurchatov Institute, Moscow: A code is being developed for fast interpretation of data with the aim of evaluating the ion temperature profile.

Two contracts outside WTZ exist in the field of neutral particle analysis: Ioffe Institute, St. Petersburg, is contributing to the measurement and interpretation of neutral particle spectra and Kurchatov Institute is performing a detailed sensitivity study for the neutral particle interpretation code.

6. KFKI, Budapest, Hungary

A guest researcher participated in the development and operation of the laser blow-off system at ASDEX Upgrade. With the ablation of low- and medium-Z metals impurity transport investigations were performed. Another part of the collaboration was the experimental investigation of the behaviour of the high-Z material, tungsten, in the plasma centre. To assist the experiments at the ASDEX Upgrade tokamak, a laboratory experiment was built to examine the properties of the ablated particles.

7. Centro de Fusão Nuclear, EURATOM IST Association, Lisbon, Portugal

This cooperation, the aim of which is to instal and operate the microwave reflectometry diagnostic on ASDEX Upgrade, focused on two main subjects in 1994. The first was to test the already installed frequency bands (16 – 40 GHz) and conduct first measurements. Though the density range was limited, the high temporal resolution (20 – 100 μs per profile) and the feasibility of electron density profile determination could be demonstrated. Next, the diagnostic was further upgraded with the Q-band (33 – 50 GHz) and the V-Band (50 – 75 GHz). With these, the probed density range is $0.4 - 6.8 \cdot 10^{19}/\mathrm{m}^3$ in O-mode polarization ($\vec{E} \| \vec{B}$) on the high and low-field sides of the plasma. First tests were also carried out with the X-mode channel ($\vec{E} \perp \vec{B}$), which will probe the outer edge of the plasma ($n_e \approx 0 - 2 \cdot 10^{19}/\mathrm{m}^3$) on the low-field side. To facilitate the data acquisition for the upgraded system, a 200 MHz VME-bus board was built and tested within this work.

8. AEA Culham, United Kingdom

In March 1994 three scientists from AEA Culham visited Garching to discuss collaboration in the fields of MHD, RF heating and current drive and edge physics. The similarities in shape with their different sizes make COMPASS-D and ASDEX Upgrade well-suited to scaling studies. In October 1994 two scientists from IPP went to Culham to hold an Executive Committee Meeting on the collaboration. Visits between the two labs were defined for 1995. On this occasion, a workshop together with JET was held. Its topic was H-Mode and Boundary/Divertor Physics. The transfer of the newly found CDH-mode to other devices and the effect of ELMs on divertor discharges were discussed.

9. Institut für Allgemeine Physik, TU Vienna, Austria

Collaboration between IPP and Institut für Allgemeine Physik concerns the development of lithium beam diagnostic methods for measuring both electron and impurity density profiles in the plasma edge. The diagnostic system on ASDEX Upgrade started operation in summer 1994. One scientist finished his dotoral thesis after a 3–year stay at IPP exploiting the first measurements with the new diagnostic system. The collaboration was financially supported by the Austrian Friedrich Schiedel Stiftung für Energieforschung, which is gratefully acknowledged by IPP.

JET Cooperation Project

(Head of Project: Prof. Dr. Michael Kaufmann)

In January 1994, JET completed a major shutdown that hat lasted almost two years. The most important changes to the machine were the installation of four in-vessel divertor coils, a new divertor target structure with carbon fibre composite (CFC) target plates and a divertor cryopump. In addition, four new antennae for up to 20 MW of ion cyclotron resonance frequency heating, a new 10 MW launcher for lower hybrid frequency current drive, eight saddle coils for plasma disruption control and various new plasma diagnostic systems, particularly for the new divertor plasma region, were installed. Some of the latter have been developed with the advice and support of the IPP, such as a new bolometer system to measure spatially and temporally resolved the total radiated power. ASDEX-type pressure gauges have been installed to investigate the neutral particle flux and recycling in the JET pumped divertor. Furthermore, the surface layer analysis of carbon tiles from the JET vessel by means of ion beam techniques at the IPP is continued.

The first plasma in the new configuration was produced on 14 February, and by 15 March, 2 MA diverted plasmas had been established successfully. The new experimental phase started then. Experimental operations were shared between three Task Forces, which addressed different aspects of the program: (i) divertor performance assessment and divertor physics; (ii) tokamak concept improvement; and (iii) high plasma performance. During 1994, the plasma current was increased to 5 MA and the total heating power reached 26 MW; a plasma stored energy of 11.3 MJ was obtained and a neutron rate of $4 \cdot 10^{16}$ neutrons/s was achieved.

Divertor performance assessment and divertor physics: an important first result of divertor experiments was the significant improvement of the power handling capability of the new divertor structure. In discharges where the plasma strike zone was swept over the divertor target with a frequency of 4 Hz, 140 MJ of plasma energy could be deposited without reaching divertor target temperatures where a strong influx of carbon (''carbon bloom'') would deteriorate plasma performance. This contrasted with only 15 MJ that could be deposited previously onto the X-point target tiles in similar discharges without producing carbon blooms.

In conjunction with studies on future divertor plasma conditions relevant to ITER, experiments were carried out to achieve a further reduction of the power flow near the divertor target. This was studied by detaching the divertor plasma from the material surfaces, and was achieved in ohmic and L-mode discharges by ramping up the plasma density with strong deuterium gas puffing. Plasma detachment was observed by a reduction of the plasma flow onto the divertor target measured by Langmuir probes embedded in the divertor target plates. During detachment, the carbon impurity flux from the target was reduced and plasma radiation from the divertor region was concentrated at the plasma X-point but still outside the core plasma. Similar experiments during discharges with H-mode confinement resulted in a transition back to L-mode confinement. So far, similar attempts at puffing a mixture of neon and deuterium also precipitate a return to L-mode when the net input power falls below the H-mode threshold. However, there is evidence for both the screening and the compression of neon in the divertor.

A step forward was made by puffing a mixture of nitrogen and deuterium gases which led to partially detached, ELMy H-mode plasmas, to which both NB and ICRF heating power was successfully coupled. For example, with 24 MW of combined heating power, the target temperature was held constant at 350° C for the 2.5 s of the heating. Further studies at higher combined heating power should provide the most convincing demonstration of the relevance of this regime to ITER.

Plasma discharges with the divertor cryopump operating at liquid helium temperature to pump deuterium resulted in increased peaking of the core plasma density profile, thus facilitating neutral beam penetration. The efficiency of the cryopump in reducing recycling from plasma facing surfaces has been exploited in the high performance hot-ion H-mode regime to the point where the NB injection particle source dominates fuelling from recycling. Hence, peaked density profiles, favoured for improved NBI, are maintained leading to improved fusion performance.

Tokamak concept improvement: advanced tokamak concept studies have been undertaken. The most important results obtained, so far, are the extension of the high β_p regime to lower safety factors, q^{95}, to higher normalised β_N and, by virtue of the frequent ELMs, to quasi steady-state. $\beta_p = 2.6$ has been obtained transiently while $\beta_p = 1.6$ and $\beta_N = 3$ were maintained simultaneously for 7 s at a toroidal field of 1.4 T. Methods of improving confinement stability by modifying the current density profile have also been explored and a plasma current of 2 MA has been driven non-inductively for 3 s using 4 MW of Lower Hybrid power.

High plasma performance: the highest fusion performance achieved during 1994 is comparable to the best obtained previously. In the ELM-free phase of a 3 MA hot-ion H-mode with 18 MW of NBI, the fusion triple product ($n_D T_{io} \tau_E$) reached 8 •10^{20} m^{-3} keVs and the maximum neutron rate was 4•10^{16} s^{-1}, within 10 % of the best achieved with deuterium in 1991/92. During ELM-free H-mode phases, the best energy confinement time achieved was a factor of 2.3 above the ITER89-P confinement scaling. Peak fusion performance appears to be limited by MHD instabilities which manifest themselves either in a fast event like an ELM or in a slow 'roll over' of the stored plasma energy and neutron yield. The best plasma performance in steady state (at a plasma current of 4 MA and an input power of 18 MW) lasts for more than four energy confinement times and the fusion parameter reached a value of 2.6•10^{20} m^{-3} keVs. At a lower plasma current of 2 MA, H-mode discharges have been maintained for 20 s corresponding to 45 energy confinement times.

To run diagnostic systems and to contribute to the exploitation of JET scientific results, IPP personnel are assigned to JET under two task agreements. Both agreements were prolonged for another two years period, leaving all provisions of the former contracts unchanged. In addition, a closer cooperation between JET and IPP in the fields of H-mode and plasma edge physics has been initiated. A workshop dealing with these topics at Culham (Nov. 1994), attended mainly by scientists from JET and IPP, can be regarded as the start of this intensified cooperation.

1. TASK AGREEMENT NO. 1

Ch. Fuchs, K.F. Mast, K. McCormick, R. Reichle

For the JET pumped divertor experiment a new bolometer diagnostic for measuring the local radiation power density was developed and installed at JET. The principal component of the new JET bolometer is a high-temperature version of the ASDEX Upgrade metal resistor bolometer. Sixteen channels of the proposed ones are in operation. To unfold the raw data, the Anisotropic Diffusion Model Tomography program developed by IPP was installed at JET. This method of reconstructing the radiation distribution from bolometer radiation measurements has been successfully applied to various plasma scenarios. Especially results for JET's neon puffing experiments are most important for characterizing the radiating JET boundary.

A lithium beam diagnostic setup was installed at JET for measuring the electron density in the plasma edge. IPP gave advice for the design and construction of the lithium injector.

2. TASK AGREEMENT NO. 2

R. Behrisch, W. Assmann (LMU München), J. Ehrenberg, S. Grigull, R. Grötschel (FZ Rossendorf), G. Haas, D. Hildebrandt, U. Kreissig (FZ Rossendorf), A.P. Martinelli, M. Mayer, D. Naujoks, V. Prozesky (Nat. Accel. Lab., Capetown, S. Africa), W. Schneider

To get information on the actual composition of the plasma-facing vessel wall material of JET and on the plasma-induced material transport at the vessel walls during plasma discharges, the 20 representative samples cut out of different areas of the JET vessel after the 1991/1992 discharge period were further investigated in respect of Be, O, C and H deposition, by Heavy Ion Elastic Recoil Detection Analysis (ERDA) as well as by sputter Auger depth profiling. Be and O concentrations of up to 20 atomic % are measured on the carbon pieces in surface layers of about 200 nm, and similar concentrations of C and O are found on the Be samples. He, H and D concentrations are typically of the order of a few atomic %. There is a correlation between the O and the Be as measured on the C samples and between the H/D and the C as measured on the Be samples.

During the 1993/94 JET discharge period 30 Long Term Samples (LTS) of carbon, partly covered by an evaporated layer of Al, were mounted at the vessel walls. These samples were removed in September 1994 and the surface layers were analyzed with MeV ion beams by RBS, NRA, PIXE and ERDA. It was found that the inboard part of the vessel walls is erosion-dominated with erosion of the Al layer and only small deposits, while the outer part is deposition-dominated with deposits up to 2 μm thick. The measured deposits have a concentration of 60 to 70 atomic % of Be, the rest is C and O with a few atomic % of H and D. The ERDA analysis also showed traces of B, N, F, Na, Mg, Si, S, Cl, K, Ca, Ti, Cr, Fe and Ni.

ASDEX-type pressure gauges were installed at 5 poloidal positions in 3 octants of the JET MKI divertor. Four gauges below the horizontal target plate and 1 gauge in the pump plenum of the cryopump. By strike point sweeping the position of the gauges relative to the strike zones is changed from inside the inner strike zone to the private flux region and to outside the outer strike zone.

The neutral gas density in the divertor and the particle removal achieved by the cryopump were investigated. In ohmic discharges and quiescent H-mode phases the pressures are in the range of 5 × 10^{-4} to some 10^{-3} mbar and during ELMs up to 10^{-2} mbar depending on plasma density and heating power. Under ohmic conditions the pressure is proportional to the square of the plasma density as found in other tokamaks. During ELMy H-mode phases (giant and grassy ELMs) the pressure especially below the inner strike zone is strongly modulated (giant ELMs by a factor of more than 10). If the cryopump is activated, the pressure in the plenum drops by a factor of 2 and the gas consumption for similar ohmic discharges rises by a factor of 2.5. The pumped flux generally exceeds the particle flux introduced by gas puff, i.e. the cryopump depletes the walls of hydrogen isotopes. The particle removal rate could be estimated at a few % of the particle flux onto the target plate.

NET/ITER COOPERATION PROJECT

(Head of Project: Prof. Dr. Karl Lackner)

Since its foundation IPP has hosted the NET Team, a group of scientists and engineers from the European countries participating in the EURATOM programme. They were called together to prepare the design of NET, the Next European Torus. NET is conceived as the next major step in the European fusion programme, and a considerable fraction of its objectives are in the technology area. IPP contributed to the NET activities both by direct secondment of personnel to the NET Team and by performing NET supporting work.

From May 1988 to the end of 1990, IPP hosted the full ITER Team (International Thermonuclear Experimental Reactor), a project with objectives similar to those of NET but with equal participation of EURATOM, Japan, Russia and USA. IPP strongly supported the ITER activities through its support of NET and are still doing so.

With the signing of Protocol I of the ITER-EDA phase it has been decided that from now on the ITER Team will reside at three locations, one of them being IPP Garching again. The Garching part of the ITER Team will concentrate its activities on physics questions and on in-vessel components. IPP will also continue to host the NET Team, which, at the same time, will function as the EC home base to ITER.

Through its scientific work, IPP Garching makes extensive and essential contributions to the ITER Engineering Design Activity. In particular, the programme of ASDEX Upgrade, centred on optimization of the poloidal divertor concept, is directly aimed at supporting ITER. A highlight of this work during the last year was the discovery of the CDH-mode, constituting a proof of principle of the compatibility of good H-mode type confinement with low power loading on the divertor target plates. Also the stellarator experiments at IPP make significant contributions to ITER. The results of these efforts are described in the chapters dealing with the ASDEX Upgrade and W7–AS projects.

The following sections therefore describe only additional, specific design efforts aimed at ITER, partly supported by NET contracts.

1. DIVERTOR PHYSICS AND PLASMA WALL INTERACTION

1.1 Scrape-off-Layer Modelling Calculations

R. Schneider, D. Reiter (IPP Jülich), K. Lackner, J. Neuhauser, B. Braams (Courant Institute, New York), D. Coster, H.S. Bosch, H. Kastelewicz, H.P. Zehrfeld

On the basis of the successful model validation work for ASDEX and ASDEX Upgrade, ITER calculations were done with the B2-EIRENE code package to study the importance of the divertor geometry with respect to power losses due to neutral recycling and impurity radiation, which are necessary to reduce the power load of ITER target plates to technically feasible values (of the order of 5 MW/m^2). Estimates and simulation calculations show that for ITER conditions neutral hydrogen losses are not large enough to reduce the power target load to technically tolerable values. Therefore, additional radiation losses from impurities are required, ideally resulting from controlled addition of recycling gases.

Two different ITER geometries are studied: a V-shaped and a gas-bag-like divertor Fig.1.1. Calculations for both configurations for a pure deuterium plasma are done for an input power of 100 MW, equally distributed into the electron and ion channels. It is thereby implicitly assumed that 200 MW is lost by radiation.

Differences between the two configurations become apparent from a density scan, at the reference input power of 100 MW. In both configurations the power flows to the target plates start to decrease significantly, even already at modest plasma densities of about $5 \cdot 10^{19} m^{-3}$. Whereas, however, for the V-shaped targets this power flow reduction is approximately equal on the

two target plates, with the energy and particle fluxes in the natural ratio arising from the basic asymmetry of the power flux into the scrape-off layer, power and particle fluxes become extremely asymmetric in the gas-bag case. The probably most revealing difference between the two configurations can be seen, however, in the magnitude of the momentum loss from the plasma. This momentum loss determines the possible radiated power fraction and is therefore very well suited to comparing the detachment behaviour of different geometries. Whereas in the V case the momentum loss increases approximately at the same plasma density on both sides, the two divertor legs behave extremely differently in the gas–bag case, with the inner leg detaching approximately at the same edge density values as in the V, but the outer leg remaining attached throughout the range of the scan.

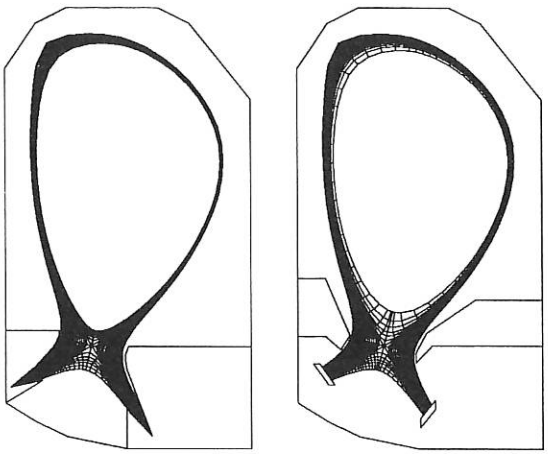

FIG. 1.1: ITER Geometries and computational grids

These different pure plasma results then have consequences for the impurity losses. To study radiation scenarios for ITER, calculations with a multifluid plasma were done for the two configurations in the form of impurity density scans, at a given power input of 200 MW and given plasma separatrix density of $6 \cdot 10^{19} m^{-3}$. Two impurity species were treated: beryllium, as target plate and first wall material, creating neutrals by sputtering, and neon as an additive. The neon content of the discharge was controlled by prescribing the density of Ne^{10+} at the innermost flux surface and setting the diffusive fluxes of all other ionization stages equal to zero at this surface.

Larger radiation power losses and better control are possible in the V-configuration owing to the stabilization compared with the gas-bag, where the plasma detaches asymmetrically on the inner leg, then triggering the formation of a strong marfe. The impurity losses rise more linearly and on a higher level for the V-configuration than for the gas-bag as a function of the prescribed neon density, as expected from the larger momentum losses for the V-shaped geometry discussed in the pure plasma density scan and demonstrating the influence of different hydrogen flow patterns for impurity loss distribution and detachment.

1.2 Role of Kinetic Effects in the Scrape-off Layer

Yu. Igitkhanov, M. Brambilla, R. Chodura

A numerical procedure for kinetic correction of a 2D fluid code for the edge tokamak plasma was developed. This procedure takes care of non-local effects caused by high energy particles. The main idea of this procedure is to simulate the property of the bulk velocity distribution by fluid equations whereas the property of the high-energy tail is calculated from a kinetic equation. The comparison of this approach with a fully kinetic treatment has shown reasonable agreement. Kinetic effects cause a reduction of the heat conductivity along the magnetic field (as compared with the usual Spitzer-Harm expression), which results in stronger temperature gradients, a reduction of the power load at the target and a decrease of the upstream plasma density to values consistent with the gas-target solution.

1.3 Analytic Models for Momentum Removal from the Scrape-off Layer

Yu. Igitkhanov

The concept of the ITER divertor is based on a dynamic gas target where a low-density cushion develops upstream from the plate. In order to sustain such a regime, most of the power has to be radiated upstream from the cushion, which in turn requires a significient pressure drop of $> 80\%$ along the field lines. This effect, due to the transfer of momentum losses towards the side–walls via charge exchange neutrals, was evaluated. For typical ITER dimensions the neutral collisionality is most likely intermediate, which requires that a kinetic approach be used to evaluate the viscous shear stress value for arbitrary neutral density. Calculations show that the efficiency of the lateral momentum transfer depends mainly on completing two processes, viz. momentum transfer via charge exchange from ions to neutrals (increasing with neutral density) and momentum transfer by the neutral gas to the side-wall (decreasing with neutral density because the mean neutral velocities approach those of the ions). As a result, the total momentum loss to the wall saturates at some neutral density level which depends on the temperature difference between hot neutrals coming from the plasma and cold neutrals from the wall, the Mach number and the distance from the wall.

1.4 Characterization of PFC Materials for NET

B.M.U. Scherzer, G. Ramos, C. Wu+

Carbon fibre composite materials doped with boron, silicon, and titanium were analyzed with respect to dopant concentration and their depth profiles before and after heating to 1800 K for 2 hours. This work was done in connection with the NET contract ERB5000 CT930032. Materials provided were produced by two manufacturers, SEP and CEREM.
The SEP materials generally show large lateral and in-depth inhomogeinity, so that only minima and maxima of dopant concentrations can be determined.
The CEREM materials doped with Si and Ti have a much finer

structure with no detectable lateral imhomogeinity. These samples, however, showed an almost linear increase in dopant concentration from the surface toward the bulk. The nominal bulk concentration could not be restored by mechanical polishing. However, due to sputtering with 3 keV D^+_3 an almost homogeneous distribution was obtained at 800 K. At higher temperatures the near-surface dopant concentration may increase above the bulk value.
Pwe heating treatment at 1800 K did not show any appreciable influence on the boron and titanium concentration distribution. In Si-doped materials a decrease of dopant concentration is observed near the surface.

2. CONFINEMENT DATA BASE ACTIVITIES

2.1 ITER H-Mode Threshold Database

J.A. Snipes[1], R.S. Granetz[1], M. Greenwald[1], F. Ryter, O.J.W.F. Kardaun, U. Stroth, A. Kus, J.C. DeBoo[2], T. Carlstrom[2], D.P. Schissel[2], K. Thomsen[3], D.J. Campbell[3], J.P. Christiansen[3], J.G. Cordey[3], Y. Miura[4], N. Suzuki[4], M. Mori[4], T. Matsuda[4], H. Tamai[4] , T. Takizuka[4], S.-I. Itoh[4], T. Fukuda[5], Y. Kamada[5], T. Matsuda[5], M. Sato[5], T. Takizuka[5], K. Tsuchiya[5], S.M. Kaye[6] ([1]Alcator C-MOD), ([2]DIII-D), ([3]JET), ([4]JFT-2M), ([5]JT-60U), ([6]PBX-M)

This year the threshold database was significantly improved by the addition of new data from DIII-D and PBX-M under boronized conditions and by the first contribution from 4 new devices: Alcator-CMOD, COMPASS-D, ASDEX Upgrade and later JT-60U. The new data from DIII-D and PBX-M show a threshold power which is a factor of about 2 lower than the previous ones. Previous JET discharges performed with heating powers close to the threshold were selected, also yielding for this device a lower threshold than last year.

The DIII-D threshold power is now in good agreement with the value obtained last year in ASDEX Upgrade, now included in the database. The contribution from Alcator-CMOD extends the density and magnetic field by factors of 4 and 2, respectively, reaching values comparable to those of ITER. The contributions of COMPASS-D and JT-60U extend the ranges of major radius (R) and aspect ratio. The analyses performed this year with the new data do not yet include the data from JT-60U. They were guided by dimensionless considerations which lead to two possible expressions compatible with the observations made in single devices: more or less linear dependence of the threshold on magnetic field and density. These are: (1) $P_{thres} = 0.025\bar{n}_e^{0.75} B_T S$ and (2) $P_{thres} = 0.4\bar{n}_e B_T R^{2.5}$ MW 10^{20} m^{-3} T m, where S is the plasma surface area. The plots of heating power versus these expressions are interpreted as H-mode existence diagrams: the lower boundary of discharges which achieved the H-mode is considered to be the threshold.

These results yield lower threshold values than previously. This is in particular due to the new data and to the interpretation of the existence diagrams. The extrapolation to ITER with the EDA design parameters at a density of 0.5 $\cdot 10^{20}$ m^{-3} yields about 100 MW and 200 MW for expressions (1) and (2), respectively.

2.2 Confinement Analysis Based on the ITER H-Mode Data Base

O. Kardaun and the H-mode Database Working Group

Offset-linear scalings were derived on the basis of the ELM-free standard dataset (N = 858) of the global confinement database (ITERH.DB2). The scaling (presented at the EPS) gives 0.0117 $I_p^{1.0}\ B_T^{0.50}\ \bar{n}_e^{0.75}\ M^{-0.25}\ R^{3.2}\ \kappa^{0.05}$ for the linear and 0.0493 $I_p^{1.0}\ B_T^{0.30}\ \bar{n}_e^{-1.0}\ M^{2.0}\ R^{-1.0}\ \kappa^{2.3}\ P_L'$ for the offset term of the thermal energy (on log scale, rmse = 11.1 %). The difference in exponents between the offset and linear terms are in accordance with the effects of interaction reported previously. The fractional reduction in rmse w.r.t. ITERH.93P (about 20 %) and confidence intervals for the exponents indicate that a simple power law is empirically clearly rejected by these data. Such a scaling may still be used for zeroth order and (in comparison with offset-linear scalings) conservative extrapolations for future devices. A strong isotope dependence of the linear term and a small one of the offset term is in agreement with results found previously at JFT-2M, and accords well with various discussions on this topic between JET and ASDEX, as well as recent TFTR D-into-T supershot experiments.

3. MODELLING OF DISRUPTION-CAUSED WALL EROSION

L.L. Lengyel, P.J. Lalousis* (*IESL.FORTH, Heraklion, Greece), P. Spathis

The major results of scenario calculations are as follows:
The erosion rate is rather high as long as the particles originating from the disrupting plasma reach a practically unshielded surface, and rapidly decreases as soon as a vapour layer forms over it. The erosion rate strongly depends not only on the energy flux carried by the plasma particles but also on the particle energies and the energy distribution function of the incident particles. Particles of the high-energy wing of the distribution function penetrate deep into the vapour shield and determine the intensity and duration of the initial vaporization burst. Monoenergetic beams deposit their energy as soon as a vapour layer forms, at some distance from the solid surface, causing erosion rates and vapour shield characteristics qualitatively and quantitatively different from those corresponding to thermal plasmas.

Since the vaporized particles, after being ionized, form a high-beta substance, the presence of the magnetic field substantially affects the evolution dynamics of the vapour layer and the resulting erosion rates.

4. HEATING SYSTEM DESIGN WORK

4.1 ICRF System

M. Brambilla, J.-M. Noterdaeme, IC Group

The work for ITER in the ICRF area concentrated on three aspects:

Participation in ITER-defined tasks in the area of design of the ICRF system and of screenless antennas, validation of computer codes and preparation of the European contribution to an ITER technical meeting and workshop on heating and current drive. Support for the design of the IC system was provided in the form of coupling calculations for the antenna and calculation of power deposition profiles for the different heating/current drive scenarios envisaged for ITER. During this work, the codes were further developed and improvements to increase the computational speed were incorporated. (See theory of ion cyclotron heating, Tokamak Division). The variational principle for IC antennas was extended to handle arrays so that the mutual inductance of coupled loops can be evaluated. The treatment of radial currents in feeders and shorts was also improved as required to deal with antennas in very large vessels. Self-consistent 3D calculations for the violin antenna (a long antenna that is resonant at the different frequencies required for the several heating and current drive scenarios proposed for ITER) indicated that 3D effects may be important and that further analysis is necessary. In the area of Faraday screenless antennas an informal meeting of representatives of the different machines which have done or are planning screenless antenna IC experiments was organized during the IAEA meeting in Seville to assess why some experiments could operate without screen and others could not. The hardware required to perform the tests in ASDEX Upgrade was designed and fabricated and first experiments are envisaged for early 1995. In 1993, an assessment of the codes available in Europe to calculate antenna coupling and power deposition profiles was started. The comparison of the codes is progressing, providing insight into their domain of applicability. This comparison will be extended in 1995 with the inclusion of the US and possibly Japan.

4.2 NBI System

J.H. Feist, B. Heinemann, E. Speth, Technology Division

In the frame of ITER EDA task D71, in which an outline design of a neutral beam injection system (beam energy 1 MeV, neutral power 50 MW) was made, two problems were investigated: the magnetic shielding of the beamline and a double gate valve between the box and torus. The ITER magnetic field at the position of the injector is $\approx$ 1 kG. The necessary reduction to <1 G from the source to the end of the neutralizer is obtained by magnetic shielding in two steps: passive shielding, consisting of 30 cm thick iron walls on both sides of the injector, and a double wall of very soft iron (20 cm / 10 cm thick, 5 cm air gap) around the injector (3.5 m in diameter), which reduces the field to less than 10 G. This residual field has to be compensated with actively controlled coils. Further calculations for this concept, which have to include the effect of various openings, will be carried out with the PROFI computer code . To separate the injector box from the tokamak for maintenance purposes, an all-metal-sealed double gate valve has to be installed inside the cryostat, which acts as a double containment. This valve, which has an opening of 1.6 $\times$0.6 m^2, has to withstand a pressure of up to 20 bars in the event of an accident. Various valve types, sealing concepts and pressure elements for the movement have been investigated in principle. Considerable development is found to be necessary for this component.

4.3 ECRH and ECCD System

T. Graubner, W.Kasparek, H. Kumric, IPF, University of Stuttgart

At the end of 1993, a concept for an optical launcher for a 50 MW ECRh/ECCD system on ITER was elaborated. On the basis of this concept, a more detailed design study was undertaken. Optimization of the system with respect to high beam quality, shielding of sensitive components, reasonable thermal loading of the mirrors, and easy maintenance was done. In particular, beam-forming techniques to minimize the beam divergence and simultaneously reduce the peak power were investigated. Among the different methods under study, namely the use of HE_{1n} mode mixtures in the feed, integration of phase-modifying reflecting surfaces into the beam path, and shaping of the total beam profile by optimizing size, location and direction of the individual beams on the common antenna mirror, the latter method has proven to be most suitable for ITER.

This led to an antenna which can be switched between perpendicular launch for heating and fixed oblique launch for current drive, which is characterized by good localization of the power in the centre of the plasma (FWHM of the total beam < 0.5 m), a relatively small aperture in the first wall of 0.14 m^2 (average power density in the port 360 MW/m^2) and a tolerable microwave dissipation on the deflecting mirror near the first wall (< 370 W/cm^2, if a beryllium-coated mirror at 200 C is assumed).

Simultaneously with these investigations, work on a launcher which allows continuous change of the injection angle between 20° and 35° continued. Depending on the space available between the magnetic field coils, it was shown that in this case it may also be possible to inject 50 MW with a single launcher. Division of the power into two launchers can be envisaged if the available space is insufficient for a 50 MW launcher.

STELLARATORS

IPP's activities in the stellarator field are concentrated on exploiting the WENDELSTEIN 7-AS experimental facility and on developing the next-step facility in the WENDELSTEIN line, WENDELSTEIN 7-X. Work on the first topic is done by Experimental Division 3, headed by F. Wagner, work on the second topic by Experimental Division 2, headed by G. Grieger.

W7-AS was newly equipped with a set of symmetrically installed limiter tiles (two in each module) which allowed to study the island divertor concept for particle and power exhaust in a first approach. The island divertor scheme will be one of the exhaust principles foreseen for W 7-X. It has clearly been documented that the magnetic structure at the edge is determined by the chain of natural islands of the configuration and that the geometrical aspects are close to the known vacuum configuration. These topological studies have been extended to higher plasma pressure and to larger shear more comparable to the situation of W 7-X. The outcome of these investigations gives confidence into the efficiency of the island divertor to handle larger power fluxes in a controlled manner. First attempts were made to model the edge plasma parameters. Studies have also been started to explore the specific island edge topology for the possibility to exhaust power by impurity radiation. The large number of X-points and the island confinement may be the naturally provided potential.

Plasma heating at 2^{nd} harmonic O-mode was demonstrated at 140 GHz. This novel result implies ECRH operation up to a density of 2.5×10^{20} m^{-3}. This allows to utilise the stellarator prospects of uncompromised high density operation also with ECRH.

H-mode studies concentrated on the operational window. With ECRH, the density threshold is found to increase with heating power. The H-mode develops in small windows of the accessible iota range. These operational islands are characterised by a negative electric field already prior to the H-mode and a distinct maximum in space potential at the separatrix.

The powerful 140 GHz gyrotron was used for collective Thomson scattering from thermal waves in the plasma. This technique allows the determination of the ion energy distribution and - in case of a Maxwellian distribution - of the ion temperature. This diagnostic has a high potential to explore α-particle dynamics in future DT devices and is therefore a rather competitive area of research. Thanks to the excellent collaboration between the IAP in Nishny Novgorod, the IPF Stuttgart and the W7-AS ECRH team, the feasibility of this scattering technique in a large fusion device was demonstrated.

With respect to W 7-X, work concentrated on the elaboration of the Phase II Proposal which was ready for submission to Euratom in June 1994. Referring to Phase I, a small re-definition of the coil shapes provided more space in the divertor region and the "sweep coils" operated in d.c. fashion as "control coils" allowed variations of the boundary structure by effecting the radial distribution of shear. A flexible divertor arrangement was developed with the goals of stationary operation already from the beginning of the exploitation phase and a throughput power of 10 MW. Such a flexible solution for the divertor and the necessary pumping capability was found indeed. With neutral injection, it was decided to use W 7-X replicas of ASDEX-upgrade beam lines which initially will be equipped with one Pini each, but which are prepared for each accepting three Pinis more so that for the Stage II heating a NBI power of 20 MW can be reached.

A contract on a DEMO coil was launched and a DEMO cryostat designed. The DEMO coil will provide information on all details of the coil production process and on the behaviour of the coil under overload conditions. The DEMO cryostat will yield detailed information on all cryogenic questions and on the feasibility of ports. The development of a cost-effective superconductor for W 7-X progressed; STAR coils made from one full double layer length were tested in the STAR test facility of KfK.

Work on the reactor properties of HELIAS-type stellarators was intensified as a result of the interaction with the W 7-X Ad Hoc Groups. Neoclassical and anomalous contributions to the transport were considered and a self-consistent electric field included. ECRH at 140 GHz was envisaged as start-up heating. Line radiation is expected to clamp the boundary temperature to rather low values and to shield the divertor plates from excessive loads. All the results support the attractiveness of Helias reactors.

Further work concerned H mode studies, contributions to the American MHH studies and quasi-axisymmetric tokamaks.

WENDELSTEIN 7-AS

(Head of Project: Prof. Dr. Friedrich Wagner)

1. OVERVIEW

After about six months of assembly and maintenance work experiments at W7-AS were resumed in March 94. The support structure of the modular coil system has now been reinforced to keep displacements of the coils within permitted limits. Operation is now possible without severe restrictions.

Additionally, W7-AS was equipped with a second limiter system adapted to the fivefold periodicity of the magnetic configuration. Its major task is to provide a nearly symmetric boundary layer suitable for edge physics studies and to protect the inboard wall and wall installations. After improving the alignment of these limiters the previous main limiters were removed, so that the inboard limiters serve as main limiters. The higher toroidal symmetry of this arrangement results in a more uniform density decrease in the plasma boundary layer and allows more exact investigation of the natural islands at the plasma boundary.

Successful particle and power exhaust under long-pulse and steady-state operation in W7-X and a reactor require the development of a divertor. For an island divertor based on natural islands at the stellarator edge, it is of decisive importance whether these islands remain fixed in geometry with increasing plasma pressure and secondary currents. Detailed studies on W7-AS at different pressure levels and various shear values have revealed rather promising results.

Detailed analysis provided new insights into confinement and transport, as well as into modes and fluctuations and their causal connection.

NBI is being upgraded from four to eight sources, which will be available in spring 95. Deuterium injection was tested for the first time in W7-AS.

ECR was successful both in heating and diagnostics. A clear heating effect was measured with 140 GHz 2nd harmonic O-mode heating in a plasma density well above the cut-off for X2 mode launch. Thus the density range in W7-X for ECRH operation can be increased to 2.5×10^{20} m^{-3}. Likewise for the first time, ECCD experiments with 140 GHz in high-density plasmas were carried out. A premiere, too, was the demonstration that a gyrotron can be used to measure the ion feature in a fusion plasma by collective Thomson scattering, this being important for investigating the velocity distribution of α-particles in D-T plasmas as under way on JET.

Further diagnostic developments include periodic multichannel Thomson scattering, toroidal plasma rotation measurement, extension of the laser blow-off system, IR thermography and amplitude modulation for the microwave reflectometry allowing measurement of the density and density fluctuation profiles simultaneously.

2. EXPERIMENTAL RESULTS

2.1 Boundary Layer and Plasma-Wall Interaction Studies

2.1.1 Edge configuration

For $\iota_a = n/m > 0.4$, the vacuum magnetic field configuration is bounded by a 5/m "natural" chain of islands. Due to the small shear, their symmetry, radial position and widths very sensitively depend on the actual ι choice and, in particular, on the radial ι profile. The latter, on the other hand, is influenced by all types of plasma currents. In order to get a reliable basis for plasma edge modelling and for designing a planned pumping island divertor, it was first necessary to check the relevance of the vacuum field calculations (small deviations of the ι scale or profiles would cause strong changes of the edge structure). Of further interest was to find out whether the 5/m island chain also remains dominant for the fundamental rational $\iota = 1/2$ and for higher plasma pressures, which is a precondition for meaningful island divertor studies.

Due to the strong sensitivity of the structures to the ι profile, this information could be derived with high accuracy from relatively simple measurements of poloidal n_e (and T_e) modulations with a Langmuir probe array. The latter was placed at a fixed radius outside separatrix and covers about 1/3 of the poloidal plasma circumference ($\Phi = 72^o$, 16 tips, $\theta = 133 - 227^o$). As an example, Fig. 1 shows n_e modulations versus ι_a for net-current-free, low-β ($\approx 0.1\%$) ECRH discharges. Bright areas (higher densities) indicate closed islands nearest to the probe tips. Towards smaller ι, the islands shift radially outward until

they become intersected by the limiters, which corresponds to the left-side sharp border of the bright areas. The structure then doubles indicating the respective X-point fans (best resolved for ι = 5/9 and 5/10).

By comparing the poloidal phases of the islands and, in particular, the points of intersection with limiters (providing a sharp criterion) with vacuum field calculations, excellent agreement is found with respect to both the absolute ι scale and the radial ι profiles. This is also supported by spatially resolved H_α and camera observations of the limiters, limiter calorimetry and radial density profiles from an energetic lithium beam (Φ = 54°). The latter closely follow the calculated separatrix position, Fig. 2. As can further be seen from Fig. 1, the 5/10 structure is not significantly perturbed by the lower-order 1/2 resonance. Respective probe array measurements performed at modified shear (<β> up to 0.8%, or induced plasma current I_p = -3 kA) give, apart from deviations in detail, evidence that the

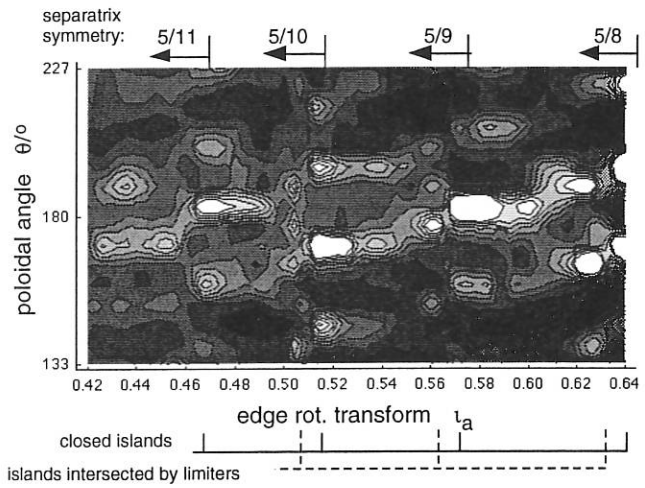

FIG. 1: Contour plot of poloidal n_e distributions in the SOL versus ι_a measured by a poloidal Langmuir probe array (s. text) for net-current-free, low-β ECRH discharges. Linear scaling, darkest: $n_e < 3\times10^{17}$ m^{-3}, brightest: $n_e > 1.5\times10^{18}$ m^{-3}. The pattern reflects the dominance of 5/m "natural" islands at the edge.

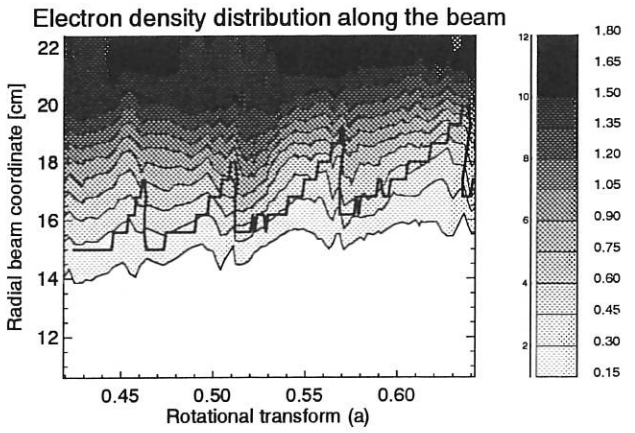

FIG. 2: Contour plot of the edge radial n_e profiles versus ι_a from the energetic lithium beam, discharge conditions as in Fig. 1. Thick solid line: separatrix position. The right-hand scale is to be multiplied by 10^{19} m^{-3}.

divertor-relevant 5/m island chains also remain dominant under these conditions.

2.1.2 *Particle transport*

For discharges with the plasma aperture bounded by the two localized, asymmetric main limiters, the n_e profiles from fast reciprocating Langmuir probes in the SOL typically show a radial modulation of the underlying exponential shape (shoulders) which changes sign after reversing the magnetic field. Examples are shown in Fig. 3. The modulation depth scales with B^{-1} and depends in a characteristic way on the poloidal probe position and limiter aperture. These features indicate a close correlation to poloidal connection lengths inhomogeneities and associated deviations of the equipotential from flux surfaces, as they are introduced by the limiters. An estimation of the respective poloidal E-field components lends support to the shoulders being caused by superimposed $E_\theta \times B$ drifts. On the other hand, the basic effect, including the change of sign after reversing the B-field, could also be qualitatively reproduced without E_θ by adding a poloidal rotation (according to radial E-fields from Langmuir probes) to a field-line-tracing Monte Carlo code with cross-field diffusion, Fig. 4. However, the most probable explanation seems to be the combined effect: plasma rotation on equipotential surfaces which deviate from the flux surfaces.

As should be expected, after replacing the asymmetric limiters by the symmetric inboard limiters (which introduce nearly homogeneous L_c) the SOL n_e profiles became much closer to exponential. Profiles taken at two different poloidal positions can be transformed to congruence by equilibrium correction of the flux coordinates (KW code), which also is a good check of the code. These features make particle transport estimates more reliable. Figure 5 shows updated SOL particle diffusion coefficients $D_\perp$ estimated from n_e profiles (fast-reciprocating Langmuir probes) at two levels of sophistication: by simple expo-

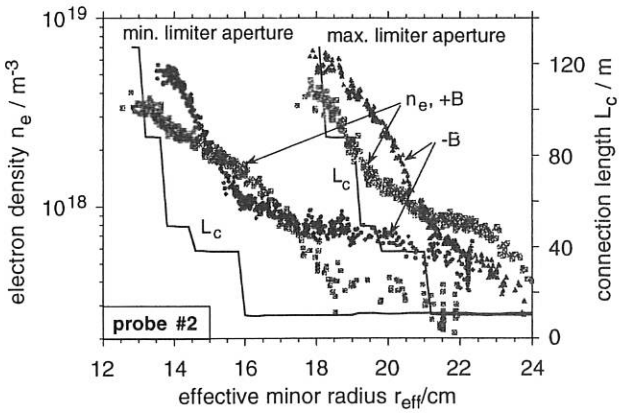

FIG. 3: SOL n_e profiles with "shoulders" from a fast-reciprocating Langmuir probe for the extreme limiter apertures and reversed B-fields. Net current-free ECRH discharges, B_0 = 1.25 T, ι_a = 0.34, P_{heat} = 350 kW, <n_e> = 1.5×10^{19} m^{-3}, probe position at Φ = 72°, θ = 0°. Calculated connection lengths L_c are indicated by solid lines. The shoulders invert when B is reversed.

nential fits and by the W7EDGE code. The latter is also 1D (radial) but considers radially varying connection lengths and takes into account varying flux tube cross-sections by parallel averaging. As can be seen from Fig. 5, the earlier published scaling of $D_\perp \propto n_{ea}^{-1}$ is well confirmed. From a respective analysis of probe and lithium beam data for limiter-bounded ECRH discharges at ι_a varying between 0.29 and 0.42, no indication for a ι dependence of $D_\perp$(SOL) was found, though the core confinement strongly depends on ι in this range.

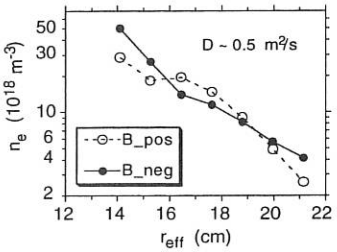

FIG. 4: Qualitative reproduction of the "shoulder" effects by field-line-tracing Monte Carlo simulation with cross-field diffusion and a superimposed poloidal rotation. $D_\perp = 0.5\ m^2\ s^{-1}$ was assumed, $v_{||}$ and v_{pol} were derived from the probe data. The profiles refer to the cases with minimum aperture in Fig. 3.

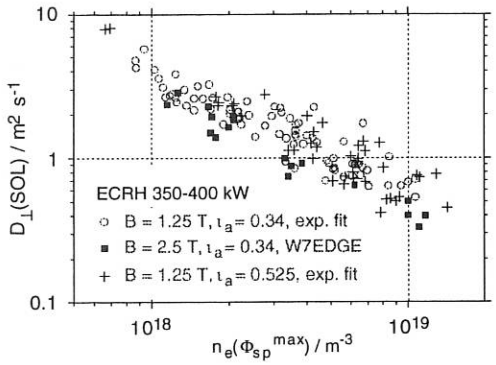

FIG. 5: Update of SOL particle diffusion coefficients $D_\perp$ versus the edge electron density n_{ea} from probe data. $D_\perp$ scales with n_{ea}^{-1}.

2.1.3 *Recycling and impact of radial plasma shift*

Global analysis of density decay experiments indicates that in case of main (top and bottom) limiter operation recycling primarily occurs at the limiters, but that a significant fraction of the particles emerging from the limiters undergo secondary recycling at the wall, e.g. via CX with plasma ions, rather than directly refuelling the plasma. This assumption is supported by EIRENE code simulations. They show a strong sensitivity of the refuelling rate to wall recycling, even for limiter bounded discharges. The total refuelling rate increases by a factor of 5 when the wall recycling coefficient is increased from 0 to 1 and the limiter recycling coefficient is kept fixed at 1.

If the plasma is shifted to the inboard limiters by means of a vertical magnetic field, improved particle control is observed. Figure 6 compares two consecutive discharges with and without vertical field. With the plasma shifted inwards the density decays faster (exponential decay time $\tau_p^* = 60$ ms compared with 200 ms), and to a lower level ($N_{p\infty}/N_{p0} = 0.13$ compared with 0.23, extrapolation from a model fit). The external gas puffing rate to maintain the same steady state density increases ($\Phi_{ex} = 5$ compared with 3×10^{20} s^{-1}) as well as the total gas consumption to build up the target density ($\int\Phi_{ex}\,dt = 1.5$ compared with 0.5×10^{20}). It is not yet clear whether the observed results are due to the different locations of the recycling sources (top / bottom versus inboard limiters), which are associated with different penetration depths of neutrals into the plasma and consequently with different CX spectra, or to a reduction of the recycling source strengths by pumping of particles at the inboard limiters or at nearby wall areas. Enhanced particle transport with the plasma shifted inwards can probably be excluded, because in parallel no degradation in global energy confinement is observed.

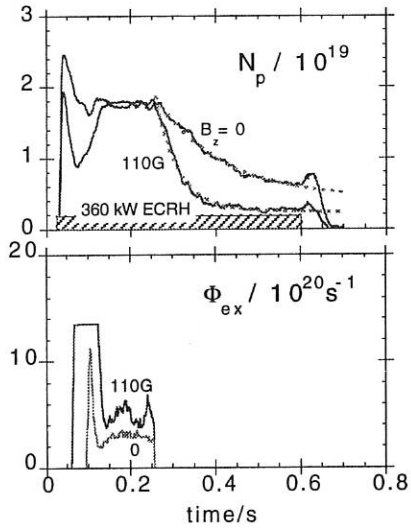

FIG. 6: Plasma electron number N_p and external gas puffing rate Φ_{ex} for typical gas switch-off experiments at different vertical magnetic fields B_z. The ECF heating pulse is indicated. Dotted curves represent fits from a recycling model.

2.1.4 *Power load distribution on the inboard limiters*

The new poloidal inboard limiters in W7-AS (similar in each toroidal field period) provide a nearly symmetric boundary layer suitable for edge physics studies and serve to protect the in-vessel installations. Each limiter consists of two blocks with 8 carbon tiles and covers a poloidal range from $\theta = 133$ to 227° close to a $\phi = 0°$ plane (triangular plasma cross-section). Their toroidal width is 12 cm. Different from the two rail limiters, this arrangement retains the symmetry properties of the magnetic configuration. Application of a vertical magnetic field results in the shifting of the power load from the rail limiters to the inboard limiters. For vertical fields ≥ 150 G at 1.27 T main field the load is almost completely directed to the inboard limiters.

Spatially resolved calorimetric (thermocouples in the limiter tiles) and thermographic measurements show almost symmetric, but non-uniform thermal load distributions over the inboard limiter surfaces. The load increases from the midplane towards the top and bottom due to increasing connection lengths in these directions (example in Fig. 7, from calorimetry). Close to

the midplane, the limiters are mutually shadowed. This is also reflected by load profiles in the toroidal direction, which show strong central peaking for tiles close to the midplane, thus indicating very short power decay lengths (Fig. 8, from thermography). Maximum specific loads could not yet be obtained with sufficient accuracy, because the viewing field of the thermographic camera is restricted to a limiter part close to the midplane only. Nevertheless, scaling measured maximum values to a heating power of 1 MW (considering higher loads as well as smaller peaking at the outer tiles), a rough estimate shows that about 10 MW/m^2 has to be expected. Similar to previous measurements with the top and bottom rail limiters, the total load on the inboard limiters was found to decrease towards higher plasma density, while the radiated power increases. The power accountability is about 70%.

In order to get more accurate thermal flux data, which is indispensable in view of the planned increase of the heating power, the thermographic camera is now rearranged to look at a whole inboard limiter.

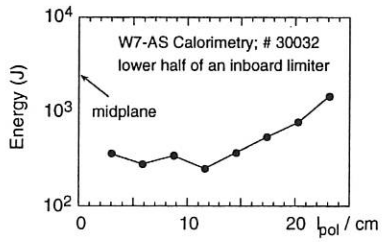

FIG. 7: Typical poloidal profile of the energy deposited on the lower half of an inboard limiter (from calorimetry). Currentless ECRH discharge, P_h = 300 kW, B_0 = 1.27 T, B_z = 125 G, ι_a = 0.341, $\langle n_e \rangle = 10^{19}$ m^{-3}. The load increases with increasing distance from the midplane.

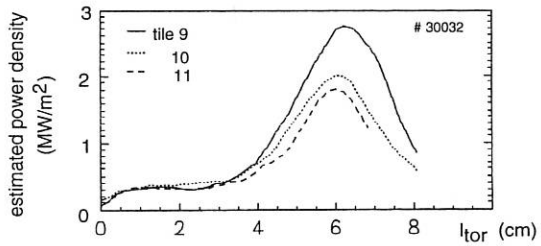

FIG. 8: Thermographically measured toroidal power density profiles across the surface of limiter tiles. Shot parameters as in Fig. 7. Tile #9 is located in the torus midplane. The centre of the tiles is at l_{tor} = 6 cm. Peaking decreases with increasing distance from the midplane.

2.1.5 *Impurity injection into the boundary layer*

In order to study the transport and radiation behaviour of particles in a region with magnetic islands, impurities are to be injected into these islands. This requires the impurity ion source to be localized with an accuracy of a few mm. This seems to be possible by impurity release from an erosion probe or by gas puffing from the leading edge of a limiter.

Prestudies were made with titanium injected into the edge plasma by an erosion probe and with nitrogen introduced from a gas valve near the wall.

Titanium injection by a reciprocating erosion probe. Using a reciprocating probe system a Ti electrode 6 mm in diameter was exposed to the edge plasma at floating potential or with temporal biasing for measuring the incident particle flux to the Ti sample. Separatrix-dominated discharges were chosen with discharge conditions which keep the magnetic configuration close to the vacuum field: P_{heat} = 360 kW, $n_e = 1 \times 10^{19}$ m^{-3}, ι_a = 0.509.

Strong effects of the impurity injection were observed in the core plasma as well as in the SOL plasma. Figure 9 shows as an example the temporal evolution of different signals (W, n, P_{rad}, Ti XII, Ti XX) with the injection at 0.39 s. Due to the injection the line-averaged density increased temporarily and was accompanied by a sudden enhancement of radiation. At this time emission of the Ti XII line and with some time delay the Ti XX line were observed, which gives evidence that the released impurity penetrated into the core plasma. The central Ti concentration reached a level of about 1%. The radiated power measured by a bolometer at a toroidal distance of about 1 m from the source increased by a factor of 3 and decreased to the undisturbed level within 30 ms after injection. The radiated power in the vicinity of the source could not be measured.

In the SOL plasma the heat flux transferred by particles to electrical probes near and far from the injection point dropped by a factor of about two due to a corresponding decrease of the electron temperature in the SOL plasma (see Fig. 10).

However, effects of impurity injection were only observed when the probe crossed a distinct location on its way into the plasma which corresponds well to the expected position of the separatrix. With the given magnetic configuration this position was reproducible within 3 mm.

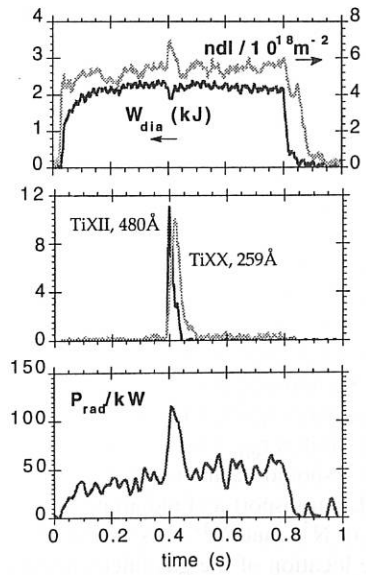

FIG. 9: The stored plasma energy, the line-averaged density, the intensities of detected emission of Ti XII and Ti XX, and the radiated power.

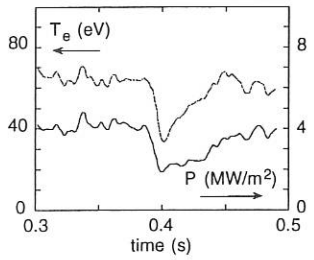

FIG. 10: The temporal evolution of the power flux transferred by particles to two probes in the SOL plasma or of the corresponding electron temperature T_e.

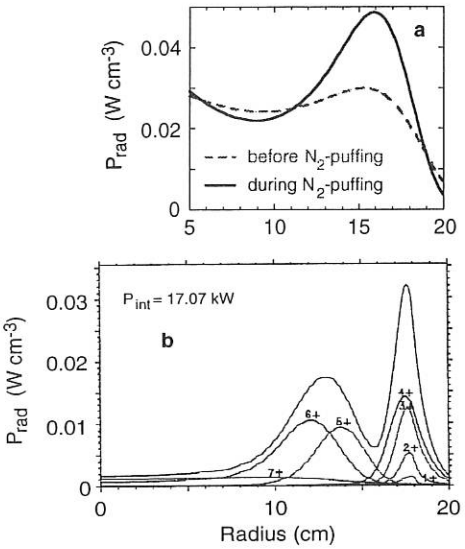

FIG. 11: (a) The radial distribution of the radiated power derived from bolometer measurements before and during gas injection. (b) The radiation profiles for nitrogen ions calculated by the IONEQ_code.

Nitrogen injection by gas puffing. Programming of the concentration of impurities is difficult in W7-AS because the device is equipped with neither a divertor nor a pumped limiter (e.g. Ne injection causes an uncontrollable density increase due to strong recycling). The experiments made at a medium line-integrated density of $n_e = 2\times10^{19}$ m^{-2} ($P_{heat} = 360$ kW, $\iota = 0.34$) have demonstrated that the control of both the plasma density and the concentration of the injected impurity in the plasma is possible with nitrogen. From the observed decay of line radiation from nitrogen ions an effective removal time t_N^* for nitrogen of about 20 ms can be derived, which is longer than the energy confinement time. Enhancement of radiation by the bolometer during nitrogen puffing was found to be restricted to the plasma boundary region, with the maximum near the radial position of the limiter, $r_{eff} \approx 0.17$ m, where ionization states of nitrogen up to 4 should occur in these discharges, as expected from the IONEQ transport and radiation code (see Fig. 11). In fact, emission of N^{3+}- and N^{4+}-ions was found at similar radial positions. The location of the gas inlet caused poloidal asymmetries for these emission lines, indicating the significance of local radiation losses near impurity sources. Further experiments will be directed to look for possibilities of a significant increase and control of the impurity radiation level at the plasma edge of W7-AS. For gas injection near or into a magnetic island a gas inlet through an inboard limiter is being prepared.

2.2 Confinement and Transport

2.2.1 *Energy confinement scaling*

The dependence of the energy confinement time on the plasma radius and rotational transform is of importance for extrapolation to W7-X and other stellarators. W7-AS is the only stellarator which can vary these parameters under otherwise identical plasma conditions. In order to deduce an improved scaling expression, a new database was assembled. A total of 296 discharges were selected from the period 1992 - 94, when frequent boronization was applied to the vacuum vessel. Only L-mode discharges at optimum confinement were selected. Care was taken to select the data so as to fill the parameter space uniformly. The well-conditioned dataset can be described by the scaling expression

$$\tau_E = 0.183\, a^{2.19}\, B^{0.7}\, n^{0.5}\, P^{-0.55}\, \iota^{0.44}\,.$$

The confinement time is found to be about improved by 15% in relation to a pre-1992 dataset.

The previous dataset was used to test the energy confinement time in W7-AS against three current confinement scaling expressions. The analyses employs Baysian statistics. The results favour Lackner-Gottardi scaling by 21 dB to ion-plateau scaling and by 37 dB over ITER-89P scaling. Work in progress is directed at a Baysian formulation of dimensionally correct scaling expressions.

2.2.2 *International stellarator database*

The new W7-AS dataset was contributed to the international stellarator database. The assembling of this database was completed with final updates for 237 discharges from ATF, 197 from CHS, 120 from Heliotron E and 13 from W7-A. The stellarator database was analysed and will be published in the near future. The deduced parameter dependences are similar to those found for W7-AS alone. An additional important result is that $\tau_E \sim R^{0.75}$.

2.2.3 *Stellarator-tokamak comparison*

Because of the differences in the magnetic configuration of stellarators and tokamaks, comparative confinement studies are an approach to learn about the importance of magnetic shear, trapped particles and plasma current on confinement.

From the similarities and differences of the confinement properties it was observed that W7-AS confinement generally trended to be more consistent with a local and diffusive transport model. For example, W7-AS energy confinement improves with density and the temperature profile does not exhibit resilience to changes in the heating location. On the other hand, W7-AS shares the unexplained degradation of confinement with heating power. In the last campaign, both density scaling and power degradation of confinement were studied in

more detail with a view to comparison with tokamak behaviour.

2.2.3.1 Density dependence of confinement

Investigation of the density scaling in W7-AS was extended to high density ECRH discharges. The experiments were done at B_t = 2.5 T and ι = 0.34. The heating power of 0.45 MW was supplied by 140 GHz ECRH. Profile information is available for the electron density and temperature from Thomson and ECE measurements and for the ion temperature from neutral particle analysers. Local transport was studied by using steady-state and heat wave analyses, both giving consistent results.

Figures 12 and 13 document the similarity which exists between the density scaling in W7-AS ECRH and tokamak ohmic discharges. The improvement of τ_E, previously observed up to $\bar{n}_e < 6\times10^{19}$ m^{-3}, saturates at higher density. This behaviour is similar to the transition from the LOC to the SOC regime in tokamaks. As in tokamaks, the saturation correlates with a saturation in the improvement of the electron transport (see Fig. 13). τ_E rises to somewhat higher densities until the ions are completely coupled to the electrons. The ion energy transport is consistent with the predictions from neoclassical theory (DKES).

It was also attempted to relate the transport coefficient to the level of density fluctuations measured by a reflectometer. For each density value, radial profiles are available in the density gradient region. The fluctuation amplitude decreases and saturates with density in the same way as χ_e does (see Sect. 2.4.3).

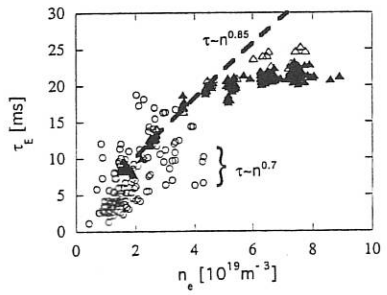

FIG. 12: Global energy confinement time of the density scan as a function of line-averaged density (triangles). A regression of the data at low density yields $\tau_E \sim n^{0.85}$ (dashed line). As a reference the data from a previous database (various discharge conditions) yielding $\tau_E \sim n^{0.7}$ are displayed (open circles).

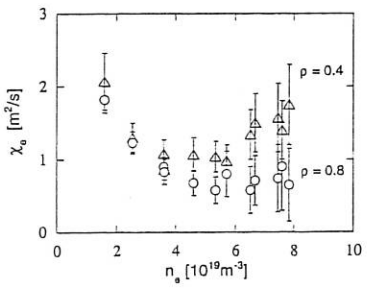

FIG. 13: Radial averages of χ_e as a function of line-averaged density. The averages were taken between r = 5 and 8.5 cm (ρ = 0.4) and r = 12 and 15 cm (ρ = 0.8).

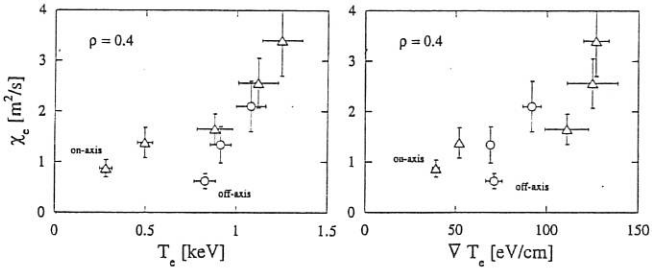

FIG. 14 Radially averaged (5 cm < r < 8.5 cm) electron heat diffusivity of the power scan as a function of electron temperature and temperature gradient.

2.2.3.2 Power dependence of confinement

Similar analyses were carried out for a power scan using on- and off-axis ECRH with the power ranging from 0.1 to 0.9 MW. The global energy confinement time of this scan is consistent with $\tau_E \sim P^{-0.55}$. The experiments were done in collaboration with the RTP team, who carried out similar experiments at the RTP tokamak. The objective was a comparative investigation of the connection of power degradation to electron temperature or the temperature gradient.

The local transport analyses of on- and off-axis heated discharges in W7-AS showed that χ_e at a plasma radius depends on the power which is deposited inside this radius, and not on the total heating power. This rules out the electron temperature as the local parameter which determines power degradation of τ_E. This can also be seen in Fig. 14, where χ_e is plotted versus T_e and ∇T_e. The transport coefficient in on- and off-axis discharges cannot be described by the parameter T_e. The data can be better interpreted with χ_e being a function of ∇T_e.

2.2.3.3 Perturbative transport studies

Perturbative transport studies are a tool to uncover a possible ∇T_e-dependence of χ_e by comparing this quantity as determined by power balance analysis (χ_e^{pb}) and heat pulse propagation (χ_e^{inc}). An explicit ∇T_e-dependence results in a significantly increased χ_e^{inc}. A remarkable difference is found between the W7-AS stellarator and the RTP tokamak. While in W7-AS agreement is found between the quantities as determined by the different methods, $\chi_e^{inc}=\chi_e^{pb}$, RTP shows $\chi_e^{inc}=$ (2-5) χ_e^{pb}. Figure 15 summarizes these findings for both machines. The RTP result can be reconciled with $W\sim P^{0.5}$ if χ_e is allowed to depend on ∇T_e. But this explanation must be ruled out in the case of W7-AS. This contradicts the power balance result and leads to the fundamental question whether it is possible to construct a local model able to explain $\chi_e^{inc}=\chi_e^{pb}$ in the case of the stellarator and $\chi_e^{inc}=(2\text{-}5)\ \chi_e^{pb}$ for the tokamak, and $W\sim P^{0.5}$ for both. For W7-AS a simple $\chi_e=\chi_e(T_e,\nabla T_e)$ does not work. The alternative to this local model is a model which allows an explicit dependence of the transport coefficients on a global parameter, e.g. $\chi_e\sim P^{0.5}$. Indications of such a dependence were found in W7-AS: ECRH switch-on and -off experiments suggested that instantaneous switching of χ_e according to $\chi_e\sim P^{0.5}$ gives a better simulation of the T_e time traces than a local $\chi_e=\chi_e(T_e,\nabla T_e)$ model. At present there prevails a difference between RTP and W7-AS which cannot be easily under-

stood in terms of a unique model. The observation that very different models, a local one and a global one, lead to the same form of power degradation is intriguing and must be further investigated.

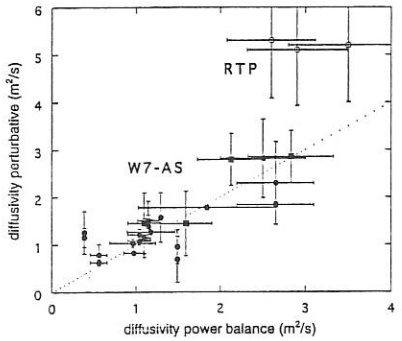

FIG. 15: Comparison of transport coefficients from power balance and heat wave studies from W7-AS and RTP.

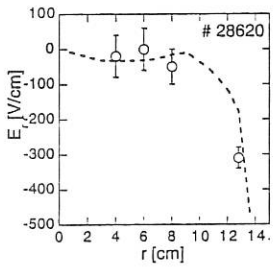

FIG. 16: The radial electric field from ambipolarity (dashed line) and as deduced from plasma rotation (circles).

2.2.4 *Ambipolar electric field*

The neo-classical transport in the LMFP regime of stellarators can be significantly reduced by the radial electric field E_r. For calculation of neo-classical transport coefficients the radial electric field is usually determined by the ambipolarity condition.

In the course of 1994 routine measurement of the poloidal plasma rotation became available. The radial electric field derived can now be compared with the ambipolar one. A systematic study has begun to test the relevance of the ambipolar field experimentally. The first discharge investigated was heated by 0.7 MW ECRH and 0.8 MW NBI, where $n_e(0) \approx 6\times10^{19}$ m^{-3}, $T_e(0) = 1.6$ keV, $T_i(0) = 750$ eV. The measured radial electric field was found to be of the order of the ambipolar one (Fig. 16). The radial behaviour is well reproduced, and the measured absolute value of E_r at the plasma edge is somewhat larger than the ambipolar electric field.

2.2.5 *W7-AS with modified mirror ratio*

Experiments in configurations with modified mirror ratios (MR = $(B_{36} - B_0)/(B_{36} + B_0)$ = 10% (*R*) and MR = -10% (*A*)) were carried out in W7-AS. Figure 17 shows the variation of W_{dia} with ι_a. The general dependence of W_{dia} on ι_a in the *R* and *A* configurations is similar to that in the standard case *S* (MR = 0.3 - 1%). Most data points are for net-current-free discharges. Those with free development of the bootstrap current I_{boot} can have differing values of W_{dia}, depending on the initial ι value. The pulse time of about 0.5 s was too short for saturation of I_{boot}. More experiments are required to extend the experiments to separatrix-dominated configurations; the minima of W_{dia} need to be better resolved for *A*. In order to compare the absolute values of the energy confinement time, the modification of the plasma radius in the three configurations has to be taken into account.

The correlation of the size of the last closed magnetic surface with the value of the mirror ratio could be confirmed by the power deposition at the two main limiters (interacting with the elliptical surface) and the inboard limiters (interacting with the triangular surface).

Discharges in the different configurations with co and ctr NBI at $\iota_a = 0.34$ were used to study the associated toroidal rotation. In the case of ctr NBI, the Ohkawa current can be seen in Fig. 18 being about 1 kA in both the *R* and *A* configurations.

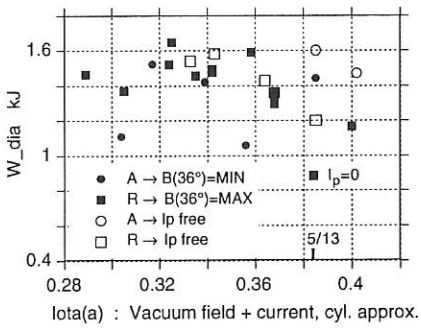

FIG. 17: Diamagnetic energy as a function of the rotational transform for ECRH plasmas (B = 1.25 T and P = 0.4 MW) in R and A configurations.

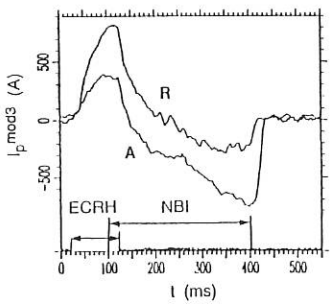

FIG. 18: Free plasma currents in the R (# 27292) and A (# 27303) configurations. A positive bootstrap current in the initial ECRH phase is offset by a negative Ohkawa current.

2.2.6 *Toroidal rotation and viscous damping*

The influence of strong toroidal magnetic field ripple on toroidal rotation was studied in the *R*, *A* and *S* configurations. In steady state, the neutral beam driving force is balanced by viscous damping, which is expected to depend on the magnetic field ripple. The measurements and calculations were carried out in collaboration with K. Ida and N. Nakajima, NIFS, Japan.

Toroidal rotation was inferred from Doppler shifts of charge exchange excited C^{5+} relative to a reference line along a single line of sight through the plasma centre intersecting the co and ctr neutral beams. The NBI of the discharges at $\iota_a = 1/3$, $B_0 = 1.27$ T were switched from co to ctr injection (400 kW) in the

1.27 T were switched from co to ctr injection (400 kW) in the course of the discharge. In cases of high ripple, toroidal rotation was found to be strongly damped (by a factor of 2 - 3) compared with the standard case with $v_\Phi \leq 15$ km/s.

The measured toroidal velocities were compared with neo-classical plateau values based on finite β NEMEC equilibrium calculations with the experimental pressure profiles. In cases of strong viscous damping (high ripple) we found reasonable agreement between the predicted and measured toroidal rotation velocities (see Fig. 19). In the standard case, however, the expected rotation from neo-classical parallel viscosity was a factor of 4 - 5 higher than the measured one (see insert), indicating the negligible role of this damping mechanism here. In this case, contributions from perpendicular viscosity have to be taken into account.

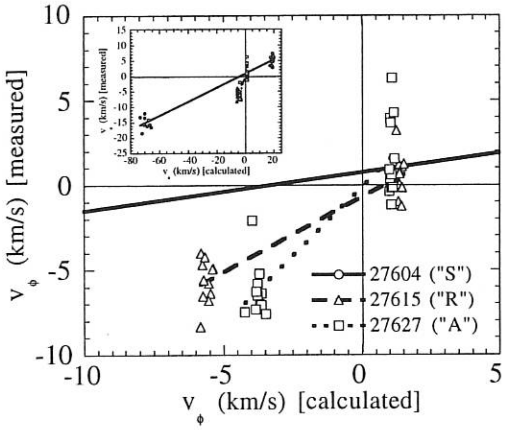

FIG. 19: Comparison of experiment and theory. The insert shows the same data on extended scales.

2.2.7 *H-mode*

The H-mode studies concentrated on exploring the conditions within the transport barrier at the edge and the operational conditions of the H-mode.

Figure 20 shows the temporal evolution of H_α, $T_i(a)$, the impurity flow velocity v_θ^I, and the floating potential of probes mounted into the limiter or that of the limiter Φ_{fl}^{lim} itself during an H-mode transition at $\iota(a) = 0.53$. The H_α trace indicates the distinct drop into the H-phase. Simultaneously, v_θ^I, (representing the E×B component as the diamagnetic contribution can be neglected), the edge electron and ion temperature (BIV), and the edge density increase at the transition. The sharp drop in floating potential at the H-transition is caused predominantly by a drop in space potential. The H-mode transition is accompanied by a stronger negative electric field at the edge. The sharp temporal development of the edge parameters can be used to explore their correlation. Φ_{fl}^{lim} scales linearly with v_θ^I in the expected manner (see Fig. 20d). At the H-transition, both v_θ^I and Φ_{fl}^{lim} jump. This jump can occur at different combinations of v_θ^I and Φ_{fl}^{lim} and can be of different magnitude.

Langmuir probe fluctuation studies in the SOL and within the transport barrier were carried out. Within the transport barrier the particle flux, obtained from correlated density and potential fluctuations, is strongly reduced after the transition. In particular the density fluctuations decrease after the transition. The decrease occurs over the whole frequency range (5 kHz ≤ f ≤ 500 kHz).

We turn to studies on the operational boundaries of the H-mode. The H-mode in W7-AS can be reached with ECRH (70 or 140 GHz) or NBI. The power threshold is lower than expected from the tokamak scaling. For $\iota(a) \approx 0.53$, the H-mode was obtained for 1.25 and 2.5 T (the two field values for 70 and 140 GHz ECRH application) with the minimal power of one gyrotron (200 kW), which corresponds to a P/S value of 0.015 MWm^{-2}.

There is clearly a lower density limit which is itself a function of heating power and other parameters. For example, the density limit of about 3×10^{13} cm^{-3} increases with larger ECRH power.

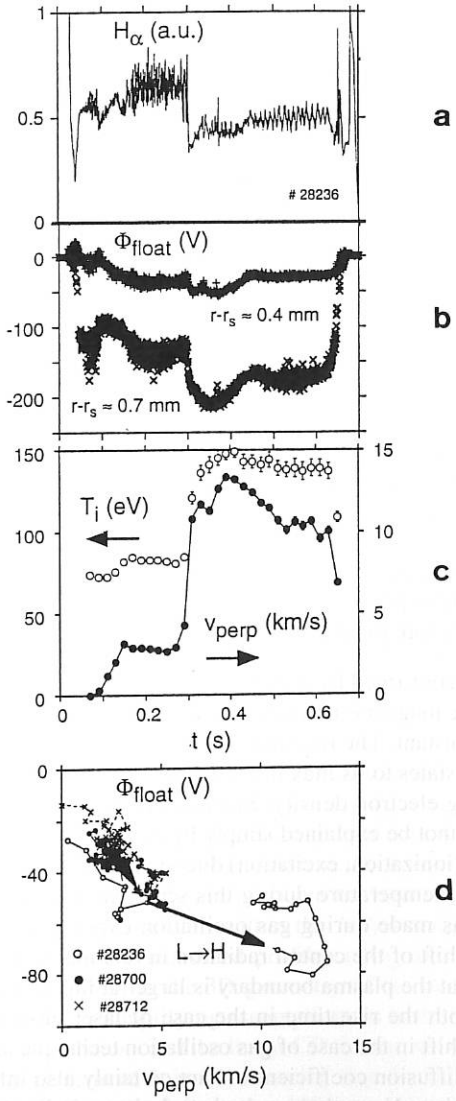

FIG. 20: (a) H_α-trace showing the H-transition. (b) Floating potential of two Langmuir probes within the transport barrier during the discharge. (c) Ion temperature $T_i(a)$ and poloidal rotation v_θ^I (BIV) at the plasma edge during the discharge. (d) Limiter floating potential Φ_{fl}^{lim} versus v_θ^I for three discharges with H-transition.

At higher heating power, T_e at the edge increases, whereas T_i drops. The coupling between T_e and T_i depends on density. For the low-density case T_i drops more strongly when the heating power is increased and the H-mode disappears. When the heating power is turned off, the H-mode transiently appears again for a short period.

At higher density the electron-ion coupling is still affected when the power is stepped up, but the plasma remains within a dithering H-mode. These investigations show a strong correlation between edge ion temperature, flow, and the H-mode threshold.

A peculiarity of the H-mode of W7-AS is its restriction to a narrow ι range $0.51 \leq \iota(a) \leq 0.53$, where it already occurs for the lowest available heating power. This ι range is characterized by the 5/9 island chain with little interference from the up-down limiters. The limiters restrict the connection length L_c at the edge to about 10 circumferences. This ι range provides good confinement also in the "L-mode". Detailed edge studies at low density in the "L-mode" have revealed that in this ι range, the space potential Φ_{sp} has a singular and precisely defined maximum. The radial E-field shows a strong step close to or at the LCFS from being positive in the SOL to negative inside the LCFS.

2.2.8 *Impurity transport*

Impurity transport in W7-AS was studied by short injection of aluminium tracer impurities into the plasma by laser blow-off and measurement of the time behaviour of their spectral line radiation. Additionally, gas oscillation experiments were performed in which the radially resolved time behaviour of the line radiation of a sinusoidal gas source (H_2S, F_3CH) was investigated.

Statistical analysis of the aluminium confinement time by laser blow-off experiments in different types of ECRH discharges indicates (approximately) $\tau \propto n^{0.9} P^{-0.8}$.

This is confirmed by density and heating power scans (Fig. 21) with the magnetic field, rotational transform and plasma radius kept constant. The rise time of the line radiation of central ionization states to its maximum value typically increases with increasing electron density. Simulations show that this observation cannot be explained simply by a change of the atomic processes (ionization, excitation) due to variations in electron density and temperature during this scan. An equivalent observation was made during gas oscillation experiments, where the phase shift of the central radiation in relation to the sinusoidal source at the plasma boundary is larger at higher electron density. Both the rise time in the case of laser blow-off and the phase shift in the case of gas oscillation technique are sensitive to the diffusion coefficient but are certainly also influenced by convection. Nevertheless, both techniques indicate better impurity confinement at higher density.

The SITAR time-dependent transport code was extended by implementing collisionality-dependent expressions for the Pfirsch-Schlüter transport and for the viscosity terms in the banana and plateau regimes. Simulations of the experimental transport results with the modified code is the subject of ongoing investigations.

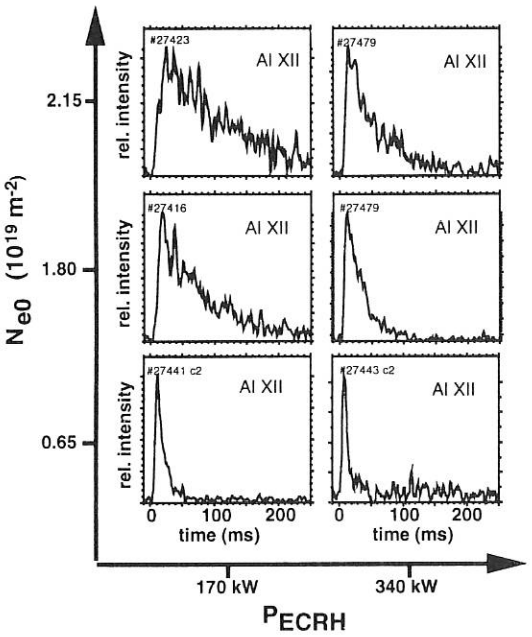

FIG. 21: Dependence of the aluminium confinement time on electron density and ECR-heating power.

2.3 Electron Cyclotron Resonance Heating (ECRH) and Current Drive (ECCD)

2.3.1 *X- and O-mode absorption with 2nd harmonic*

A good knowledge of both the total absorbed heating power and the radial power deposition profile is of great importance for transport investigations with both steady-state and perturbative methods. Coherent power modulation techniques, where the perturbed electron temperature is measured by space- and time-resolved ECE diagnostics, were applied to determine the power deposition profiles in ECR-heated plasmas with high accuracy. The analysis is particularly simple for 2nd harmonic X-mode (X2) launch, because the launched waves are completely absorbed in a single transit through the plasma at typical W7-AS parameters. The modulation frequency was scanned from 100 Hz to 10 kHz for different launching scenarios in long-pulse operation and analysed by Fourier methods. ECRH power deposition profiles were measured for two cases, one where a wide (defocused) and one where a narrow (focused) microwave beam was launched. As seen from Fig. 22, where the FWHM of the measured deposition profiles is plotted together with an extrapolation towards infinite modulation frequency, the diffusive broadening can be neglected at modulation frequencies of a few kHz. The difference in the deposition profile width inferred from the different widths of the launched beams is well resolved.

A more sophisticated evaluation of the same experimental data base makes use of a self-consistent modelling of the stimulated heat wave propagation at various frequencies taking into account fast particle effects in the particular magnetic field topo-

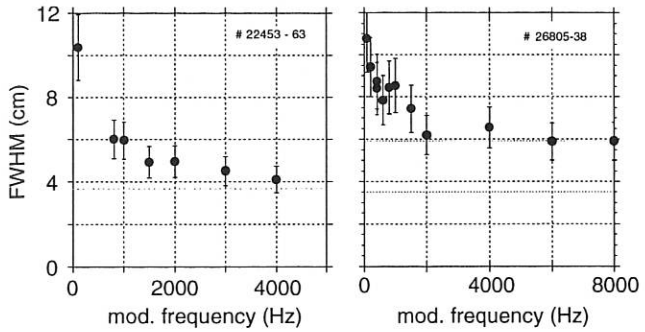

FIG. 22: Measured FWHM of ECRH power deposition profiles for a narrow (focused, left) and wide (defocused, right) microwave beam as a function of the modulation frequency.

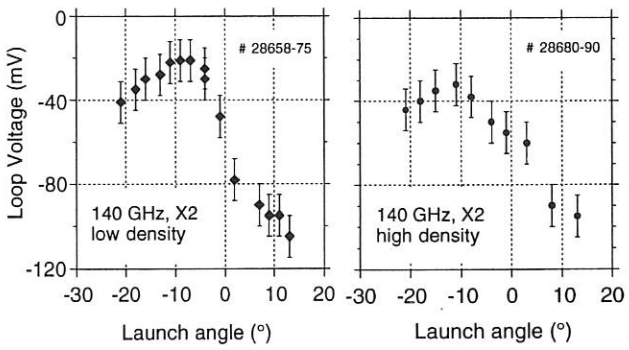

FIG. 23: ECCD with 140 GHz, 2nd harmonic X-mode launch: The loop voltage required for compensation of both the bootstrap current and the EC driven current component is displayed as a function of the launch angle for low (1.5×10^{19} m^{-3}, left) and high density (7×10^{19} m^{-3}, right).

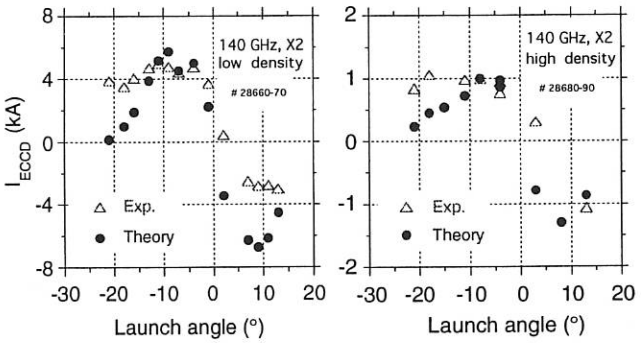

FIG. 24: Comparison of the EC-driven current derived from the measured plasma profiles and loop voltage (triangles) with the theoretical ECCD modelling (dots) for the two cases of Fig. 23.

logy of W7-AS. Some broadening of the deposition profile due to trapped particle drifts is derived from the experimental data and the total absorbed power obtained by this method is in excellent agreement with the theoretical predictions.

An extension of plasma operation towards twice the plasma density for X2-mode, i.e. towards 2.5×10^{20} m^{-3} for 140 GHz at 2.5 T, would be possible with 2nd harmonic O-mode (O2) heating. This mode has, however, a weak single-pass absorption at typical W7-AS plasma parameters but may become an interesting candidate for the W7-X next-step stellarator. We therefore examined 2nd harmonic O-mode absorption experimentally. A clear heating effect was measured with 0.7 MW ECRH power launched into a NBI-sustained target plasma with n_{e0} = 2.0×10^{20} m^{-3}, which is well above the cut-off density for X2-mode launch. An absorbed power of about 140 kW was estimated with central deposition, whereas the calculated single-pass absorption from ray tracing was 50 kW at the given parameters, indicating multipass absorption.

2.3.2 *ECCD at high density*

The existing experimental data base on ECCD was extended towards high densities by launching 140 GHz at W7-AS. Here the cut-off density limit is $n_{e,crit} = 1.2\times10^{20}$ m^{-3} for X2-mode launch from the low-field side. The small EC-driven currents at the high density can be measured with good accuracy because they are not masked by large inductive currents as in tokamaks. The plasma net current was feedback-controlled ($I_p = 0 \pm 200$ A) by compensating both the pressure-driven bootstrap current and the EC-driven current component with an inductively driven current. A deterioration of the global confinement by the current-induced change of the edge rotational transform is avoided by this method. A change of the magnetic shear at fixed $\iota(a)$ is, however, introduced, which modifies the confinement to some degree. The required loop voltage is plotted in Fig. 23 as a function of the launch angle of a narrow 0.4 MW microwave beam. Two cases with low ($n_{e0} = 1.5\times10^{19}$ m^{-3}, T_{e0} = 2.5 keV) and high plasma density ($n_{e0} = 7\times10^{19}$ m^{-3}, T_{e0} = 0.9 keV) are shown. The loop voltage at perpendicular launch (0^o, no ECCD) is required to compensate the bootstrap current alone. Positive (negative) launch angles correspond to co (counter)-current drive with respect to the bootstrap current direction. The bootstrap current I_{boot} (DKES code) and the inductively driven current I_{ind} were calculated (neo-classical conductivity) for each shot on the basis of the measured temperature and density profiles. A linear superposition of the three current components is assumed, and the 'missing current' $\Delta I = I_p - I_{boot} - I_{ind}$ is then attributed to the EC-driven current and plotted in Fig. 24 as a function of the launch angle. The residual plasma current I_p is in general negligible as compared with the bootstrap and inductive currents. The comparison with an independent theoretical ECCD modelling based on linear theory is shown for both cases. The EC-driven current is calculated within the "adjoint approach" taking into account the measured profiles of n_e and T_e and trapped particle effects in the 3D geometry of the stellarator. Keeping in mind the simplifying assumptions in both the bootstrap current calculations and the linear CD theory, we arrive at a remarkable agreement. It is worth noting that the EC-driven currents ΔI are determined from the difference of two larger quantities, I_{boot} and I_{ind}, especially in the high-density case. The absolute values of the driven current as well as the characteristics of the launch angle dependence are well described and support previous results at W7-AS in the low-density regime at 1.25 T, 2nd harmonic X-mode ECCD with 70 GHz.

2.4 Modes and Fluctuations

2.4.1 *Global Alfvén Eigenmodes*

The most prominent MHD activity during NBI in the range 15-40 kHz seems to be well explained in terms of Global Alfvén Eigenmodes (GAE), which are excited by the injected energetic particles. This type of Alfvén waves results from the low shear, which, on the other hand, leads to the absence of Toroidal Alfvén Eigenmodes (TAE) as observed in tokamaks. The stability of GAE's is an important issue for the future W7-X device and also for advanced tokamaks with extended regions of flat q profiles. Particularly in a reactor, GAE/TAE-induced α-particle losses could lead to reduced heating power and enhanced wall damage.

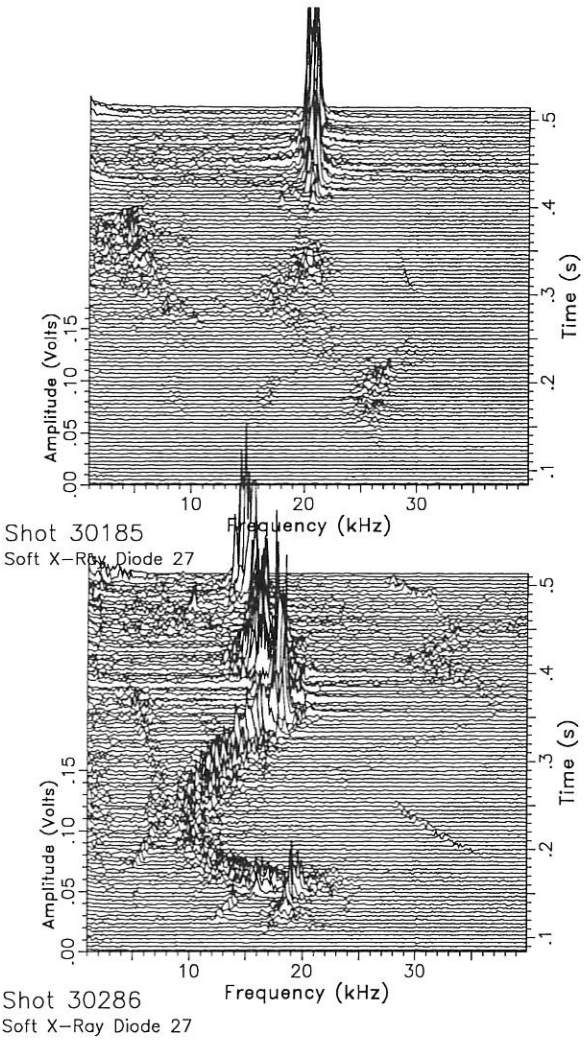

FIG. 25: Frequency spectra (soft X-ray emission) for cases with $H^0 \rightarrow H^+$ (upper part) and $D^0 \rightarrow D^+$ (lower part) injection (50 keV). Due to the different ion mass the frequencies are clearly shifted in accordance with values predicted for the (m,n) = (3,1) GAE (B = 1.25 T, $\iota \gtrsim 1/3$). The amplitudes are largest in the later phase of the discharge (high density leads to low enough Alfvén velocity, and low β leads to reduced shear stabilization).

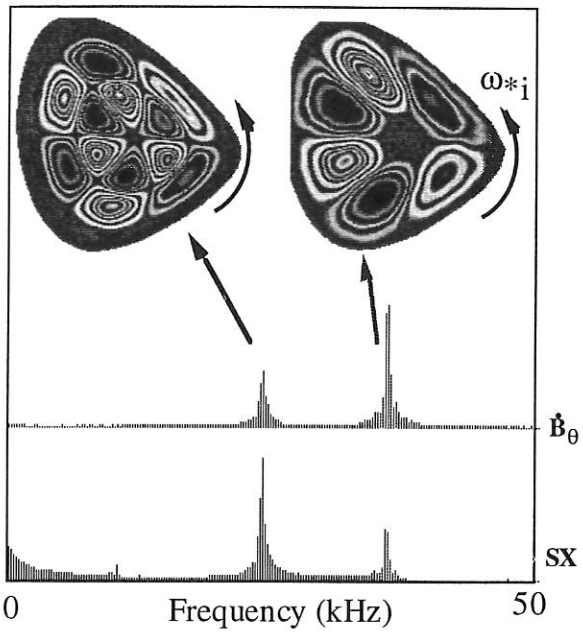

FIG. 26: GAE mode structure ((m,n) = (3,1) radial displacement) from soft X-ray reconstructions. Different radial eigenfunctions are found for the two frequency-shifted lines.

Understanding the conditions under which the GAE's are driven unstable is still an issue under investigation. These modes are preferentially excited in phases where the plasma energy has already started to decay as the density limit is approached, which is determined by the available heating power. In this case the energetic particle drive ($\propto \beta_{fast}$) is expected to decay faster than the electron Landau damping ($\propto \beta_e$). The experiments together with gyrofluid code calculations indicate that additional effects connected with changes of the magnetic shear, the Alfvén velocity, the beam deposition and fast particle profiles, and the beam slowing-down distribution can play an important role. In particular, experiments were performed where GAE's could be destabilized by lowering T_e by impurity gas puffing. Investigations of the particle-wave resonance condition were continued by comparing the different behaviour of co- and counter-injected particles and by changing the injected ion mass. No significantly different GAE behaviour was found on comparing $H^0 \rightarrow H^+$ with $D^0 \rightarrow D^+$ injection. This is expected since both the particle and the Alfvén velocities have the same mass scaling. The reduced GAE frequency in the $D^0 \rightarrow D^+$ case (Fig. 25) is consistent with the change of the Alfvén velocity and therefore can be considered as further evidence of Alfvén waves.

Although the GAE modes are nonresonant ($\iota \neq n/m$), only low-n modes, for which the helicity is closely aligned with the equilibrium field, are found in agreement with the gyrofluid calculations. Reconstruction of the poloidal and radial mode structure was achieved by combined analysis of soft X-ray, ECE and Mirnov oscillations. Satellite lines in the frequency spectra are caused by mode components with a node in their radial eigenfunction (Fig. 26).

2.4.2 *MHD stability of configurations at ι = 0.35*

The stability of W7-AS with respect to pressure-driven modes is dominated by the stabilizing influence of its vacuum magnetic well. The well can be reduced by applying a vertical field and thus shifting the plasma inwards. Previous investigations addressed the question of ideal stability and showed an experimentally relevant stability limit only for large vertical field ($B_z / B_0 \geq 0.015$). This work has now been extended to investigate the stability with respect to resistive interchange modes in the standard low-iota (ι = 0.35) configuration, including configurations with different toroidal magnetic field ripple r_t ($r_t = B_{01} / B_{00}$, B_{mn} = Fourier coefficients of magnetic field strength; r_t is roughly the negative mirror ratio MR as defined in Sect. 2.2.5).

The stability analysis using the JMC code is based on free-boundary equilibria calculated with the NEMEC code. The pressure profiles used were proportional to $(1\text{-}s)^2$ (s = normalized toroidal magnetic flux). The toroidal current was assumed to vanish within each flux surface. Figure 27 shows the stability boundaries of 4 configurations with different toroidal magnetic field ripple (r_t = 0, ±10%, -20%) which have a similar ratio of vertical field strength to mean magnetic field strength.

The standard and positive toroidal ripple configurations show the same resistive interchange stability boundaries. The decreased stability properties of the negative toroidal magnetic ripple configurations can be explained by an additional decrease of the vacuum magnetic well due to the toroidal ripple.

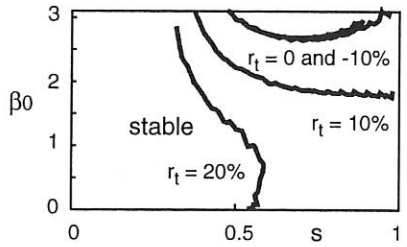

FIG. 27: Stability boundaries for resistive interchange across the plasma depending on the central β-value.

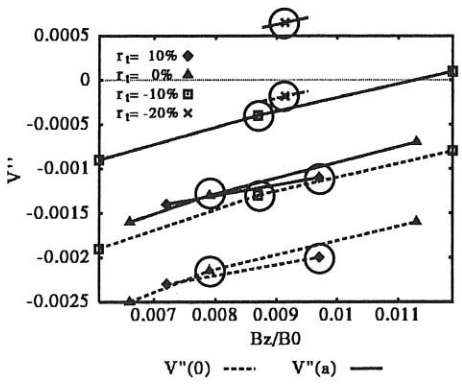

FIG. 28: Vacuum magnetic well at the plasma boundary and on axis for different toroidal magnetic ripple configurations as a function of the vertical field strength.

This can be seen in Fig. 28, where the values of the vacuum magnetic well at the plasma boundary and on axis are plotted for different toroidal ripple configurations and various vertical field strengths. The encircled configurations are those shown in Fig. 27.

Investigations considering the stability of ideal and resistive ballooning modes have been started and are in progress.

2.4.3 *Density fluctuations*

The phase fluctuations of a reflected mm-wave as measured by reflectometry contain information about the density fluctuations at or close to the probed cut-off layer. By heterodyne-detection technique the relevant phase fluctuations can be measured independently of amplitude fluctuations in the reflected beam. Due to the broadband capability of the system at W7-AS radial positions corresponding to densities 1 to 6 × 10^{19} m^{-3} are probed during a single discharge.

In the context of transport investigations at W7-AS the parameter dependence of electron density fluctuations was studied in ECRH-heated discharges by performing a density and a power scan. For each shot density fluctuation profiles are measured under stationary plasma conditions with the mm-wave frequency ramped up every 10 ms to probe different radial positions. Density fluctuations Δn are evaluated from the rms value of the phase fluctuations by means of the gradient of the density profile (Δn/Δr) at the respective cut-off layer position. Thomson scattering data are taken for the profile information.

Figure 29 shows the increase of the density fluctuation level towards the plasma edge, with the line-averaged density as a parameter. As the density increases up to 5×10^{19} m^{-3} the fluctuation level drops for all probed radial positions. No further reduction is observed for densities higher than that (compare Sect. 2.2.3.1)

A scan of ECRH heating power (0.1 MW < P_{ECRH} < 0.8 MW) was performed at two values of averaged density ($n = 2.5\times10^{19}$ m^{-3} / 4.0×10^{19} m^{-3}) in order to investigate the power degradation of energy confinement. As shown in Fig. 30, density fluctuations surprisingly decrease if the heating power is increased. A similar reduction of fluctuation level with ECRH power is observed for the electron temperature fluctuations while the electron heat diffusivity obtained from both power balance and heat wave analysis increases with heating power.

2.4.4 *Temperature fluctuations*

Our novel technique of ECE correlation radiometry, viewing the same plasma volume along two different lines of sight in a Hanbury-Brown and Twiss-like intensity interferometer arrangement, has proved the existence of fluctuations of the electron temperature in the radial range 0.55 < r/a < 0.75 in the plasma core of W7-AS. Until now only pure ECR-heated plasmas have been explored. The relative fluctuation level is below 1% and consists of clearly separable turbulent low (< 15 kHz) and high (< 150 kHz) frequency components in a ratio of about

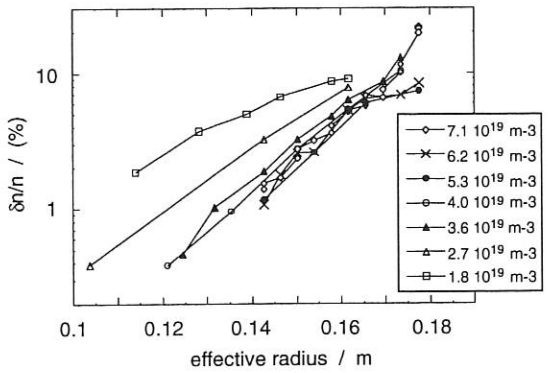

FIG. 29: Density fluctuations $\Delta n/n$ in the gradient region as a function of effective radius obtained during a density scan. The relevant line-averaged densities are given as a parameter. Note the log scale. All discharges are heated with 450 kW ECRH.

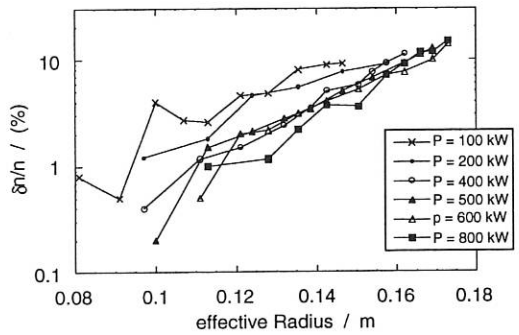

FIG. 30: Density fluctuation profiles obtained during a power scan. The average density is 4×10^{19} m^{-3} ; discharges with a lower average density ($n = 2.5\times10^{19}$ m^{-3}) show similar results.

2 to 1 of the relative amplitudes. Figure 31 shows a typical fluctuation spectrum. The two components exhibit different behaviour concerning their radial and poloidal correlations: the high-frequency component shows a poloidal velocity which has not been observed at low frequencies. A poloidal velocity of the fluctuating structure of about 4 - 5 km/s in the electron diamagnetic drift direction can be derived. For the low-frequency component a radial velocity of 50 m/s can be derived, directed from the plasma centre to the edge.

First parameter dependence studies were conducted to collect indirect evidence from parameters which are known to affect the global confinement. It was expected that a rise in the relative fluctuation level $\tilde{T}_e/T_e$ correlates with a decrease of confinement, indicating the possible transport relevance of temperature fluctuations. Of interest are scans of the density, the magnetic configuration by changing the rotational transform, and the ECRH heating power. As an example, Fig. 32 shows the dependence of the normalized fluctuation level on heating power and also plots the confinement time for comparison. The surprising result is that the fluctuation level decreases, whereas the confinement deteriorates. The density and the iota scan show the same tendency but with larger error bars.

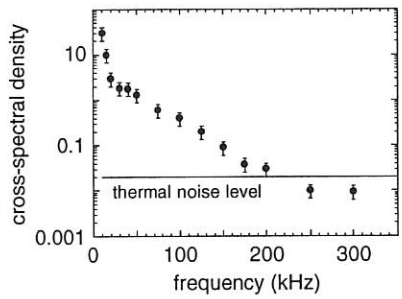

FIG. 31: Typical turbulent temperature fluctuation spectrum.

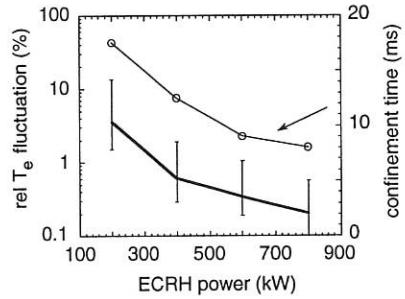

FIG. 32: The rms values of the electron temperature fluctuations and the energy confinement time as a function of the ECRH power. The central electron density is 3×10^{19} m^{-3}. The error bars give the uncertainty of the measurement due to possible cross-talk in phase and from density fluctuations.

2.4.5 *Microwave scattering*

Density fluctuations were measured by microwave scattering with resolution in both real space and wave vector space. The μ-wave diagnostic operates at 156 GHz. Four different scattering angles (6°, 12°, 40° and 50°) of forward scattering are accessible, corresponding to scattering wave vectors between 340 and 2800 m^{-1}. The useful frequency range is about ±400 kHz around the irradiated probing signal.

Parameter scans of density and power were started to explore the applicability of the diagnostic and look for potential correlations with transport. Regularly, turbulent scattering spectra are found which are symmetric around the central frequency with a bandwidth of about 100 kHz, depending on the scattering angle and density. At densities below about 3×10^{19} m^{-3} an unexpected feature was observed: in addition to the symmetric spectrum, a relatively broad (around 40 kHz) peak was observed, shifted by 140 kHz (see Fig. 33). The phenomenon is observed at all scattering angles. Especially the component antiparallel to the scattering wave vector, that means frequencies below zero, was well pronounced. The corresponding component at +140 kHz was always smaller and less pronounced at larger scatter angles. The phenomenon might be caused by poloidally moving structures. A preliminary calculation results in a velocity of around 5 km/s in the ion diamagnetic drift direction. The feature is still under evaluation.

It was attempted to use the diagnostic capabilities to determine the temporal evolution during an L-H transition. Correlations

were calculated between the scattered power within various spectral ranges and signals as obtained by H_α detectors, Mirnov coils, reflectometry and probes. Although the time resolution is approximately 100 µs, the relatively slow L-H transition in W7-AS allows no conclusive determination of the time dependence of density fluctuations with respect to the other diagnostics and the local origin of the transition.

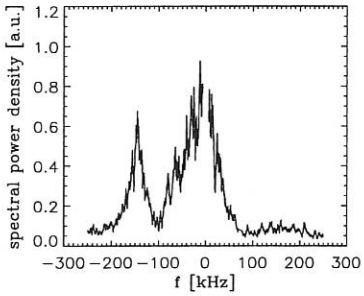

FIG. 33: The scattering spectrum as obtained in a purely ECR-heated plasma with central electron density of 2.5×10^{19} m^{-3}. The scattering angle is 50°. Besides the symmetric turbulent spectrum, an additional feature is observed shifted to -140 kHz. It might be due to a structure poloidally rotating with approximately 5 km/s in the ion diamagnetic drift direction.

2.4.6 *Fluctuations in the scrape-off layer*

Fluctuations in the scrape-off layer of tokamaks and stellarators are investigated because of their importance for the transport coefficients in the SOL and hence for the power density at the target plates of a reactor.

Measurements with arrays of Langmuir probes and observation of the H_α light from the plasma edge performed on the former ASDEX tokamak and on W7-AS provide the experimental basis for a linearized model. Magnetic field curvature and finite electrical resistivity of the sheath at the target plate or limiter are considered as fundamental components of the SOL turbulence in both stellarators and tokamaks.

While the theoretical basis seems to be understood (the model still needing further refinement by finite Larmor radius effects, realistic geometry and atomic physics effects), the usual nonlinear treatment by a mixing length estimate is far from satisfactory.

A first glance at the raw signals suggests treating the turbulence as a superposition of single events of finite extent in time and space. An algorithm was developed to decompose a multichannel signal into a sum of functions with given shape in time and space and variable amplitude, size, lifetime, velocity and position in time and space. A number of statistical analyses were performed on this database. Figure 34 shows an example of conditional averaging.

Data around about 40 selected events with large values of the ratio amplitude / size were averaged. At one side of the events with positive potential there is a cluster of negative events and vice versa. The "companions" are spread out in time. Pairs are oriented in such a way that the plasma flows radially outward between the poles.

In contrast to conventional conditional averaging, this method allows one to separate reference events and surrounding events and apply conditions on surrounding events, permitting detailed analysis of the interaction of structures in the fully developed turbulence.

Progress in theoretical understanding of turbulence must be accompanied by improvement of experimental techniques. A cornered probe array was designed to get information on radial structures in the turbulence. Langmuir probe measurements by the fast voltage sweep technique were continued.

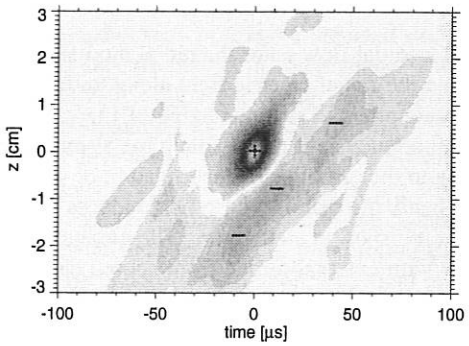

FIG. 34: Averaged surroundings of events with positive potential in the centre.

3 DIAGNOSTIC DEVELOPMENT

3.1 Periodic Multichannel Thomson Scattering

During the previous experimental phase of W7-AS preparations were made for the first tests with the new periodic multichannel Thomson scattering system using a pulsed (20 Hz) Nd:YAG laser. This system will deliver space and time resolved electron temperature and density profiles throughout a plasma discharge. Technical details of the experimental set-up have already been reported (s. Annual Reports 1992 and 1993).

The detection optics and the polychromators were aligned by simulating the laser and the observation volumes with a special lamp constructed for this purpose. The lamp was fixed on the laser axis and the volumes were imaged onto the entrance slits of the corresponding polychromators.

The alignment of the laser through the vertical ports 2.11 and 2.12 was done by means of an internal and external aperture system, an external telescope and He-Ne lasers. The internal apertures reduce the stray light from the laser, whereas the external apertures can be used to verify the alignment of the laser at any later stage.

The synchronization of the laser and the detection electronics with the plasma discharge is crucial for reliable operation of the entire diagnostic. This was done by obtaining appropriate trigger signals from the main experiment, and the time windows were chosen such as to minimize the time during which the laser and certain critical voltages of the detection electronics were activated.

Eight polychromators from a total of sixteen were tested. Their spatial distribution was: three for the plasma centre, three for the plasma gradient, and two for the plasma edge. Signals from these measurements were examined to ensure that their origin was indeed the scattered laser light in the plasma.

At present, the laboratory set-up for measuring the relative spectral sensitivities of the polychromator channels is under construction. Furthermore, the hardware required for the automatic data acquisition during the next experimental phase will also be installed.

3.2 Toroidal Rotation Measurement

Poloidal and toroidal flow enter the radial momentum balance and determine the radial electric field along with the diamagnetic flow component. The knowledge of the radial electric field is of importance as it may explain the H-mode transport barrier owing to the turbulence de-correlation of sheared flow; on the other hand, the radial electric field reduces the neo-classical ion heat transport in stellarators. The measurement of the toroidal flow with external torque from neutral beam injection allows to study anomalous viscosity and the role of the neo-classical contribution (see Chapt. 2.2.6).

Plasma rotation is measured by the spectral Doppler line shift of impurity line radiation, in W7-AS stemming mainly from boron or helium. Additionally, this line radiation is excited by charge exchange between injected beam neutrals and impurities. Background radiation can be subtracted by pulsing the neutral beam. A well-defined aperture of the neutral beam makes spatially resolved information accessible. The poloidal plasma rotation can be measured by observing line radiation in the direction of the major radius and tangentially to the magnetic flux surfaces, and the toroidal plasma rotation by observing tangentially to the torus.

To complete the old poloidal rotation measurement system, a new device for measuring the toroidal rotation was installed at the end of 1994. The impurity line radiation is guided via an optical imaging system and a quartz fibre bundle direct to the entrance slit of a 50 cm monochromator. The arrangement of the fibres is such that slit image curvature effects are neglected. A Peltier-cooled CCD camera system is attached directly to the monochromator for the near-UV and visible spectral ranges. The camera is controlled by a PC, first processing of the raw data is done here, and finally the data can be transferred via FTP to UNIX machines for further processing.

3.3 Extended LBO System at W7-AS

The existing laser blow-off system at W7-AS was duplicated and the new unit positioned almost opposite, having the same port geometry and plasma cross-section (Fig. 35a). The new location is in the deposition area of the neutral heating beams and in the direct vicinity of some spectroscopic diagnostics (VISPEC, VUV rotating mirror probe, grazing incidence spectrometer) which can be used to diagnose the ablation beam.

The lasers of both systems are identical single-shot multimode ruby lasers (pulse width 30 ns at max. energy 1.5 J) which are focused through a quartz glass window onto the target inside the machine. The 49×49 mm glass target plate is evaporated with a few microns thin layer of the investigated material (Al, Fe, etc.) on the plasma-facing side. The laser beam transmits the glass target from the rear side and ablates the material at the plasma-facing side. The short beam of impurity atoms enters the plasma and can be studied spectroscopically. The laser energy can be changed by varying the charging voltage, and the spot size by defocusing the beam onto the target.

Both systems were supplied with a small optical observation port (Fig. 35a) at the target chamber which observes the ablation beam direct from the rear side. The light from both systems was connected via fibre light guides to the entrance slit of one visible spectrometer, which allows spectrally selected observation of only one or both systems (if the two systems are fired at different times). Measurements of the time behaviour of radiation from lowest ionization states (or even neutrals) arising from the early penetration process of the investigated material into the plasma were performed and provided information about the beam quality. This is important for simulation of the time behaviour of the line radiation from the following higher ionization states during the transport process to the plasma centre. Observation of Al I,II,III lines shows that the LBO beam consists of a quick component of neutral atoms reaching the plasma within approximately 0.2 ms after the laser has fired and a broad slow component of clusters arriving up to 2 ms later (Fig. 35b). The relative abundances of both components depend on the laser energy density on the target, the material and the thickness. Nearly pure atomic beams could be produced with high laser energy density and the use of thin targets (0.5 micron).

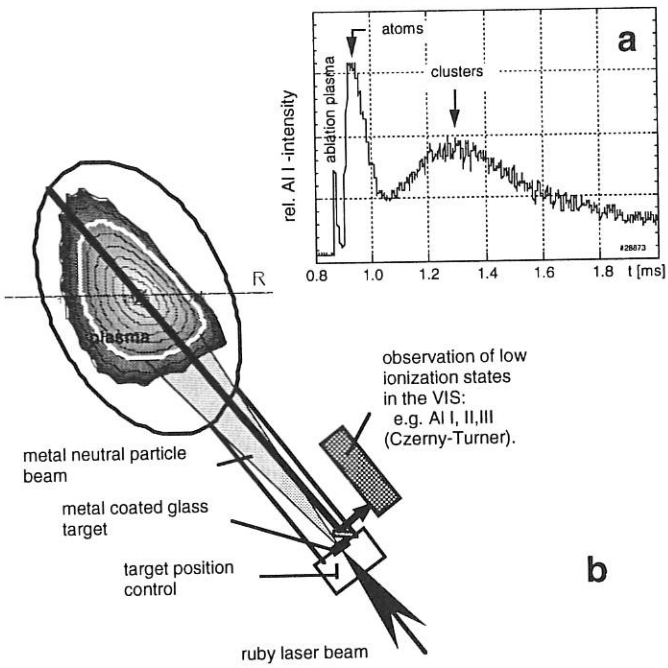

Fig. 35: (a) Time trace of Al I (394.4 nm) line radiation during penetration of the LBO beam into the plasma, (b) Set-up of the LBO systems at W7-AS.

3.4 Collective Thomson Scattering with 140 GHz Gyrotron Radiation

Collective Thomson Scattering (CTS) of EM radiation from thermal plasma fluctuations, in principle, allows one to measure the velocity distribution function of plasma ions and their composition in the plasma. Experiments with IR and FIR lasers showed the basic capability of CTS. The lack of proper sources, however, prevented CTS from being established as a routine plasma diagnostic. A joint project was started in 1992 with the Institute of Applied Physics (IAP), Nizhny Novgorod, Russia, and Institut für Plasmaforschung (IPF), University of Stuttgart, to investigate the basic capability of high-power gyrotrons (electron cyclotron MASERS) as narrow-band sources for CTS. Similar proposals were made for CTS at the JET (Culham) and FTU (ENEA Frascati) tokamaks. The W7-AS project was granted special financial support by the German Federal Government. We have now demonstrated for the first time that a gyrotron can be used to measure the ion feature in a fusion plasma, which offers promising prospects for future CTS diagnostics.

The experiments were performed in the W7-AS stellarator with a source power of 0.45 MW at 140 GHz. As plasma start-up in W7-AS is realized with 70 GHz ECRH, the magnetic induction was restricted to resonant values of 1.25 T (2nd harm., 70 GHz) or 2.5 T (1st harm., 70 GHz). Operation at 1.25 T provides optimum conditions for scattering, because the ECE background, which is at 4th harmonic for 140 GHz, is of the order of a few eV only. The ion feature was measured in the parameter range of 0.4×10^{20} m^{-3} < n_{e0} < 0.9×10^{20} m^{-3} and 0.3 keV< $T_e \approx T_i$ < 0.5 keV in NBI-heated discharges with tangential injection. The measured spectra are well represented by theoretical modelling. Operation at 2.5 T (2nd harm. at 140 GHz) is characterized by a strong ECE background and resonant absorption of incident and scattered radiation. The scattered spectra show a broad nonthermal feature in the frequency range < 0.5 GHz, where the ion line is expected. Additional injection of a perpendicular 22 keV neutral beam destabilizes a lower hybrid wave, which is clearly detected by CTS as a narrow spectral peak on top of the broad-band spectrum. The driving mechanism of this instability requires further investigation.

The measurements of the ion feature constitute a proof-of-principle experiment for investigating the velocity distribution of α-particles in D-T plasmas as under way on JET.

3.5 IR Thermography on W7-AS

An infrared camera system (detector: 120×160 pixels InSb focal plane array; detection wavelength: 4.7 + 0.5 μm; spatial resolution: 2 mm/pixel; time resolution: 20 ms/frame; arrangement: viewing upper half of one inner limiter; data acquisition: PC-based, connected to a Micro VAX or a Sun workstation) went into operation in autumn 1994. The IR camera is based on a highly sensitive indium antimonide focal plane array working at liquid nitrogen temperature. The optical system consists of a sapphire window and a multi-element lens.

The camera is calibrated and thus the absolute surface temperature can be determined.

3.6 Edge Density Profile Measurements by AM-Reflectometry

At W7-AS a broadband heterodyne reflectometer is being operated to investigate density fluctuations from the observed phase fluctuations of the reflected mm-wave. This diagnostic capability was extended by incorporating amplitude modulation (AM) of the signal launched to the plasma. The measured phase delay of the AM envelope function, i.e. the time delay of the reflected mm-wave, is used to reconstruct density profiles. As both the carrier and AM envelope phases are measured, the density fluctuation profile and density profile are obtained simultaneously. Tuneable solid-state oscillators in combination with active frequency multiplication allow the entire frequency range (76 to 110 GHz, corresponding to densities 1 to 6×10^{19} m^{-3}) to be probed within less than 1 ms. The density profiles obtained with this diagnostic agree well with Thomson scattering and lithium beam data (Fig. 36a). The use of the X-mode together with the magnetic field gradient in the toroidal plane chosen ($\phi = 33^{o}$) also gives access to the more inner part of the profile, where the gradient is rather small. Figure 36b shows the density profile development during an NBI-heated discharge, for example. At the beginning of the discharge with still rather low densities the probed part of the profiles ranges up to 6 cm into the plasma. For t > 200 ms even the highest frequencies used are in cut-off. From 300 to 500 ms, where density ramp-up is controlled by additional gas puffing, the probed gradient region is shifted further outward. For profile recovery by numerical Abel inversion one has to assume an edge profile up to the

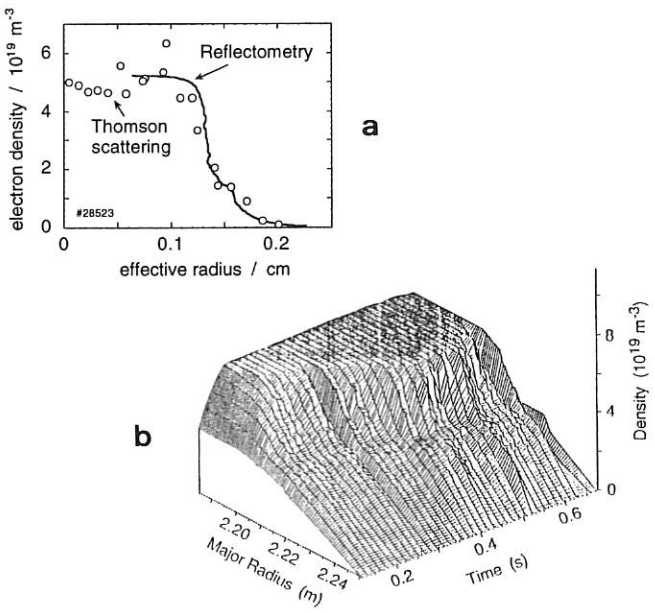

FIG. 36: (a) Comparison of the density profiles obtained from reflectometry (solid line) and Thomson scattering (dots) for a discharge with combined heating (NBI and ECRH). Reflectometry gives a high spatial resolution but mainly probes the gradient region. (b) Profile development during an NBI-heated discharge.

lowest probed density. It is fitted to the probed part via the gradient. At least one free parameter remains in the position of the plasma edge, i.e. where the density is equal zero. The gradient of the obtained profiles is rather independent of this initialization profile, while the computed absolute plasma position more clearly depends on this assumption.

3.7 LENA

The Low-Energy Neutral particle Analyzer (LENA) has been running during experimentation on W7-AS. Charge exchange neutral fluxes and energy distributions are taken in the energy interval of 20 to 1300 eV every 145 µs using a time-of-flight arrangement.

LENA data were taken for almost every shot. The reaction of the low-energy CX fluxes and spectra to variation of the main plasma parameters was documented. The determination of T_i profiles near the plasma edge is still an elaborate procedure and was possible only in a few cases.

After removal of the old main limiters and operation with symmetric "inboard limiters" the CX fluxes increased considerably. Also the variation of the CX spectra with $\bar{n}_e$ is quite different. This indicates that the neutral atom distribution in the vicinity of LENA has drastically changed. A new determination of the spatial distribution of the neutral gas sources for the calculation of T_i profiles is therefore required.

3.8 Re-absorption-corrected CX-measurements

The ion temperature profile is important input to confinement studies. Especially in high-density and NBI discharges precise measurements are mandatory for such studies. At W7-AS, the ion temperature is routinely deduced from Neutral Particle Analyzers (NPA). With increasing density the NPA spectra are deformed due to re-absorption of the neutral particles on their trajectory out of the plasma. An improved analyses code (CIT) has now been developed which takes into account re-absorption by ionization and charge exchange. CIT simulates the active beam and the neutral particle fluxes in the full 3D geometry and has the capability of inferring a unique T_i profile which has to describe simultaneously a set of spectra taken along different lines of sight. This method reduces the ambiguity of the T_i determination and, furthermore, systematic deviations of energy channels can be diagnosed (see Fig. 37).

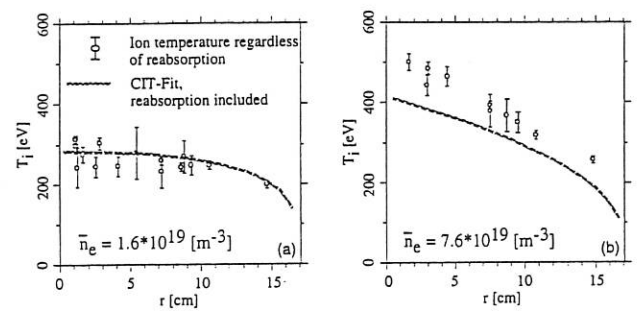

FIG. 37: Comparison of the routinely determined ion temperature regardless of re-absorption with a profile as inferred from CIT. At low density, the results are consistent (a), while at densities > 6×10^{19} m^{-3} the inclusion of re-absorption leads to smaller T_i values (b).

4. MACHINE OPERATION AND TECHNICAL ACTIVITIES OF W7-AS AND AUXILIARY SYSTEMS

As usual, the following topics highlight the main technical activities on W7-AS, such as machine operation and changes, developments, new installations and repair work as well as the technical status of control and plasma heating systems.

4.1 Main Activities of W7-AS

During the long shut-down phase starting in August 1993 the machine was subjected to a variety of modifications and repair work (see Annual Report 1993), which were finished in spring 1994. Very critical and time and personnel-consuming was the installation of the nine identical graphite limiters at the inner vessel walls and the work on the additional coil supports and the newly constructed FC77 cooling system for the critical modular field coils of type 3. After this very long and intense shut-down phase with a series of further machine work W7-AS restarted successfully on 21 March 1994. The very complex additional support structure for the ten coils of type 3 came up to expectation. W7-AS is now operable at nominal parameters with main field values of up to 2.5 T without severe restrictions. Continuous measurements of coil movements now afford hope of untroubled operation of the magnetic components of the machine.

During the first experimentation phase till 19 August 1994 a total of 2,637 discharges were carried out in 53 experimentation days. For about 855 of these discharges the machine was operated at about 2.5 T. After a short shut-down phase till October 1994, described below, a second experimentation period followed, with 1,445 discharges, of which 471 shots were carried out at the full field values and about 200 shots were done without plasma but providing single fields for tests of the feedback system.

During the short maintenance phase in late summer 1994 a major effort was expended on the new inner limiter system. These limiters are arranged as pairs in upside-down symmetry at the inner vessel walls near the triangular plane. For investigations of the temperature behaviour during plasma discharges the limiters are equipped with thermocouples. Expected were limiter loads in up-down symmetry but the spatially resolved calorimetric measurements showed non-symmetric temperature behaviour which could only be explained by non-symmetric thermal load associated to deviations of the nominal positions of the limiters. Precise measurements with a special water-level gauge yielded deviations as listed in Tab. 1, requiring readjusting of the limiters to the nominal positions. As new thermal measurements during the following experimentation campaign have shown readjustment of the limiters was very successful.

Measurements of connection lengths in the plasma edge have clearly shown that the two toroidal up-down limiters, one at the top and one at the bottom of elliptical plasma cross-sections, break the symmetry of the magnetic configuration. After detailed discussions it was decided to dismantle the toroidal limiters during this shut-down phase to provide a more symmetric configuration during the next experimentation campaign. Other work in this shut-down period was the changing of several glass windows to quartz ones to reduce the risk of damage during 140 GHz heating. After finishing all maintenance work machine operation restarted on 20 October 1994 and continued till 21 December 1994. Restart of machine operation is expected in March 95.

Reconstruction of the standard remote-controlled boronization system on W7-AS to a fully automated programme-controlled device is on schedule and will later allow stand-alone boronizations (SAB) every night. The alterations of the valve system, gas cabinet and exhaust device are already finished and the boronization system will be recommissioned during the restart of W7-AS. The installation of the programmable controlling unit (SPS) is under way. Total automation of the door-locking system in L7 and parts of L7A, which is also on schedule, calls for major installation work because 18 doors have to be equipped with electropneumatic remote-controlled locking units. The availability of the complete system is expected for autumn 1995.

Module	Lower Limiters	Upper Limiters
1	+ 1 mm	+ 3 mm
2	- 7 mm	- 3 mm
3	- 6 mm	- 5 mm
4	0 mm	+ 2 mm
5		+ 5 mm

Tab. 1: Measured deviations from the nominal positions of the inboard limiters before readjusting. In module 5 no lower limiter is installed.

4.2 Control Systems

Reliability and operation convenience of the W7-AS feedback system were greatly improved by a new set of PID controllers. These electronic circuits avoid saturation effects and can be remote controlled by programming or with several interlock signals.

The control data acquisition system was also extended. Up to 16 new channels can be stored and individually retrieved within a few seconds on a Macintosh. This is very helpful for quick testing of new installations and supervision of control parameters during plasma physics operation.

Furthermore a new timer system was designed on the basis of commercial computer boards using modern high-level visual programming language. The time resolution can be as good as 1 ms and all parameters are adjustable remotely by mouse clicking from any control computer in the network.

4.3 140 GHz ECRH System

Replacement of two out of four 70 GHz (0.2 MW, 3 s) transmission lines by 140 GHz transmission lines for the contractual gyrotrons from GYCOM (0.5 MW, 3 s), is on schedule. The matching optics at the gyrotron end and the waveguide section (about 20 m), including beam monitors, waveguide switches and dummy loads for both calorimetric measurements and long-pulse operation were installed on schedule. The transmission efficiency of both lines was measured at low power and meets the design values. The first two contractual gyrotrons were sequentially delivered to IPP after successful tests at full specified performance at the factory site. Both gyrotrons were tested at IPP under short-pulse conditions. Long-pulse tests had to be postponed because the superconducting magnets showed some mechanical long-term instability and had to be shipped back to the manufacturer for reinforcement of the coil support structure. Long pulse tests with the full transmission system and launcher are scheduled for the first half of 1995 after reassembly of the magnets and gyrotrons at IPP .

4.4 Neutral Injection into W7-AS

4.4.1 Upgrading the injection power to 3 MW

The four additional sources were installed on the two existing beamlines. All the power supply, control and cooling systems were connected and commissioning was started. The first of the new sources started operation in December without any problems, and 1.7 MW was injected into a plasma at 1.27 T and $\iota = 0.351$. The plasma energy content of 14 kJ did not exceed the value reached before with 1.5 MW. However, that was achieved with freshly boronized walls.

The remaining three new systems are being commissioned, so that the full power of 3 MW is expected to be available for the next campaign of experiments starting in March 95 after the present shut-down of W7-AS.

4.4.2 Study of perpendicular injection into W7-AS

A study was carried out to investigate the possibility of nearly perpendicular injection into W7-AS. The motivation for this study originated from W7-A, where the near-perpendicular injection geometry (determined by technical considerations) led to a large fraction of non-confined fast ions. As a consequence, a strong radial electric field was built up, as demonstrated by the accompanying poloidal rotation. This electric field apparently improved both the confinement of the fast ions and the background plasma confinement. Obviously, a similar improvement would be highly desirable, could it be achieved in W7-AS.

The attempt to inject near-perpendicularly into W7-AS requires a compromise between a sufficiently big angle (w.r.t. perp.) for transmission (through the existing beam ports, which are "tangentially" oriented), on the one hand, and a sufficiently small angle to create enough orbit losses, on the other hand. A technically reasonable solution was found with an angle of

around 15° and an ASDEX injector equipped with two sources. Transmission will be near 73% for this case, and for densities above 0.7×10^{20} m^{-3} this will result in an ion current loss of about 17 A (as computed with FAFNER). The strength of the subsequent electric field and the potential effect on confinement as well the accompanying effects of the impurities sputtered from the walls need further detailed consideration.

4.4.3 Deuterium injection into W7-AS

Different hydrogen isotopes injected by the beams offer the possibility of studying mass dependences of wave frequencies (such as the Alfvén wave) and transport coefficients. D^0 injection also offers better control of the hydrogen content for studying minority heating scenarios with ICRH. A further incentive is the possibility of measuring the neutral beam heating efficiency by the neutron production rate due to fusion collisions between beam and plasma deuterons.

A problem with deuterium injection is the neutron shielding of the W7-AS torus hall. A deuterium test injection experiment was therefore arranged with reduced personnel and extended radiation detection. The evaluation of the measurements is under way. The results will determine the conditions under which deuterium injection can be carried out.

4.5 ICRH

The broad ICRH antenna installed in W7-AS was modified in two steps: First it was equipped with shielding elements, already mentioned in the Annual Report 1993, and installed to reduce the effects of antenna currents parallel to the magnetic field. Secondly, a complete Faraday screen was installed. In both cases the antenna impedance showed sudden changes during the RF pulse and power limitation due to arcing at less than 100 kW, but again no heating was seen. It must be believed that the RF interacts with the plasma and neutral gas density of the helical plasma edge at the totally open upper and lower antenna sides. There is evidence of electric breakdown in these areas. Therefore, in a further modification the top and bottom of the antenna will be closed.

The conventional double loop antenna is now planned to be installed in summer 1995.

4.6 W7-AS Data Acquisition and Processing

The activities of the W7-AS Data Acquisition and Processing Group in 1994 were geared to one major goal: preparing for the shutting down of the Amdahl-5890/CMS-based data analysis platform hitherto in use and replacing it with a modern UNIX-based data analysis network (UDAN) along the lines of the proposal first made in 1991. The IBM R6000 / AIX ("Power") systems was selected.

In-house software already running on ULTRIX was ported to AIX fairly quickly, often only needing to be recompiled. Significant delays were incurred in making licenses for commercial products available to W7-AS users, in part due to emergency budgetary constraints. The most difficult job was porting the huge volume of user-written programs and W7-AS system libraries from CMS and VMS to AIX, whereby a great deal of CMS-and VMS-specific code had to be rewritten. Considerable difficulties had to be overcome in adapting the system management techniques developed for ULTRIX to the fundamentally different AIX operating environment. This daunting task is well under way to its projected completion by mid-March 1995.

A number of major changes were made to the global structure of the data acquisition and analysis systems. Most significant was the planned elimination of the central VAX data collection computer (W7MAIN) in favour of directly transferring diagnostic data to the UNIX data analysis systems. The diagnostic data acquisition systems were modified significantly, replacing the DECnet-based data transfer system with one based on TCP/IP, and converting all acquired binary data from VAX to AIX-compatible standard formats (IEEE floating point and Big Endian). In cooperation with the Garching Computer Centre, all W7-AS shot files archived in HADES were converted to the new data format and transferred to the AFS-based mass storage system between September and November of 1994. The existing HADES archive will be maintained for at least one year for security reasons. 30 magnetic disks with a total capacity of 120 Gbyte were installed on the AIX computers to serve as cache to hold a sample of about 5000 of the "most interesting" shots for quick access.

A number of other software products were ported to or installed under AIX, including ORACLE/IDA data base access software and the IDL interactive graphics package, among others.

The routine tasks of operating and maintaining the existing W7-AS data acquisition system, incorporating new data acquisition subsystems or improving existing ones occupied a significant fraction of the W7-AS data processing group's manpower. Diagnostics were added for Mini-Soft-X-Ray (MSOX) and Langmuir probes (in cooperation with IPB in Berlin).

WENDELSTEIN 7-X

(Head of Project: Dr. Günter Grieger)

1. WENDELSTEIN 7–X GROUP

C.D. Beidler, H. Greuner, E. Harmeyer, N. Jakšić,[1] J. Junker, N. Karulin,[2] J. Kißlinger, H. Maaßberg, F. Rau, H. Renner, J. Simon-Weidner,[1] H. Wobig

1.1 Wendelstein 7–X Studies

In 1994 the Wendelstein 7-X studies were continued and focused on special questions of the machine components and their technical feasibility. The phase II proposal for the W 7-X project[3] concerning the technical design of the device was completed. Increased attention was given to the divertor structures and plasma boundary physics. Neoclassical transport, electric fields and plasma rotation were investigated. Special attention was given to questions of a Helias reactor: The start-up scenario, the modular coil system, and the divertor of a stellarator reactor were treated.

1.1.1 Force and stress calculations

Magnetic force and the associated mechanical stress and strain analyses were continued for the standard case of Wendelstein 7-X, as well as for the different operational cases. Each coil winding pack of the system consists of 120 windings of a cable-in-conduit conductor with a co-extruded aluminium jacket. It is embedded in a coil housing of stainless steel. The mutual intercoil support structure was chosen as a cross-connected framework in order to minimize structural material. The support structure was improved applying local reinforcements in the radial and lateral directions.

In order to compute the stresses and strains of the coil system the ADINA finite-element code was used. The elastic material data of the ABB conductor were applied. In the calculations the effects of the cooling-down of the coil module and the influence of sliding on stresses were considered. The results of the optimization of the support scheme were represented on the SOFT Conference in Karlsruhe /431/. These investigations are being done by members of the ZTE Division.

1.1.2 Divertor studies

1.1.2.1 Divertor of W 7-X

With respect to the phase II proposal for the W 7-X project the technical design of the divertor system has been completed. Components which fulfil the requirements of the planned experiment with steady-state operation at an input power of 10 MW can be realized on the basis of present knowledge. The divertor design of W 7-X provides a flexible solution of the energy and particle exhaust of a HELIAS device. Unique features to study plasma boundary and transport are included. Variation of the magnetic configuration and control of the neutral particle balance are valuable tools for investigating the physical phenomena at the boundary to optimize operation with respect to reducing impurity reflux and power load to the target plates during long-pulse discharges. In stellarators - without MHD limitations by disruption - operation at high densities and high radiative losses will be favoured and may allow a significant reduction of the power load to the target plates.

a) Magnetic configuration

Since the structure of the boundary region may be decisive for plasma-wall interaction and impurity inflow, an important theoretical and experimental domain of research in W 7-X will be how to optimize this structure. The magnetic topology at the boundary of the HELIAS is characterized by a non-axisymmetric 3D configuration where

---

[1] ZTE Division

[2] Guest from Kurchatov Institute, Moscow

[3] Wendelstein 7-X, Phase II Application for Preferential Support, IPP June 1994, CCFP 62/6.1.

"helical edges" are formed in the outermost magnetic surface on the outboard side of each period at the location of strongest curvature of this surface. Spatially, a helix-like line connects the lower and upper ends of indented cross-sections one field period apart. There, field lines starting close to but beyond the LCMS and crossing the helical edge show the strongest radial displacements. The LCMS is either defined as the last closed magnetic surface of the confinement area surrounded by an ergodized boundary region outside or by the inner separatrix if islands are present at the boundary and intersected by divertor plates. Without additional coils this "inherent diversion" can be used for energy and particle exhaust from the plasma. Sufficient flexibility in the particular magnetic configurations allows systematic studies of the transport at the boundary by modifying the interaction area at the target plates and the structure of the connection lengths of the open field lines. On the other hand, effects due to finite β are small owing to the positional stability of the optimized HELIAS configuration[4] and the minimized bootstrap currents.

b) Open divertor solution

So far 10 divertor units have to be arranged as seen in Fig. 1.1. Positioning of target plates to reflect the 5-fold symmetry along the helical edge[5] makes an open divertor possible: energy and particle fluxes are deposited on the target plates without the problem of leading edges for various magnetic parameters, and the interaction of charged particles leaving the plasma with the vessel wall is avoided. "Resonant" fields additionally superimposed by means of small control coils provide flexibility and allow controlled modification of the boundary and fluxes to the target in static and dynamic operation ("sweeping").

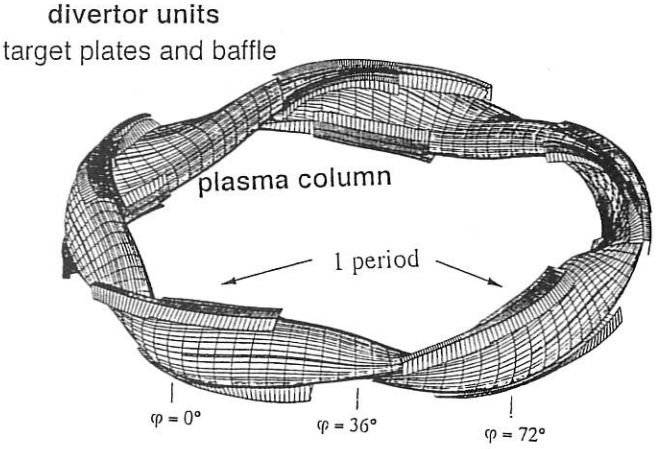

FIG. 1.1: Plasma column and positioning of the 10 divertor units.

c) Control coils

Saddle-shaped coils with dimensions of about 0.3×1.8 m^2 can be located behind the target plates. Currents of up to 25 kA in these control coils allow one to control the size and phase of the islands and also to introduce an ergodic region at the plasma boundary. The main features of the control coil are:

- Variation of the connection length and distance between target plates and separatrix.
- Distribution of power on target plates. A sweeping effect is introduced when energizing the coils by AC currents; the transient magnetic field of the sweep coils oscillates the strike points on the target plates.
- Compensation of error fields. A further application of the control coil system is compensation of symmetry-breaking error fields, e.g. due to small construction inaccuracies of the device.

d) Modelling

Models describing the SOL and fluxes for expected plasma parameters with an input power of up to 10 MW were developed on the basis of a 3D description of the field lines at the boundary and 1D particle and energy transport along the field lines. The EIRENE code is used to calculate the neutral particle densities and evaluate the possibilities of effective pumping. Finer segmentation and further improvement of the divertor geometry was achieved in the last year, resulting in a more uniform load on the targets. In order to concentrate the neutrals in the divertor region and minimize the interaction of high-energy neutral particles with the wall of the vessel, the target plates are combined with baffle plates[6].

Neutral gas behaviour: The neutral particle density, pumping efficiency of cryopumps and localization of charged particle sources were estimated with the EIRENE code for typical parameters. The density calculated in the pumping chamber is about 10^{19} m^{-3}, assuming a plasma particle flux of 6×10^{23} s^{-1} on the targets, and a SOL density of 3×10^{19} m^{-3}. With the same parameters, the pumping rate is calculated by modelling the cryopanels as absorbing surfaces. An absorbed flux of 7.5×10^{21} s^{-1} is found, which is 1.2% of the flux incident on the targets. The neutral density in the pumping chamber and the pumping rate depend on the SOL parameters; both increase as the ionisation length of the neutrals. In the case of a He plasma one finds about the same neutral densities in the pumping chamber. As a measure of the particle flux gain in the SOL, the local ionization rates were calculated as a function of the boundary densities. Already with a relatively low SOL density of 3.5×10^{19} m^{-3} more than 99% of the recycled particles are ionized inside the SOL, and with a density of 7.5×10^{19} m^{-3} one obtains nearly 100%. On the basis of this calculation, a plausible recycling scenario is shown in Fig. 1.2. The regulating "tools" for the particle content in the SOL are the gas-puff on the source side and the number of activated cryopanels on the absorbing side.

---

[4] Hayashi T., Schwenn, U., Strumberger, E., Jpn. J. Appl. Phys. 31, (1992), 2580.

[5] Nührenberg, J., Strumberger, E., Contr. Plasma Physics 32 (1992), 212.

[6] Kisslinger, J. et al. EPS Lisboa (1993), 17C, II, 587.

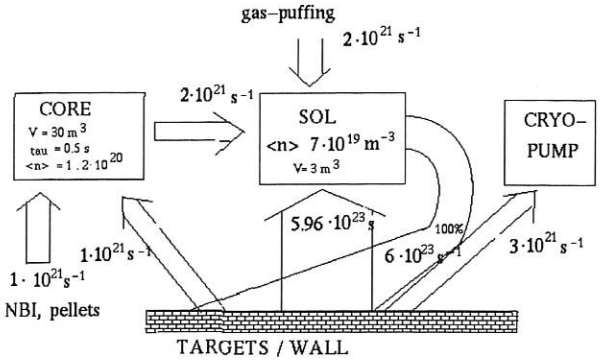

FIG. 1.2: Particle recycling scenario in the high-recycling regime of W 7-X, estimated from global particle fluxes and calculations of plasma sources.

1.1.2.2 Technical design

At present, design studies are being done to combine the particular elements of the divertor for W 7-X inside the vessel and analyse the compatibility with heating and diagnostics requirements: target plates with supporting structure and cooling circuits, installation of "sweep" coils, baffles and integrated pumps. The positioning of target plates is optimized in respect of the following criteria:

- Concentration of the plasma outflow on the target plates, and separation of the plasma from the vessel.
- Maximal power load of 10 MW/m^2, requiring that the field lines be incident at an angle of 1-2^o to the target.
- Variation of the magnetic configuration for the rotational transform range $5/6 \leq \iota \leq 5/4$. Integration of baffles and cryopumps for efficient pumping and stationary operation dealing with external fluxes of 5×10^{21} part./s (NBI, pellet, gas feed etc.) and pressures in the range of up to 10^{-3} mbar in the divertor.

a) Target plates

The target plates consist of single target elements. The 2 target plates of one divertor unit are spliced into 144 target elements (1/10 of the total value of the device) spanning an area of 2.2 m^2. The target elements are standardized. The width is 50 mm and the length between 270 and 500 mm. Flat carbon tiles (CFC: SEP N11) are brazed to the cooling structure. The cooling structure is made of the molybdenum alloy TZM. Twelve to fifteen target elements are mounted in modules. Finally, the modules will form the calculated 3D area. The modules and the water pipes are electrically insulated and fixed in the vessel.

b) Baffles

The baffles see relatively low heat flux with a typical power load of 50-200 kW/m^2. Therefore, the baffle plates can use fine-grain graphite tiles clamped to a water-cooled stainless-steel structure. The baffle area per unit is 3 m^2. The bake-out temperature will be 350^o C.

c) Carbon-armoured first wall (carbon shield)

The carbon-armoured first wall is similar in design to the baffle plates. The averaged power deposition is expected to be limited to 100 kW/m^2. Tiles of fine-grain graphite are mounted on a water-cooled structure. The area of the carbon tiles in W 7-X is $\approx$100 m^2.

d) Pumping

Two independent systems for pumping will be installed. To control the neutral pressure inside the divertor and allow additional particle sources for controlling plasma parameters, turbomolecular pumps and additional high-speed cryopumps will be used. The 10 divertor units are decoupled and can be operated independently of each other with variable pump speed. The turbomolecular pumps define the basic pumping system of W 7-X and will also be used for pumping the divertor units during the discharge with an acceptable pump speed: For H2 the effective pump speed per pump unit is estimated to be 4200 l/s. The cryopanels are positioned on the inner side of the vessel between the diagnostic ports. Four cryopanels per divertor unit will be arranged. The LHe supply is independent for each panel. Therefore, single panels can be used to vary the pump rate. The cryogenic effective pump speed of one divertor box is estimated to be 15000 l/s, continuous in time for about 3 h at a pressure of 1×10^{-3} mbar.

1.1.3 Numerical fits for describing neoclassical transport in the long-mean-free-path regime

A standard least-squares fit technique has been applied to several data sets, generated numerically by the Drift Kinetic Equation Solver (the DKES code, van Rij and Hirshman, Phys. Fluids B1 (1989) 563), to provide a rapid description of the neoclassical transport properties of a number of experimental stellarator devices. The fits are provided in terms of the mono-energetic diffusion coefficient D, which is assumed to have the form $D^{-1} = D_{1/\nu}^{-1} + D_{\sqrt{\nu}}^{-1} + D_{\nu}^{-1}$, where $D_{1/\nu} = \alpha_{1/\nu} E_r^0 \nu^{-1}$, $D_{\sqrt{\nu}} = \alpha_{\sqrt{\nu}} E_r^{-3/2} \nu^{1/2}$ and $D_{\nu} = \alpha_{\nu} E_r^{-2} \nu$ are expressed in terms of the 90-degree deflection frequency ν, the radial electric field E_r, and the respective fitting coefficients α. For the classical stellarators W7-A and L2, the values determined for α agree well with those expected from analytic theory. For Advanced Stellarators such as W7-AS and devices of the Helias type, the values of α can vary considerably, but the assumed dependence of D on ν and E_r remains valid; examples are provided in Fig. 1.3. These fits have been incorporated into the 1-D transport code, ASTRA.

1.1.4 H-mode studies

Poloidal shear flow and a resulting reduction of radial plasma losses are the dominant features of H-mode confinement in tokamaks. The spin-up of poloidal shear flow may be caused by various mechanisms such as Stringer spin-up or turbulent Reynolds stresses. The damping mechanism is magnetic pumping or the gyro-relaxation effect. The equations governing poloidal and toroidal plasma flow have been formulated in general stellarator geometry, which also provides a general expression for the magnetic pumping effect. Numerical evaluation of the collisional magnetic

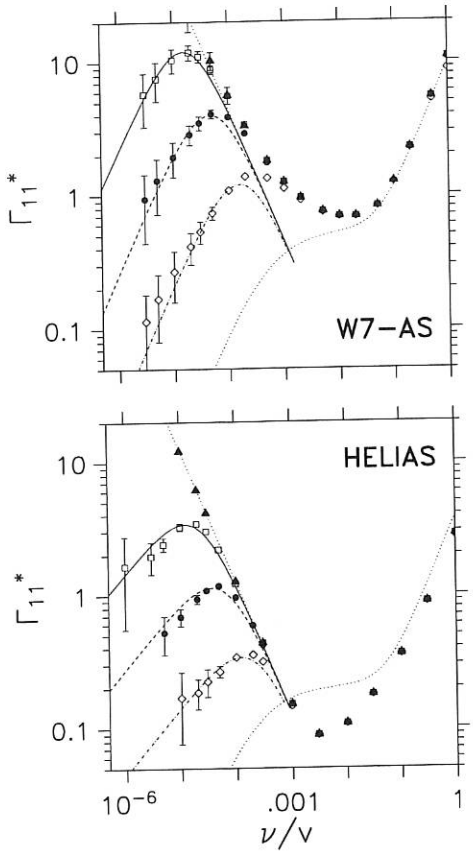

FIG. 1.3: Normalized mono-energetic transport coefficients Γ_{11}^*, at half the plasma radius versus ν/v for W7-AS and a Helias configuration. DKES results (with error bars) are given by data points and least-squares fits by lines for the E_r/v values: 0 (▲, dotted line), 10^{-4} (□, solid line), 3×10^{-4} (●, dashed line), and 10^{-3} (◇, dot-dash line). The axisymmetric contribution is also indicated (additional dotted line).

pumping term showed a distinct difference between the Wendelstein 7-AS configuration and the Wendelstein 7-X configuration. Magnetic pumping in W 7-X is appreciably smaller than in W 7-AS. Provided the same excitation mechanism is present in both configurations, this result suggests that plasma rotation and transition to H-mode should be more easily achievable in W 7-X than in W 7-AS.

1.2 Reactor Studies

1.2.1 Start-up scenario

Start-up scenarios in a Helias reactor were analyzed using the ASTRA code, which computes the evolution of $T_i(r,t), T_e(r,t)$ and the density $n(r,t)$. The ASTRA code,[7] which was developed for tokamak geometry, was modified to stellarators by including the neoclassical transport coefficients of Helias configurations[8]. The anomalous thermal conduction of electrons is modelled according to

$$\chi_{e,an} = 1.5 \frac{1.6}{R} \left(\frac{2.2}{B}\right)^2 \frac{T_e^{3/2}}{(1.1 - r^2)^4} \quad [\frac{m^2}{s}].$$

This transport coefficient describes L-mode confinement in ASDEX[9] and fits to Wendelstein 7-AS data. Furthermore, the radial electric field is computed self-consistently by utilizing the condition of ambipolarity. This radial electric field appreciably reduces the neoclassical ion transport and prevents excessive loss of localized ions. As heating method ECR heating at 140 GHz is envisaged and the power is deposited in a small region in the plasma centre. Power deposition is fixed, and self-consistent calculation of the power is in preparation. Radiation losses (bremsstrahlung and line radiation) are included, the line radiation being localized to the boundary region.

The result shows that the initial plasma with $T = 3.5$ keV can be heated to ignition by a net heating power of 50 MW. The ignited plasma is stabilized against thermal instabilities by a soft onset of enhanced plasma losses at the expected beta limit of $< \beta > \approx 4.5\%$. Ignition is reached at relatively low temperatures. The plasma parameters of the burning state are summarized in the following table.

		$B_o = 5$ T	$B_o = 4.7$ T
Average major radius	[m]	22	22
Average plasma radius	[m]	1.76	1.76
Fusion power	[MW]	3090	3050
α-heating power	[MW]	618	610
Neutron power	[MW]	2472	2440
Plasma energy	[MJ]	878	852
Ion temperature	[keV]	11.3	10.9
Electron density	[10^{20} m^{-3}]	4.0	4.0
Average β	[%]	4.54	4.98
Peak β	[%]	14.3	15.8
Helium content	[%]	5	2
Energy confinement time	[s]	2.01	1.93

TABLE I: Parameters of a Helias reactor.

1.2.2 Divertor of the reactor

The divertor concept proposed for the Helias reactor is derived from the island divertor concept of W 7-X. The difference to W 7-X is the fixed magnetic configuration, where

[7] Pereverzev, G.V., et al., Report IPP 5/42, 1991.

[8] Beidler, C.D., et al., Report IPP 2/318, 1993.

[9] Lackner, K., et al., Plasma Physics and Contr. Fusion **31**, (1989), 1629.

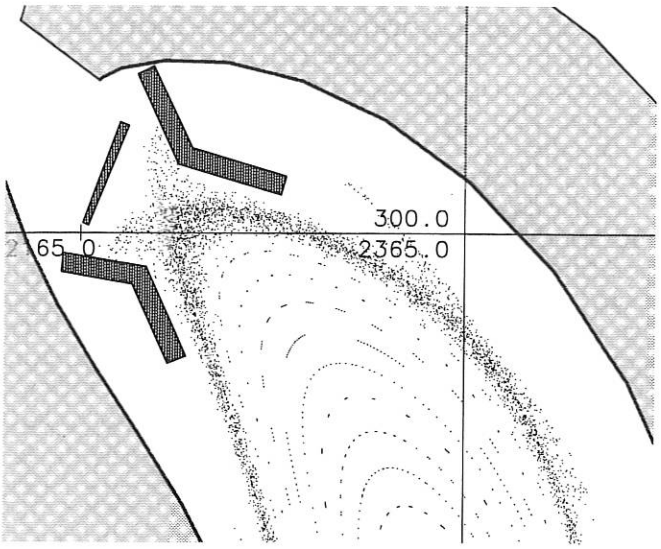

FIG. 1.4: Cross-section of the Helias reactor at the toroidal plane $\varphi = 0$ (upper part of the up-down symmetric figure). Shown in radial sequence are: flux surfaces, scrape-off layer, and divertor unit, as well as contours of the first wall, blanket and shield.

a more closed divertor design is afforded by utilizing the island shape, see Fig. 1.4.

Each of the 10 divertor units (2 per field period) consists of two target plates adjusted to the outstreaming plasma fans. Additional baffle plates accompany the highly loaded target plates and prevent neutrals from moving into the main chamber. Another baffle plate separates the pumping chamber from the divertor region, increasing the pumping efficiency. The angle between the target plates and the diverted plasma fans is chosen so that reflected neutral particles move towards the separatrix. The toroidal length of the divertor is about 14 m, located between $\varphi = -18^o$ and $\varphi = +18^o$; further geometrical data are collected in Table II.

Connection length, target to target	[m]	22
Connection length, target to target	[m]	1350
Connection length, X-point to target	[m]	300
Length of one divertor unit	[m]	14
Width of the target plates	[m]	0.5
Total area of the target plates	[m^2]	140
Total area of the baffle plates	[m^2]	260
Highly loaded area	[m^2]	40
Angle of incidence	[^{o}]	1

TABLE II: Characteristic data of the divertor.

Calculations of the power density by Monte Carlo technique — assuming a diffusion coefficient of 1 m^2s^{-1} — show that 20 to 30% of the α-particle power may be deposited by particles on the target plates if the power density is constrained to a maximum of 10 MW/m^2. The larger part of the power must be removed in a different manner; e.g. by radiation in the plasma boundary.

1.2.3 MHH studies

MHH, the Modular Helias-like Heliac, is described by D.T. Anderson and P.R. Garabedian in Nucl. Fus. **34** 881 (1994) and is being investigated by a group of US scientists as reference configuration for SPPS, the US Stellarator Power Plant Study, with similar assumptions for plasma performance and material characteristics as in the ARIES-IV tokamak reactor. The latter is detailed in the Report UCLA-PPG-1461, 1994 by F. Najmabadi et al. Typical values for MHH as per July 1994 are a major plasma radius of 14 m, a rotational transform on axis of $\iota_0 = 1.1$, an average axis field of 5 T, and a minor plasma radius of about 1.6 m with a rotational transform of $\iota_a = 1.3$. There are 4 field periods and 8 non-planar coils per period. J.F. Lyon et al. estimate competitive values for the cost of energy for both systems in a paper to the IAEA Conference, Sevilla, September 1994.

As a part-time activity, undertaken within the IEA Implementing Agreement for Cooperation in the Development of the Stellarator Concept, we evaluated vacuum field properties of MHH with comparison to those of W 7-X and HSR, the Helias Stellarator Reactor derived from W 7-X. The optimization principles pursued for W 7-X and HSR are different from those of MHH. Nevertheless, radial profiles of ι and the magnetic well are similar for MHH and the high-ι case of W 7-X. This might be due to the fact that MHH is similar to HSX, the new "quasihelical" advanced stellarator under construction at Madison, WI (USA), which was developed in co-operation between D.T. Anderson and IPP Garching. The magnetic ripple near the axis is larger in W 7-X than in MHH; due to the lower number of coils per field period it is larger in MHH near the edge. Four modified coil configurations, MHH-A through MHH-D, were specified, which differ in their coil cross-sections and current densities. Their vacuum fields are rather similar; the peak fields at the coils (12.6 to 15.4 T) and associated peak forces (250 to 760 MN/m^3) are different, however. These data enabled our US colleagues to improve their scaling studies of these quantities with the coil dimensions and current densities. An initial step towards a divertor for MHH has been performed along the line pursued for W 7-X. A few remarks on reactor aspects were touched in our studies: the ignition/burn scenario as a result of a simple one-dimensional approach, and some questions of reactor maintenance for MHH. An internal report was written with a recommendation to define new coil shapes with an increased value of the major radius in order to improve the divertor prospects and reduce the peak fields.

2. STELLARATOR PHYSICS STUDIES

W. Dommaschk, S. Gori, F. Herrnegger, W. Lotz, P. Merkel, C. Nührenberg, J. Nührenberg, A. Schlüter, U. Schwenn, E. Strumberger.
Guests: T. Hayashi,[1] K. Ichiguchi,[1] N. Nakajima,[1] S. Murakami,[1] M. Yokoyama.[2]

2.1 Introduction

In 1994 the work of the Stellarator Physics Group was concentrated on W7–X phase II issues – in particular divertor physics studies /212, 213/ –, and on beginning to augment the level of theoretical description of stellarators /523/. Work bridging the theoretical and configurational gap between tokamaks and optimized stellarators was also begun.

In Sec. 2.2, an example of an application of the methods developed for the theoretical design of W7–X to a question which may be relevant for tokamak research is described.

The well-behavedness of finite-β equilibrium surfaces is the object of advanced equilibrium studies /88, 201, 202, 419, 500, 501/ undertaken as collaborative work together with NIFS (HINT code) and PPPL (PIES code). Section 2.3 describes some of this work.

In Sec. 2.4, divertor physics work is described which is directly related to the current version of a technical divertor realization in W7–X.

2.2 Quasi-axisymmetric Tokamaks

Creation of rotational transform – as a prerequisite for toroidal confinement – in tokamaks is traditionally done with an inductively driven toroidal current. More recently, the plasma-driven bootstrap current as well as externally, noninductively driven toroidal currents have received increasing attention because of their importance for stationary operation. Problems associated with these methods are, for example, that the bootstrap current does not create central rotational transform and that all these methods – per se – do not decrease the potential for instabilities driven by a large toroidal current. Thus it might be worthwhile to replace part of the current by an externally created rotational transform. Experimentally, suppression of disruptions and tearing modes was achieved by replacing a fraction of the toroidal current by an externally created $\ell = 2$-type rotational transform. Computationally, studies of tokamak-stellarator hybrids have recently been started. A problem associated with such hybrids is that the ideal-tokamak axisymmetry is sacrificed. This means not only that the assessment of, for example, the MHD properties becomes much more complicated and has to be done with 3D codes, but also that non-MHD aspects such as neoclassical aspects may become dominant. A specific question in this context was investigated /166/: Can axisymmetric tokamaks be generalized into quasi-axisymmetric tokamaks, i.e. truly 3D configurations of the tokamak type with an axisymmetric structure of $|\vec{B}|$ in magnetic coordinates? The answer is affirmative; Figs. 1, 2 and 3 describe an example.

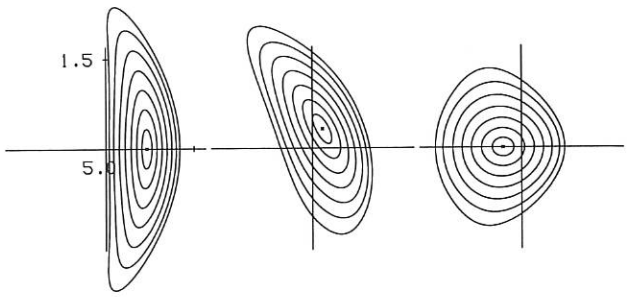

FIG. 1: Flux surface cross-sections of a quasi-axisymmetric configuration with 2 periods; $0.91 > \iota > 0.32$, $\langle\beta\rangle \approx 0.03$.

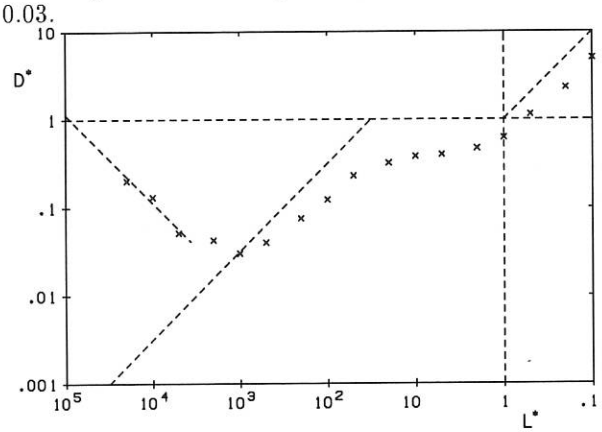

FIG. 2: Normalized transport coefficient D^* versus normalized mean free path L^* (for notation, see Phys. Fluids **31** *(1988) 2984). The dashed lines (additional to those indicating the normalizations) give the PS, plateau, and banana results for the equivalent circular tokamak and the $1/\nu$ line representing the lmfp Monte Carlo results from which the equivalent ripple (below one per mill) is obtained.*

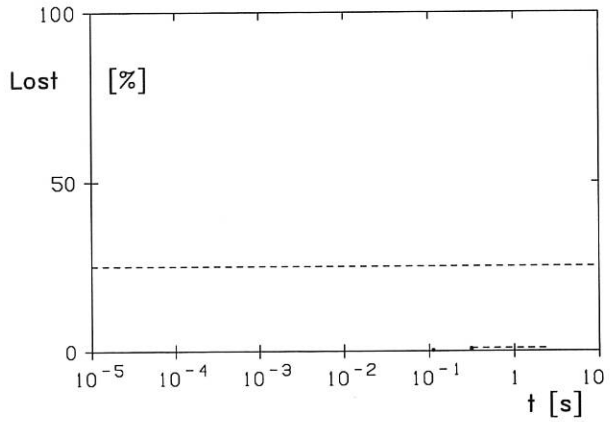

FIG. 3: Collisionless α-particle losses in the quasi-axisymmetric configuration of Figs. 5 and 6 as a function of the time of flight. Particles are started at aspect ratio 10; the upper dashed line shows the fraction of reflected particles. The number of reflected particles followed is 100; each symbol indicates the loss of one particle; the lower dashed line indicates that no further particle is lost.

[1] National Institute for Fusion Science, Nagoya, Japan.

[2] Kyoto University, Kyoto, Japan.

2.3 3D MHD Equilibrium Calculations with Advanced Codes

Two 3D equilibrium codes which do not a priori require the existence of regularly nested magnetic surfaces, the HINT[3] and the PIES[4] codes, have been applied to W7–X and other stellarator equilibria. Their comparative application will increase confidence in finite-β island-size and separatrix computations. A major achievement with PIES was the computational achievement of an $\langle\beta\rangle = 0.05$ W7–X equilibrium for the case of no medium-order resonance in the plasma region /501/. The HINT code studies of self-healing of islands have been extended to MHD unstable equilibria to clarify the relation of this phenomenon to analytical theories of finite-β island behavior. Figure 4 shows the self-healing of a 5/5 island chain in an unstable $\ell = 1,\ 2$ stellarator.

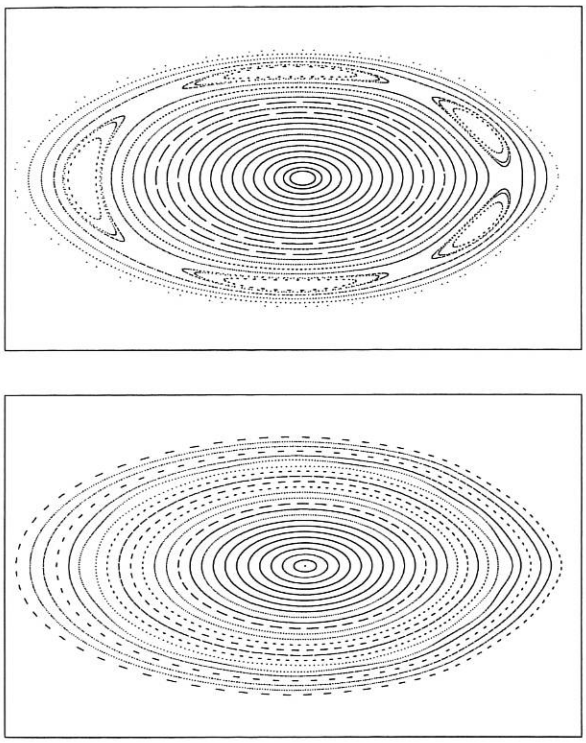

FIG. 4: Poincaré plot of vacuum field (top) and finite β ($\langle\beta\rangle \approx 0.01$) self-healed equilibrium (bottom) of an unstable $\ell = 1,\ 2$ stellarator with five periods and aspect ratio ≈ 10.

2.4 Divertor Studies for Phase II of W7–X

The magnetic field structure in the edge region is studied by way of the field line map interconnecting the plasma facing surfaces of the target and baffle plates for three rotational transforms ($\iota = 5/6, 5/5$ and $5/4$). When these field lines are ordered according to their lengths, ordered layers are found. Fig. 5 shows five such ordered layers – representing field line lengths from more than 200 to less than 15 m – in the bean-shaped cross-section for $\iota = 5/6$ (top), $\iota = 5/5$ (middle) and $\iota = 5/4$ (bottom). These maps show the differences in the structure of the open-field line mantle occurring in the transition from a thin island structure embedded in closed magnetic surfaces (so that the open field lines are caused by the divertor plates themselves) to a structure in which a separatrix is surrounded by genuinely open field lines.

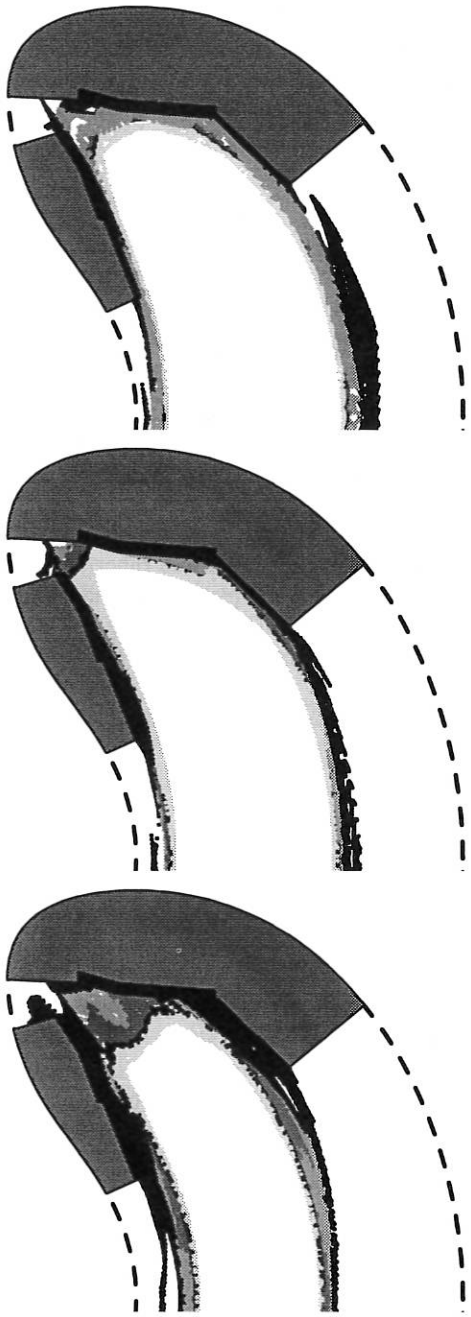

FIG. 5: Field line map interconnecting the divertor troughs for three values of ι at the separatrix: $\iota = 5/6$ (top), $\iota = 5/5$ (middle) and $\iota = 5/4$ (bottom). The field line lengths of the five layers (light grey, dark grey, middle dark grey, middle light grey, black from inside to outside) are: more than 200 m, 200 – 100 m, 100 – 45 m, 45 – 15 m, less than 15 m.

[3] T. Hayashi, in: *Theory of Fusion Plasmas*, Chexbres, Switzerland (1988), SIF (Bologna 1989) 11.

[4] A. Reiman, H. Greenside, Comp. Phys. Comm. **43** (1986) 157.

3. W 7-X TECHNICAL R & D

W. Bitter[1)], B. Fleischer[1)], H. Greuner, R. Holzthüm[1)], S. Huber[1)], N. Jaksic[1)], S. Kamm[1)], F. Kerl [1)], H. Münch, M. Pillsticker, J. Sapper, J. Simon-Weidner[1)], B. Sombach[1)], F. Schauer, I. Schoenewolf, J. Tretter[1)], F. Werner, A. Wieczorek

R. Heller, K. P. Jüngst, W. Maurer, KfK-ITP

3.1 Outline

The small capacity of the technical team in 1994 was again concentrated on two essential tasks: On the one hand, the overall technical concept of the W 7-X experiment was worked out and the "Application for EURATOM Preferential Support, Phase II" was formulated. Its examination by an "ad hoc group" of experts started in November 1994 and consumed then the major capacity of the team for explanations and in-depth discussions, still going on. On the other hand, the contract for the DEMO coil could be placed with industry, the call for tender action for the DEMO cryostat was carried out and first test results on a broader basis could be achieved at KfK.

3.2 R & D Work

After a delay of about 9 months due to administrative problems, the contract for the full size DEMO coil was placed with industry. The leading engineer and manufacturer is NOELL GmbH, Würzburg (D), the winding pack will be manufactured by ANSALDO, Genua (I). The work for this contract has started with the transfer of all necessary data files and technical information to IPP's partners. The contract is running with good progress, the delivery of the coil is scheduled to be in October 1996.

A smaller order was placed with industry for the procurement of a refrigerator plant for 100 W, 4 K to be installed at IPP for testing the DEMO cryostat. Also this work is in full swing, the delivery and commissioning of this plant will start in autumn 1995.

The call for tender action for the DEMO cryostat produced four valid offers. The contract for this complex full size vessel arrangement will be placed with industry in spring 1995. The delivery time is planned to be two years. The quoted share of delivery from industry is shown in Fig. 1.

The second STAR-test coil was delivered to IPP by TESLA with a short delay. It was equipped with the encasing and the electrical and hydraulical terminals, pretested and delivered to the test bed at KfK. A first test run happened in November 1994 and showed - in spite of some problems with the test bed - the principle functioning of the cooling circuits and the current operation of the coil. More detailed results are underway.

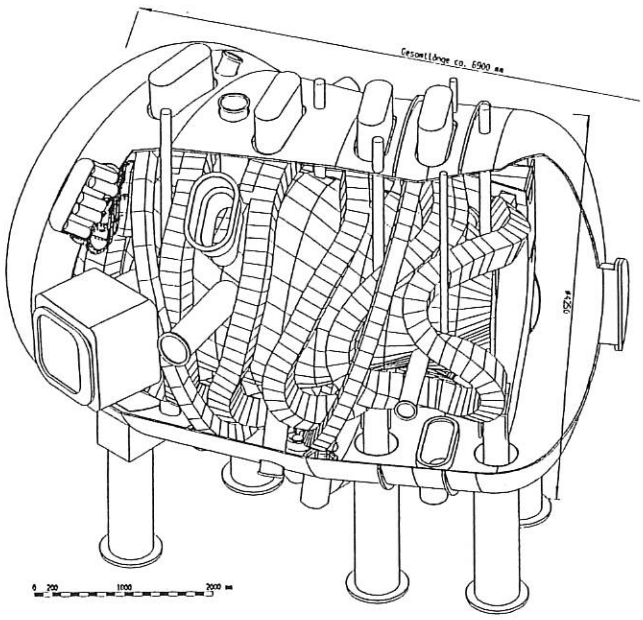

FIG. 1: Test cryostat, 1/10 of W 7-X

3.3 Basic Machine Design

The basic machine design was completed for the purpose of the above mentioned application for pref. sup., phase II, on the basis of the coil data set available up to now. A full costing for the W 7-X plant at the new site of Greifswald was carried out.

The design of the heating systems (ECRH, NBI, and ICRH) was integrated into the plant design as well as the design of the energy supply and the central cooling system.

An assembly of all essential site conditions was worked out as an input information for the "master plan" to be worked out by the architect.

A schedule for the whole plant was worked out as well as the demands for staff.

3.4 Divertor Activities

Following the recommendations of the "Phase I Ad Hoc Group", a divertor concept for the machine on the basis of full steady state operation capability was designed. The technical lay- out led to a design with flat tile divertor elements. Some of these elements were ordered from industry to be tested with full thermal load and as reference pieces for a safe and

---

[1)] Central Technical Department

economic quality management for the later series production of about 1,500 elements. Fault conditions for the divertor and the whole heat removal system design have been fixed. (Fig. 3)

3.5 Neutral Injection into W 7-X

(Neutral beam group, Technology Division)

Neutral beam heating is envisaged for W 7-X as a powerful and well-proven method of bulk heating for plasma ions and electrons. It will be used to drive the plasma into the high-density, high-ß regime very much in the same way as on W 7-AS: ECRH or some non-resonant RF heating will provide start-up and produce a target plasma of sufficiently high density in order to trap a substantial fraction of the neutral beam, which will then further build up the plasma density and ß.

The ultimate neutral beam power (stage II heating) will attain 20 MW, delivered by two injector boxes of the ASDEX Upgrade type. In stage I of neutral beam heating only a quarter of this power will be implemented. The injectors will deliver either 55 keV H^0 or 60 kV D^0 in stage I; in stage II is also 100 kV D^0 envisaged. Due to the stellarator requirement that current driven by neutral beams be cancelled and in order to increase the experimental flexibility, the total power has to be delivered by a symmetric pair of counter-directed injectors.

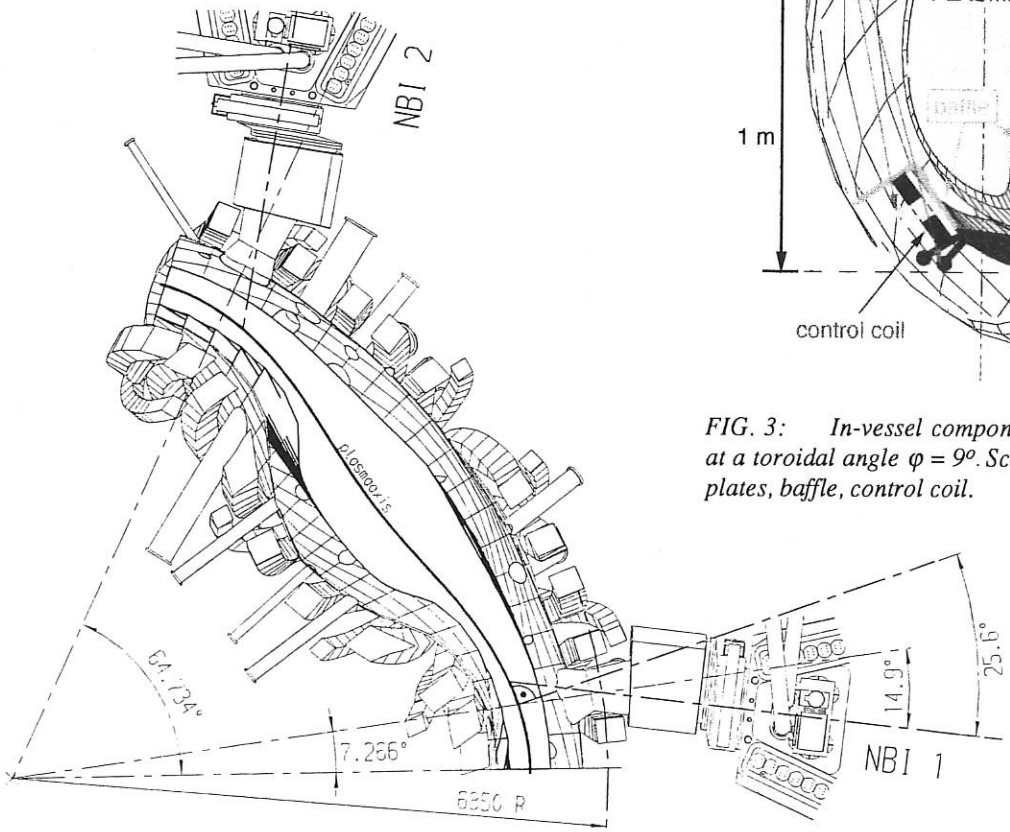

FIG. 2: Injection geometry for W 7-X NBI.

The injection geometry will be around 20^0 w.r.t. perpendicular (see Fig. 2). Each of the two beamlines will be capable of housing four PINIs (plug-in neutral injectors), but will initially in stage I be equipped with one PINI only, thereby delivering up to a total of 5 MW for pulse lengths of up to 10 seconds.

The transfer of beam power to the W 7-X plasma will be very efficient. Shinethrough losses above an average density of 10^{20} m^{-3} will be around 10% or lower, and orbit losses due to the optimized magnetic field configuration will be negligible. Power deposition is centre-peaked for all densities except for 60 kV D^0 injection, where the profiles become flat to slightly hollow at the highest values above 3 x 10^{20} m^{-3}.

The main progress in 1994 was made in setting up the corresponding part of phase II application for preferential support of stage I heating and defending it before the EURATOM Ad-hoc group.

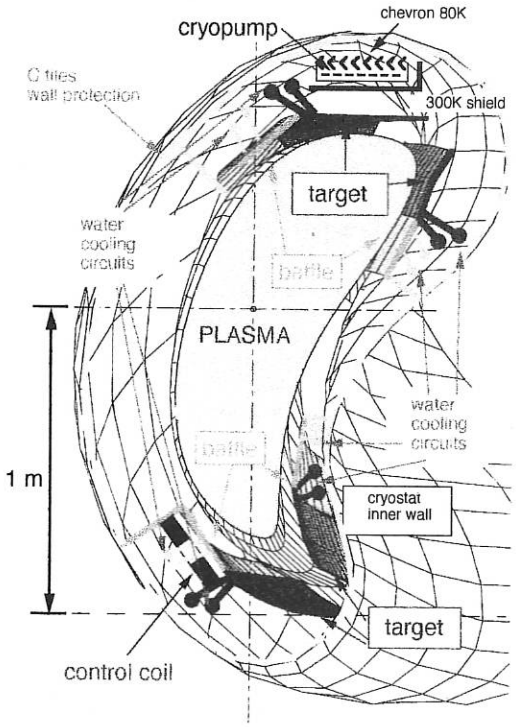

FIG. 3: In-vessel components: cross-section of the device at a toroidal angle φ = 9°. Schematic overview includes target plates, baffle, control coil.

IEA IMPLEMENTING AGREEMENT
for Cooperation in Development of the Stellarator Concept
EUROPEAN ATOMIC ENERGY COMMUNITY / US DEPARTMENT OF ENERGY

1. OBJECTIVES OF THE AGREEMENT

The objective of the Implementing Agreement, first concluded in 1985, is to "improve the physics base of the Stellarator concept and to enhance the effectiveness and productivity of research and development efforts related to the Stellarator concept by strengthening co-operation among Agency member countries". To achieve this, it was agreed to exchange information, conduct workshops, exchange scientists, do joint theoretical, design and system studies, coordinate experimental programmes in selected areas, exchange computer codes, and perform joint experiments. In 1990 the Agreement was extended until 1995. The contracting parties are EURATOM, the U.S. DoE, Japan (since October 1992), and Australia (since October 1993). In September 1994, Russia became an Associate Contracting Party.

2. STATUS OF THE AGREEMENT

In 1994 the 19th meeting of the Executive Committee was held in Seville, Spain, on September 28, in conjunction with the IAEA International Conference on Plasma Physics and Controlled Nuclear Fusion Research. The main topics of this meeting were the progress of the collaboration, Russia´s accession to the Implementing Agreement, the future participation of Ukrainian laboratories, the status of the experiments, and especially the future of the collaboration. It was agreed to intensify the cooperation on reactor studies under the Implementing Agreement. The dialogue started in 1993 with that part of the tokamak programme which is oriented towards steady-state operation has been intensified. The first joint workshop will be organized by IPP in February 1995.

3. REPORT ON 1994 ACTIVITIES

In 1994, fourteen physicists participated in the exchange of scientists. From Japan H. Zushi (from Kyoto), S. Kubo, M. Fujiwara, K. Ida, K. Itoh, S. Itoh and K. Tanaka (all from Nagoya) visited Garching, their stays lasting between 4 and 20 days. They were interested in several aspects of plasma turbulence and turbulence theories, and experimental methods of turbulent fluctuations. There were several long-term visits of scientists from Oak Ridge to IPP in 1994. Staying from May 9 to September 23, J.F. Lyon coordinated the cooperation between IPP and Oak Ridge in the fields of ICRH physics and divertor design. D. Spong calculated GAE modes for W 7-AS with the Oak Ridge gyro-fluid code during his visit to IPP from July 8 to August 1. A.C. England was concerned with the ICRH broad antenna at W 7-AS during his 4-week stay in October/November. T. Luce studied similarities and differences of the energy transport in the W 7-AS stellarator and DIII-D tokamak from June 25 to July 31.

U. Gasparino from IPP is spending about two years in Japan, since March 1994, to study neoclassical treatment of RF-induced transport, the kinetic description of RF heating, heating and current drive in 3D geometry, and the bootstrap current in 3D geometry. U. Stroth from IPP visited the institute in Nagoya to set up a stellarator data base from November 13 to December 11. P. Merkel from IPP stayed 6 weeks in Princeton in spring to study advanced equilibria with the PIES code.

Divisions and Groups

THE SCIENTIFIC DIVISIONS OF IPP

Experimental Plasma Physics Division 1
Director: Prof. M. Kaufmann

ASDEX Upgrade
- divertor experiment for investigating the ITER/NET plasma boundary in a reactor-relevant divertor configuration and parameter regime, especially the questions of heat deposition, wall erosion, and particle exaust under good confinement conditions
- investigation of the magnetics of an ITER-type plasma

JET collaboration
- operation of diagnostics at JET and general collaboration

Experimental Plasma Physics Division 2
Director: Dr. G. Grieger

Wendelstein 7-X
- preparation of construction
- further evolution of numerical and analytical methods of investigating equilibrium, stability and transport in three-dimensional toroidal configurations incl. plasma heating, particle and power exhaust
- engineering, R & D and prototype development

Contributions to stellarator reactor systems studies

Preparation of Greifswald site

Experimental Plasma Physics Division 3
Director: Prof. F. Wagner

Wendelstein 7-AS (Advanced Stellarator)
- stellarator with improved confinement conditions
- toroidal plasma confinement in the stellarator
- net-current-free plasmas, plasma production and heating by neutral injection, and high-frequency waves
- plasma stability and impurity effects

Technology Division
Director: Prof. R. Wilhelm

Neutral injection
- development and construction of the injection systems for W 7-AS, ASDEX Upgrade and W 7-X
- implementation of injection experiments

Electron cyclotron resonance heating
- preparation of ECRH for ASDEX Upgrade
- cooperation with ECRH project on W 7-AS

Ion cyclotron resonance heating
- preparation and implementation of ICRH experiments for W 7-AS, ASDEX Upgrade and W 7-X

Plasma technology (see also Surface Physics Division)
- development, characterization and modelling of low-pressure plasma processes for thin-film formation

Surface Physics Division
Directors: Prof. V. Dose
Prof. J. Küppers

Surface physics
- atomistic characterization of surfaces

Plasma wall interactions (analytical)
- interactions of atoms, ions and electrons with solid surfaces
- wall fluxes in the boundary layer of plasma devices
- limiter and wall analyses

Plasma wall interaction (preparative) (see also Technology Division)
- preparation and characterization of thin film coatings for plasma devices

Theory Division
Director: Prof. D. Pfirsch

Theoretical basis of plasma physics
- analytical and numerical MHD computations
- nonlinear instabilities
- models for anomalous transport
- high-frequency current drive
- turbulence theory

Tokamak Physics
Director: Prof. K. Lackner

Tokamak physics
- experiment-oriented theoretical work for the design and interpretation of tokamak experiments such as ASDEX, ASDEX Upgrade, JET and NET/ITER
- experimental work on plasma edge physics on ASDEX Upgrade

Computer Science Division
Director: Prof. F. Hertweck

Development of the AMOS/D system
Development of data acquisition systems for experiments at IPP
Studies in parallel computer architectures
Studies in neural networks

Berlin Division
Director: Prof. G. Fußmann

Experimental and theoretical investigations on impurities (production, transport, and radiation) in ASDEX Upgrade and W 7-AS

Plasma generator PSI-1
- operation and characterization of a high-current discharge
- plasma interaction with solid surfaces

Arc physics (especially vacuum arcs)

EXPERIMENTAL PLASMA PHYSICS DIVISION 1

(Prof. Dr. Michael Kaufmann)

Division E1 comprises two groups:

1. ASDEX Upgrade Operation and Diagnostics I

Head: W. Köppendörfer
Deputy Head: B. Streibl

Albrecht, M., Ch., Behler, K., Bessenrodt-Weberpals, M., Bosch, H.-S., Buchelt, E., de Blank, H.J., Deschka, S., Dorn, C., Drube, R., Dux, R., Eberhagen, A., Engstler, J., Fink, J., Finkelmeyer, H., Garcia-Rosales, G., Gehre, O., Gernhardt, J., Goss, H., Gruber, J., Haas, G., Herppich, G., Hohenöcker, H., Hupfloher, H., Jacobi, D., Kaplan, E., Kass, Th., Klement, G., Kollotzek, H., Kornherr, M., Krüger, P., Maraschek, M., Mast, K.F., Mattes, K., Meisel, D., Merkel, R., Mertens, V., Neu, G., Raupp, G., Reichert, G., Richter, H., Salmon, N., Schilling, H.-B., Schittenhelm, M., Schramm, G., Schneider, H., Schweizer, S., Seidel, U., Sokoll, M., Suttrop, W., Stober, J., Treutterer, W., Troppmann, M., Ulricht, M., Vernickel, H., Wolf, K., Zasche, D., Zehetbauer, Th., Zohm, H.

This group is concerned with the operation of the tokamak experiment ASDEX Upgrade and its peripheral installation. This group also conducts a part of the experimental investigations. This work is described under the ASDEX Upgrade project.

2. Diagnostics II

Head: H. Röhr
Deputy Head: H. Salzmann

Alexander, M., Asmussen, K., de Peña Hempel, S., Ebersberger, B., Engelhardt, W., Fahrbach, H.-U., Field, A., Herrmann, W., Ignacz*, P., Junker, W., Kallenbach, A., Kurzan, B., Lang, P.T., Lang, R., Murmann, H., Neu, R., Sandmann, W., Schönmann, K., Steuer, K.-H.

This group is responsible for the development of plasma diagnostics and pellet injectors for ASDEX Upgrade, JET and other experiments. In addition, plasma physics investigations with these diagnostics are conducted by the group. The activities are detailed under the projects ASDEX Upgrade, JET Cooperation and W VII-AS.

EXPERIMENTAL PLASMA PHYSICS DIVISION 2

(Dr. Günter Grieger)

The activity of the Experimental Plasma Physics Division 2 is concentrated mainly on the WENDELSTEIN 7-X Project (see Sec. WENDELSTEIN 7-X Project).

The relevant team is:

W 7-X

C.D. Beidler, W. Dommaschk, H. Greuner, G. Grieger, E. Harmeyer, F. Herrnegger, J. Junker, N. Karulin, J. Kißlinger, W. Lotz, P. Merkel, H. Münch, C. Nührenberg, J. Nührenberg, M. Pillsticker, F. Rau, H. Renner, J. Sapper, F. Schauer, I. Schoenewolf, U. Schwenn, E. Strumberger, A. Wieczorek, H. Wobig.

The team is supported by contributions from Kernforschungszentrum Karlsruhe (KfK), Institut für Technische Physik, and by the Central Technical Department of IPP.

EXPERIMENTAL PLASMA PHYSICS DIVISION 3

(Prof. Dr. Friedrich Wagner)

The W7-AS group comprises Experimental Plasma Physics Division 3. The work of which is fully reported in the section "Stellarator, Wendelstein 7-AS". The members are as follows:

Experimental Plasma Physics Division 3
R. Balbin[1], J. Baldzuhn, K. Behringer[9], R. Brakel, B. Brañas[1], R. Burhenn, G. Cattanei, A. Chih Yao Teo[10], J. Das, A. Dodhy, D. Dorst, A. Elsner, M. Endler, K. Engelhardt, V. Erckmann, T. Estrada[1], Y. Feng, U. Gasparino, J. Geiger, T. Geist, S. Geißler, L. Giannone, C. Görner[10], P. Grigull, H. Hacker, M. Haese[11], H.J. Hartfuss, O. Heinrich[10], G. Herre[10], M. Hirsch, J.V. Hofmann, E. Holzhauer[9], K. Ida[6], R. Jaenicke, M. Kaiser, F. Karger, M. Kick, A. Kislyakov[2], G. Kocsis[7], C. Konrad[10], H. Kroiss, G. Kuehner, A. Kus, H. Laqua, L. Ledl[11], T. Luce[4], E. De la Luna[1], J.F. Lyon[5], H. Maassberg, C. Mahn, W. Mandl, N. Marushchenko[3], K. McCormick, V.E. Moiseenko[3], H. Niedermeyer, W. Ohlendorf, M. Peters[8], V. Plyusnin[3], H. Ringler, M. Romé, N. Ruhs, N. Rust[10], J. Saffert, F. Sardei, S. Sattler[10], F. Schneider, U. Schneider, E. Simmet, D. Spong[5], U. Stroth, G. Theimer[10], E. Unger[10], F. Wagner, A. Weller, E. Würsching, D. Zimmermann, M. Zippe, S. Zoletnik[7]

1) Guest from CIEMAT, Madrid (Spain)
2) Guest from IOFFE Institute, St. Petersburg (CIS)
3) Guest from Kharkov Inst. (Ukraine)
4) Guest from General Atomics, San Diego (USA)
5) Guest from Oak Ridge National Laboratory (USA)
6) Guest from Nat. Inst. for Science, Nagoya (Japan)
7) Guest from KFKI Research Inst., Budapest (Hungary)
8) Guest from FOM-Instituut, Nieuwegein (Holland)
9) Guest from IPF Stuttgart (Germany)
10) Doctoral fellow
11) Undergraduate

Technical Teams W7-AS:
W. Andres, J. Bömerl, H. Czich, R. Dunkel, G. Grünwald, E. Hausner, F. Hoffmann, J. Hofner, H. Holitzner, R. Horn, G. Hussong, E. Katzmarek, A. Kellerbauer, H. Rixner, S. Schraub, R. Semler, J. Stadlbauer, U. Weber, G. Zangl, the Operatoring Team, the Assembly Group, and the Data Acquisition Team

Experimental Plasma Physics Division 2
K. Kisslinger, F. Rau, J. Sapper, H. Wobig, and the workshop of Experimental Division 2.

ECRH (Electr. Cycl. Resonance Heating):
W. Kasparek, G.A. Müller, P.G. Schüller (IPF Stuttgart)
H.U. Nickel (KfK Karlsruhe)
S. Fil'chenkov, A.V. Kostrov, L. Kukin, L. Lubyako, A. Shtanyuk, E. Suvorov, (IAP, Nizhny Novgorod, CIS)

ICRH (Ion Cycl. Resonance Heating):
W. Becker, F. Braun, R. Fritsch, C. Hoffmann, F. Hofmeister, J.M. Noterdaeme, Ph. Verplancke, H. Wedler, F. Wesner (Technology Division)
A.C. England, D. Rasmussen (Oak Ridge National Lab., USA)

NBI (Neutral Beam Injection):
K. Freudenberger (till July 94), W. Ott, F.-P. Penningsfeld, F. Probst, E. Speth, R. Süss, A. Teubel (Technology Division), W. Melkus (Central Technical Services)

Plasma Surface Interaction Group:
R. Behrisch, V. Dose, K. Ertl, Y. Furuyama, H. Verbeek, J. Roth, A. Schiavi

Division Berlin:
A. Herrmann, D. Hildebrandt, B. Jüttner, D. Naujoks, P. Pech, H.-D. Reiner, H. Wolff

Computer Centre:
S. Heinzel, H. Lederer

Central Technical Services:
B. Brucker, G. Förster, H.-J. Kutsch, E. Maier, J. Perchermeier and the workshop.

GENERAL THEORY DIVISION

(Prof. Dr. Dieter Pfirsch)

The areas treated in the General Theory Division are: nonaxisymmetric equilibria, linear and nonlinear instabilities, reconnection, turbulence, transport, cyclotron radiation. These studies are done in the framework of macroscopic and microscopic theories. Particular topics addressed are: resistive instabilities, sawtooth oscillations, MHD and drift wave turbulence, L/H-transition, negative-energy waves and corresponding nonlinear instabilities, transport across chains of magnetic islands. The study of a number of nonlinear phenomena entailed extensive numerical work. With respect to numerical methods, nonlinear systems of ordinary and partial differential equations are investigated.

1 MHD THEORY

1.1 Dynamics of the Sawtooth Collapse in Tokamak Plasmas

D. Biskamp, J. F. Drake*, and M. Walter
(*University of Maryland, USA)

Fast quasi-collisionless reconnection such as driven by electron inertia, which dominates over resistive reconnection in large, hot tokamak plasmas, qualitatively changes the dynamics of the sawtooth collapse. The collapse is predicted to occur in two steps, a fast Kadomtsev-like complete reconnection phase followed by a rapid reformation of a $q_o < 1$ configuration. The latter reconnection is driven by the strong flows generated during the first phase. Numerical simulations show that the final central q-value is similar to the original one, but the extent of helical flux reversal depends on the initial current profile, being particularly pronounced for a profile with a shoulder at the $q = 1$ surface. The theory provides a natural explanation of a long-standing puzzle, reconciling the apparent persistance of $q_o < 1$ with the central energy and density losses.

1.2 Existence of Three-Dimensional MHD Equilibria with Poloidally Closed Field Lines

A. Salat

The existence of MHD equilibria was investigated analytically for the subclass of nonaxisymmetric toroidal configurations with poloidally closed field lines and symmetry with respect to an equatorial plane. Two types of nonaxisymmetry are considered: a) noncircular magnetic axis, b) circular axis but variations of the geometry and/or magnetic field along the axis. It was proved that no equilibrium of type a) exists. As regards type b), it was shown that neither the ellipticity of the cross section, nor the triangularity, nor higher-order deformations up to and including the seventh order are allowed to vary. For still higher orders the same was made plausible. Hence type b) equilibria are also practically ruled out.

The nonexistence proof does not hold in the limit of vanishing aspect ratio and straight axis. For this straight case exact three-dimensional solutions of the MHD equations are presented. The configurations have neither cylindrical nor helical symmetry. All field lines are plane and closed around the axis. The magnetic surfaces have nested elliptical cross sections whose ellipticity along the axis is an arbitrary function.

1.3 MHD Stability Investigations

D. Lortz, G. O. Spies, and A. Zeiler

(a) Axisymmetric $m = 1$ modes in plane plasma-vacuum equilibria, which reduce to rigid shifts in the limit of cylindrical symmetry, have been investigated. It is shown that in elliptically corrugated equilibria stability depends on the direction of the shift (leading to the well-known vertical-shift instability), whereas in triangular or even higher-order corrugated equilibria the direction of the shift is of no importance.

(b) The theory of resistive peeling modes has been worked out for topologically toroidal slab equilibria. Such modes are unstable if, and only if, both the current density and the magnetic shear are discontinuous across the plasma-vacuum interface. The growth rates, when measured in units of the Alfvén frequency, remain finite in the ideal limit of large Lundquist numbers.

(c) The classical spheromak (current density proportional to the magnetic field, spherical plasma-vacuum interface, homogeneous magnetic field at infinity) is unstable to global magnetohydrodynamic tilting modes, even if a perfectly conducting rigid wall bounds the vacuum region.

1.4 Nonlinear Ideal Magnetohydrodynamics with Surface Currents

D. Pfirsch

A formulation of nonlinear MHD with surface currents and plasma flow on the basis of a Hamilton principle has been derived. In particular, transition conditions containing contributions from the plasma flow are obtained for the first time. The formulation is also applied to the linearized theory around static equilibria. It yields the well-known energy principle.

1.5 On Resistive MHD Stability

H. Tasso

(a) A general stability condition previously derived by the author is proved to persist to second order ϵ^2 in the perturbation despite the addition of several antisymmetric operators of first order ϵ in the linearized stability equation. This implies that more physics can be treated.

(b) Energy and Lyapunov methods are elegant and efficient for linear stability for both the fixed and the free boundary problems. By contrast energy methods for nonlinear stability of free boundary problems are very hard to establish. Compressibility causes basic difficulties in terms of nonvanishing surface integrals for the fixed boundary case.

1.6 2D Electron Magnetohydrodynamics and Collisionless Reconnection

D. Biskamp, E. Schwarz, and J. F. Drake

On time scales $< \Omega_i^{-1}$, the plasma behavior is determined by the electron dynamics interacting with the selfconsistent magnetic fields, described by the electron magnetohydrodynamics (EMHD). Strong current density gradients excite whistler turbulence with modes primarily perpendicular to the current direction, which suggests a 2D model. High resolution simulations of flux tube coalescence in EMHD have been performed. Current sheets have lengths $\Delta \sim c/\omega_{pe}$, while the width δ is determined by residual dissipation effects η. For sufficiently small η, i.e. small δ/Δ, current sheets are unstable giving rise to strong turbulence, which propagates into the downstream region. This turbulence provides an effective collisionless dissipation mechanism in the limit $\eta \to O_+$. Reconnection rates $\partial_t \psi$ are found to be independent of c/ω_{pe} and η.

2 TURBULENCE, TRANSPORT AND WAVES

2.1 Nonlinear Instability Mechanism in 3D Collisional Drift Wave Turbulence

D. Biskamp and A. Zeiler

Numerical simulations of 3D collisional drift wave turbulence reveal a behavior basically different from that found in previous 2D studies. The linear instability saturates due to energy transfer to small k_z leading to formation of convective cells. The turbulence is sustained by nonlinear transfer processes between $k_z = 0$ and $k_z \neq 0$ modes, the latter acting as a catalyst. The system tends to relax to a nonturbulent poloidal shear flow.

2.2 Tokamak Edge Turbulence

J. F. Drake, A. Zeiler, and D. Biskamp

The development of a first principles theory of the L/H transition requires an understanding of transport in Ohmic and L mode plasma. Similarly, the design of the ITER divertor requires an understanding of transport in SOL plasma. We have developed a set of 3D nonlinear equations in a realistic tokamak geometry which desribe resistive ballooning and drift waves in tokamak edge plasmas. These equations are solved in a novel flux tube coordinate system. The simulations allow to make predictions of absolute fluctuation levels and transport. The structure of the turbulence is controlled by a single parameter α, which is a measure of diamagnetism of the edge. For $\alpha < 0.5$ the turbulence is dominated by resistive ballooning modes and the resultant transport has a strongly ballooning character. Ohmic and L-mode edge plasmas in ASDEX, TEXT, ASDEX-U, DIII-D and C-Mod fall into this regime. For $\alpha > 1.0$ the magnetic curvature plays no essential role and the turbulence results from slab-like dissipative drift waves. In this regime all linear modes are stable. Nevertheless, a nonlinear instability sustains the turbulence. H-mode plasmas fall into the high α regime.

2.3 Electromagnetic Effects in Drift Wave Turbulence

S. J. Camargo, B. D. Scott, and D. Biskamp

Drift wave turbulence studies usually do not consider magnetic fluctuations. We are studying numerically a new extension of the Hasegawa-Wakatani equations that includes magnetic fluctuations. The main parameter of the system β is related to the usual ratio of thermal to magnetic pressure. When β is increased the effect of the magnetic fluctuations are more important, however causing significant changes in the system only for $\beta > 1$.

2.4 Quasi-Neutral Collisional Drift Fluids

D. Pfirsch and D. Correa-Restrepo

The usual theoretical description of drift wave turbulence makes use of various approximations, the effects of which are difficult to assess, in particular the conservation laws for energy and momentum. New collisional multi-species drift fluid equations are derived by a method which allows to prove in an elegant and consistent way conservation laws and to obtain the expression for energy dissipation. The results are not only interesting from a theoretical point of view, but also as a useful tool for numerical calculations.

2.5 Negative-Energy Perturbations in Axisymmetric Maxwell-Vlasov Equilibria

D. Correa-Restrepo and D. Pfirsch

(a) Negative-energy perturbations have been investigated for a class of two-dimensional configurations, which have no poloidal currents, $\beta_p = 1$, by evaluating the free energy expression derived by Morrison and Pfirsch for internal perturbations for a class of symmetric equilibria with distribution functions depending only on the total particle energy H and the conserved canonical momentum P. Owing to the toroidal current necessary for equilibrium in the presence of pressure gradients, at least one of the equilibrium distribution functions must be anisotropic, i.e. must explicitly depend on P. As a consequence these configurations allow negative-energy perturbations.

(b) The results obtained for $\beta_p = 1$ have been extended to the case of general axisymmetric configurations. These investigations make extensive use of the Poisson bracket formalism. In order to generate the currents necessary for a general axisymmetric equilibrium in the presence of pressure gradients, the equilibrium distribution function of at least one particle species must depend not only on the particle energy H and the canonical momentum in the toroidal direction P, but also on at least one of the other two constants of motion. Because of this dependence the configurations allow negative-energy perturbations.

2.6 Inverse Method for the Investigation of Nonlinear Instabilities

D. Pfirsch and H. Weitzner*
(*New York University, New York, USA)

Earlier work on explosively unstable similarity solutions of Hamilton's equations with Hamiltonians homogeneous of degree N and satisfying resonance conditions is applied to study the nonlinear stability of linearly stable equilibria with neighboring positive- and negative-energy waves. In the inverse method an explosively unstable similarity solution is assumed and one solves for the coefficients of the terms in a Hamiltonian of some given structure. Through some general arguments and many examples one concludes that explosively unstable solutions occur generally for wide ranges of coefficient values.

2.7 Tokamak Transport Based on the Thirteen Moment Model

M. K. Tippett and H. Weitzner

A new model for collisional transport in a tokamak plasma has been analyzed. The model is obtained from Grad's two-fluid thirteen-moment equations by estimating the order of magnitude of the various effects and neglecting those that are small. The model includes small particle flows, pressure anisotropy and temperature variation within flux surfaces.

2.8 Transport across Chains of Magnetic Islands

M. Schiegl and D. F. Düchs

In layers with magnetic islands both curvature and gradients of the magnetic field cause drifts in the plasma particles to such an extent that their orbits can cross the island chain. The space of initial conditions for various types of orbits is determined to obtain an estimate for collisional transport enhancement. This procedure is being extended to overlapping island chains.

2.9 Tokamak Magnetic Fields with 3-Dimensional Perturbations

D. F. Düchs, A. Montvai (FOM Netherlands)
K. Graf Finck v. Finckenstein (TH Darmstadt),
K. Riedel (NYU, USA)

Perturbed tokamak magnetic fields are most suitably computed in Hamiltonian formulation by special mapping procedures. Symplectic features can be used favorably for calculating the maps. The code for these field calculations is used as an example for the problem of determining an error estimate for numerical results. Computations of the long time evolution in a system with overlapping islands do not agree well with results from analytic calculations.

2.10 Emission of Extraordinary Waves from an Inhomogeneous Plasma

R. Croci

The asymptotic solution of the system of Vlasov- Maxwell equations for a plasma slab with an externally given current distribution has been derived for weak absorption, weak equilibrium density inhomogeneity, and homogeneous magnetic field. The importance of the proposed method lies in the fact that, different from the usual turning points method no model equations or phenomenological assumptions are introduced; particularly important is that wavelengths are not restricted to be larger than the Larmor radius. The example presented to illustrate the results considers the emission at the harmonics of the electron gyrofrequency of a population of fast electrons; the theoretical results are in qualitative agreement with the experiments.

2.11 Dynamical Systems and Discretization

R. Meyer-Spasche

The dynamical behavior of solutions of differential equations and of related difference equations has been compared. Convergence of difference schemes is much more easily described in closed time intervals ($t \leq T$) than in open intervals ($t \to \infty$). How instabilities and spurious solutions arise has been investigated in terms of dynamical systems theory for several model problems.

2.12 Multiple Solutions for Non-Linear Partial Differential Equations

D. F. Düchs, K. Graf Finck v. Finckenstein
(TH Darmstadt), and F. Pohl

For the example of nonlinear diffusion equations with nonlinear source terms the existence and the stability of multiple solutions has been investigated. Different numerical procedures have been compared. Of special interest are steady-state solutions and their accessibility from various ranges of initial conditions. For some cases of nonlinear boundary conditions asymmetric steady-state solutions have been found for *symmetric* initial conditions.

TOKAMAK PHYSICS

(Head of Project: Prof. Dr. Karl Lackner)

The main task of this division is theoretical and experimental support of IPP tokamak activities. Consequently, the major part of its work is reported in the sections regarding ASDEX Upgrade, JET and ITER/NET. The activities described below concern either more basic aspects of fusion plasma physics or the development of models and codes not exclusively linked to one particular experiment.

Head: K. Lackner, Deputy: J. Neuhauser
Team: G. Becker, A. Bergmann, M. Brambilla, K. Büchl, A. Carlson, R. Chodura, D. Coster, W. Feneberg, S. Fiedler, O. Gruber, O. Kardaun,, L. Lengyel, P. Martin,, G. Pautasso, K. Reinmüller,, R. Schneider, W. Schneider, J. Schweinzer, B. Scott, M. Weinlich, H. Werthmann, R. Wunderlich,H.-P. Zehrfeld

Guests: A. Boozer, College of William & Mary, Williamsburg, B. Braams, New York University, Yu. Igitkhanov, Kurchatov Institute, Moscow, E. Kakoulidis, G. Kyriakakis N. Tsois, Demokritos, Athens, G. Kristof, Technical University, Budapest, P. Lalousis, IESF.FORTH, Heraklion, P. McCarthy, H. Callaghan, University of Cork, A. Ushakov, I. Veseleva, V. Rozhansky, Technichal University, St. Petersburg, R. Zanino, Politecnico, Torino,

1. TRANSPORT MODELLING OF ITER AND ASDEX UPGRADE WITH 1.5–D BALDUR CODE

Special versions of the 1.5-D BALDUR predictive transport code were developed and applied in simulations of high-density scenarios of ITER with peaked and flat density profiles. The code self-consistently computes 2-D equilibria and solves 1-D transport equations with empirical transport coefficients. The emphasis of the recent studies was on scenarios with flat density profiles and a high, fixed radiative power loss in the main chamber, caused by argon and neon puffing. It was shown that self-sustained steady-state thermonuclear burn is reached for 370 s, and that it is compatible with the flat density profiles and strong radiation losses. The required global and local energy and particle transport was determined. In the argon and neon scenarios, the radiation-corrected energy confinement times are 4 s and 3.5 s, respectively, which are achievable according to the ITER ELMy H-mode scalings. Neon is superior due to its smaller radiative loss within the separatrix (37 % of the total radiation in the main chamber). High radiative losses from the confinement zone, mainly by bremsstrahlung, cannot be avoided. In steady state, a helium fraction of 5 % is computed. The fractions of helium, argon and neon and the corresponding fuel dilution are substantially lower than with peaked density profiles. A comprehensive empirical scaling law for the one-fluid effective heat diffusivity in ELMy H-mode plasmas was derived and validated against experimental data from different tokamaks. The transport law was successfully applied in modellings of high-density discharges of ASDEX Upgrade.

2. RECENT DEVELOPMENTS IN COMPUTATIONAL DRIFT WAVE STUDIES

A three-dimensional computational model of the electron component of fluid drift dynamics has been built in arbitrary axisymmetric flux surface configuration. Radial Fourier transforms are not used, as the system is periodic only in the angles. A flux coordinate system aligned to the magnetic field is used, allowing comparatively few grid nodes in the parallel direction (R. Dewar and A.H. Glasser). A scrape-off layer (SOL) is included, with Debye-sheath boundaries parallel to the field lines at a toroidally symmetric limiter. This makes the global nature of the computation necessary, as the interface between the closed- and open-field-line regions and between the core and SOL may be very narrow. Especially at the L→H transition, the "plasma edge region" in its entirety may be as narrow as 1 to 2 cm. In this model the profiles are variables carried on equal footing with the turbulence, and the plasma is maintained by external heating, treated in an edge computation as an outward heat flux across the inner boundary, and by edge fuelling via an inward flux of neutral atoms across the outer boundary, ionized by collisions with electrons. This model will deliver

its results on the electron fluid system in the coming year.

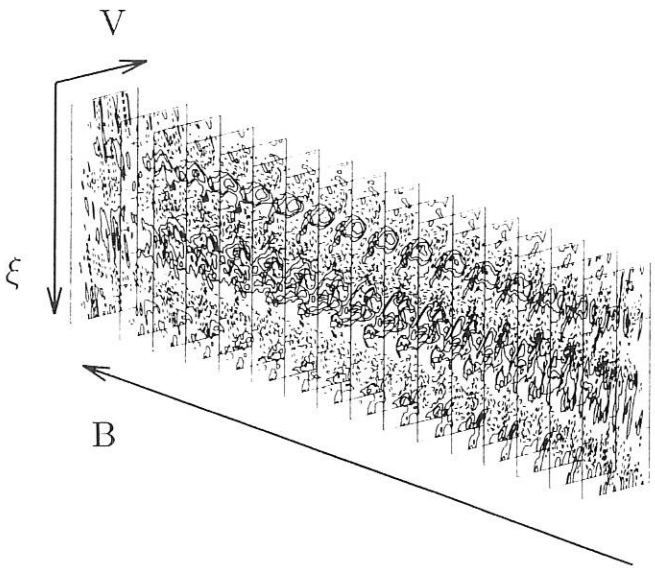

FIG. 2.1: Three dimensional structure of tokamak edge temperature fluctuations, in the flux coordinates V (flux surface volume), ϑ (poloidal angle mapped onto a field line), and ξ (field line label, opposite to the electron drift direction). The range of ϑ is once around the torus, with the ends on the inside, and that of ξ is 1/7 the way around the flux surface. In V, the box size is about 3 cm. This shows that rather large scales of fluctuation result from collisional drift wave turbulence.

A two-dimensional (2D) computational model has been constructed from the foregoing, by applying the poloidal/toroidal periodicity constraint to yield a parallel wavenumber, $k_{\|}$, as a function only of the radial position and the toroidal Fourier mode index. As long as the plasma is hot enough that the electron dynamics take the minimum parallel gradient allowed by the geometry, this can be expected to yield accurate results. The computational scheme is the same as that for the 2D slab, which allows very large grids, or carrying a run for several milliseconds of physics time, sufficient in an edge computation to put the profiles in stationary equilibrium. Computation of the TEXT edge by this method has reproduced all of the features of both the turbulence and the profiles – including the E×B shear layer – but with the exception that it failed ot exhibit a particle pinch: the density gradient was flat interior to the region where the neutral density was appreciable. This is perhaps due to the underestimation of $\kappa_{\|}$ at short perpendicular wavelength. The drift plane model fails in the SOL, where the minimum $\kappa_{\|}$ imposed by the Debye sheath is much too small to cause effective parallel dissipation. The 2D SOL models in current use by other authors are thereby put in question, since they are similar to the drift plane model in SOL.

Electromagnetic effects on drift wave turbulence using a 2D slab model were studied. In pressure gradient driven turbulence, the electromagnetic contribution to heat and particle transport is negligibly small, due to randomisation by the E×B turbulence of the phase of $\tilde{B}_r$.

3. IMPROVED CALCULATION OF THERMAL FORCES AND HEAT FLUXES IN THE B2 CODE

New subroutines for the multi-fluid B2 code were implemented to calculate the classical parallel heat fluxes and thermal forces in a multi-ion plasma in 21 moments approximation. The routines are based on the average-charge state formulation of the equations which constitute the relation between the heat fluxes, the parallel velocity differences, a higher moment of the distribution function and the temperature gradients. The number of coupled linear equations to be solved here is reduced from twice the number of fluids (charge states) to twice the number of different species (masses); e.g. for a plasma with H, C and Ne the number is 8 instead of 36 including two equations for the electrons.

4. 2–D PARTICLE SIMULATION STUDIES

Two-dimensional particle simulations are done for a magnetized plasma between two absorbing walls, one containing a Langmuir probe to which an oscillating voltage is applied. If the probe potential is positive so that electrons are collected, then the potential of the flux tube connected to the probe rises, and the time-varying electric field at the edge of the flux tube causes a polarization drift of ions across the magnetic field. This enhances the electron current to the probe and results in a hysteresis of the electron branch of the current-voltage characteristic of the probe. The maximum electron current is up to twice as strong as the electron source flux, so that the density in the flux tube decreases. The hysteresis effect is observed at any angle of the magnetic field, and its strength is proportional to ω up to $0.1\omega_{ci}$ and tends to saturate at higher frequencies.

The diamagnetic and $E \times B$ drifts in the vicinity of an absorbing wall are studied with non-uniform particle source (see Fig.4.1).

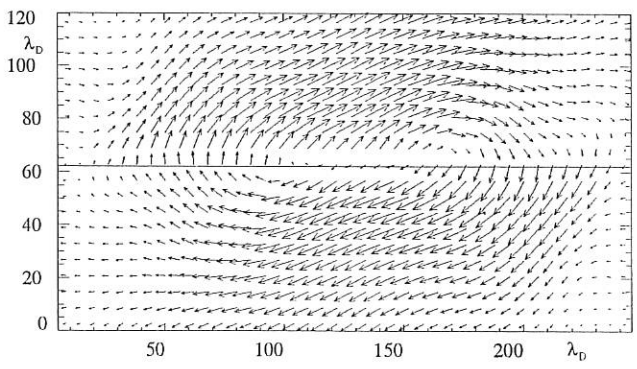

FIG. 4.1: Ion flow between two absorbing walls (top, bottom) in a particle simulation with a non-uniform source along the central line (maximum density in the centre). The magnetic field is tilted by 10° to the paper normal. $v_{ti}/\omega_{ci} = 10\lambda_D$.

At the edge of the magnetic sheath, where usually the boundary conditions for fluid codes are posed, the particle flux can be reversed at places where the drift is directed away from the target. However, close to the wall the flux is directed everywhere towards the target. Finally, the simulations are to provide boundary conditions for fluid models which include these drift motions.

As a first step towards simulating the instability inducing a unipolar arc, particle simulations of the plasma in front of a wall with an electron-emitting area are performed.

5. FLUID MODELLING OF THE PLASMA FLOW AT A DIVERTOR

Modelling of a SOL plasma by Navier-Stokes fluid equations requires boundary conditions at the sheath in front of the limiter or the divertor target for the flow velocity of each ion species of a multi-component plasma. Such boundary conditions are not available from the properties of the sheath and the (absorbing) target. The Bohm condition usually used as boundary condition is a limiting condition and not a boundary condition in the strict sense and remains to be only one condition in the case of more than one ion species. In order to meet this deficiency the fluid model was extended. This extended form of the fluid equations allows for arbitrarily large viscosities and needs no boundary conditions for the fluid velocities of the ion species. The fluid velocities at the boundary fulfill the Bohm condition on their own. The extended fluid model is checked numerically against a fully kinetic model for different situations (i.e. different collisionalities, magnetic field orientations etc.).

6. THEORY OF ION CYCLOTRON HEATING

The effect of Coulomb collisions on the absorption of H.F. waves in plasmas in the absence of resonant particles and spatial dispersion (cold-plasma limit) was reconsidered. Using the Landau form of the collisional operator, exact expressions for the collisional dissipation by pairs of charged species with arbitrary mass and charge ratios were obtained in terms of their mobility tensors.

Accurate semi-analytic expressions for the surface admittance matrix of large plasmas were derived and tested by comparison with those obtained by numerically integrating the wave equations. They can appreciably speed up modelling of ICRH antennas in large tokamaks like ITER. For this purpose, the question of boundary conditions at the plasma surface in the Finite Larmor Radius approximation (with three independent waves in the plasma to be matched to the two existing in vacuum) was elucidated.

A simple, yet accurate approximation was found for the toroidal Plasma Dispersion function, which describes the effects of space dispersion (non-locality along magnetic field lines) on the propagation and absorption of waves near ion cyclotron resonances in tokamak plasmas. It can easily be implemented in codes solving the wave equations in toroidal geometry, allowing a quantitative discussion of the effects of toroidicity on ion cyclotron damping and on linear mode conversion to ion Bernstein waves.

7. FUELLING BY PELLETS

The temporal evolution of pellet clouds in magnetically confined hot plasmas was calculated with the help of a two-fluid model consisting of the ionized and neutral components. Unlike in previous models, the inductive electric field associated with the time variation of the distorted magnetic field (high-beta interaction of the cloud with the applied field) and the effect of the cloud viscosity were also taken into account. The results were compared with those stemming from two alternative models and used for bench-marking calculations: a single-velocity model with the $\vec{j} \times \vec{B}$ force based on the local conductivity value and an ion-stop model in which the particles were instantaneously stopped upon ionization and were only used as collision centers for momentum depletion. The results stemming from the three models show a high degree of consistency.

Up-to-date pellet ablation models as well as models describing the erosion of divertor plates during disruptions (hot spots, etc.) require reliable information on the confinement radius of the vaporized substance and the bulk characteristics of the vapour cloud thus formed (temperature, density, ionization degree, etc.), following the moment of stopping of the transverse expansion of the ablated and subsequently ionized substance. Scenario calculations were performed for hydrogen and carbon pellets with the help of a time-dependent MHD code that includes finite-rate atomic processes, radiative losses (in the case of carbon), and electrostatic and magnetic shielding effects. A systematic variation of the four input parameters representing the backgroung plasma and the ablation rate: T_{e0}, n_{e0}, B_0, $\dot{N}$, was performed. The multiple regression analyses applied to the corresponding data sets resulted in scaling laws both for hydrogen and carbon. The scaling laws are now being checked.

8. SURFACE VAPORIZATION DURING DISRUPTIONS

Plasma particles incident on divertor plates during disruptions cause intense erosion of the surface. The slowed-down and stopped charged particles change the charge balance within the layer and contribute to the build-up of an electrostatic shielding field. An up-to-date model was developed for calculating it.

SURFACE PHYSICS DIVISION

(Prof. Dr. Volker Dose
Prof. Dr. Jürgen Küppers)

Scientific activities in the Surface Physics Division proceed via three routes, which we call plasma wall interaction (analytical), plasma wall interaction (preparative) and surface science. Our work on analytical problems of plasma wall interaction is for the purpose of this report further divided into two categories. Those activities which take place in intimate collaboration with fusion devices are included in the respective chapters on tokamaks and stellarators. Additional laboratory work described in this chapter is grouped under the title plasma wall interaction processes. Contributions to the field of plasma wall interaction (preparative) are described in a separate section entitled plasma technology. This project is a joint venture with the IPP Technology Division. More fundamental studies, summarized under the heading of surface science, comprise a continuation of previous activities in magnetism and contributions to the Sonderforschungsbereich 338. The latter concentrates on adsorption at solid surfaces and integrates work at the Munich Universities and IPP and MPQ.

Head: V. Dose, Deputy Head: E. Taglauer,

M. Anton[4], A. Annen[1], R. Behrisch, E. Berger[1], E. Bertel, J. Biener[1], T. Burtseva[5], V.N. Chernikov[6], T. Detzel[3], M. Donath, W. Eckstein, K. Ertl, Th. Fauster, R. Fischer[3], Y. Furuyama[7], A. Garrett[8], St. Grigull[1], S. Grudeva-Zotova[9], B. Gubanka[1], P. Hanesch[1], A. Horn[2], W. Jacob, A. v. Keudell[1], H. Knauf[10], U. Kögler[10], K. Krieger, J. Krumrey[2], M. Küstner[1], S. Labich[1], K. Lange[1], M. Langhoff[1], W. von der Linden, Ch. Linsmeier[3], C. Lutterloh[1], J. Lehmann[1], A.P. Martinelli, R. Matzdorf[11], M. Mayer[3], N. Memmel[3], S. Miller[1], D. Naujoks[3], F. Passek[3], P. Pecher[1], V.N. Petrov[12], H. Plank[3], W. Poschenrieder, V. Prozesky[13], G. Ramos-Lopez[1], G. Rangelov[3], J. Reinmuth[1], S. Reiter[3], P. Roos[1], W. Roos[17], J. Roth, P. Sandl[3], A. Schenk[3], B. Scherzer, A. Schiavi[3], St. Schömann[14], U. Schubert[1], R. Schwörer[3], R. Siegele[3], G. Staudenmaier, A. Steltenpohl[2], G. Thornton[15], M. Unger[2], P. Valášek[1], G. Venus, H. Verbeek, R. Vichev[9], W. Wallauer[1], W. Wang[16], M. Wittmann[3], S. Wolf[1], G. van Wyk[17].

1 Doctoral Candidate
2 Undergraduate Student
3 Post Doc
4 Guest, EPFL Lausanne, Switzerland
5 Guest, Efremov Institute, St. Petersburg, Russia
6 Guest, Kernforschungszentrum Jülich
7 Guest, Kobe University of Mercantile Marine, Japan
8 Guest, Cambridge University, UK
9 Guest, Bulgarian Academy of Sciences, Sofia, Bulgaria
10 Guest, KFA Jülich, Germany
11 Guest, Universität Kassel, Germany
12 Guest, Technical University, St. Petersburg, Russia
13 Guest, National Accelerator Center, Kapstadt, SA
14 Guest, Universität Leipzig, Germany
15 Guest, University of Liverpool, UK
16 Guest, Academia Sinica, Shanghai, China
17 Guest, Univ. of the Orange Free State, Bloemfontein, SA

1. PLASMA WALL INTERACTION

1.1 Erosion of Plasma-facing Materials

Erosion of plasma-facing materials strongly influences the design of advanced divertors for ITER. Erosion is important for the estimates of both plasma contamination and the lifetime of plasma-facing structures. Physical sputtering due to light plasma ions was investigated in detail and adequate analytical expressions were derived. Selfsputtering of surfaces due to returning energetic impurity ions may lead to run away erosion if values larger than unity are reached. Selfsputtering yields are enhanced at grazing ion incidence but may be strongly influenced by surface roughness. New results were obtained for Ni and Be, and first mathematical approaches to describe the surface roughness are presented.

Chemical erosion and radiation-enhanced sublimation are additional erosion mechanisms for graphite and carbon-based compounds. Also for chemical erosion analytic fitting formulae were derived. Chemical erosion as well as radiation-enhanced sublimation can be controlled by the use of B, Si or Ti-doped graphites and Carbon Fibre Composite (CFC) material, where enhanced erosion of carbon leads to a protective surface layer highly enriched in the dopant concentration.

1.1.1 *Self-sputtering of nickel and beryllium at oblique incidence*

(E. Hechtl*, W. Eckstein, J. Roth)
(*LMU Munich)

The bombardment of nickel with selfions and krypton for comparison is investigated for energies between 60 eV and 8 keV and for angles of incidence between normal incidence and 75° both experimentally and by computer simulation. Experimental weight loss measurements determine for Ni the sum of the reflection coefficient and the sputtering yield ($R_N + Y$), while for the recycling inert gas only Y is obtained. As predicted by the simulation, the experimental results clearly show the effect of the planar surface binding potential, which is 4.46 eV for nickel ions and 0 eV for krypton. Due to this difference the incoming nickel ions are accelerated towards the nickel target and approach the target at a decreased angle of incidence, which is not the case for krypton ions. It also demonstrates that in the experimental weight change method at large angles of incidence (75°) the particle reflection coefficient R_N dominates the result ($R_N + Y$) at low energies (~100 eV), whereas at high energies (>1 keV) the sputtering yield (Y) is the leading part.

For beryllium the selfsputtering yield was measured at 1 keV as a function of the angle of incidence (see contributions of Physik-Department of the Technical University of Munich). The experimental data increase with angle of incidence, but much less than computed results for a planar surface. It is assumed that the surface roughness of the beryllium samples is responsible for the reduced increase with angle of incidence.

1.1.2 *Erosion on simultaneous bombardment with carbon and hydrogen ions*

(D. Naujoks, W. Eckstein, R. Behrisch)

Simultaneous bombardment of wall components with low-energy carbon and hydrogen ions may result in a build-up of the carbon which is not compensated by erosion due to the hydrogen ions. Critical carbon concentrations for this effective reduction of the wall erosion are about 3.5 % in agreement with erosion measurements on a limiter probe exposed in TEXTOR.

1.1.3 *Measurement and characterization of surface roughness of graphites*

(M. Küstner, W. Eckstein, V. Dose, J. Roth)

Qualitative measurements on different graphites have shown previously that the increase of the sputtering yield with angle of incidence is reduced with increasing surface roughness. Only best polished surfaces exhibited the steep angular dependence calculated for flat surfaces (TRIM.SP). On artificial test-surfaces it could be shown that two parameters determine the angular dependence, i.e the distribution of actual angles of incidence on the tilted surface and, for strong topography, the shadowing of sputtered particles on neighbouring surface structures.

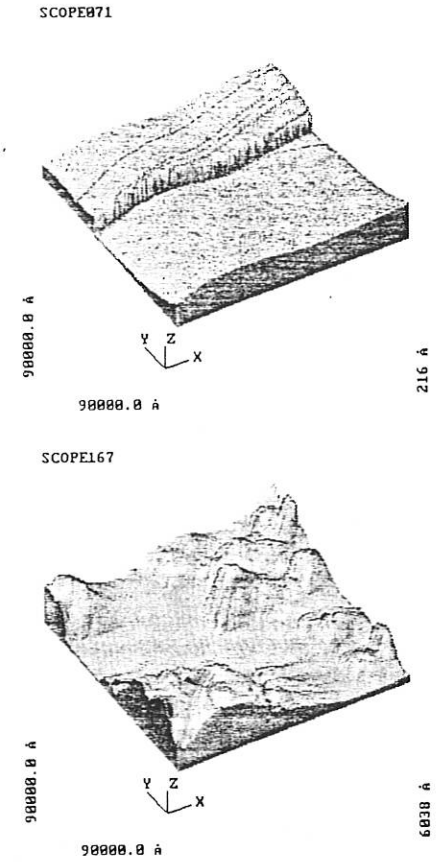

FIG.1: STM images for HOPG (top) and EK98 (bottom). The image size is 9x9 μm² with a resolution of 128x128 pixel. The maximum change in the vertical level is 216Å for HOPG and 6038 Å for EK 98.

In order to characterize the surface roughness of differently prepared graphites, the surfaces are monitored with a scanning tunnel-microscope (STM). Figure 1 shows the results for highly oriented pyrolytic graphite (HOPG) featuring an atomically flat surface with isolated steps and an isotropic fine grain graphite (EK 98) with large pores and crystallites.

A typical image of 9x9 μm^2 contains 128x128 pixels. In order to reduce the data volume, a principal components analysis is done, which retains 99 % of the image information for a data volume reduced by a factor 8 in the case of EK 98. On these reduced surfaces the distribution of effective angles of incidence will be determined and used as input parameter for computer simulations for sputtering, such as TRIM.SP.

1.1.4 *Surface segregation during ion bombardment of alloys*

(S. Schömann, G. van Wyk, E. Taglauer)

On Au_3Cu alloy crystals segregation of Au in the first layer on the (001) surface was found. Ion bombardment results in intermixing of Cu into the first layer, but due to preferential sputtering of Cu its concentration in the first layer is limited. Entropy driven desegregation sets in at temperatures above

600 K, from which behaviour a segregation energy of 47 kJ/mole was determined.

On AlNi(001) enrichment of Al is found in the first layer, combined with Ni enrichment in the second layer. Details of the segregation kinetics are studied by ion bombardment.

1.1.5 Analytical formula for chemical sputtering of carbon

(C. Garcia-Rosales, J. Roth)

One critical problem in today's fusion devices using graphite as first wall material concerns the erosion of surface material by chemical sputtering via hydrocarbon formation due to hydrogen bombardment from the plasma. This effect may lead to a considerable impurity flux into the plasma, as shown in recent measurements at the ASDEX-Upgrade tokamak. In order to calculate the contribution of chemical sputtering to carbon erosion and impurity flux into the plasma, it is convenient to have at one's disposal an analytic expression based on laboratory experiments. Up to now an empirical formula was proposed which only crudely describes the broadening of the temperature dependence of the chemical sputtering at incident energies ≤ 200 eV. This low-energy effect leads to a considerable erosion already at room temperature and to the absence of a threshold energy for carbon erosion. Following the results from recent studies the chemical erosion is now described by the sum of two separate processes: the well-known process leading to the pronounced maximum at 800 K for ion energies above 150 eV and a new process acting at ion energies below 150 eV and surface temperatures below 740 K. The thus derived analytic equation describes well the chemical erosion by deuterium ions in the energy range of 10 to 10 000 eV and temperatures between 300 and 1000 K.

In the comparison of pure graphites with boron-doped graphites it could be shown that only the high-energy process can be considerably reduced while the low-energy, low-temperature process remains unchanged by doping.

1.1.6 Sputtering and surface composition change of carbon-silicon compounds under D^+ bombardment

(H. Plank, R. Schwörer, J. Roth)

SiC-fibre-reinforced material (SiC/SiC) was investigated in respect of its sputtering behaviour, chemical erosion and surface composition change due to D^+ bombardment at energies between 20 eV and 1 keV and at temperatures up to 1000 K. The sputtering yields were determined from the weight loss of the target. A comparison with earlier results obtained from SiC samples with different structure and fabrication (e.g. single crystals, plasma-sprayed materials) shows that SiC/SiC has no different erosion behaviour. A weak chemical erosion with a maximum at 500 K was observed at D^+ energies below 100 eV. The chemical erosion is below 10 % of the value for pure graphite.

Due to the energy dependence of the methane release and the penetration depth of D^+ ions, it is expected that there is a surface composition change of SiC (bulk composition 50 at% Si, 50 at% C) at low D^+ energies. This was investigated with Auger Electron Spectroscopy (AES) in off-beam-time intervals. The enrichment of Si strongly depends on the ion energy and target temperature. A Si surface concentration of 92 at% was observed at 20 eV D^+ and 500 K. The Si surface enrichment reflects the temperature and ion energy dependence of the chemical erosion of SiC/SiC.

In comparison with SiC/SiC, a CFC material doped with 10 at% Si (LS 10) was investigated. Figure 2 shows the fluence dependence of the surface enrichment in Si for both materials. While for SiC the steady-state surface concentration was reached after $2.5*10^{19}$ D^+ / cm^2, for LS 10 it was reached only after $50 * 10^{19}$ D^+ / cm^2 (Fig.2). The saturation value at the surface for SiC at room temperature is about 85 at% Si and for LS10 about 56 at% Si. For 500 K, at the temperature of maximum chemical erosion, the surface concentration of Si in LS10 reached 70 at%.

The large fluence needed for Si enrichment in LS10 can be understood from the structure of the material. SiC grains of dimensions of about 1 µm are embedded in a CFC matrix and have to be etched out due to the ion bombardment. Thus several µm of material has to be eroded until the surface is covered with SiC grains protecting the underlying carbon material. The resulting surface structure is shown in Fig. 3. These findings have important consequences for the use of multicomponent materials as first-wall armours in fusion reactors. Due to intense ion bombardment a surface structure will be created which has favourable properties in respect of erosion, while the bulk has favourable properties in view of thermomechanical quality.

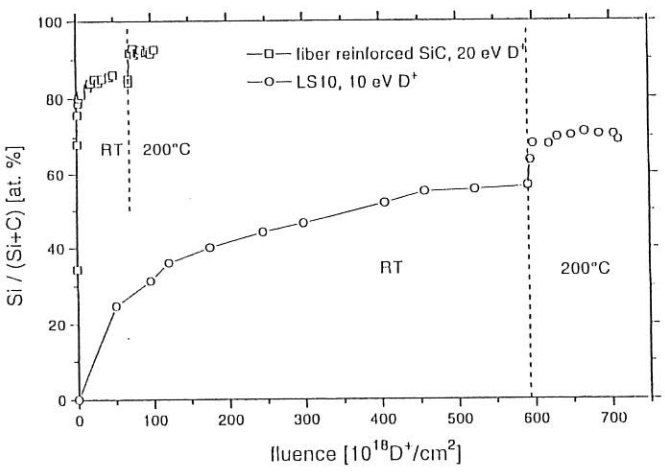

FIG. 2: Silicon surface concentration vs. fluence for D^+ - bombardment at room temperature. The saturation concentration for SiC is reached much faster than for LS10 indicating structural effects.

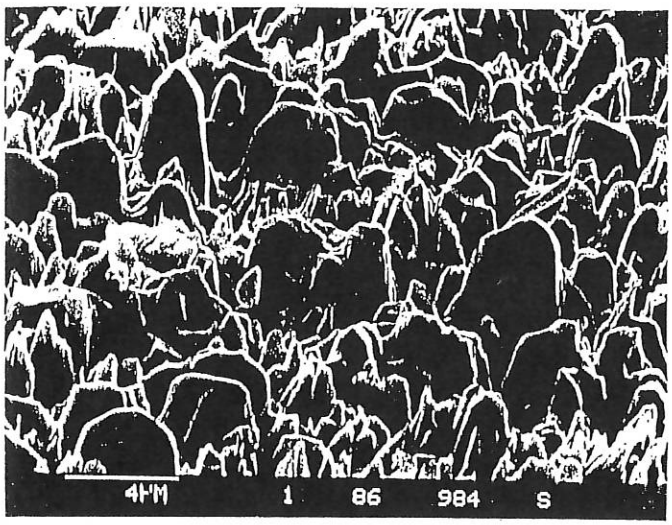

FIG. 3: REM picture of the bombarded area of LS10 at a magnification of 6000. A column structure developed during bombardment. X-ray analysis yields a silicon-layer on top of the columns, while the underlying bulk is carbon rich.

1.1.7 Line-of-sight measurements of the radiation enhanced sublimation of graphite

(P. Franzen, J.W. Davis* and A.A. Haasz*)
(*University of Toronto, Institute of Aerospace Studies)

The radiation-enhanced sublimation (RES) of pyrolytic graphite (HPG99) was measured during D^+ irradiation, by line-of-sight quadrupole mass spectroscopy (LOS-QMS). The quadrupole mass spectrometer was modified to block the transmission of reflected beam particles. This modification allowed the measurement of RES at temperatures below 1000 K, where physical (and chemical) sputtering dominates the erosion of graphite. Figure 4 shows the temperature dependence of the RES yield for 1 keV D^+ irradiation. The RES yield at ambient temperature is of the order of 10^{-3} C/D for 1 keV D^+, about one order of magnitude lower than the physical sputtering yield.

The temperature dependence of RES can be explained by means of a model based on fundamental physics. Frenkel pairs (C interstitials and vacancies), created by the ion beam, are able to diffuse through the graphite lattice. C interstitials which reach the graphite surface are weakly bound and can therefore sublime thermally. At low temperatures, the vacancies are immobile and RES is governed by the competition of interstitial diffusion and desorption and Frenkel pair recombination. Because the activation energies of these processes are similar (of the order of 0.3 eV), the dependence of the RES yield on temperature is weak. At temperatures above 1200 K, the vacancies also become mobile - the activation energy of vacancy diffusion is about 3.2 eV - and can disappear by annihilation with natural defects or by a collapse of vacancy lines leading to an increasing interstitial concentration; hence, the RES yield increases almost exponentially with increasing temperature. At these high temperatures (above 1200 K) the interstitial diffusion is very fast, so that RES is governed by vacancy diffusion.

Interstitial-vacancy recombination and vacancy annihilation are asssumed to be diffusion limited with recombination and annihilation radii of the order of several Å. The prefactors of interstitial and vacancy diffusion are obtained from random walk theory, the activation energies from the literature. The only fitting parameter is the desorption rate of interstitials from the graphite surface.

1.1.8 Divertor and limiter materials, surface layer analysis

(R. Behrisch, W. Assmann*,T. Burtseva,
C. Garcia-Rosales, S. Grigull, V. Prozesky, J. Roth)
(*LMU Munich)

Improved carbon materials obtained by doping with different concentrations of Ti and of B were produced and are being tested in respect of sputter erosion and hydrogen trapping. Sputtering-induced enrichment of the dopant in the surface layers is correlated with the observation of carbide crystallites on the surface. Two carbon tiles of the ASDEX-Upgrade divertor were replaced with Ti-doped carbon (RG-Ti) and their thermal and erosion behaviour during the present discharge period is being investigated.

For a fast, sensitive and quantitative analysis of vessel wall components from ongoing plasma experiments, especially layers composed of low Z-atoms, which may build up on the vessel walls of fusion experiments through plasma-induced material transport, the ERD (heavy ion recoil detection analysis) technique was further developed and the data evaluation programs were improved and provided. They were and are being applied for the analysis of a large number of samples from the vessel walls of JET.

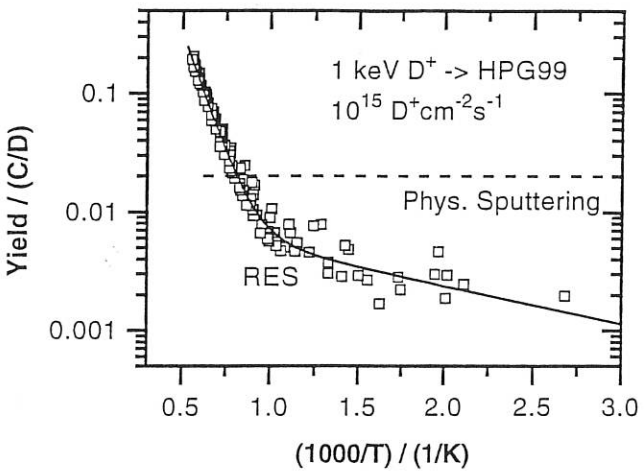

FIG. 4: Temperature dependence of the RES yield for 1 keV D^+ irradiation of HPG99. The solid curve through the data points is computed from the atomistic model.

1.2 Retention and Recycling of Plasma Ions

Retention of hydrogen isotopes implanted into the surfaces of plasma-facing materials, but also retained in layers of eroded and redeposited atoms, depends strongly on the material used. Codeposition is observed in fusion experiments in all carbon-containing layers. The details of film deposition, especially from hydrocarbon radicals, and the hydrogen content have therefore been investigated.

The plasma density control in fusion experiments and the helium dilution of the plasma strongly depend on the recycling behaviour of the first wall. Additionally to kinetic reflection and re-emission after recombination to molecules in recent investigations also ion-induced detrapping from saturated near surface layers was identified as a recycling mechanism. These processes were investigated with strong emphasis on graphites and carbon-based materials.

1.2.1 Hydrogen content of carbon films grown by CH_3^+ ion beam bombardment

(H. Plank. W. Wang, J. Roth)

The hydrogen content of carbon films grown by CH_3^+ ion beam bombardment onto pyrolitic graphite and silicon substrates was investigated by thermal desorption spectroscopy (TDS). In order to determine the H/C ratios of the films, the carbon content was evaluated using experimental deposition coefficients for CH_3^+ bombardment. The H/C ratios were also determined by ion beam analysis for comparison.

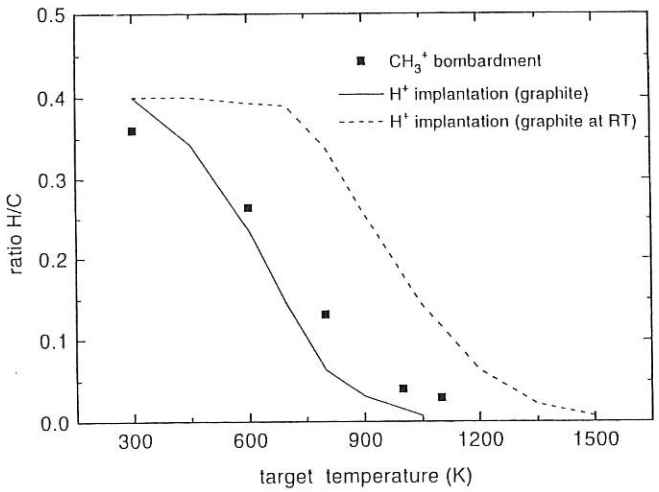

FIG. 5: Temperature dependence of H/C ratios of films deposited by CH_3^+ ion bombardment of Si and pyrolytic graphite. H/C ratios from H^+-implanted pyrolytic graphite are shown for comparison.

The H/C ratio of the deposited layers is independent of the CH_3^+ ion energy but strongly governed by the substrate temperature. It decreases from about 0.4 at 300 K to 0.03 at 1100 K. The temperature dependence of the H/C ratio is shown in Fig. 5, where average values are given for CH_3^+ ion deposition in the energy range of 150 eV to 3 keV. The H/C ratio decreases faster than anticipated from thermal desorption due to the additional effects of chemical erosion in the range 600-900 K and ion-induced detrapping of the adsorbed hydrogen in the a-C:H layer. Similar data have previously been reported for hydrogen implantation into graphite and are given for comparison. The fast decrease of the hydrogen codeposition with surface temperature may lead to considerably reduced estimates for the tritium inventory in future thermonuclear rectors, such as ITER.

1.2.2 Hydrogen inventory in graphite exposed to plasma

(M. Langhoff, B.M.U. Scherzer)

The hydrogen inventory in graphite during and after plasma exposure is investigated. Deuterium ions are implanted into graphite by an RF discharge with a mean energy of 150 eV and a flux of $4 \cdot 10^{18}$ at/(s·m^2). The total deuterium flux onto the target, including neutral deuterium atoms, is greater than $1.2 \cdot 10^{19}$ at/(s·m^2). An energetic He beam (2.6 MeV) allows in-situ measurements of the deuterium inventory in the graphite by means of ERD (elastic recoil detection analysis). Simultaneously the beam is used for RBS (Rutherford backscattering spectrometry) to monitor impurities on the target arising from erosion of the surrounding chamber walls.

The deuterium inventory is found to be twice as high as observed in graphite implanted only with ions of the same energy. It is believed that this is due to the build-up of a deuterium-rich C:D layer. Calculations show that this can be explained by a stitching process of desorbing CD_3 radicals from the surface. The formation of the C:D layer is supported by an enhanced cross-section for ion-induced release of deuterium by the energetic analyzing beam.

If impurities such as iron are deposited on the surface at low concentration, the formation of the C:D layer is hindered. The deuterium inventory drops. The formation of a needle structure, however, leads to an increase of the surface area and therefore to an increase in the deuterium inventory.

Measurements at elevated temperatures (600 K) show that the C:D layer is stable with respect to the deuterium inventory. A transient uptake of hydrogen in graphite up to 600 K could not be observed.

1.2.3 *Detrapping of deuterium in carbon at low bombarding energies*

(M. Mayer, W. Eckstein, B.M.U. Scherzer)

It was shown that at low implantation energies (≤100 eV) of deuterium in graphite below saturation the detrapping of this implanted deuterium by protium at the same energy occurs even at the lowest fluences (10^{15}/cm^2). This effect lowers the concentration of hydrogen implanted in graphite (below saturation) and has to be considered in the implantation at low energies. The effective detrapping cross-section increases by a factor of 10, going from 500 eV to 50 eV, which explains that this detrapping effect was not seen for higher energies.

1.2.4 *Range of hydrogen in light target materials*

(M. Mayer, W. Eckstein)

Calculated ranges and half-widths of the depth distributions of protium and deuterium in Be, C and Si are compared with experimental data published by Leblanc and Ross. Our values calculated with the TRIM.SP Monte Carlo program are found to be in good agreement with the experimental data; changes in the use of different interaction potentials and inelastic energy loss models did not appreciably change the outcome in the energy range investigated. This is remarkable to note, because other simulation programs based on the same assumptions show results deviating by a factor up to 5 from the experimental data.

1.2.5 *Re-emission, desorption and microstructure evolution of graphites under He ion bombarment*

(V. Kh. Alimov*, B.M.U. Scherzer, V.N. Chernikov, H. Ullmaier**)
(*Institute for Physical Chemistry, Russian Academy of Science, Moscow; **Institut für Festkörperforschung, KFA Jülich)

Helium re-emission, trapping, and thermal desorption from ordered graphite (HOPG and HPG) of different orientation, polycrystalline graphite (EK 98), and Ti-doped graphite (RG-Ti-91) bombarded by 40 keV He ions were measured at irradiation temperatures of 300 K and 800 K. The microstructure evolution of the implanted specimen was investigated by Transmission Electron Microscopy (TEM).

While He- re-emission from basal-oriented HOPG is dominated by blistering and flaking, edge-oriented HPG shows different re-emission states at room temperature assigned to He release from intrinsic cavities, early bubble formation, and bubble coalescence, respectively. At 800 K 100 % re-emission is quickly reached due to diffusive mobility of He.

Due to low He mobility normally to the graphite planes no thermal desorption is observed from basal-oriented HOPG up to 1200 K for small implanted fluences.

In contrast to conclusions by Niwase, graphite implanted at room temperature up to damage of 10 dpa and more cannot be regarded as amorphous, but shows a turbostratic structure.

1.2.6 *Radiation damage by helium and deuterium implantation in HOPG graphite and diamond*

(G.A. Ramos Lopez, B.M.U. Scherzer)

The experimental work on damage production in single crystalline graphite (HOPG) and diamond by channelling ion beam analysis was completed. For the production of damage in both materials the chemical interaction of the incident ions with the target material (e.g. hydrogen with carbon) is of minor importance. The large defect concentrations in graphite observed by channelling are explained by splitting into small misaligned crystallites and by local disorder of lattice atoms around point defects. Because of the anisotropy of the graphite structure strong blistering is found only in implantation parallel to the c-axes.

2. SURFACE SCIENCE

The second triennial period of Sonderforschungsbereich (SFB) 338 ends in June 1995. Concluding reports were filed and a new proposal was submitted for a third period. The surface science group contributes to SFB 338 with three projects entitled "Ion scattering on adsorbates", "Model catalysts for the investigation of metal support and metal / promotor interaction" and "Surface states and the dynamics of metal surfaces". Modern calculational methods were introduced to improve the evaluation of experimental data.

2.1 SFB 338

(E. Bertel, R. Fischer, P. Hanesch, S. Labich, J. Lehmann, Ch. Linsmeier, N. Memmel, S. Reiter, P. Roos, P. Sandl, A. Steltenpohl, E. Taglauer, S. Wolf in collaboration with H. Knözinger, LMU Munich, and K.D. Rendulic, TU Graz)

The step dynamics on Cu(115) at room temperature was characterized by scanning tunnelling microscopy (STM): while regular monoatomic steps have a low kink density and a stable position on the surface, double steps show strong kink migration with an activation energy of about 0.1 eV. The facetting of the surface upon oxygen adsorption into (104), (014) and (113) faces was visualized. Especially (113) facets show strong reconstruction and will be further studied mainly with respect to adsorption sites. This reconstruction is completely reversible upon oxygen desorption.

The growth and structure of ultrathin gold and palladium films on Ru(0001) were studied by low-energy ion scattering. For both metals up to a coverage of two monolayers layer-by-layer growth was found. The distance between the interfacial

gold and ruthenium layers as well as the distance between the top two gold layers was determined to be 2.4±0.15 Å. In contrast to the previously studied Fe/Cu and Co/Cu systems no interdiffusion of substrate and film material could be observed in the gold films.

The ubiquitous spectroscopic problem of decomposing overlapping lines and, thereby, accurate coverage determination in ion scattering spectroscopy is solved for a particularly ill-posed example of Pd adsorption on a Ru(001) surface employing Maximum Entropy. The total scattering signal consists of 13 partially overlapping isotope lines, which are resolved using non-biasing prior information.

The studies examining metal-support interactions at supported rhodium catalysts were extended to main group oxides, namely alumina and silica. In contrast to Rh/TiO_2, no encapsulation was observed for Rh/Al_2O_3. XPS measurements at Rh/TiO_2 model catalysts after heat treatment under UHV conditions revealed a reduction of the support, which was not observed for heat treatment in hydrogen at ambient pressures. For further studies of the Rh/SiO_2 system, model supports of thin SiO_2 films on molybdenum were prepared and examined by X-ray Photoelectron Spectroscopy (XPS).

The study of low-dimensional electronic states was continued by measuring the dispersion anisotropy of the Shockley surface states on Cu(110). A surface resonance was identified in the centre of the surface Brillouin zone on Pt(111). This completes the systematics of Shockley surface states on the fcc(111) faces of the d^9-transition metals and the noble metals. Comparison of the surface state data with the adsorption enthalpies of rare gases and the dynamics of H_2 dissociation on these surfaces reveal a significant influence of the surface states on the physisorption potential, the dissociation barriers and hence the reactivity of metal surfaces (collaboration with K.D. Rendulic, Inst. f. Festkörperphysik, TU Graz). On the basis of these results, a novel mechanism for the promotion of catalytic reactions was put forward.

2.2 Surface Magnetism

(Th. Detzel, M. Donath, V. Dose, K. Ertl, B. Gubanka, W. von der Linden, F. Passek, J. Reinmuth, P. Valášek, M. Vonbank, in collaboration with A. Hubert, University of Erlangen, J. Noffke, TU Clausthal and V.N. Petrov, TU St. Petersburg)

The relationship between atomic arrangement, spin-dependent electronic structure and magnetic properties in systems with fewer than three dimensions was studied by Kerr microscopy, spin- and angle-resolved inverse photoemission (IPE), and spin-resolved appearance potential spectroscopy (APS).

The lifetimes of image-potential-induced surface states on magnetic surfaces were qualitatively explained by assuming electron-hole-pair production as dominant decay channel.

The series of investigations on ultrathin fcc Fe films on Cu(001) was pursued with IPE experiments. Attention was focused on the thickness range between 5 to 10 monolayers where only one or two layers are ferromagnetic. The exchange splitting of an electronic surface state proved the ferromagnetic layers to be located right at the surface. In addition, this particular state was shown to be a sensitive detector of the fcc crystal structure of the topmost iron layers.

Investigations of the magnetic and structural properties of an alloy surface, $FeNi_3(111)$, were started by characterizing the magnetic domain structure of the surface using Kerr microscopy. Spin-resolved APS aims at studying structural and magnetic phase transitions at the alloy surface by separately probing the Fe and Ni signals.

Appearance potential spectra of heavy fermion systems are calculated and analyzed in the frame of the Gunnarsson-Schönhammer approach for the Anderson impurity model (this procedure was successfully used to describe a wide variety of one-particle spectroscopies of 4f systems). We used a generalization of the Gunnarsson-Schönhammer approach to determine the two-particle response function. We find excellent agreement with the experimental data for $CeNi_5$ and $CePd_3$.

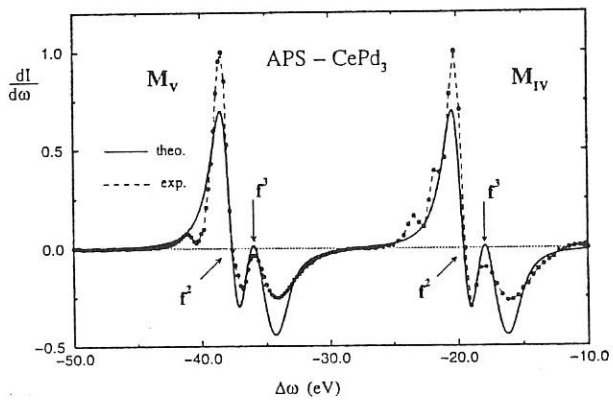

FIG. 1: Theoretical result (solid line) for the first derivative of the APS intensity for $CePd_3$ compared with normalized experimental data (dashed line).

TECHNOLOGY DIVISION

(Prof. Dr. Rolf Wilhelm)

The main task of the Technology Division is the development and operation of the various plasma heating systems at IPP's two major facilities. For a more detailed description of these projects (viz. neutral beam injection and ion cyclotron heating on ASDEX Upgrade and W7-AS, and electron cyclotron heating on AUG) the reader is referred to the respective sections of this report. The following sections present some further information on specific technical developments and experimental and theoretical work within the plasma heating programme or in connection with general reactor aspects.

1. NEUTRAL INJECTION HEATING

Group leader: E. Speth
Deputy: W. Ott

M. Ciric, J.-H. Feist, K. Freudenberger*, B. Heinemann, W. Kraus, H. Lohnert[1], P. McCarthy[2], W. Melkus[1], S. Obermayer, F.-P. Penningsfeld, F. Probst, R. Riedl, W. Schärich, A. Stäbler, R. Süß, A. Teubel, O. Vollmer, K. Wittenbecher

* till July 94
1 Central Technical Services
2 Tokamak Physics Division

1.1 Results from the RF Source Development

M. Ciric, J.-H. Feist, W. Kraus, E. Speth

The development work on the RF source concentrated mainly on two fields:

a) understanding of the performance and optimization of the configuration of the source itself;
b) commissioning and optimization of the new power-regulated RF generator.

In the former field a comparison of various configurations was made concerning reliability, required RF power (for full beam current) and beam transmission. As a consequence, it was decided to return to the previous configuration with an external RF coil because - compared with the source version with the internal RF coil - a higher power efficiency, better beam quality, and much better reliability were observed (see ASDEX Upgrade).

In the latter field a new 120 kW RF generator at 1 MHz with regulation of the output power, as a prototype of the future supplies for the second injector, was installed and started operation in autumn. It is a self-excited oscillator, equipped with a tetrode and power regulation and modulation by control of the screen grid and the control grid, respectively. Different rise times can be chosen in steps of between 300 µs and 1 ms, which is quite important for reliable PINI operation (notching of the RF plasma after a high-voltage breakdown). The generator delivers more than 125 kW; the nominal regulated output is 120 kW on a load impedance of 100 Ω. Lower impedances are optional.

Furthermore, a new ferrite-core RF/high-voltage transformer with 38 ring cores was developed. It has a current transmission ratio of 1:4 to minimize transmission losses and forms part of the impedance matching network. The cores are air-cooled. An efficiency of 0.8 A of the extracted beam current per kW of RF power was achieved with this setup.

1.2 Numerical Work

F.-P. Penningsfeld, A. Teubel, P. McCarthy

The two versions of the FAFNER Monte Carlo code (with/without radial electric field) simulating neutral beam injection into stellarators and the NIPOR program, which takes data sets of the local power deposition for fast analytical estimations, are now being routinely used to determine the NBI efficiency into W7-AS.

A study on perpendicular injection to achieve better confinement by creating an additional electric field was conducted. The geometrical constraints were determined with the DENSB code, whereas the optimal injection geometry as well as radial electric field effects on fast ion losses were studied with the FAFNER routines (see W7-AS for details).

FAFNER2 was applied to W7-X to determine fast orbit losses of injected particles. Fast orbit losses are negligible (<1%) in this device due to the optimized Helias configuration.

Additionally, FAFNER2, which is a parallelized code, was applied to ASDEX Upgrade. It was benchmarked with PENCIL

for a typical AUG configuration. The birth profiles were in good agreement. Differences in the deposition profiles are mainly due to an underestimation of charge-exchange processes in PENCIL. The new code can be taken to simulate NBI into 2D tokamak plasmas.

2. ION CYCLOTRON RESONANCE HEATING

Group Leader: F. Wesner
Deputy: F. Hofmeister

W. Becker, F. Braun, H. Faugel, R. Fritsch, C. Hoffmann, J.-M. Noterdaeme, S. Puri, Ph. Verplancke[1], H. Wedler

[1] Doctoral Fellow of N.F.W.O., Belgium

2.1 Fast ICRH Reactions of the RF Generators to ELM's during the H-mode

F. Braun, Th. Sperger

During type-1 ELM's, occurring during the H-mode in tokamaks with high heating power, the coupling of ICRH antennas is strongly changed, resulting in reflection peaks similar to those caused by arcing. The RF power is immediately cut-off in these cases since such reflection peaks are normally used for arc detection. As matching circuits, used hitherto in some experiments to compensate coupling variations, cannot cope with these fast coupling changes, type-1 ELM's constititue a general new problem for ICRH devices. On ASDEX Upgrade cut-off during ELM's has so far only been avoided up to about 1 MW by matching to impedances between the values of ELM's and ELM-free phases.

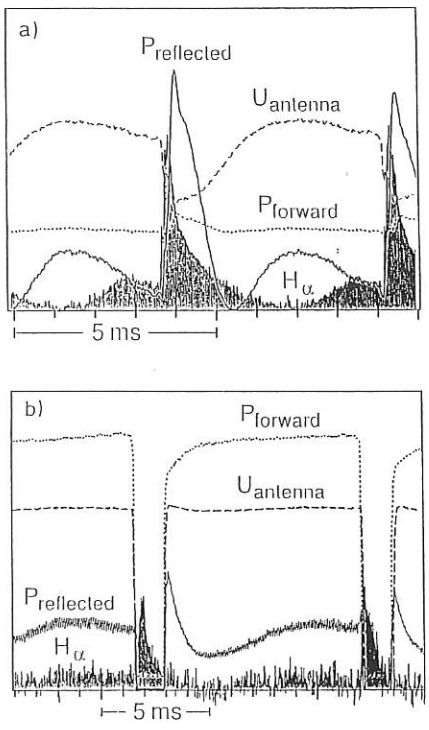

FIG. 1: Reaction of the antenna coupling and of the RF circuit on type-1 ELM's. The sharp and high reflection peak normally triggers a safety cut-off (a). This can be prevented by a fast reduction of the generator power (in this case to zero), triggered by an ELM-signal (H_α or ring voltage) before the antenna coupling is changed (b).

This problem was overcome by developing a fast micro-computer device (68332 processor) which is triggered by an ELM signal and immediately reduces the generator power. It turned out that, with the ring voltage as trigger signal, this power reduction can be achieved fast enough to avoid reflection peaks. This device has been successfully tested: Figure 1 shows the reflection peak (a) and its prevention (b). In the case shown, when the power was reduced to zero, and with high ELM frequencies, the average RF power is reduced by about 20 %.

With a smaller power reduction and additional logic decisions, also possible with the microcomputer within the short time sllowed, , the average heating power is now reduced by about just 5 % (the power is only reduced if the reflection exceeds an adjustable value, and is immediately raised when it again becomes small enough).

2.2. Further Development in RF Matching

F. Hofmeister, H. Faugel

With the aim of improving the matching estimate for the next shot tuner positions, phase measuring, and linear rectifier electronics were developed. Additionally to the former way of measuring the scalar ratio of net power to squared maximum voltage in each antenna feeder line, predicting the tuner positions for matching is now assisted by measurements of the vectorial quantity of the reflection coefficient in the generator feeder line on the generator side of the tuner pair. This method improves matching in situations with plasma coupling conditions changing from shot to shot or in finding a matching compromise in the cases of type-1 ELM's at high additional heating power or an H-mode transition within the ICRH pulse. It is also a prerequisite for planned feedback tuning within an ICRH pulse. This can be done either in a relatively long (>2 s) pulse by letting the tuners run with their maximum speed of approximately 45 mm per s or by the very fast way of changing the frequency during the shot. The latter way has its limits in the generator bandwidth and needs a particular network configuration, which involves some drawbacks in operational flexibility. Both methods have been prepared for implementation in 1995.

2.3 Completion of the 200 MHz Bandwidth Langmuir Probe System

Ph. Verplancke

Theoretical work on RF Langmuir probes (see Annual Report 1993) indicates that interesting new physics appear at RF frequencies, offering prospects of new SOL diagnostics. Six Langmuir probes, flush-mounted in the lower outer divertor plate of ASDEX Upgrade, were put into operation at the start of 1994. The challenging 0 - 200 MHz measurement system is discussed here, first results being presented in the section on AUG diagnostics.

The probes are connected to coaxial cables with a teflon dielectric, withstanding the tokamak bakeout and suitable for vacuum operation. The power necessary to sweep through the current-voltage characteristic of the 200 mm^2 graphite probes, lies in the range of a few hundred W and is delivered by a 1 kW, 10 kHz - 200 MHz wide band, tube chain amplifier. This device is earthed to the tokamak and supplied with power via an insulating transformer to avoid the use of a wide-band DC break in the coaxial cable. Additionally, a DC bias voltage can be applied via a so-called T-bias, consisting of a choke coil and capacitor. To achieve stiffness of the amplifier output voltage during fast frequency sweeps with the changing and nonlinear Langmuir probe load, a bifilar 9:1 ferrite impedance transformer was built and put between the amplifier and the load.

Voltage and current are measured in the time domain, with a DC-200 MHz bandwidth, about 7 m from the probes, and transformed to the probe position with the classical transmission line formulas. This fully avoids the problem of compensating for cable currents, which would in any case only be possible in a narrow frequency band. Careful design of the voltage measuring probes allowed us to achieve a flat frequency response with only resistors. The current measuring probes combine a high common mode rejection ratio, resistive measurement for DC-10 kHz, and a transformer for the 10 kHz 200 MHz range. The circuits to combine both bands were developed, since commercially available systems only work up to 50 MHz. Analog-to-digital conversion is done with a 200 MHz digital oscilloscope, still earthed to the tokamak. Control and data acquisition are realized via General Purpose Interface Bus with an optical fibre extension to achieve galvanic insulation from the control room.

Explorative studies of new high-frequency physics of flush-mounted Langmuir probes were carried out (see section on AUG diagnostics). Work is now focussing on the displacement currents in the ion magnetic sheath as a possible diagnostic for ion edge temperature.

2.4 Plasma Dielectric Tensor in a Tokamak

S. Puri

A precise evaluation of the plasma dielectric tensor in an axi-symmetric toroidal geometry is conducted using the exact Grishanov-Nekrasov[1)] integral form valid in the large aspect ratio and vanishing Larmor radius approximation.

The difficult integrations over velocity, azimuthal angle and phase angle are performed using a combination of Dawson integrals and the steepest-descent approaches. The results become exact in the limit as the ratio of the toroidal circumference to parallel wavelength approaches infinity.

The irrelevance of wave-particle phase decorrelation in the low-collisionality, hot thermonuclear plasmas is pointed out. Collisional effects become important only at low temperatures as the collision frequency becomes comparable to the particles' transit frequency around the torus.

Absorption is positive definite for all radial as well as azimuthal locations (without the need to average over the azimuth) for a Maxwellian plasma. The errors in the physical models that lead to echo-like effects with consequent non-positive-definite local absorption are pointed out.

3.0 ECRH ON ASDEX UPGRADE

(ECRH Group, in cooperation with IPF Stuttgart and IAP Nizhni Novgorod)

Group leader: F. Leuterer
Deputy: M. Münich

F. Brandl, H. Brinkschulte, F. Monaco, G. Pereverzev, F. Ryter, M. Zouhar

3.1 Gyrotron Operation

Within the collaboration with IAP Nizhni Novgorod we have put one gyrotron with 0.5 MW/0.5 s into operation on a stone load. Two parameter sets for high power output were tested, one at 70 kV/24 A with an output power of 500 kW, the other at 62 kV/ 24 A with an output power of 430 kW. For both cases the magnetic fields in the cryomagnet and gun magnet have to be adjusted to maximize the power output. The quoted powers are measured direct at the gyrotron output with 50 ms pulses into a calorimetric load and thus also contain possible contributions from non-Gaussian modes. The gyrotron was then connected via a three-mirror quasioptical line to a high-power stone load, and pulses of up to 0.5 s were achieved.

3.2 Gyrotron Operation in the Stray Magnetic Field of the Tokamak

The impact of the AUG poloidal magnetic field on gyrotron performance was first tested with a dummy tube, i.e. a tube where the collector top is removed and replaced by a glass disc. The collector surface is sprayed with a fluorescent coating so that the beam deposition can be seen in low-voltage operation. Without the perturbing stray field the electron beam is deposited cylindrically symmetric. In the presence of the stray field the distortion of the beam trajectory is weak on the collector side pointing towards the tokamak, while it is strong on the opposite side. This is because the perturbations due to the horizontal and vertical components of the stray field have opposite and equal signs, respectively, and thus have a compensating or an additive effect. These observations were obtained while AUG was running 800 kA discharges, with a stray field amplitude of about 13 G. At full performance of 1.6 MA we expect a stray field amplitude of about 30 G. Assuming that the deviation of the beam deposition scales linearly with the stray field amplitude, we estimate that from the beam deposition point of view we should be able to run this tube even at full AUG parameters.

We also operated the actual gyrotron in the presence of the stray field, which changes sign during an AUG shot. We

---

1) N.I. Grishanov, F.M. Nekrasov, Fiz. Plasmy **16** (1990) 230

performed 100 ms pulses both at the beginning of an AUG shot and at the end. In each case the gun magnetic field, which determines the beam compression, had to be slightly readjusted in order to take the additional vertical component of the stray field into account. In the cavity region of the gyrotron the stray field is negligible, as long as the tube is not operated at its stability limit.

3.3 Absorber for Millimetre Wave Radiation

The gyrotron output also contains power in unwanted modes, which do not hit the mirrors and finally end up at the walls of the mirror boxes, where they should be absorbed. Water pipes mounted on these walls provide one possibility. We looked for surface coatings with absorbing material on a metallic wall. Layers of mineral compounds (containing bound water) 5 to 8 mm thick were not satisfactory. They showed strong interference as a function of the angle of incidence of the microwave beam, indicating that the absorption per transit is not sufficient. A coating of "Bügellack", used in high-voltage engineering, about 0.3 to 0.4 mm thick showed a low reflection of about 30% over a wide range of angles, with no indication of interference between the waves reflected from the dielectric surface and the metallic wall . Theoretically this can be modelled with a material with $\varepsilon \approx 6 + i2.5$. Such an imaginary part corresponds to a skin depth of the order of the layer thickness and to a conductivity of about 20 $(\Omega m)^{-1}$. Because of the thin absorbing layer we expect that the deposited heat can be rapidly transferred to the underlying aluminium structure. Pulses of 0.5 MW/0.5 s at 140 GHz were transmitted through a mirror box thus coated. The present coating is certainly not sufficient for long pulse, for which we still need to find a material with similar dielectric properties but high thermal strength and conductivity.

4. REACTOR ORIENTED STUDIES

A. F. Knobloch

The ongoing tokamak reactor studies were continued with a view to arriving at a more general description of the accessible configurations and parameter sets for both pulsed and steady-state next-step and prototype conceptual reactors.

The relations for the optimum aspect ratio (for definition see IPP Annual Report 1993) derived on the basis of a certain ratio of the average neutron wall load to a combination of input parameters show a notable aspect ratio dependence of all reactor parameters and of their respective accessible domains.

It was now found possible to derive the aspect ratio without any predetermined reactor operating parameter. This approach requires involving the assumed energy confinement scaling (taken in the power product form), which allows identification of the impact of alternative scalings and the pertaining enhancement factors (which have to be adjustable) on the preferred configuration. The general aspect ratio equation implies the power product scaling exponents in characteristic combinations leading to notably different relations for different scalings. With fixed input assumptions on the specific plasma properties, the maximum toroidal field, and the blanket/shield thickness, all dimensional and operating parameters of possible consistent reactor configurations follow directly from the respective optimum or off-optimum aspect ratio, with the option of including aspect ratio dependent relations between input parameters.

For a better understanding of the fundamental differences between the properties of unshielded tokamak experiments and shielded reactor concepts it is interesting to derive also the design relations for a zero blanket/shield thickness. In that case the aspect ratio is determined only by one geometry factor and the relation to the optimum situation.

A tokamak reactor formulary was compiled from which to derive in a straightforward manner possible reactor parameter combinations based on certain input data. This supports a structured evaluation of the accessible parameter range. So far additional limitations such as the ones imposed by tolerable divertor operating conditions are not included.

A few preliminary observations - supporting earlier results and substantiated by the the present ITER EDA parameter set[1] - are: While for an unshielded experiment the optimization of the aspect ratio leads to $A < 3$ (as chosen for JET), the inclusion of about 1 m of blanket/shield distance yields $A \sim 4$ with some impact of the input parameter combination. In order to obtain a JET-like aspect ratio for a reactor, one has to deviate notably from the pertaining optimum geometry. This, by comparison, leads to a notably higher plasma current. Furthermore, below the optimum aspect ratio the inductive burn pulse duration at the rated operating conditions strongly reduces from typically hours down to, for instance, about 1000 s (which is low; a steady-state plasma current density distribution, for example, is not achieved). Pulsed reactor concepts with inductive current drive for long burn pulses require larger than optimum aspect ratio, typically $A > 5$ for about 10 h, and a reduced toroidal field. In view of the lack of understanding of energy confinement, hence of the present necessity to extrapolate from one development step to the next one, the basis for pulsed reactors[2] is poor, besides the fact that they do not appear to be of practical and economic interest.

Steady-state operation calls for high current drive efficiency and a large bootstrap fraction, high plasma temperature, high Troyon coefficient, larger q and toroidal field, supported by a larger aspect ratio with the plasma current being reduced. Such a high-Q situation, however, also calls for a larger confinement enhancement factor f_H. A low aspect ratio next-step reactor designed for pulsed operation, high plasma current, and large f_H (assuming the largest f_H value found tolerable for the ELMy H-mode) may not attain steady-state conditions with low current drive efficiency even with a reduced plasma current.

The conclusion results that the next step in tokamak reactor development must be directly relevant to and extrapolatable to a prototype steady-state reactor.

---

1) P.H. Rebut et al., ITER Papers and Posters, 15th Int. Conf on Plasma Phys. and Contr. Fusion, Seville 1994.

2) R.W. Conn et al., Assessment of Fusion Power Plants Based on Pulsed Tokamak Operation: The Pulsar Study, 15th Int. Conf on Plasma Phys. and Contr. Fusion, Seville 1994.

PLASMA TECHNOLOGY

(Prof. Dr. Volker Dose
Prof. Dr. Rolf Wilhelm)

The Plasma Technology group is concerned with three tasks: Surface coatings are produced by means of plasma-enhanced chemical vapour deposition (PECVD) for special applications, mainly in fusion plasma devices. New or improved PECVD procedures or devices are being developed for this purpose. As the scientific part of the activity, plasma, plasma edge, and thin film diagnostics are employed in order to correlate the discharge parameters with the properties of the resulting coatings and improve understanding of the basic mechanisms of plasma deposition. The third goal is a modelling of the deposition process which allows the discharge conditions to be adjusted in a predictable way in order to optimize a desired property of the growing film.

In 1994, the main activities were in-situ characterization of the growth and etching of hydrogenated carbon films, modification of an ECR plasma chamber to allow measurement of the particles fluxes onto the substrate, and modification of a deposition chamber to permit handling of toxic and explosive precursor gases which are used to deposit boron containing thin films. A new experiment was set up with the aim of studying multipactor discharges and their interaction with surfaces.

V. Dose (Division Head)[1], W. Fukarek (until 31.01.94), S. Grudeva-Zotova[5], F. Höhn[2], W. Jacob[1], A. v. Keudell[1], J. Krumrey[4], K. Lange[1], P. Pecher[1], J. Perchermeier[3], J. Reinmuth[4], R. Wilhelm (Division Head)[2].

1 Surface Physics Division
2 Technology Division
3 Central Technical Services
4 Undergraduate Student
5 Short-term visitor (University of Sofia, Bulgaria)

1. INVESTIGATION OF MULTIPACTOR DISCHARGES

(Cooperation with ICRH Group)

A new experiment was set up to investigate multipactor (MTP) discharges at a frequency of 50 MHz. The vacuum system consists of two separate chambers. One chamber contains the electrodes used to strike and run MTP discharges and is equipped with a quadrupole mass spectrometer to study the gas release during a discharge. The second chamber contains an Auger electron spectrometer that is used to investigate the surface composition of one electrode, which can be transferred under vacuum from the discharge chamber to the analysis chamber. The whole setup allows the state of the electrode surface before and after a MTP discharge to be studied. The work is accompanied by a theoretical study of MTP discharges and their transition to a plasma.

2. IN-SITU PLASMA DIAGNOSTICS

2.1 Optical Emission Spectroscopy (OES)

In an exploratory experiment we investigated the question whether OES of certain noble gas (mainly helium and argon) emission lines yields information on the electron energy distribution function (EEDF) in our low-pressure plasmas. At present the question is still unanswered, but the physical requirements are established and a number of useful and unuseable helium lines were identified. Theoretical investigations showed that a number of lines with a significantly different electron excitation cross-section allow, in principle, partial reconstruction of the EEDF.

2.2 Mass-selected Ion Energy Distributions from a Methane ECR Plasma

The diagnostics of the fluxes of plasma species onto the substrate are of appreciable importance for understanding plasma deposition processes. We, therefore, started an effort to measure mass-selected ion energy distributions from a

methane electron cyclotron resonance (ECR) plasma. The mass and energy of ions passing through an orifice in the substrate electrode were analyzed in the pressure range from 0.06 to 1.5 Pa by means of a commercial energy mass analyzer. As found earlier in mass-integrated measurements, the mean energy and the full-width-at-half-maximum (FWHM) of the mass-resolved ion energy distributions decrease with increasing pressure. This is shown in Fig.1 for CH_5^+ ions. Other ions have very similiar energy distributions. Very interesting is the change of the composition of the ion flux with increasing pressure. While at low pressure CH_3^+ is the most prominent ion, CH_5^+ ions are dominant above about 0.4 Pa, and above 1 Pa even $C_2H_3^+$ and $C_2H_5^+$ as well as $C_3H_3^+$ and $C_3H_5^+$ appear with higher intensity than CH_3^+.

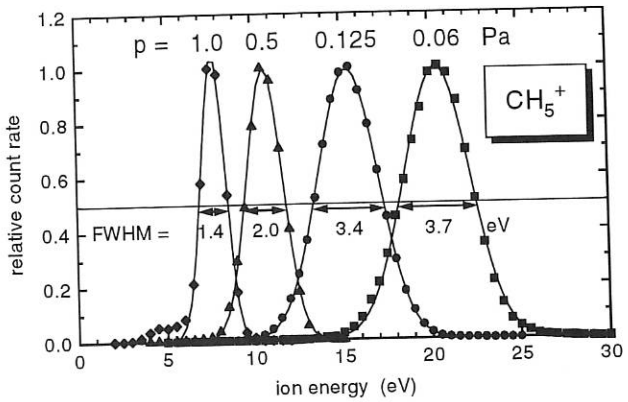

FIG. 1: Energy distributions of CH_5^+ ions as a function of the chamber pressure measured in a methane ECR discharge.

3. SURFACE MECHANISMS DURING C:H GROWTH

Deposition and erosion of plasma-deposited hydrogenated carbon (H:C) films were studied in-situ by spectroscopic ellipsometry. Ellipsometry measures the change of the polarization state of a linearly polarized light beam upon reflection from the growing thin film. From the analysis of the ellipsometry signal the film thickness and the optical constants of the film material can be deduced with high accuracy.

In a series of experiments where the energy of impinging ions was varied, we could show that hydrogen ions have a decisive influence on the film structure. Energetic hydrogen ions penetrate the film and modify a surface-near layer. The thickness of this modified layer depends on the penetration depth and, therefore, on the ion energy. This modified layer exists during deposition from methane and during etching in a hydrogen plasma. Its thickness is shown in Fig. 2. During etching we find a thicker modified layer than during deposition. Also shown in Fig. 2 are the ranges of hydrogen and CH_4^+ ions in a hydrocarbon film as calculated by TRIM.SP. By comparing these calculated ranges with the modified layer thickness it is evident that only hydrogen ions can account for this effect.

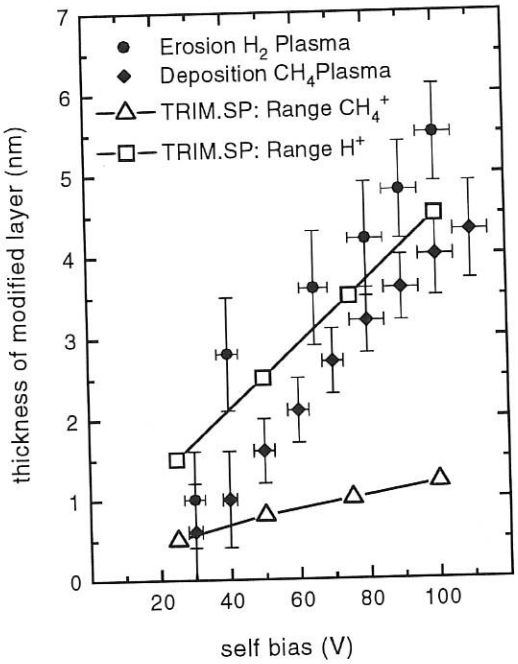

FIG. 2: Thickness of the ion-induced modified layer as measured by ellipsometry. Also shown are the ranges of carbon and hydrogen ions in a polymer-like C:H film as calculated by TRIM.SP.

4. HYDROGENATED BORON / CARBON FILMS

An existing deposition chamber was modified with a heatable, RF-driven electrode and a sample introduction system. This chamber permits handling of toxic and explosive precursor gases and is being used for the deposition of amorphous, hydrogenated boron (a-B:H) and carbon-boron films (a-B:C:H). In a first set of experiments, amorphous, hydrogenated carbon (a-C:H) films, which will serve as a reference for boron-containing films, were deposited and analyzed. The deposited a-C:H films possess properties which are typical of such films and the correlation of the film properties with the deposition conditions is in good agreement with what is known from literature data.

In a second set of experiments, a-B:H films were deposited as a function of the applied RF power. It turned out that these films have a rather high internal stress and tend to delaminate from the substrate. For sufficiently high applied powers the deposited films are long-term stable at ambient atmosphere; at low power, however, the films degrade on a time scale of several days. XPS and IR analyses showed a substantial uptake of oxygen and carbon in these unstable films. By analogy with a-C:H films we find a decreasing hydrogen content in the deposited a-B:H films with increasing RF power, but the total amount of incorporated hydrogen is about 20% lower. Thermal desorption spectroscopy revealed that hydrogen effusion appears at lower temperatures in a-B:H as compared with a-C:H.

BERLIN DIVISION

(Head of Division: Prof. Dr. G. Fussmann)

The research capacity of the Berlin Division of IPP is partly dedicated to joint work with the experimental and theoretical groups in Garching and partly to independent investigations in Berlin. The activities are concentrated on edge plasma physics, impurity transport, and plasma-wall interaction in both types of fusion experiments at IPP, the tokamak and the stellarator.
The current cooperation with the ASDEX Upgrade team includes spectroscopic investigations of the divertor region, IR thermography of divertor plates, and Langmuir and collector probe measurements in the divertor and scrape-off layer. The Berlin Division is contributing to W7-AS with IR thermography of limiters and investigations of the edge plasma with probes of different kinds. First experiments were carried out to study the impurity transport after injection into local magnetic island structures. Contributions to these IPP projects are presented in the relevant sections of this report.
The large probe manipulator as part of the SOL diagnostics of ASDEX Upgrade was completed and put into operation. The boundary layer spectrometer was installed at AUG for observation of the boundary and divertor regions in the VUV spectral range.
The plasma generator PSI-1 is being routinely operated for studying the plasma behaviour near material surfaces, the physics of materials under high particle and heat flux conditions, and plasma-wall interaction. The plasma of the generator is also being used to test newly developed diagnostics, e.g. electron density determination by He-beam injection and two-photon spectroscopy.
The surface analysis laboratory equipment primarily designed to analyze and handle large probes from fusion experiments was completed by X-ray-induced photo electron spectroscopy.
Technical preparations are under way to construct an electron beam ion trap (EBIT). This will be used mainly for determining atomic data of highly ionized heavy ions with the aim of studying high-Z materials for nuclear fusion devices.
The theory group is involved in various studies of edge physics problems, e.g. the effect of neutral particles on the radiative thermal instability in SOL plasmas, numerical marfe studies, and investigation of erosion and redeposition processes.
Plasma polarization experiments in W7-AS and arcing investigations in AUG are being conducted in close cooperation with a WIP (Scientists' Integration Programme) group from Humboldt University, Berlin, which is dealing with fundamental problems of arc cathode spots in vacuum.

P. Bachmann, M. Behnke, H. Behrendt, W. Bohmeyer, E. Dietrich, L. Dietrich, H. Grote, K. Grützmacher[3], E. Hantzsche[4], A. Herrmann, S. Hesse, D. Hildebrandt, S. Hirsch, B. Jüttner[4], M. Kammeyer, H. Kastelewicz, P. Kornejew[1], M. Laux, H. Meyer, B. Napiontek, D. Naujoks, E. Pasch[2], P. Pech, H. Pursch[4], R. Radtke, H.-D. Reiner, V. Rohde, M. I. de la Rosa[3], A.M. Runov[5], J. Sachtleben, J. Seidel[3], A. Stareprawo, A. Steiger[3], D. Sünder, U. Wenzel, H. Wolff

1 Seconded from Experimental Division 1
2 Seconded from KFA Jülich
3 Physikalisch-Technische Bundesanstalt, Berlin (PTB)
4 Funded by the "Scientists' Integration Programme" (WIP)
5 Guest, Kurchatov Institute, Moscow, Russia

1. PLASMA GENERATOR PSI-1

The activities at the PSI-1 plasma generator were concentrated on developing and comparing different diagnostics for electron density and temperature.

A fast-reciprocating single Langmuir probe was used to measure radial profiles of electron density and temperature. The Thomson scattering diagnostic has the advantage that additional premises are not necessary for interpretating the results. A Nd:YAG laser (20 Hz, 1 J, 9 ns) and silicon avalanche diodes for the detection channels were used. The system was calibrated with one rotational anti-Stokes Raman line scattered from molecular hydrogen.

The determination of plasma parameters by injecting a thermal helium beam and detecting the line intensities of different HeI lines was tested as an alternative plasma edge diagnostic method. The efficiency of this method depends on the penetration depth of the neutral helium atoms determined by the divergence of the beam. Different nozzle geometries and a nozzle/skimmer combination were therefore studied. The functional dependence of the population density of excited HeI

levels on plasma parameters was found by solving a system of rate equations including the levels with principal quantum numbers 1 to 6. The calculated HeI-line intensities were compared with data determined by passive spectroscopy, whereas the density of metastables was measured by laser-induced fluorescence. A comparison of the three diagnostics was made.

Figures 1 and 2 show the radial dependence of n_e and T_e for a hydrogen discharge (I = 200 A, p_{cath} = 1 Pa, p_{target} = 50 mPa). For n_e the agreement between the beam diagnostic and the Thomson scattering is good, whereas the probe measurements give higher densities. For T_e the differences between the three diagnostics are smaller than 30%.

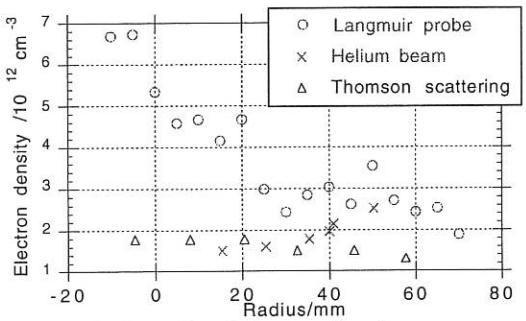

FIG. 1: Radial profile of electron density.

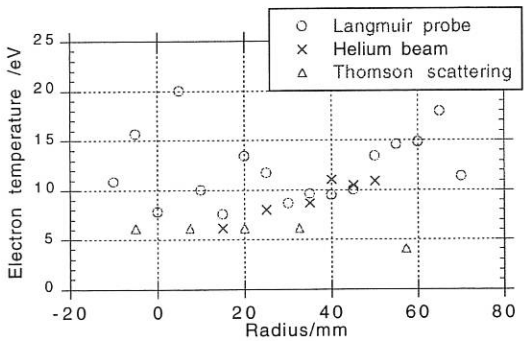

FIG. 2: Radial profile of electron temperature.

Two-photon induced L_α fluorescence of atomic hydrogen allows isotope-selective, and temporally and spatially resolved measurements of small neutral densities. PTB Berlin and IPP cooperate in developing this technique as a novel diagnostic for magnetically confined fusion plasmas. For this purpose, pulsed radiation around 243 nm is required, which can be produced with high efficiency for the first time by a new type of single-mode solid-state laser spectrometer developed at PTB Berlin.

First investigations at the plasma generator PSI-1 were done to demonstrate the capability of the new method and prove theoretical predictions. To provide Doppler-free excitation, two counterpropagating circularly polarized laser beams (8 mJ each in 2.5 ns) were directed into the target chamber of PSI-1 perpendicularly to the plasma beam. The induced L_α fluorescence was observed from a small volume (∅ 3 mm, 8 mm long) which was imaged on a windowless photomultiplier by a MgF_2 lens with a collecting solid angle of 13 msr. Distinct signals were first observed from a deuterium plasma, and two important properties of the induced fluorescence signal could be verified: (i) within the laser bandwidth of 500 MHz, the two-photon resonances in the plasma and in a reference cell occur at the same laser wavelength, (ii) the pulse duration of the induced L_α fluorescence signal is less than 10 ns, in agreement with theoretical predictions.

Future work will concentrate on the determination of kinetic temperatures and number densities in a wide range of plasma parameters for different hydrogen-deuterium mixtures. A new design of the L_α fluorescence detection system and pulse energies of 50 mJ, as already generated, will greatly improve the detection limit.

2. THE MIDPLANE MANIPULATOR AT AUG

The midplane manipulator system for AUG was put into operation (see AUG Project/Diagnostics, this report). First investigations were carried out with a reciprocating Langmuir probe. Two sensors pointing in the two toroidal directions were used to measure plasma parameters at the plasma boundary. Typical radial profiles obtained by one of the two sensors are shown in Fig. 3. The results of the other sensor are strongly affected by the near ICRH guard limiter. The decay length of the plasma density was determined to be 18 mm. The temperature rises from 5 eV deep in the SOL to 30 eV close to the separatrix. The floating potential rapidly changes near the separatrix.

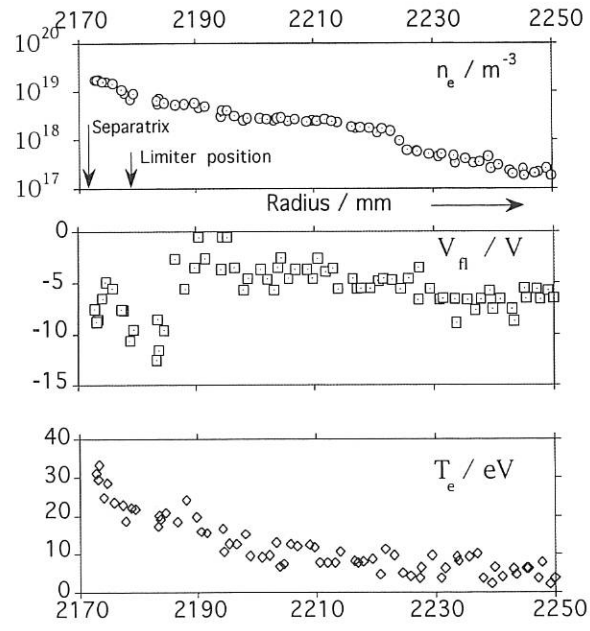

FIG. 3: Radial profiles of the electron density, floating potential, and electron temperature, shot #5284 (850 kA, $4.6 \cdot 10^{19}$ m^{-3}) at t = 3.1 s.

3. THE BOUNDARY LAYER SPECTROMETER

In 1994 the boundary layer spectrometer was completed and successfully installed at AUG (Fig. 4). For technical

description see this report, AUG Project/Diagnostics. Future investigations will mainly concentrate on influx measurements, impurity transport, CX reactions of impurities, and ion temperature measurements.

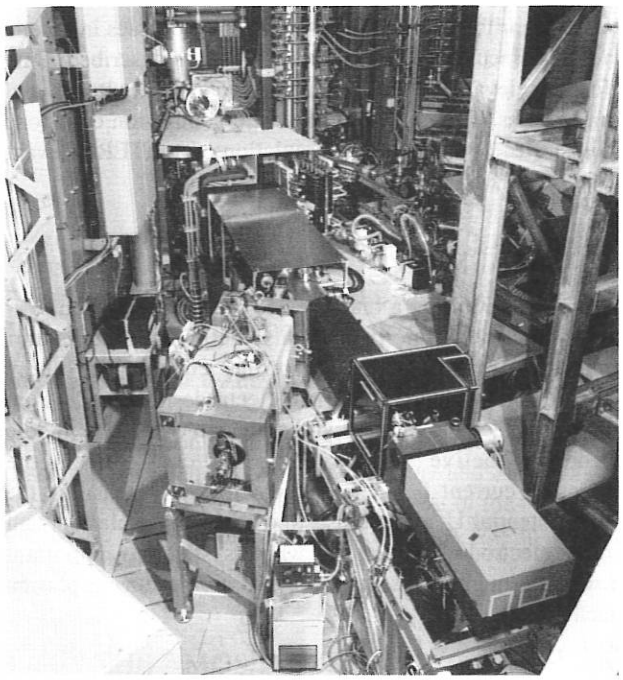

FIG. 4: The boundary layer spectrometer at AUG. The VUV branch is located on the left side, the visible branch on the right.

4. THE UHV LABORATORY

The SIMS-AES device was used for systematic surface analysis of different probes and plasma-facing solid components from fusion experiments. Erosion and redeposition phenomena were studied on collector probes from W7-AS, carbon tiles from JET, and also special ASDEX Upgrade divertor plates with tungsten inlays.

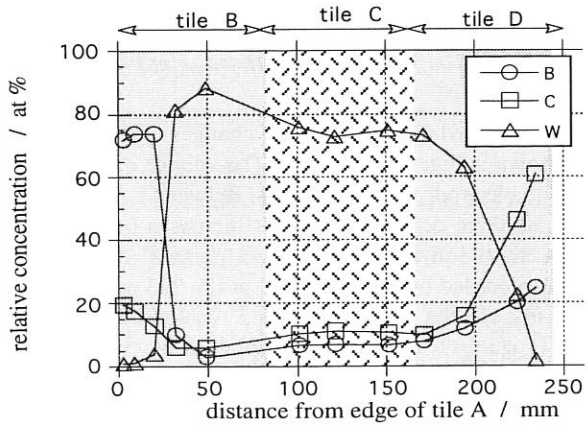

FIG. 5: Relative concentration of the elements B, C, and W in the surface layer of the AUG divertor target plates with tungsten inlay after exposure.

A typical result of the AES analysis of AUG divertor target tiles with tungsten inlays is shown in Fig. 5. These target plates marked A to D were mounted in the outer part of divertor segment 1 in the order A, B, C, D with increasing major radius. The plates were exposed to about 400 shots after boronization. The increased erosion of the boron layer clearly reflects the area of contact of the separatrix with the plate. The innermost point of contact is located about 50 mm from the edge of tile B. Beginning from this point, the separatrix moves in the outward direction during the shots. The erosion of tungsten and its redeposition in the immediate proximity was found to be very small.

The optical profilometer was used for investigating the erosion pattern on divertor target plates of AUG and limiter tiles of W7-AS. In both cases increased erosion of graphite on certain edges coupled with prompt redeposition in the vicinity could be observed. The possibility of prompt redeposition occurring was confirmed by model calculations.

5. STUDY OF HIGH-Z MATERIALS FOR TARGET APPLICATION

Recent investigations have shown that high-Z materials seem to be a very promising alternative for target plates in divertor tokamaks and stellarators. Several studies are being devoted therefore to different aspects of these materials.

5.1. Erosion of Tungsten

During simultaneous bombardment with plasma ions and non-recycling impurity ions the composition of the exposed surface and subsequently the sputtering yields change due to the implantation of the impurity ions. The question whether erosion of the target material or deposition of the impurity atoms occurs strongly depends on the plasma conditions, the target atom species, and the exposure time. An analytical model was developed to describe these processes and the results agree well with experimental results and those obtained by computer simulation using the TRIDYN code.

5.2. The Effect of "Prompt Redeposition"

In the case of shallow magnetic field line inclination a major fraction of the eroded and subsequently ionized particles can be redeposited onto the plate during the first gyration - a process named "prompt redeposition". On the assumption of a cos δ distribution of the eroded particles and including the effect of the ionization length distribution, the fraction of promptly redeposited particles can be calculated analytically. In a more adequate description of the prompt redeposition process the effect of the sheath electric field and the multiple ionization effect have to be included. The above effects were considered in more detail using the ERO code. There is good agreement between the analytical model and the results calculated with ERO for the simplified model.

5.3. Spectroscopic Investigations

Spectroscopic investigations of tungsten erosion in AUG were extended to very high plasma densities during NBI. All detectable tungsten lines are very weak. Moreover, a sharp

intensity decrease in front of the target is observed. The line intensities grow with NBI power. The findings are in line with the expected very high fraction of promptly redeposited particles as well as with the temperature dependence of tungsten sputtering. A more quantitative interpretation requires knowledge of atomic data not yet available. Therefore spectroscopic studies of tungsten erosion were started at the plasma generator PSI-1 with the aim of establishing the connection between measured line intensities and the flux of released particles.

6. THEORY

6.1. Radiative Thermal Instability and Bifurcation in Tokamak Plasmas

A radial hydrodynamic model which describes the dynamics of the plasma and neutral particles self-consistently is used to investigate the radiative thermal instability in the SOL by applying a linear stability analysis of existing equilibrium states. Phase space trajectories are analyzed to derive the conditions of their existence and bifurcation. Neutrals are shown to force bifurcation. Unstable perturbations, localized in the SOL, may lead to a strongly radiating cold plasma belt which is shifted to the wall with increasing energy input and connection length.

6.2. Plasma Cooling due to Impurity Injection into Magnetic Islands

The energy loss of the plasma due to radiation of impurities injected into magnetic islands, which is proportional to $n_e\, n_{imp}\, L(T_e)$, with $L(T_e)$ being the radiation function, becomes large when the densities in the islands are high and L attains a maximum value. Therefore, both the particle and energy fluxes of the plasma within the islands and around them are investigated by means of MHD and Monte Carlo calculations. One result is that, owing to high particle confinement, impurity injection into magnetic islands leads to more effective plasma cooling and lowering of the energy fluxes to the target.

6.3. Numerical Marfe Studies for a Deuterium-Carbon Plasma at ASDEX Upgrade

An advanced version of the B2 plasma code was used to investigate the formation and nonlinear behaviour of marfes in a D-C-plasma for realistic ASDEX Upgrade single-null divertor geometry and realistic experimental scenarios. All charge states are treated as separate fluids. It was shown that a marfe can readily be stabilized by external feedback control using the radiated power as control parameter. The whole set of stationary states can be represented in a diagram of steady states by a double-valued function where the two branches describe marfe-free and marfe plasma states, respectively. The internal mechanism sustaining a marfe, i.e. a localized region of enhanced density and lowered temperature relatively to the surrounding medium, was investigated.

6.4. Kinetic Description of Elastic Processes in Hydrogen-Helium Plasmas

Recent experiments with high-density divertor plasma operation in tokamaks and future design projects have revived interest in the earlier work on elastic collision processes between neutral and charged components in hot plasmas. In revisiting these papers, classical methods were employed to calculate deflection functions, cross-sections, and collision rates. An algorithm for implementing these processes in kinetic Monte Carlo neutral gas transport models was described. Data fits for the relevant quantities were provided for hydrogen and helium species. The relevance of elastic neutral-ion collisions was illustrated by a numerical simulation of an ITER-relevant divertor model.

7. PLASMA POLARIZATION AT W7-AS

Plasma polarization by a biased electrode was tested on W7-AS to study the feasibility of this method for stellarator geometries. The polarization probe consists of three concentrically mounted cylindrical electrodes 1-3 made from graphite that face the plasma with their end caps. The middle electrode 2 (active surface about 28 cm^2) injects the polarization current I_2, the inner electrode 1 measures the floating potential U_1 at the closest position to the plasma, and the outer electrode 3 shields the whole system. An important step was thorough degassing to avoid arcing during plasma contact.

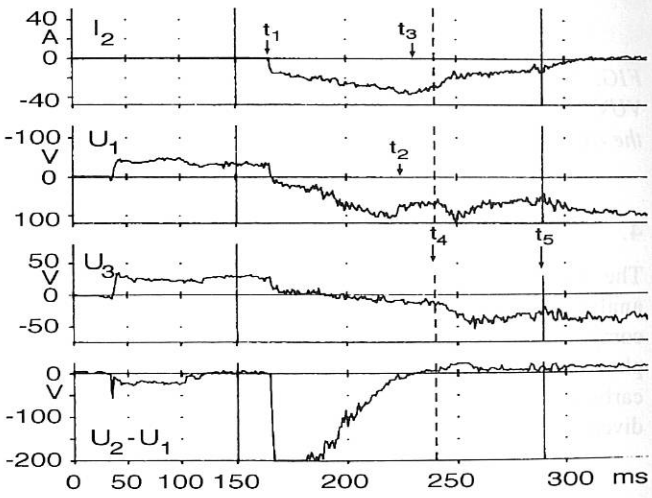

FIG. 6: Set of signals at the three electrodes of the polarization probe.

Polarization caused the characteristic changes of the measuring signals shown in Fig. 6 for # 28799. The voltage of -270 V was switched to electrode 2 at t_1 = 167 ms. Between t_4 = 240 ms and t_5 = 290 ms there occurred transient increases of the plasma energy, central ion temperature, and plasma rotation. This event was preceded by changes of U_1 at t_2 = 223 ms and of I_2 at t_3 = 230 ms, but the outer electrode 3 reacted only at t_4. The delay of t_4 against t_2 and t_3 can be explained by changes of the temperature distributions at the wall and electrodes at different times. Interestingly, for $t \geq t_4$ the potential difference U_2-U_1 between the current-conducting electrode 2 and the floating inner electrode 1 is no longer negative, although the former electrode still receives ion currents >10 A. Further work is necessary to distinguish fluctuations not connected with the polarization and to study the plasma behaviour in more detail.

COMPUTER SCIENCE DIVISION

(Prof. Dr. Friedrich Hertweck)

F. Hertweck, Ch. Brosig, G. Czapski, R. Dohmen, H. Fisser, H. Friedrich, A. Graf (on leave); K. Hallatschek, P. Heimann, J. Maier, M.G. Pacco-Düchs, I. Precht, H. Richter, Ute Schneider, D. Stolz, Ch. Tichmann, R. Tisma, M. Zilker

Great part of the activities of the division were related to the maintenance and further development of the data acquisition system for ASDEX Upgrade. In particular, the transition from a central mainframe to a fully distributed system was initiated. This was done in close collaboration with the ASDEX Upgrade project. In the field of parallel processing, the systems for the acquisition and processing of large amounts of data (Mirnov and Soft Xray diagnostics) were enhanced. Additionally, a prototype PowerPC parallel system was built as a possible replacement of the current transputer systems. The study of neural network algorithms for analyzing diagnostic data was started. Further effort was made to develop programs for, or to port programs to, commercial "number-crunching" parallel machines.

1. THE AMOS/D SYSTEM

In 1994, as in the year before, the activities of the Computer Science Division were concerned with the further development of the AMOS/D system. Particularly, additional diagnostics were installed and the ever-increasing amounts of data required a permanent adaptation. At the end of the year, the fifty plus diagnostics were producing up to 120 MB of raw data per shot.

1.1 The AMOS/2 Central System

The central part of the AMOS/D System is a virtual machine known as AMOS/2, which runs on an IBM 3090/150 with 64 MB of memory and 16 GB of disk space.

This machine supports the following functions.

- online reception of ASDEX Upgrade shotfiles and their storage on disk;
- intershot data analysis with complex analysis programs;
- management of the ASDEX Upgrade shotfile archive.

As the new generation of workstations is more powerful than a mainframe, it was decided to transfer the first two of the above-mentioned functions onto a SUN workstation cluster (with four processors and 512 MB of memory). This offers the following advantages:

- the greater CPU power may still be expanded by increasing the number of processors (up to eight);
- the large memory of currently 512 MB is able to accomodate shotfiles of 120 MB;
- the diagnostic programs are running in a normal UNIX environment;
- easy access is possible by remote login from the user workstations;
- the Dependence Data Base is established as a central server.

The first steps in this migration process were taken. The shotfile monitor, which so far had been running in AMOS/2 on the IBM 3090, was ported to the SUN compute server without any loss of functionality. During a transition phase a coexistence of the two versions of the shotfile monitor is required in order to comply with a very important requirement: the experimental activity of ASDEX Upgrade should never be disturbed or even interrupted.

1.2 The Dependence Data Base (DDB)

The shotfile Dependence Database DDB is an online database. It shows the interdependence of level-0 shotfiles (containing raw data) and level-n shotfiles generated from lower-level shotfiles ($n > 0$). An entry for each level-n shotfile shows the dependence on all its predecessors (i.e. the shotfiles that were

used to generate it). This is done more or less automatically when such a level-n shotfile is generated. The DDB also permits to find all successors of a particular shotfile: by declaring it "invalid", all its successors can also be set to "invalid". This online database has been in operation in AMOS/2 on the IBM 3090 since early 1994. The process of porting the DDB to the UNIX compute server was almost completed.

1.3 The AMOS/2 Archive System

The AMOS/2 Archive System has been in operation for many years using a StorageTek silo. Towards the end of the year, shotfiles for more than 5,000 shots, comprising about 140.000 files (1 per diagnostic per shot) with a total amount of 180 GB of data, were stored. Only the currently important files are residing on disk.

The first steps for a migration to the Andrew File System AFS supported by the RZG Computing Centre were taken. The AFS will also comprise an archiving facility based on a new technology (D2-tapes by EMASS).

The AFS is expected to offer a better service, also because the FDDI networking facilities can be used. The first diagnostics are running successfully on the compute server, which is at the same time an AFS server.

1.4 The AMOS/D Communications Network

In 1994, the backbone network of AMOS/D was converted to FDDI. For that purpose, the nodes that connect the diagnostics to the network were upgraded to obtain newer and faster CPUs. The software also had to be modified. Throughout the year, the network showed a high reliability and availability.

1.5 CAMAC Interface for the SPARC-Sbus

As there is no commercial product to attach CAMAC crates directly to a SPARC, two prototype Sbus interface cards were developed and successfully tested. They allow the Kinetic Systems 3920 and 3922 CAMAC crate controllers to be attached to the Sbus. The production of the modules and software development are under way.

1.6 Fortran 90

In 1994, Fortran 90 compilers for several platforms became available, especially from NAG, IBM, and Cray as well as a compiler for the PC. In order to make the transition from Fortran 77 to Fortran 90 easier for the users, courses were given. The PPLOT plotting library was converted into a Fortran 90 module and also the Dependence Data Base Manager was ported.

1.7 Summary Shotfiles for ITER

Summary shotfiles, as described below, are a useful concept for anyone who wants to get a global picture of a particular tokamak discharge. While some informal reviewing was already being done by the ASDEX Upgrade team, this more formal approach was undertaken upon request by the ITER group.

ASDEX Upgrade measurement data are stored in shotfiles. There is one shotfile for each shot and each diagnostic and the files are known as level-0 shotfiles. Since raw measurement data are only useful for the involved scientists, higher-level shotfiles containing evaluated data may be generated. In this way, a hierarchy of level-n shotfiles is created. It should be noted that the structure of level-n shotfiles is the same as that of level-0 shotfiles.

For the global survey of the contents of shotfiles a summary shotfile can be produced, containing the essential data needed to assess the quality or relevance of a particular shot.

A software package was implemented to extract any desired signals from the set of shotfiles for a shot. The ASDEX Upgrade shotfile access procedures were modified to handle the name ambiguity of signals (it is likely that two diagnostics use the same signal names, like temperature, density, ...).

This package was extended to be able to read shotfiles from other machines than ASDEX Upgrade; these are usually presented as ASCII-files (like the ASCII format of the JT shotfiles).

2. PARALLEL PROCESSING

The activities in the field of parallel processing include the development of transputer systems as well as the usage of commercially available systems.

2.1 The Mirnov and Soft Xray Computers

The two diagnostics Mirnov and Soft Xray are using MULTITOP parallel computers specially developed for ASDEX Upgrade. They consist of VMEbus modules with four T800 processors per board and four MB of memory per processor. The computers were upgraded to 32 processors for Mirnov (128 MB memory and 64 signal inputs) and 64 processors for Soft Xray (256 MB memory and 128 signal inputs).

The software for these two computers was updated in order to enhance the system performance and to include additional acquisition modes, in particular external interrupt control.

The performance requirements of the algorithms are clearly approaching the limits of the T800 CPUs (about 1 Mflop/s).

2.2 A New Generation of MULTITOP Computers

Due to the apparently limited performance of the currently used MULTITOP systems - regarding both CPU-power and memory capacity - feasibility studies were carried out to find a suitable replacement. A prototype system was built by using four powerPC TRAM-modules from Parsytec. The system was tested and its performance analyzed; one powerPC 601 offers a performance increase by a factor of 50 over a T800.

One of the system's greatest advantages is the availability of standard high-level software.

2.3 The nCUBE Computer System

The nCUBE machine is obviously approaching the end of its useful life, because the RZG computing centre is planning the installation of a much greater parallel system. However, in retrospect, the nCUBE was worth the investment: it was a valuable tool for developing and testing software for parallel computers, thus increasing our know how. It was heavily used throughout the year for many-particle codes. It turned out that all the programs that were developed for the nCUBE could easily be ported to other parallel systems.

2.4 Benchmark Studies of other Parallel Computers

An algorithm for restructuring 3D-arrays, originally designed for the nCUBE, was ported to several other parallel systems in order to test the performance of communication between processor nodes. The tested systems were the nCUBE (hypercube topology), the Intel Paragon (2D open mesh), the IBM SP2 (multistage network), and the Cray T3D (3D toroidal grid).

2.5 Neural Network Algorithms

The new area of neural network algorithms is likely to have an impact on the methods of data analysis for plasma diagnostics.

In some first studies, we wanted to show whether it is possible to detect significant events in the signals of a tokamak discharge. The results were quite encouraging, but it turned out that the power of the existing workstations was hopelessly insufficient for training larger neural networks.

Fortunately, other scientists from neighbouring institutes are also interested in these new techniques. A Siemens SYNAPSE–1 computer was acquired by Prof. G. Morfill (Max-Planck-Institute for Extraterrestrial Physics) in December 1994 and we will be able to use this new machine for our work in this area. Since both institutes are using similar methods of data analysis, we will both benefit from an intensive cooperation.

CENTRAL TECHNICAL SERVICES

(Dr.-Ing. Harald Rapp)

The Central Technical Services (ZTE) of Max-Planck-Institut für Plasmaphysik support the experimental divisions with the design, construction and operation of experiments and their diagnostics. They also provide and run all kinds of utilities for facility operation and employ approximately 170 workers, technicians and engineers. Task-sharing between the research groups, industry and the Central Technical Services is standard practice for minimizing costs and manpower and for providing technical support meeting experimental needs.

1. MECHANICAL DESIGN AND CALCULATION

(J. Simon-Weidner)

There are 25 technicians and engineers in the department, four of them calculating mechanical stresses and thermal loads in coils, vacuum vessels, supports and divertors. The computer network consists of 40 workstations, including those in the experimental divisions. Work on stresses due to halo currents in ASDEX Upgrade and improvement of the ICRH antennae proceeded in 1994. Calculation and construction work on divertor target plates for ASDEX Upgrade and the W7-X stellarator was started. Major effort was given to the progress of the W7-X design. This primarily concerns the call for tender of the modular demo coil and the test cryostat. A big task was the assistance for phase II of the W7-X Euratom approval, which is still in progress. Other tasks of the department mainly concern the design of experimental equipment such as high-frequency components, plasma diagnostics and compatibility studies.

2. ELECTRONICS DEVELOPMENT

(D. Arz)

The department consists of 2 groups for developing measurement and control techniques and for high-voltage switching and control for NBI and ECRH. Another small group services equipment for electronic measurement. A variety of apparatus in a wide range of power and frequency was developed and built. Commissioning and maintenance of 20 high-voltage switchboxes were continued and provided high operational reliability of the plasma heating systems. A new development task was initiated using VME bus systems for experimental control and interaction of common industrial and special experimental equipment.

3. MATERIALS TECHNOLOGY

(E. Trcka)

The department offers a variety of technical services for materials testing, experimental vacuum equipment and surface processing. The latter comprise chemical, galvanic and vapour deposition surface preparation as well as galvano-plastics for diagnostic and high-frequency applications. Vacuum testing is a routine task for quality guarantee of the mechanical manufacturing process. In the course of the design of high-power antennae, testing and investigation of materials and highly stressed mechanical elements became important.

4. ELECTRIC POWER SUPPLY

(W.R. McGlaun)

The department is responsible for the electric power supply of IPP and the experiments. The staff operates 4 flywheel generators, with a total power of 580 MVA and an available energy of 2.6 GJ . The energy is transmitted via a modular system of thyristor-controlled converters (462 MVA in total) and diode rectifiers to the experimental loads. Also the high-voltage supply for the plasma heating systems is operated by the department. After 7 year´s duty a complete inspection was carried out on a flywheel generator in 1994. Control links between the experiment and the generators and rectifier stations were improved in order to meet the complex demands of ASDEX Upgrade.

5. FACILITY OPERATION

(H. Rapp)

The department is charged with planning and supervising installations for heating, cooling, cranes and other facility equipment. During the report period a furnace and the complete control of the heating station were replaced. In the frame of the department´s responsibility for environmental protection, a task force was set up to identify all installations which may pollute air or water or violate legal regulations.

6. WORKSHOPS

(M. Keiner)

More than 90 of the ZTE personnel work in workshops and with supporting groups. The capacity meets the basic needs for con structing and assembling experimental setups. If necessary, additional capacity is purchased from industry. There are workshops for mechanical fabrication and joinery, electrical and electronic manufacturing, maintainance of utility installations and apprentice training. Some of the craftsmen routinely participate in construction or repair work during shut-down phases of experiments. In 1994 some modern machine tools were put into operation in order to meet quality requirements.

ADMINISTRATION

(Dr. Thomas Köstlin)

The administration and general services of Max-Planck-Institut für Plasmaphysik are organized in departments. Six of them are presented here:

PERSONNEL DEPARTMENT

The personnel department is responsible for administrative matters relating to personnel. The personnel figures of the institute for 1993 were as follows:

Total personnel	988
Scientists	279
Technicians	433
Directorate and Staff Representative Council	21
General Services	65
Administration	68
Other personnel	122

PURCHASING AND CONTRACTS DEPARTMENT

The purchasing and contracts department is responsible for all contracts and orders carried out by IPP, Garching and Berlin. This year, about 9,000 purchase orders were placed. Included were complex contracts, many of them having been signed after a Europe-wide call for tenders. Furthermore, all export and import formalities are handled within this department: about 160 international and European shipments were made in 1994.

LEGAL AND PATENT DEPARTMENT

The legal department attends to patent applications and supervision, contracts of cooperation, and licensing of patents in cooperation with Garching Innovation GmbH, a subsidiary of the Max Planck Society. In 1994 the division supervised 116 patents and similar rights.

FINANCE DEPARTMENT

The finance department is responsible for financial planning and all financial transactions and fiscal matters of IPP.

Total budget in 1994:	161.1 MDM
This budget was financed as follows:	
Federal Republic of Germany through Federal Ministry of Research and Technology (BMFT)	89.4 MDM
Bavaria	9.1 MDM
Berlin	0.8 MDM
Mecklenburg-Vorpommern	0.3 MDM
EURATOM	39.8 MDM
Other income	21.7 MDM

SITE AND BUILDINGS DEPARTMENT

The site and buildings department is in charge of planning, construction, structural alteration and reconditioning of buildings and main service facilities. Building maintenance is also provided for the neighbouring Max Planck Institutes of Astrophysics and Extraterrestrial Physics, the European Southern Observatory and the Berlin Division of IPP.

SOCIAL DEPARTMENT

The social department gives assistance to employees seeking housing, provides accommodation for guests in IPP residences, and runs the transport pool, bus and cleaning services.

Publications

Publications and Conference Reports

1. *Abramov*, V.A., P. Bachmann, D.Kh. Morozov** and *D. Sünder:* The Influence of Neutral Particles on the Radiative Thermal Instability in SOL Plasmas. Contrib. Plasma Phys. **34**, 271-276 (1994).

2. *Alimov*, V.Kh., R.Kh. Zalavutdinov** and *B.M.U. Scherzer:* Oxygen Retention in D-Ion-Irradiated B_4C and Boron-Doped Graphites. J. Nucl. Mater. **212-215**, 1461 (1994).

3. *Bachmann, P.* and *D. Sünder:* Radiative Thermal Instability of the Tokamak Edge Region. In: Proc. 21st EPS Conf. Control. Fusion and Plasma Phys., Montpellier 1994, Eds. E. Joffrin, P. Platz, P.E. Stott. ECA 18B. Europ. Phys. Soc., Geneva 1994, 794-797.

4. *Baldzuhn, J., W. Ohlendorf* and *WVII-AS-Team:* A Comparison of Improved Confinement Regimes in W7-AS. In: Proc. 21st EPS Conf. Control. Fusion and Plasma Phys., Montpellier 1994, Eds. E. Joffrin, P. Platz, P.E. Stott. ECA 18B. Europ. Phys. Soc., Geneva 1994, 384-387.

5. *Ballico, M.* and *H. Lederer:* Plasmafusionsforschung: Serielles und paralleles Rechnen mit nur einem Programmcode auf Cray YMP, nCUBE2, Workstations mit PVM und KSR1. In: Forschung und wissenschaftl. Rechnen. Berichte und Mitteilungen, Heft 1. MPG, München 1994, 232-234.

6. *Becker, G.:* Transport Simulations of the Ignited ITER with High Helium Fraction. Nucl. Fusion **34**, 507-518 (1994).

7. *Behrendt, H., W. Bohmeyer, L. Dietrich, G. Fußmann, H. Greuner, H. Grote, M. Kammeyer, P. Kornejew, M. Laux and E. Pasch:* Development and Test of Edge Plasma Diagnostics at the PSI-1 Plasma Generator. In: Proc. 21st EPS Conf. Control. Fusion and Plasma Phys., Montpellier 1994, Eds. E. Joffrin, P. Platz, P.E. Stott. ECA 18B. Europ. Phys. Soc., Geneva 1994, 1328-1331.

8. *Behringer, K.:* Plasma Edge Spectroscopy. In: Proc. 4th Course and Workshop on Magnetic Confinement Fusion, UIMP Santander 1992, Eds. P.E. Stott, J. Sanchez. Ciemat, Madrid 1994, 152-166.

9. *Behringer, K.:* Spectroscopic Studies of Impurity Densities and Impurity Transport. In: Proc. 4th Course and Workshop on Magnetic Confinement Fusion, UIMP Santander 1992, Eds. P.E. Stott, J. Sanchez. Ciemat, Madrid 1994, 137-151.

10. *Beidler, C.D.* and *W.N.G. Hitchon*:* Ripple Transport in Helical-Axis Advanced Stellarators: A Comparison with Classical Stellarator/Torsatrons. Plasma Phys. Control. Fusion **36**, 317-353 (1994).

11. *Beidler, C.D., W. Lotz* and *H. Maaßberg:* Neoclassical Transport Scalings for Stellarators in the Long-Mean-Free-Path Regime. In: Proc. 21st EPS Conf. Control. Fusion and Plasma Phys., Montpellier 1994, Eds. E. Joffrin, P. Platz, P.E. Stott. ECA 18B. Europ. Phys. Soc., Geneva 1994, 568-571.

12. *Bergmann, A.:* Two-Dimensional Particle Simulation of Langmuir Probe Sheaths with Oblique Magnetic Field. Phys. Plasmas **1**, 3598-3606 (1994).

13. *Bertel, E.:* Symmetry of Surface States. Phys. Rev., B **50**, 4925-4928 (1994).

14. *Bertel, E.* and *U. Bischler:* One-Dimensional Surface States on Metal Surfaces. Surf. Sci. **307-309**, 947-952 (1994).

15. *Bessenrodt-Weberpals, M.:* Förderung des wissenschaftlichen Nachwuchses im IPP. MPG Spiegel 2, 40-42 (1994).

16. *Bessenrodt-Weberpals, M.:* Graduiertenförderung in der Max-Planck-Gesellschaft am Beispiel des MPI für Plasmaphysik. Phys. Bl. **50**, 168-169 (1994).

17. *Bessenrodt-Weberpals, M., M. Maraschek, H. Zohm, ASDEX-Upgrade-Team* and *NI-Team:* Sawtooth Filtering by Singular Value Decomposition. In: Proc. 21st EPS Conf. Control. Fusion and Plasma Phys., Montpellier 1994, Eds. E. Joffrin, P. Platz, P.E. Stott. ECA 18B. Europ. Phys. Soc., Geneva 1994, 1312-1315.

18. *Biener, J., A. Schenk, B. Winter, C. Lutterloh, U.A. Schubert* and *J. Küppers:* Hydrogenation of Amorphous C:H Surfaces by Thermal H(D) Atoms. Surf. Sci. **307-309**, 228-234 (1994).

19. *Biener, J., A. Schenk, B. Winter, U.A. Schubert, C. Lutterloh* and *J. Küppers:* Spectroscopic Investigation of Electronic and Vibronic Properties of Ion Beam Deposited and Thermally Treated Ultrathin C:H Films. Phys. Rev., B **49**, 17307-17318 (1994).

20. *Biskamp, D.:* Cascade Models for MHD Turbulence. Phys. Rev., E **50,** 2703-2711 (1994).

21. *Biskamp, D.:* Magnetic Reconnection. Phys. Rep. **237**, 179-247 (1994).

22. *Biskamp, D.* and *U. Bremer:* Dynamics and Statistics of Inverse Cascade Processes in 2D Magnetohydrodynamic Turbulence. Phys. Rev. Lett. **72**, 3819-3822 (1994).

23. *Biskamp, D., S.J. Camargo* and *B.D. Scott*: Spectral Properties and Statistics of Resistive Drift-Wave Turbulence. Phys. Lett., A **186**, 239-244 (1994).

24. *Biskamp, D.* and *J.F. Drake:* Dynamics of the Sawtooth Collapse in Tokamak Plasmas. Phys. Rev. Lett. **73**, 971-974 (1994).

25. *Brakel, R., J. Das, Y. Feng, P. Grigull, H. Niedermeyer, F. Sardei, U. Schneider, WVII-AS-Team* and *ECRH-Group:* Recycling and Particle Control Studies in the W7-AS Stellarator. In: Proc. 21st EPS Conf. Control. Fusion and Plasma Phys., Montpellier 1994, Eds. E. Joffrin, P. Platz, P.E. Stott. ECA 18B. Europ. Phys. Soc., Geneva 1994, 388-391.

26. *Brambilla, M.:* A Note on the Toroidal Plasma Dispersion Function. Phys. Lett., A **188**, 376-383 (1994).

27. *Brambilla, M.:* Fast Evaluation of the Quasilinear Ion Distribution Function During Ion Cyclotron Heating. In: Proc. 21st EPS Conf. Control. Fusion and Plasma Phys., Montpellier 1994, Eds. E. Joffrin, P. Platz, P.E. Stott. ECA 18B. Europ. Phys. Soc., Geneva 1994, 960-963.

28. *Brambilla, M.:* Quasi-Linear Ion Distribution Function During Ion Cyclotron Heating in Tokamaks. Nucl. Fusion **34**, 1121-1143 (1994).

29. *Büchl, K., A. Carlson, A. Herrmann, J. Neuhauser, U. Seidel, M. Ulrich, M. Weinlich* and *ASDEX-Upgrade-Team:* Brigth Spots on the Divertor Plates of ASDEX-Upgrade During Stationary Phases. In: Proc. 21st EPS Conf. Control. Fusion and Plasma Phys., Montpellier 1994, Eds. E. Joffrin, P. Platz, P.E. Stott. ECA 18B. Europ. Phys. Soc., Geneva 1994, 710-713.

30. *Camargo, S.J., D. Biskamp* and *B.D. Scott:* High Resolution Simulations of 2-D Dissipative Drift-Wave Turbulence. In: Proc. 21st EPS Conf. Control. Fusion and Plasma Phys., Montpellier 1994, Eds. E. Joffrin, P. Platz, P.E. Stott. ECA 18B. Europ. Phys. Soc., Geneva 1994, 564-567.

31. *Cesario*, R., F. de Marco*, A. Cardinali** and *M. Brambilla:* RF Sheath Formation and Plasma Density Rise During the Ion Bernstein Wave Heating Experiment of Tokamak Plasmas. Nucl. Fusion **34**, 1527-1531 (1994).

32. *Correa-Restrepo, D.* and *D. Pfirsch:* Negative-Energy Perturbations in General and in Arbitrary One-Dimensional Vlasov-Maxwell Equilibria. Phys. Rev., E **49**, 692-708 (1994).

33. *Correa-Restrepo, D.* and *D. Pfirsch:* Negative Energy Perturbations in Symmetric Maxwell-Vlasov $\beta_p = 1$ Equilibria. In: Proc. 21st EPS Conf. Control. Fusion and Plasma Phys., Montpellier, 1994, Eds. E. Joffrin, P. Platz, P.E. Stott. ECA 18B. Europ. Phys. Soc., Geneva 1994, 1398-1401.

34. *Coster, D., B. Braams*, J. Neuhauser, R. Schneider, H. Zohm, ASDEX-Upgrade-Team, NBI-Team,* et al.*:* B2-EIRENE Modelling of ELMs on ASDEX-Upgrade. In: Proc. 21st EPS Conf. Control. Fusion and Plasma Phys., Montpellier 1994, Eds. E. Joffrin, P. Platz, P.E. Stott. ECA 18B. Europ. Phys. Soc., Geneva 1994, 846-849.

35. *Cramer, J.* and *E. Bertel:* Adsorbate-Site Determination by Surface-State Spectroscopy ? Appl. Phys., A **59**, 459-461 (1994).

36. *De Blank, H.J.:* An Energy Principle for Guiding Centre Equilibria with Flow. In: Proc. 21st EPS Conf. Control. Fusion and Plasma Phys., Montpellier 1994, Eds. E. Joffrin, P. Platz, P.E. Stott. ECA 18B. Europ. Phys. Soc., Geneva 1994, 1394-1397.

37. *De Blank, H.J.:* MHD Instabilities in Tokamaks. Fusion Technol. **25**, 2T, 85-96 (1994).

38. *De Blank, H.J.:* Plasma Equilibrium in Tokamaks. Fusion Technol. **25**, 2T, 39-44 (1994).

39. *De Blank, H.J., H. Zohm* and *ASDEX-Upgrade-Team:* Test of Theory of the L-H Transition in ASDEX Upgrade Discharges. In: Proc. 21st EPS Conf. Control. Fusion and Plasma Phys., Montpellier 1994, Eds. E. Joffrin, P. Platz, P.E. Stott. ECA 18B. Europ. Phys. Soc., Geneva 1994, 632-635.

40. *Denisov*, G.G., A.A. Fraiman*, V.A. Isaev*, V. Erckmann, T. Geist,* et al.*:* Collective Scattering of Powerful Gyrotron Radiation at W7-AS. In: Proc. 2nd Int. Workshop on Strong Microwaves in Plasmas, Nizhny Novgorod 1993, Ed. A.G. Litvak. Chuvashia, Cheboksary 1994, 172-184.

41. *Detzel, Th.* and *N. Memmel:* Substrate Diffusion in Metastable Ultrathin Films: Iron on Cu(001). Phys. Rev., B **49**, 5599-5606 (1994).

42. *Dohmen, R.:* Comparison between a Message Passing and a Global Shared Memory Parallel Computer by Means of a Concrete Monte Carlo Algorithm. In: Parallel Processing: CONPAR94-VAPP VI, Lecture Notes in Computer Science 854. Springer Verl., Berlin 1994, 473-484.

43. *Dohmen, R.:* Towards an Automatic Portation of Programs from nCUBE2 to KSR1. In: Parallel Scientific Computing, Lecture Notes in Computer Science 879. Springer Verl., Berlin 1994, 177-189.

44. *Dommaschk, W.:* A Necessary Condition for Omnigenity in Stellarators. J. Plasma Phys. **51**, 261-269 (1994).

45. *Donath, M.:* Magnetismus an Oberflächen: Spinabhängige Elektronische Struktur. Phys. Bl. **50**, 673-677 (1994).

46. *Donath, M.:* Spin-Dependent Electronic Structure at Magnetic Surfaces: The Low-Miller-Index Surfaces of Nickel. Surf. Sci. Rep. **20**, 251-316 (1994).

47. *Drake, J.F., R.G. Kleva** and *M.E. Mandt*:* Structure of Thin Current Layers: Implications for Magnetic Reconnection. Phys. Rev. Lett. **73**, 1251-1254 (1994).

48. *Du Plessis*, J.* and *E. Taglauer:* Surface Concentration Modification of PdPt Alloys by Noble Gas Ion Sputtering. Surf. Interf. Anal. **22**, 556-560 (1994).

49. *Düchs, D.:* European Plasma Theory Institute, Theory Development Needed. Europhys. News **25**, No. 2, 22-24 (1994).

50. *Düchs, D.* and R. *Chodura:* Proc. 4th Int. Workshop on Plasma Edge Theory in Fusion Devices. Contrib. Plasma Phys. **34**, 101-492 (1994).

51. *Düchs, D.* and *T. Hellsten*:* Status and Prospects of Controlled Thermonuclear Fusion. Hyperfine Interact. **82**, 577-594 (1994).

52. *Düchs, D., A. Montvai** and *Ch. Sack*:* Response to Comments on the Paper "On Diffusion of Magnetic Field Lines by A.R. Esterkin". Plasma Phys. Control. Fusion **36**, 167-168 (1994).

53. *Eckstein, W.:* Backscattering and Sputtering with the Monte-Carlo-Program. Radiat. Eff. Defects Solids **130-131**, 239-250 (1994).

54. *Eisenhut*, B., J. Stober, G. Rangelov* and *Th. Fauster:* Growth and Structure of Thin Au Films on Ag(111). Phys. Rev., B **49**, 14676-14683 (1994).

55. *Eliashberg*, G.M., W. von der Linden*: The Mott Transition and Superconductivity. JETP Letters **59**, 441-445 (1994).

56. *Erckmann, V.* and *U. Gasparino:* Electron Cyclotron Resonance Heating and Current Drive in Toroidal Fusion Plasmas. Plasma Phys. Control. Fusion **36**, 1869-1962 (1994).

57. *Erckmann, V., U. Gasparino, H. Maaßberg, WVII-AS-Team, NBI-Team,* et al.*:* Recent Results with 140 GHz ECRH at the W7-AS Stellarator. In: Proc. IAEA Tech. Comm. Meeting on RF Launchers for Plasma Heating and Current Drive, Naka 1993, Eds. T. Yamamoto, H. Kimura, T. Imai. JAERI, Tokai, Ibaraki 1994, 140-145.

58. *Erckmann, V., N. Karulin, H. Wobig, WVII-AS-Team, NBI-Team,* et al.*:* High Density Operation with 140 GHz ECRH: Experiments at the W7-AS Stellarator, Prospects for the W7-X Stellarator. In: Proc. 21st EPS Conf. Control. Fusion and Plasma Phys., Montpellier 1994, Eds. E. Joffrin, P. Platz, P.E. Stott. ECA 18B. Europ. Phys. Soc., Geneva 1994, 1008-1011.

59. *Erckmann, V., WVII-AS-Team, NBI-Team,* et al.*:* ECRH and ECCD with 70 and 140 GHz at the W7-AS Stellarator. In: Proc. 2nd Int. Workshop on Strong Microwaves in Plasmas, Nizhny Novgorod 1993, Ed. A.G. Litvak. Chuvashia, Cheboksary 1994, 154-171.

60. *Estrada*, T., M. Hirsch, T. Geist, H.-J. Hartfuß,* et al.*:* Reflectometry Measurements During L- to H-Transitions in the W7-AS Stellarator. In: Proc. 21st EPS Conf. Control. Fusion and Plasma Phys., Montpellier 1994, Eds. E. Joffrin, P. Platz, P.E. Stott. ECA 18B. Europ. Phys. Soc., Geneva 1994, 404-407.

61. *Fauster, Th.:* Calculation of Surface States Using a One-Dimensional Scattering Model. Appl. Phys., A **59**, 634-639 (1994).

62. *Fauster, Th.:* Quantization of Electronic States on Metal Surfaces. Appl. Phys., A **59**, 479-486 (1994).

63. *Fauster, Th.:* Two-Photon Photoemission. Prog. Surf. Sci. **46**, 177-187 (1994).

64. *Fiedler, S., K. McCormick, J. Schweinzer,* et al.: Lithium Beam Spectroscopy on ASDEX-Upgrade for Determination of Density Profiles in the Plasma Edge. In: Proc. 21st EPS Conf. Control. Fusion and Plasma Phys., Montpellier 1994, Eds. E. Joffrin, P. Platz, P.E. Stott. ECA 18B. Europ. Phys. Soc., Geneva 1994, 1272-1275.

65. *Fischer*, N., S. Schuppler*, Th. Fauster* and *W. Steinmann*:* Coverage-Dependent Electronic Structure of Na on Cu(111). Surf. Sci. **314**, 89-96 (1994).

66. *Fischer, R., R. Nolte* and *K.-H. Steuer:* Short Intense Hydrogen Gas Impulses for Transport Studies in Fusion-Plasmas Produced by Laser Thermal Desorption from Titanium Hydrid. Rev. Sci. Instrum. **65**, 2306-2309 (1994).

67. *Franzen, P.* and *E. Vietzke:* Atomic Release of Hydrogen from Pure and Boronized Graphites. J. Vac. Sci. Technol., A **12**, 820-825 (1994).

68. *Friedl, A., W. Fukarek, W. Möller* and A. *Koch:* In situ Characterization of Plasma-Deposited a-Ch:H Thin Films by Spectroscopic Infrared Ellipsometry. Rev. Sci. Instrum. **65**, 2882-2889 (1994).

69. *Fuchs, J.C., K.-F. Mast, A. Herrmann* and *K. Lackner:* Twodimensional Reconstruction of the Radiation Power Density in ASDEX Upgrade. In: Proc. 21st EPS Conf. Control. Fusion and Plasma Phys., Montpellier 1994, Eds. E. Joffrin, P. Platz, P.E. Stott. ECA 18B. Europ. Phys. Soc., Geneva 1994, 1308-1311.

70. *Fukarek, W.* and *H. Kersten*:* Application of Dynamic in situ Ellipsometry to the Deposition of Tin-Doped Indium Oxide Films by Reactive Direct-Current Magnetron Sputtering. J. Vac. Sci. Technol., A **12**, 523-528 (1994).

71. *Garcia-Rosales, C.:* Erosion Processes in Plasma-Wall Interactions. J. Nucl. Mater. **211**, 202-214 (1994).

72. *Garcia-Rosales, C.:* First-Wall Erosion in Fusion Devices. J. Nucl. Mater. **212-215**, 97-100 (1994).

73. *Garcia-Rosales, C.:* Surface near Depletion of Dopants. In: Proc. 6th Int. Workshop on Carbon Materials, Jülich 1993, Eds. B. Krahl-Urban, D. Clemens. KFA, Jülich 1994, 81-89.

74. *Garcia-Rosales, C., R. Behrisch, D. Hildebrandt, B. Jüttner, W. Schneider, H. Wolff* and *ASDEX-Upgrade-Team:* Erosion at the Divertor Tiles of ASDEX Upgrade. In: Proc. 21st EPS Conf. Control. Fusion and Plasma Phys., Montpellier 1994, Eds. E. Joffrin, P. Platz, P.E. Stott. ECA 18B. Europ. Phys. Soc., Geneva 1994, 718-721.

75. *Garcia-Rosales, C., W. Eckstein* and *J. Roth:* Revised Formulae for Sputtering Data. J. Nucl. Mater. **218**, 8-17 (1994).

76. *Garcia-Rosales, C.* and *J. Roth:* Revised Formula for Chemical Sputtering of Carbon. In: Proc. 21st EPS Conf. Control. Fusion and Plasma Phys., Montpellier 1994, Eds. E. Joffrin, P. Platz, P.E. Stott. ECA 18B. Europ. Phys. Soc., Geneva 1994, 770-773.

77. *Garcia-Rosales, C., J. Roth* and *R. Behrisch:* Sputtering and Surface Composition Modifications of Ti Doped Graphite RG-Ti at Temperatures up to 2000 K. J. Nucl. Mater. **212-215**, 1211-1217 (1994).

78. *Geiger, J., A. Weller, F. Rau, WVII-AS-Team* and *NBI-Team:* Stability Analysis of Pressure Driven Modes in W7-AS. In: Proc. 21st EPS Conf. Control. Fusion and Plasma Phys., Montpellier 1994, Eds. E. Joffrin, P. Platz, P.E. Stott. ECA 18B. Europ. Phys. Soc., Geneva 1994, 372-375.

79. *Giannone, L., R. Balbin, H. Niedermeyer, M. Endler, G. Herre, C. Hidalgo, A. Rudyj, G. Theimer, P. Verplancke, WVII-AS-Team,* et al.: Density, Temperature and Potential Fluctation Measurements by the Swept Langmuir Probe Technique in Wendelstein 7-AS. Phys. Plasmas **1**, 3614-3621 (1994).

80. *Grieger, G., J. Nührenberg, H. Renner, J. Sapper* and *H. Wobig:* HELIAS Stellarator Reactor Studies and Related European Technology Studies. Fusion Eng. Des. **25**, 73-84 (1994)

81. *Guilhem*, D., P. Ghendrih*, A. Grosman*, H. Renner,* et al.: Experimental Investigation of Power Deposition on the Ergodic Divertor Target Plates in TORE-SUPRA. In: Proc. 21st EPS Conf. Control. Fusion and Plasma Phys., Montpellier 1994, Eds. E. Joffrin, P. Platz, P.E. Stott. ECA 18B. Europ. Phys. Soc., Geneva 1994, 750-753.

82. *Hantzsche, E.:* Approaches to Two-Dimensional Models of Expanding Vacuum Arc Plasmas. In: Proc. 16th Int. Symp. on Discharges & Electrical Insulation in Vacuum (ISDEIV), Moscow-St. Petersburg 1994, Ed. G.A. Mesyats. SPIE Proc. 2259, SPIE, Washington 1994, 128-131.

83. *Hantzsche, E.:* Expansion Model of the Neutral Component in Vacuum Arc Spot Plasmas. Contrib. Plasma Phys. **34**, 703-709 (1994).

84. *Hantzsche, E.:* Space Charge Sheaths with Electron Emission. In: Proc. 21st EPS Conf. Control. Fusion and Plasma Phys., Montpellier 1994, Eds. E. Joffrin, P. Platz, P.E. Stott. ECA 18B. Europ. Phys. Soc., Geneva 1994, 926-929.

85. *Hantzsche, E.* and *B. Jüttner:* On the Appearance of Vacuum Arc Spots Imaged by the Emitted Light. In: Proc. 16th Int. Symp. on Discharges & Electrical Insulation in Vacuum (ISDEIV), Moscow-St. Petersburg 1994, Ed. G.A. Mesyats. SPIE Proc. 2259, SPIE, Washington 1994, 132-135.

86. *Hartfuß, H.-J., M. Endler, V. Erckmann, U. Gasparino, L. Giannone, P. Grigull, G. Herre, M. Kick, G. Kühner, H. Niedermeyer, H. Ringler, F. Sardei, U. Stroth, S. Sattler, F. Wagner, A. Weller, WVII-AS-Team, NBI-Team* and *ECRH-Group:* Physics Studies in W7-AS. Plasma Phys. Control. Fusion **36**, B17-B37 (1994).

87. *Hartfuß, H.-J., T. Estrada*, M. Hirsch, T. Geist,* et al.: Broadband Heterodyne Reflectometer at the W7-AS. Rev. Sci. Instrum. **65**, 2284-2290 (1994).

88. *Hayashi*, T., T. Sato*, P. Merkel, J. Nührenberg* and *U. Schwenn:* Formation and 'Self-Healing' of Magnetic Islands in Finite-β Helias Equilibria. Phys. Plasmas **1**, 3262-3268 (1994).

89. *Hechtl*, E., W. Eckstein* and *J. Roth:* Reflection and Self-Sputtering of Nickel at Oblique Angles of Ion Incidence. Nucl. Instrum. Methods Phys. Res., Sect. B **90**, 505-508 (1994).

90. *Herrnegger, F., W. Dommaschk* and *A. Schlüter:* Optimized Advanced Stellarators of Linked Mirror Type. In: Proc. 21st EPS Conf. Control. Fusion and Plasma Phys., Montpellier 1994, Eds. E. Joffrin, P. Platz, P.E. Stott. ECA 18B. Europ. Phys. Soc., Geneva 1994, 360-363.

91. *Hetzel, R., W. von der Linden* and *W. Hanke:* Pairing Correlations in a Two-Layer Hubbard Model. Phys. Rev., B **50**, 4159-4162 (1994).

92. *Hirsch, S., K. Asmussen, W. Engelhardt, A. Field, G. Fußmann, G. Lieder, D. Naujoks, R. Neu, R. Radtke, U. Wenzel* and *ASDEX-Upgrade-Team:* Study of High-Z Target Plate Materials in the

Divertor of ASDEX-Upgrade. In: Proc. 21st EPS Conf. Control. Fusion and Plasma Phys., Montpellier 1994, Eds. E. Joffrin, P. Platz, P.E. Stott. ECA 18B. Europ. Phys. Soc., Geneva 1994, 730-733.

93. *Hoffmann, C., F. Braun, W. Suttrop, J.-M. Noterdaeme, H.-U. Fahrbach, W. Herrmann, ASDEX-Upgrade-Team* and *ICRH-Team:* ICRF Power Modulation Experiments on ASDEX-Upgrade. In: Proc. 21st EPS Conf. Control. Fusion and Plasma Phys., Montpellier 1994, Eds. E. Joffrin, P. Platz, P.E. Stott. ECA 18B. Europ. Phys. Soc., Geneva 1994, 838-841.

94. *Hofmann, J.V. , K. Ida*, J. Geiger, F. Rau, J. Baldzuhn, M. Kick, G. Kühner, F.-P. Penningsfeld, W. Ott, H. Ringler, WVII-AS-Team, ECRH-Group* and *NI-Group:* Toroidal and Poloidal Rotation in the W7-AS Stellarator. In: Proc. 21st EPS Conf. Control. Fusion and Plasma Phys., Montpellier 1994, Eds. E. Joffrin, P. Platz, P.E. Stott. ECA 18B. Europ. Phys. Soc., Geneva 1994, 392-395.

95. *Hofmeister, F., F. Braun* and *F. Wesner:* The RF System and Matching Procedure for ASDEX and ASDEX Upgrade. Fusion Eng. Des. **24**, 83-89 (1994).

96. *Holzhauer*, E., G. Dodel*, M. Endler, J. Gernhardt, L. Giannone, K. McCormick, V. Mertens, H. Niedermeyer, A. Rudyj, G. Theimer, F. Wagner, H. Zohm, ASDEX-Team,* et al.*:* The H-Mode in the ASDEX Tokamak. Plasma Phys. Control. Fusion **36**, A3-A11 (1994).

97. *Hytry, R., W. Möller* and *R. Wilhelm:* Running Waveguide Discharge for Inner Coating of Metal Tubes. Appl. Phys. Lett. **64**, 3401-3403 (1994).

98. *Igitkhanov, Yu.L., G. Janeschitz*, A.S. Kukushkin*,* et al.*:* Momentum Removal from Subsonic and Supersonic Plasma Flows in the ITER Divertor. In: Proc. 21st EPS Conf. Control. Fusion and Plasma Phys., Montpellier 1994, Eds. E. Joffrin, P. Platz, P.E. Stott. ECA 18B. Europ. Phys. Soc., Geneva 1994, 714-717.

99. *Igitkhanov, Yu.L., A.S. Kukushkin*, A.M. Runov** and *R. Chodura:* Application of BGK Collision Operator for Kinetic Correction of Fluid Models. Contrib. Plasma Phys. **34**, 216-220 (1994).

100. *Igitkhanov, Yu.L., A.S. Kukushkin** and *A.M. Runov*:* The Impact of Kinetic Effects on the ITER Divertor Plasma. In: Proc. 21st EPS Conf. Control. Fusion and Plasma Phys., Montpellier 1994, Eds. E. Joffrin, P. Platz, P.E. Stott. ECA 18B. Europ. Phys. Soc., Geneva 1994, 766-769.

101. *Igitkhanov, Yu.L., M.I. Mikhailov** and *W. Feneberg:* Fluid Description of Edge Plasma Transport in a Non-Orthogonal Coordinate System. Contrib. Plasma Phys. **34**, 398-403 (1994).

102. *Igitkhanov, Yu.L.* and *A.M. Runov*:* Implication of Kinetic Effects for Fluid Codes. Contrib. Plasma Phys. **34**, 221-225 (1994).

103. *Jacob, W., M. Engelhard, W. Möller* and *A. Koch:* Absolute Density Determination of CH Radicals in a Methane Plasma. Appl. Phys. Lett. **64**, 971-973 (1994).

104. *Jänicke, R., H.-J. Hartfuß, A. Weller, H. Zohm* and *WVII-AS-Team:* Confinement and Fluctuations at $\mathfrak{t} \approx 1/2$ for Discharges with and without net Toroidal Currents in the W7-AS Stellarator. In: Proc. 21st EPS Conf. Control. Fusion and Plasma Phys., Montpellier 1994, Eds. E. Joffrin, P. Platz, P.E. Stott. ECA 18B. Europ. Phys. Soc., Geneva 1994, 396-399.

105. *Junker, W., H.-S. Bosch, K. Büchl, O. Gruber, G. Haas, H. Kastelewicz, M. Kaufmann, W. Köppendörfer, K. Lackner, M. Laux, V. Mertens, J. Neuhauser, H. Röhr, R. Schneider, K.-H. Steuer, ASDEX-Upgrade-Team, NI-Team,* et al.*:* Comparison of Experimental MARFE Observations in ASDEX Upgrade with B2 Calculations. In: Proc. 21st EPS Conf. Control. Fusion and Plasma Phys., Montpellier 1994, Eds. E. Joffrin, P. Platz, P.E. Stott. ECA 18B. Europ. Phys. Soc., Geneva 1994, 680-683.

106. *Jüttner, B., K. Büchl, M. Weinlich* and *ASDEX-Upgrade-Team:* Arcing in ASDEX-Upgrade. Contrib. Plasma Phys. **34**, 472-477 (1994).

107. *Jüttner, B., W. Löffler, C. Weber* and *G. Ziegenhagen:* Dependence of the Non-Stationary Behavior of Arc Cathode Spots on the Discharge Duration. In: Proc. 16th Int. Symp. on Discharges & Electrical Insulation in Vacuum (ISDEIV), Moscow-St. Petersburg 1994, Ed. G.A. Mesyats. SPIE Proc. 2259, SPIE, Washington 1994, 70-75.

108. *Kaiser, R.* and *A. Salat:* Surface Current Equilibria from a Geometric Point of View. Phys. Plasmas **1**, 281-295 (1994).

109. *Kallenbach, A., C. Garcia-Rosales, A. Field, M. Kaufmann, R. Neu, S. de Pena Hempel, W. Poschenrieder, K.-H. Steuer, ASDEX-Upgrade-Team* and *NBI-Team:* The Impact of Chemical Erosion on the Global Impurity Balance in the ASDEX Upgrade Tokamak. In: Proc. 21st EPS Conf. Control. Fusion and Plasma Phys., Montpellier 1994, Eds. E. Joffrin, P. Platz, P.E. Stott. ECA 18B. Europ. Phys. Soc., Geneva 1994, 774-777.

110. *Kallenbach, A., G. Fußmann, H.-M. Mayer, ASDEX-Upgrade-Team, et al.:* The Influence of Spatially and Temporally Varying Edge Conditions on the Interpretation of Spectroscopic Flux Measurements. Plasma Phys. Control. Fusion **36**, 1299-1306 (1994).

111. *Kallenbach, A., R. Neu, W. Poschenrieder* and *ASDEX-Upgrade-Team:* The Contribution of Chemical Erosion to the Carbon Content in the ASDEX Upgrade Tokamak. Nucl. Fusion **34**, 1557-1565 (1994).

112. *Kardaun, O.* and *ITER-H-Mode-Database-Working-Group:* Offset-Linear Scalings Based on the ITER H-Mode Confinement Database. In: Proc. 21st EPS Conf. Control. Fusion and Plasma Phys., Montpellier 1994, Eds. E. Joffrin, P. Platz, P.E. Stott. ECA 18B. Europ. Phys. Soc., Geneva 1994, 90-93.

113. *Kedves*, M.A., J.S. Bakos*, G. Bürger*, P. Ignacz,* et al.*:* Measurement of the Spatial Distribution of the Non-Intrinsic Impurities on Tokamak Deposition Probes by LIMS. In: Proc. 21st EPS Conf. Control. Fusion and Plasma Phys., Montpellier 1994, Eds. E. Joffrin, P. Platz, P.E. Stott. ECA 18B. Europ. Phys. Soc., Geneva 1994, 1336-1339.

114. *Keudell, A. von* and *W. Möller:* A Combined Plasma-Surface Model for the Deposition of C:H Films. J. Appl. Phys. **75**, 7718-7727 (1994).

115. *Kisslinger, J., C.D. Beidler, E. Harmeyer, F. Rau, H. Renner* and *H. Wobig:* Island Divertor for the Stellarator Wendelstein 7-X. In: Proc. 21st EPS Conf. Control. Fusion and Plasma Phys., Montpellier 1994, Eds. E. Joffrin, P. Platz, P.E. Stott. ECA 18B. Europ. Phys. Soc., Geneva 1994, 368-371.

116. *Kocsis*, G., J.S. Bakos*, G. Bürger*, P. Ignacz,* et al.*:* Aluminium Blow-off with Targets of Different Thickness and Structures. In: Proc. 12th ESCAMPIG, Noordwijkerhout 1994. Europ. Phys. Soc., Geneva 1994, 356-358.

117. *Krasheninnikov*, S.I.* and *R. Chodura:* Kinetics of Plasma Flow in the Recycling Region. Contrib. Plasma Phys. **34**, 210-215 (1994).

118. *Kreissig*, U., R. Grötzschel** and *R. Behrisch:* Simultaneous Measurement of the Hydrogen Isotopes H, D, T and 3 He with HIERD. Nucl. Instrum. Methods Phys. Res., Sect. B **85**, 71-74 (1994).

119. *Küppers, J., J. Biener, A. Schenk, B. Winter* and *C. Lutterloh:* Elementary Reactions at Carbon Surfaces under Impact of H. In: Proc. 21st EPS Conf. Control. Fusion and Plasma Phys., Montpellier 1994, Eds. E. Joffrin, P. Platz, P.E. Stott. ECA 18B. Europ. Phys. Soc., Geneva 1994, 1524-1527.

120. *Kuteev*, B.V., V.Yu. Sergeev*, S.M. Egorov*, P.T. Lang, K. Büchl, P. Cierpka, R.S. Lang,* et al.*:* Impurity Pellet Injection Systems for Tokamak Diagnostics and Burn Control. Fusion Technol. **26**, 938-944 (1994).

121. *Lackner, K.:* Figures of Merit for Divertor Dimilarity. Comments Plasma Phys. Controll. Fus. **15**, 359-365 (1994).

122. *Lackner, K., H.-S. Bosch, D. Coster, O. Gruber, G. Haas, A. Herrmann, A. Kallenbach, M. Kaufmann, V. Mertens, J. Neuhauser, F. Ryter, M. Weinlich, H. Zohm, M. Albrecht, M. Alexander, K. Asmussen, M. Ballico, K. Behler, K. Behringer, M. Bessenrodt-Weberpals, M. Brambilla, K. Büchl, A. Carlson, H.J. de Blank, S. de Pena Hempel, S. Deschka, C. Dorn, R. Drube, R. Dux, A. Eberhagen, W. Engelhardt, H.-U. Fahrbach, H.-U. Feist, S. Fiedler, D. Fieg, A. Field, J.C. Fuchs, G. Fußmann, C. Garcia-Rosales, O. Gehre, J. Gernhardt, W. Herrmann, S. Hirsch, P. Ignacz, B. Jüttner, W. Junker, T. Kass, K. Kiemer, W. Köppendörfer, H. Kollotzek, M. Kornherr, K. Krieger, B. Kurzan, P.T. Lang, R.S. Lang, M. Laux, M. Maraschek, K.-F. Mast, H.-M. Mayer, D. Meisel, R. Merkel, H. Murmann, B. Napiontek, D. Naujoks, G. Neu, R. Neu, J.-M. Noterdaeme, G. Pautasso, W. Poschenrieder, G. Raupp, H. Richter, T. Richter, H. Röhr, J. Roth, N. Salmon, H. Salzmann, W. Sandmann, H.-B. Schilling, M. Schittenhelm, H. Schneider, R. Schneider, W. Schneider, K. Schönmann, G. Schramm, J. Schweinzer, U. Seidel, M. Sokoll, E. Speth, A. Stäbler, K.-H. Steuer, J. Stober, B. Streibl, W. Suttrop, W. Treutterer, M. Troppmann, M. Ulrich, H. Vernickel, O. Vollmer, H. Wedler, U. Wenzel, F. Wesner, R. Wunderlich, D. Zasche, H.-P. Zehrfeld,* et al.*:* Recent Results From Divertor Operation in ASDEX Upgrade. Plasma Phys. Control. Fusion **36**, B79-B92 (1994).

123. *Lang, P.T., M. Alexander, K. Büchl, R.S. Lang, V. Mertens, J. Neuhauser, H. Zohm* and *ASDEX-Upgrade-Team:* Influence on the Plasma Performance by Multipellet Injection into ASDEX Upgrade. In: Proc. 21st EPS Conf. Control. Fusion and Plasma Phys., Montpellier 1994, Eds. E. Joffrin, P. Platz, P.E. Stott. ECA 18B. Europ. Phys. Soc., Geneva 1994, 306-309.

124. *Lang, P.T., P. Cierpka, R.S. Lang,* et al.*:* Compact Gas Gun Injection System for Variably Sized Solid Pellets. Rev. Sci. Instrum. **65**, 2316-2321 (1994).

125. *Langhoff, M.* and *B.M.U. Scherzer:* Time Resolved Measurements of Hydrogen Inventory in Graphite under Plasma Exposure. In: Proc. 21st EPS Conf. Control. Fusion and Plasma Phys., Montpellier 1994, Eds. E. Joffrin, P. Platz, P.E. Stott. ECA 18B. Europ. Phys. Soc., Geneva 1994, 782-785.

126. *Laux, M., W. Junker, A. Herrmann, K. Büchl, A. Field, G. Haas, K.-F. Mast, V. Mertens, B. Napiontek, J. Neuhauser, M. Weinlich, U. Wenzel* and *ASDEX-Upgrade-Team:* Bistable Behaviour of the ASDEX-Upgrade Divertor near the Transition to the x-Point MARFE. In: Proc. 21st EPS Conf. Control. Fusion and Plasma Phys., Montpellier 1994, Eds. E. Joffrin, P. Platz, P.E. Stott. ECA 18B. Europ. Phys. Soc., Geneva 1994, 726-729.

127. *Lengyel, L.L.* and *P.N. Spathis:* A Self-Consistent MHD Ablation Model: Pellet Penetration Depth Prediction for a Reactor-Temperature Plasma. Nucl. Fusion **34**, 675-685 (1994).

128. *Lengyel, L.L.* and *P.N. Spathis:* Evolution of Radiating Vapour Shield at Divertor Plates During Disruption. In: Proc. 21st EPS Conf. Control. Fusion and Plasma Phys., Montpellier 1994, Eds. E. Joffrin, P. Platz, P.E. Stott. ECA 18B. Europ. Phys. Soc., Geneva 1994, 778-781.

129. *Lieder, G., K. Behringer, A. Field, C. Garcia-Rosales, S. Hirsch, A. Kallenbach, B. Napiontek, D. Naujoks, W. Poschenrieder R. Radtke, J. Roth, M. Weinlich, ASDEX-Upgrade-Team,* et al.*:* Spectroscopic Investigation of Molecular Impurities in the ASDEX Upgrade Divertor. In: Proc. 21st EPS Conf. Control. Fusion and Plasma Phys., Montpellier 1994, Eds. E. Joffrin, P. Platz, P.E. Stott. ECA 18B. Europ. Phys. Soc., Geneva 1994, 722-725.

130. *Linden, W. von der:* What Can We Learn from QMC Simulations? In: Proc. 4th Int. Conf. in Physics Computing, Prag 1993, Eds. R.A. de Groot, J. Nadrchal. World Scientific Publ., Singapore 1994, 102-108.

131. *Linden, W. von der, K. Ertl* and *V. Dose:* Maximum Entropy Reconstruction of Local Emissivity Profiles from Soft X-Ray Chord-Measurements. In: Contrib. to High-Temperature Plasma Physics. Eds. K.H. Spatschek, J. Uhlenbusch. Akademie Verl., Berlin 1994, 131-142.

132. *Linsmeier, Ch.:* Auger Electron Spectroscopy. Vacuum **45**, 673-690 (1994).

133. *Linsmeier, Ch.:* Auger Electron Spectroscopy. In: Surface Science Techniques. Eds. J.M. Walls, R. Smith. Pergamon Press, Oxford 1994, 25-42.

134. *Lortz, D.:* Comments on the Paper: "Comments on the Extended Energy Principle". Plasma Phys. Control. Fusion **36**, 1227-1232 (1994).

135. *Lortz, D.* and *G.O. Spies:* Spheromak Instability. Phys. Plasmas **1**, 682-683 (1994).

136. *Lortz, D.* and *G.O. Spies:* Stability of Force-Free Plasma-Vacuum Equilibria. Phys. Plasmas **1**, 249-259 (1994).

137. *Lortz, D.* and *A. Zeiler:* Stability of Straight Tokamak Equilibria without Wall Stabilization. Phys. Plasmas **1**, 670-681 (1994).

138. *Lummila*, J., L. Halonen*, P.T. Lang,* et al.*:* Interpretation of New $^{13}CD_3F$ Submillimeter-Wave Laser Lines Using High Resolution Infrared Spectroscopy. J. Chem. Phys. **100**, 877-890 (1994).

139. *Lutterloh, C., A. Schenk, J. Biener, B. Winter, J. Küppers* and *U.A. Schubert:* D(H) Atom Impact Induced Eley-Rideal Hydrogen Abstraction Reaction Toward HD at Fully Hydrogenated C:H(D) Surfaces. Surf. Sci. **316**, 1039-1043 (1994).

140. *Maaßberg, H., C.D. Beidler* and *W. Lotz:* Neoclassical Transport Scalings for Stellarators in the Long-Mean-Free-Path Regime. In: Proc. 21st EPS Conf. Control. Fusion and Plasma Phys., Montpellier 1994, Eds. E. Joffrin, P. Platz, P.E. Stott. ECA 18B. Europ. Phys. Soc., Geneva 1994, 568-571.

141. *Mandl, W.:* First Results from the new NIR Z_{eff} Diagnostic on W7-AS. Stellarator News 34, 7-8 (1994).

142. *Mandl, W.* and *C. Mahn:* First Results from the new Z_{eff} Diagnostic at W7-AS Based on the Measurement of Bremsstrahlung in the NIR Spectral Region. In: Proc. 21st EPS Conf. Control. Fusion

and Plasma Phys., Montpellier 1994, Eds. E. Joffrin, P. Platz, P.E. Stott. ECA 18B. Europ. Phys. Soc., Geneva 1994, 1276-1279.

143. *Martinelli, A.P., R. Behrisch* and *A.T. Peacock*:* Modification of the Carbon and Beryllium Walls in JET by Erosion, Redeposition and Deuterium Trapping after the 1991 Discharge Period. J. Nucl. Mater. **212-215**, 1245-1249 (1994).

144. *Mayer, M.* and *W. Eckstein:* Monte Carlo Calculations of Hydrogen and Deuterium Range Distributions in Light Target Materials. Nucl. Instrum. Methods Phys. Res., Sect. B **94**, 22-26 (1994).

145. *Mayer, M., B.M.U. Scherzer* and *W. Eckstein:* Trapping and Reflection Coefficients for Deuterium in Graphite at Low Energy and Oblique Incidence. Nucl. Instrum. Methods Phys. Res., Sect. B **85**, 560-565 (1994).

146. *McCormick, K., S. Fiedler, P. Platzer*, J. Schweinzer,* et al.: High Energy Lithium-Beam-Spectroscopy Diagnostics on the Wendelstein 7-AS Stellarator: First Results. In: Proc. 21st EPS Conf. Control. Fusion and Plasma Phys., Montpellier 1994, Eds. E. Joffrin, P. Platz, P.E. Stott. ECA 18B. Europ. Phys. Soc., Geneva 1994, 1268-1271.

147. *Memmel, N.* and *Th. Detzel:* Growth, Structure and Stability of Ultrathin Iron Film on Cu(001). Surf. Sci. **307-309**, 490-495 (1994).

148. *Mertens, V., H.-S. Bosch, K. Büchl, A. Carlson, J.C. Fuchs, O. Gruber, G. Haas, A. Herrmann, W. Junker, A. Kallenbach, M. Kaufmann, W. Köppendörfer, K. Lackner, M. Laux, K.-F. Mast, J. Neuhauser, F. Ryter, A. Stäbler, O. Vollmer, M. Weinlich, H. Zohm, ASDEX-Upgrade-Team* and *NBI-Team:* Divertor Performance of High Density H-Mode Discharges in ASDEX Upgrade. In: Proc. 21st EPS Conf. Control. Fusion and Plasma Phys., Montpellier 1994, Eds. E. Joffrin, P. Platz, P.E. Stott. ECA 18B. Europ. Phys. Soc., Geneva 1994, 326-329.

149. *Mertens, V., W. Junker, M. Laux, M. Schittenhelm, K. Büchl, K.-F. Mast, A. Carlson, A. Field, J.C. Fuchs, O. Gehre, O. Gruber, A. Herrmann, G. Haas, A. Kallenbach, M. Kaufmann, W. Köppendörfer, K. Lackner, G. Lieder, J. Neuhauser, F. Ryter, H. Salzmann, W. Sandmann, K.-H. Steuer, M. Weinlich, U. Wenzel, H. Zohm, ASDEX-Upgrade-Team,* et al.: Experimental Investigation of Marfes and the Density Limit in the ASDEX Upgrade. Plasma Phys. Control. Fusion **36**, 1307-1325 (1994).

150. *Milch, I.:* Fusionsleistung mit Rekordwerten. MPG-Spiegel 1, 27-28 (1994).

151. *Milch, I.:* Mikrowellengrill fürs Plasma. Schweizer Maschinenmarkt **4**, 28-29 (1994).

152. *Milch, I.:* Plasmaphysik - Rechenprogramm für Fusionsexperimente. AGF-Jahresheft, 12-13 (1994).

153. *Milch, I.:* Rechenprogramm für die Plasmarandschicht. MPG-Spiegel 5, 87-88 (1994).

154. *Milch, I.:* Zündstoff Sonne. Fusionsforschung: Der lange Weg zur Nutzung der Fusionsenergie. Kultur & Technik **18**, 14-21 (1994).

155. *Möller, W.:* Computer Simulation of Ion-Beam Assisted Film Growth. Nucl. Instrum. Methods Phys. Res., Sect. B **89**, 322-324 (1994).

156. *Möller, W.* and *W. Eckstein:* Capabilities of Dynamic BCA Simulations. Radiat. Eff. Defects Solids **129**, 19-23 (1994).

157. *Möller, W., W. Fukarek, A. von Keudell* and *K. Lange:* Mechanisms of the Deposition of Hydrogenated Carbon Films. In: Proc. Symp. on Dry Process, Tokyo 1994. Inst. of Electrical Eng. of Japan, Tokyo 1994, 117-124.

158. *Naujoks, D., J. Roth, K. Krieger, G. Lieder* and *M. Laux:* Erosion and Redeposition in the ASDEX-Upgrade Divertor. J. Nucl. Mater. **210**, 43-50 (1994).

159. *Naujoks, D., R. Behrisch, V. Philipps** and *B. Schweer*:* Erosion and Redeposition on Carbon Probes in the Boundary Plasma of TEXTOR. Plasma Phys. Control. Fusion **36**, 2021-2030 (1994).

160. *Neu, R., R. Dux, J.C. Fuchs, W. Junker, A. Kallenbach, V. Mertens, S. de Pena Hempel, K. Schönmann* and *ASDEX-Upgrade-Team:* Influence of the Carbon and the Oxygen Concentration on the Density Limit in ASDEX Upgrade. In: Proc. 21st EPS Conf. Control. Fusion and Plasma Phys., Montpellier 1994, Eds. E. Joffrin, P. Platz, P.E. Stott. ECA 18B. Europ. Phys. Soc., Geneva 1994, 6-9.

161. *Neuhauser, J., H.-S. Bosch, B. Braams*, O. Gruber, M. Kaufmann, K. Lackner, R. Schneider, B. Streibl, H.-P. Zehrfeld, ASDEX-Upgrade-Team,* et al.: Divertor Options for ITER and ASDEX-Upgrade: Results of Modeling. In: Proc. 21st EPS Conf. Control. Fusion and Plasma Phys., Montpellier 1994, Eds. E. Joffrin, P. Platz, P.E. Stott. ECA 18B. Europ. Phys. Soc., Geneva 1994, 706-709.

162. *Niedermeyer, H., M. Endler, L. Giannone, K. McCormick, A. Rudyj, G. Theimer, ASDEX-Team, WVII-AS-Team,* et al.: Turbulent Fluctuations in the Scrape-off Layer of the ASDEX Tokamak and the W7-AS Stellarator. In: Proc. 21st EPS Conf. Control. Fusion and Plasma Phys., Montpellier 1994, Eds. E. Joffrin, P. Platz, P.E. Stott. ECA 18B. Europ. Phys. Soc., Geneva 1994, 874-877.

163. *Noterdaeme, J.-M., M. Brambilla, D. Coster, J. Gernhardt, C. Hoffmann, F. Hofmeister, J. Neuhauser, R. Schneider, H. Zohm, ASDEX-Upgrade-Team, ICRH-Team, NI-Team,* et al.: Changes in the Edge Plasma Due to ELMs, a Study Using Coupling Measurements in the ICRF Range. In: Proc. 21st EPS Conf. Control. Fusion and Plasma Phys., Montpellier 1994, Eds. E. Joffrin, P. Platz, P.E. Stott. ECA 18B. Europ. Phys. Soc., Geneva 1994, 842-845.

164. *Noterdaeme, J.-M., C. Hoffmann, M. Brambilla, K. Büchl, A. Eberhagen, A. Field, J.C. Fuchs, O. Gehre, J. Gernhardt, O. Gruber, G. Haas, A. Herrmann, F. Hofmeister, A. Kallenbach, G. Lieder, V. Mertens, H. Murmann, S. de Pena Hempel, W. Poschenrieder, T. Richter, F. Ryter, N. Salmon, H. Salzmann, W. Schneider, F. Wesner, H.-P. Zehrfeld, H. Zohm, ICRH-Team* and *ASDEX-Upgrade-Team:* First Results of Ion Cyclotron Resonance Heating on ASDEX Upgrade. In: Proc. 10th Topical Conf. Radio Frequency Power in Plasmas, Boston 1993. Eds. M. Porkolab, J. Hosea. AIP Conf. Proc. 289. AIP Press, New York 1994, 12-23.

165. *Noterdaeme, J.-M., F. Wesner, M. Brambilla, R. Fritsch, H.-J. Kutsch, M. Söll** and *ICRH-Team:* The ASDEX Upgrade ICRH Antenna. Fusion Eng. Des. **24**, 65-74 (1994).

166. *Nührenberg, J., W. Lotz* and *S. Gori:* Quasi-Axisymmetric Tokamaks. In: Proc. Joint Varenna-Lausanne Int. Workshop on Theory of Fusion Plasmas, Varenna 1994, Eds. E. Sindoni, F. Troyon, J. Vaclavik. Editrice Compositori, Bologna 1994, 3-12.

167. *Pautasso, G., A. Herrmann, K. Lackner* and *ASDEX-Upgrade-Team:* Energy Balance During Disruption Associated with Vertical Displacement Events. Nucl. Fusion **34**, 455-458 (1994).

168. *Pautasso, G., O. Gruber, K.-F. Mast, K. Büchl, J.C. Fuchs, C. Garcia-Rosales, A. Herrmann, K. Lackner, J. Neuhauser, W. Schneider* and *ASDEX-Upgrade-Team:* A Study Toward Self-Consistent Modelling of Current Quench. In: Proc. 21st EPS Conf. Control. Fusion and Plasma Phys., Montpellier 1994, Eds. E. Joffrin,

P. Platz, P.E. Stott. ECA 18B. Europ. Phys. Soc., Geneva 1994, 222-225.

169. *Penningsfeld, F.-P.:* Fast Access to Neutral Injection Heating Profiles Applied for the Stellarator W7-AS. In: Proc. 21st EPS Conf. Control. Fusion and Plasma Phys., Montpellier 1994, Eds. E. Joffrin, P. Platz, P.E. Stott. ECA 18B. Europ. Phys. Soc., Geneva 1994, 932-935.

170. *Peters*, M., H.-J. Hartfuß, U. Stroth, V. Erckmann, L. Giannone, H. Maaßberg,* et al. *:* A Comparative Heat Pulse Propagation Study on RTP and W7-AS. In: Proc. 21st EPS Conf. Control. Fusion and Plasma Phys., Montpellier 1994, Eds. E. Joffrin, P. Platz, P.E. Stott. ECA 18B. Europ. Phys. Soc., Geneva 1994, 158-161.

171. *Pfirsch, D.* and *R.N. Sudan*:* Small Scale Magnetic Flux-Averaged Magnetohydrodynamics. Phys. Plasmas **1**, 2488-2514 (1994).

172. *Pfirsch, D.* and *H. Weitzner*:* Inverse Method for the Investigation of Nonlinear Instabilities Associated with Negative-Energy Modes. Phys. Rev., E **49**, 3368-3375 (1994).

173. *Pinkau, K.:* Experimente mit dem Sternenfeuer: Option für die Energieversorgung von morgen. AGF-Forschungsthemen 7, 9-11 (1994).

174. *Preuss, R., A. Muramatsu*, W. von der Linden, P. Dietrich,* et al.*:* Spectral Properties of the One-Dimensional Hubbard Model. Phys. Rev. Lett. **73**, 732-735 (1994).

175. *Rabe, A., N. Memmel, A. Steltenpohl* and *Th. Fauster:* Room Temperature Instability of Co/Cu(111). Phys. Rev. Lett. **73**, 2728-2731 (1994).

176. *Ramos, G.* and *B.M.U. Scherzer:* Radiation Damage and Trapping of Helium in HOPG-Graphite. Nucl. Instrum. Methods Phys. Res., Sect. B **85,** 479-483 (1994).

177. *Rangelov, G., P. Augustin*, J. Stober and Th. Fauster:* Epitaxial $CoSi_2$ Formation on Si(100) Studied by Photoelectron Diffraction. In: BESSY Jahresbericht 1993, Ges. für Synchrotronstrahlung mbH, Berlin 1994, 299-300.

178. *Rangelov, G., P. Augustin, J. Stober* and *Th. Fauster:* Initial Stages of Epitaxial $CoSi_2$ Formation on Si(100) Surfaces. Phys. Rev., B **49**, 7535-7544 (1994).

179. *Rangelov, G., P. Augustin*, J. Stober* and *Th. Fauster:* Reaction of Ultrathin Co Layers with Si(111) and Si(100) Surfaces. Surf. Sci. **307**, 264-268 (1994).

180. *Rangelov, G.* and *V. Dose:* Inverse Photoemission. Bulg. Chem. Comm. **26**, 159-192 (1994).

181. *Rau, F.:* Conferences and Symposia Stellarators. Nucl. Fusion **34**, 301-311 (1994).

182. *Rau, F., C.D. Beidler, R. Brakel, J. Geiger, P. Grigull, E. Harmeyer, G. Herre, J.V. Hofmann, M. Kick, J. Kisslinger, G. Kühner, W. Mandl, H. Niedermeyer, H. Ringler, H. Walter, H. Wobig, WVII-AS-Team, ECRH-Group* and *NBI-Group:* Extended Parameter Range in W 7-AS Experiments at Various Values of the Mirror Ratio. In: Proc. 21st EPS Conf. Control. Fusion and Plasma Phys., Montpellier 1994, Eds. E. Joffrin, P. Platz, P.E. Stott. ECA 18B. Europ. Phys. Soc., Geneva 1994, 400-403.

183. *Resch*, Ch., H.F. Berger*, K.D. Rendulic** and *E. Bertel:* Adsorption Dynamics for the System Hydrogen/Palladium and its Relation to the Surface Electronic Structure. Surf. Sci. **316**, L1105-L1109 (1994).

184. *Richter, H., G. Neu, G. Raupp* and *D. Zasche:* System Integration of the ASDEX-Upgrade Timing System. IEEE Trans. Nucl. Sci. **41,** 178-180 (1994).

185. *Richter, T.* and *H. Vernickel:* The Cooling Water Calorimetry System at ASDEX Upgrade Tokamak. Rev. Sci. Instrum. **65**, 1613-1615 (1994).

186. *Rusteberg*, C., M. Lindmayer*, B. Jüttner* and *H. Pursch:* On the Ion Potential Distribution of High Current Arcs in Vacuum. In: Proc. 16th Int. Symp. on Discharges & Electrical Insulation in Vacuum (ISDEIV), Moscow-St. Petersburg 1994, Ed. G.A. Mesyats. SPIE Proc. 2259, SPIE, Washington 1994, 170-177.

187. *Ryter, F., M. Alexander, J.C. Fuchs, O. Gruber, A. Kallenbach, M. Kaufmann, W. Köppendörfer, V. Mertens, W. Schneider, A. Stäbler, O. Vollmer, H. Zohm, ASDEX-Upgrade-Team, ICRH-Team* and *NI-Team:* Condition of the L-H and H-L Transitions and Operating Regimes in ASDEX Upgrade. In: Proc. 21st EPS Conf. Control. Fusion and Plasma Phys., Montpellier 1994, Eds. E. Joffrin, P. Platz, P.E. Stott. ECA 18B. Europ. Phys. Soc., Geneva 1994, 330-333.

188. *Ryter, F., K. Büchl, J.C. Fuchs, O. Gehre, O. Gruber, A. Herrmann, A. Kallenbach, M. Kaufmann, W. Köppendörfer, K.-F. Mast, V. Mertens, R. Neu, S. de Pena Hempel, K.-H. Steuer, H. Zohm, ASDEX-Upgrade-Team, NI-Team* and *ICRH-Team:* H-Mode Results in ASDEX Upgrade. Plasma Phys. Control. Fusion **36**, A99-A104 (1994).

189. *Ryter, F., K. Büchl, J.C. Fuchs, A. Herrmann,* et al.*:* H-Mode Results in ASDEX Upgrade. Plasma Phys. Control. Fusion **36**, A99-A104 (1994).

190. *Ryter, F.* and *ITER-H-Mode-Database-Working-Group:* The H-Mode Operational Window as Determined from the ITER H-Mode Database. In: Proc. 21st EPS Conf. Control. Fusion and Plasma Phys., Montpellier 1994, Eds. E. Joffrin, P. Platz, P.E. Stott. ECA 18B. Europ. Phys. Soc., Geneva 1994, 334-337.

191. *Sanchez*, J., B. Branas*, E. de la Luna*, H.-J. Hartfuß, M. Hirsch, T. Geist,* et al.*:* Advanced Techniques for Microwave Reflectometry. Plasma Phys. Rep. **20**, 1-6 (1994).

192. *Sandl, P.* and *E. Bertel:* Surface States, Local Bonding, and Surface Reconstruction: Na on Cu(110). Surf. Sci. **302**, L325-L330 (1994).

193. *Sardei, F., P. Grigull, G. Herre, J. Kisslinger* and *M. Richter-Glötzl:* Parametrization of Open Magnetic Structures for Modelling Plasma Transport in the Boundary of W7-AS. Contrib. Plasma Phys. **34**, 113-119 (1994).

194. *Sattler, S., H.-J. Hartfuß* and *WVII-AS-Team:* Electron Temperature Fluctuations in the Core of the W7-AS Stellarator. In: Proc. 21st EPS Conf. Control. Fusion and Plasma Phys., Montpellier 1994, Eds. E. Joffrin, P. Platz, P.E. Stott. ECA 18B. Europ. Phys. Soc., Geneva 1994, 1220-1223.

195. *Sattler, S., H.-J. Hartfuß* and *WVII-AS-Team:* Experimental Evidence for Electron Temperature Fluctuations in the Core Plasma of the W7-AS Stellarator. Phys. Rev. Lett. **72**, 653-656 (1994).

196. *Schimmel*, Th., B. Winzer*, R. Kemnitzer, J. Küppers,* et al. *:* Layer-by-Layer Growth and Decomposition of an Organic Crystal Observed in Real Time by Atomic Force Microscopy. Adv. Mater. **6**, 307-311 (1994).

197. *Schlüter, M.:* On an Inconsistency in the Toroidal Standard Model of Drift-Wave Theory. Plasma Phys. Control. Fusion **36**, 1241-1244 (1994).

198. *Schneider, R., D. Reiter*, K. Lackner, J. Neuhauser, D. Coster, H.-S. Bosch, H. Kastelewicz,* et al.: B2-Eirene Scrape-off-Layer Calculations. In: Proc. Joint Varenna-Lausanne Int. Workshop on Theory of Fusion Plasmas, Varenna 1994, Eds. E. Sindoni, F. Troyon, J. Vaclavik. Editrice Compositori, Bologna 1994, 273-286.

199. *Schweinzer, J.:* Atomare Daten für Lithiumstrahlspektroskopie. In: Proc. 15. Arbeitstagung Energiereiche Atomare Stöße, Riezlern 1994, Eds. B. Fricke, et al. GSI, Darmstadt 1994, 82-84.

200. *Schweinzer, J., D. Wutte** and *H.P. Winter*:* A Study of Electron Capture and Excitation Processes in Collisions of Multiply Charged Ions with Lithium Atoms. J. Phys., B (London). At. Mol. Opt. Phys. **27**, 137-153 (1994).

201. *Schwenn, U.:* The Computational Stellarator. In: Proc. 6th Joint EPS-APS Int. Conf. on Physics Computing, Lugano 1994, Eds. R. Gruber, M. Tomassini. Europ. Phys. Soc., Geneva 1994, 471-480.

202. *Schwenn, U., T. Hayashi*, P. Merkel* and *J. Nührenberg:* W7-X Vacuum and Finite-β Magnetic Field Structure Resolved with the HINT 3D Equilibrium Code. In: Proc. 21st EPS Conf. Control. Fusion and Plasma Phys., Montpellier 1994, Eds. E. Joffrin, P. Platz, P.E. Stott. ECA 18B. Europ. Phys. Soc., Geneva 1994, 364-367.

203. *Scott, B.D.:* Electromagnetic Effects on Electron Fluid Drift Turbulence. In: Proc. 21st EPS Conf. Control. Fusion and Plasma Phys., Montpellier 1994, Eds. E. Joffrin, P. Platz, P.E. Stott. ECA 18B. Europ. Phys. Soc., Geneva 1994, 560-563.

204. *Sergeev*, V.Yu., S.M. Egorov*, B.V. Kuteev*, P.T. Lang, K. Büchl, M. Kaufmann, R.S. Lang, L.L. Lengyel, V. Mertens, ASDEX-Upgrade-Team,* et al.: Plasma Diagnostics at ASDEX- Upgrade by Means of Carbon Pellet Injection. In: Proc. 21st EPS Conf. Control. Fusion and Plasma Phys., Montpellier 1994, Eds. E. Joffrin, P. Platz, P.E. Stott. ECA 18B. Europ. Phys. Soc., Geneva 1994, 1364-1367.

205. *Silva*, A., M.E. Manso*, P. Varela*, M. Albrecht, A. Kallenbach, H. Zohm, ASDEX-Upgrade-Team,* et al.: Density Profile Measurements from Ultra Fast Broadband Reflectometry on ASDEX Upgrade. In: Proc. 21st EPS Conf. Control. Fusion and Plasma Phys., Montpellier 1994, Eds. E. Joffrin, P. Platz, P.E. Stott. ECA 18B. Europ. Phys. Soc., Geneva 1994, 1188-1191.

206. *Söldner*, F.X., F. Leuterer, R. Bartiromo*, R. Büchse, O. Gehre, M. Kornherr, K. McCormick, H. Murmann, G. Pereverzev,* et al.: Profile Control with Lower Hybrid Waves on ASDEX. Nucl. Fusion **34**, 985-1016 (1994).

207. *Spies, G.O* and *J. Li:* Relaxed Plasmas in External Magnetic Fields. Phys. Plasmas **1**, 2901-2907 (1994).

208. *Stäbler, A., J. Sielanko*, S. Götz** and *E. Speth:* Computer Simulation of the Reionization Effects for the ASDEX Upgrade Neutral Beam Injector. Fusion Technol. **26**, 145-152 (1994).

209. *Steuer, K.-H.:* Kernfusion - Forschung für die Energie der Zukunft. In: Zukunft Aktuell: Energie - eine Lebensfrage der Menschheit. Ev. Presseverband für Bayern, München 1994, 97-111.

210. *Stober, J., B. Eisenhut*, G. Rangelov* and *Th. Fauster:* Initial Stages of the Thermal Nitridation of the Si(100) Surface with NH_3 and NO. A Surface Sensitive Study of Si 2p Core-Level Shifts. Surf. Sci. **321**, 111-126 (1994).

211. *Strüber*, U., A. Kastner** and *J. Küppers:* Growth and Properties of Thin Ag Films on Pt(00) Surfaces. Thin Solid Films **250**, 101-110 (1994).

212. *Strumberger, E.:* Divertor Studies for Optimized Helias Configurations. In: Proc. 21st EPS Conf. Control. Fusion and Plasma Phys., Montpellier 1994, Eds. E. Joffrin, P. Platz, P.E. Stott. ECA 18B. Europ. Phys. Soc., Geneva 1994, 702-705.

213. *Strumberger, E.:* Field Line Mapping and Edge Modeling for Helias Configurations. Contrib. Plasma Phys. **34**, 120-126 (1994).

214. *Stühler*, J., M. Hirsch, G. Schaack**, et al.: Raman Spectroscopy of the Paramagnetic Spin Flip in $Cd_{1-x}Mn_xTe$, the Role of Band-Gap Excitons as Intermediate States, and Optically Detected Electron-Nuclear Double Resonance. Phys. Rev., B **49**, 7345-7356 (1994)

215. *Taglauer, E.:* Probing Surfaces with Ions. Surf. Sci. **299-300**, 64-76 (1994).

216. *Taglauer, E.* and *Z. Bangwei*:* Post-Bombardment Surface Segregation and Preferential Sputtering of Two-Phase AgNi Alloys. J. Vac. Sci. Technol. **12**, 167-170 (1992).

217. *Tanzi*, C.P.* and *H.J. de Blank:* New Method to Analyse Internal Disruptions with Five-Camera Soft X-Ray Tomography on RTP. In: Proc. 21st EPS Conf. Control. Fusion and Plasma Phys., Montpellier 1994, Eds. E. Joffrin, P. Platz, P.E. Stott. ECA 18B. Europ. Phys. Soc., Geneva 1994, 226-229.

218. *Tasso, H.:* Linear and Nonlinear Stability in Resistive Magnetohydrodynamics. Ann. Phys. (N.Y.) **234,** 211-224 (1994).

219. *Tasso, H.:* On Drift Wave Spectra in 1D and 2D. Nuovo Cim., B **109**, 207-209 (1994).

220. *Tasso, H.:* Two Stability Problems Related to Resistive Magnetohydrodynamics. Phys. Plasmas **1**, 3132-3134 (1994).

221. *Teubel, A.* and *F.-P. Penningsfeld:* Influence of Radial Electric Fields on the Heating Efficiency of Neutral Beam Injection in the W7-AS Stellarator. Plasma Phys. Control. Fusion **36**, 143-152 (1994).

222. *Throumoulopoulos*, G.* and *D. Pfirsch:* Negative Energy Perturbations in Circular Cylindrical Equilibria within the Framework of Maxwell-Drift Kinetic Theory. In: Proc. 21st EPS Conf. Control. Fusion and Plasma Phys., Montpellier 1994, Eds. E. Joffrin, P. Platz, P.E. Stott. ECA 18B. Europ. Phys. Soc., Geneva 1994, 1390-1393.

223. *Throumoulopoulos*, G.N.* and *D. Pfirsch:* Negative-Energy Modes in a Magnetically Confined Plasma in the Framework of Maxwell-Drift Kinetic Theory. Phys. Rev., E **49**, 3290-3309 (1994).

224. *Vollmer, O., P.J. McCarthy*, A. Stäbler, F. Ryter, J.-H. Feist, O. Gruber, A. Herrmann, A. Kallenbach, O. Kardaun, V. Mertens, E. Speth, H. Zohm, ASDEX-Upgrade-Team,* et al.: Neutral Beam Heating in ASDEX Upgrade. In: Proc. 21st EPS Conf. Control. Fusion and Plasma Phys., Montpellier 1994, Eds. E. Joffrin, P. Platz, P.E. Stott. ECA 18B. Europ. Phys. Soc., Geneva 1994, 936-939.

225. *Vollmer, O., A. Stäbler, J.-H. Feist, K. Freudenberger, B. Heinemann, H. Lohnert, S. Obermayer, R. Riedl, W. Schärich, E. Speth* and *K. Wittenbecher:* Commissioning and First Operation of the ASDEX Upgrade Neutral Beam System. In: Proc. 15th IEEE/NPSS Symp. Fusion Eng., Hyannis 1993. IEEE, Piscataway 1994, 451-454.

226. *Wagner, F.:* New Subjects in the H-Mode. Plasma Phys. Control. Fusion **36**, A319-A328 (1994).

227. *Wagner, F., J. Baldzuhn, R. Brakel, R. Burhenn, V. Erckmann, P. Grigull, H.-J. Hartfuß, G. Herre, M. Hirsch, J.V. Hofmann, R. Jänicke, A. Rudyj, U. Stroth, A. Weller, WVII-AS-Team,* et al.: H-Mode of W7-AS Stellarator. Plasma Phys. Control. Fusion **36**, A61-A74 (1994).

228. *Wedler, H., F. Wesner, W. Becker* and *R. Fritsch:* Vacuum Insulated Antenna Feeding Lines for ICRH at ASDEX Upgrade. Fusion Eng. Des. **24**, 75-81 (1994).

229. *Weller, A., D.A. Spong*, M. Hirsch, R. Jänicke, M. Kick, C. Konrad, F.-P. Penningsfeld, S. Sattler, WVII-AS-Team* and *NBI-Group:* Energetic Particle Destabilized Global Alfvén Eigenmodes in the Stellarator W7-AS. In: Proc. 21st EPS Conf. Control. Fusion and Plasma Phys., Montpellier 1994, Eds. E. Joffrin, P. Platz, P.E. Stott. ECA 18B. Europ. Phys. Soc., Geneva 1994, 408-411.

230. *Weller, A., D.A. Spong*, R. Jänicke, A. Lazaros, F.-P. Penningsfeld, S. Sattler, WVII-AS-Team and NBI-Group:* Neutral Beam Driven Global Alfvén Eigenmodes in the W7-AS Stellarator. Phys. Rev. Lett. **72**, 1220-1223 (1994).

231. *Wolle*, B., Y. Feng, S. Koch*,* et al.: Measurement of Neutron Emission Profiles and Neutron Spectra by Means of Nuclear Emulsions. In: Proc. 21st EPS Conf. Control. Fusion and Plasma Phys., Montpellier 1994, Eds. E. Joffrin, P. Platz, P.E. Stott. ECA 18B. Europ. Phys. Soc., Geneva 1994, 282-285.

232. *Woloch*, F., G. Kamelander** and *O. Gruber:* Scaling of the Rebut-Lallia-Watkins Transport Model for ASDEX Discharges. In: Proc. Joint Varenna-Lausanne Int. Workshop on Theory of Fusion Plasmas, Varenna 1994, Eds. E. Sindoni, F. Troyon, J. Vaclavik. Editrice Compositori, Bologna 1994, 345-350.

233. *Zeiler, A.:* On the Stability of Axisymmetric Modes in Straight Tokamaks. Phys. Plasmas **1**, 3378-3382 (1994).

234. *Zheng L.-J.* and *S.-T. Tsai*:* Mercier Criterion in Tokamaks with Anisotropic Energetic Particle Component. Phys. Plasmas **1**, 636-642 (1994).

235. *Zhukova*, Yu.N., E.S. Mashkova*, V.A. Molchanov*, W. Eckstein,* et al.: Angular Dependence of Sputtering Yield for Relief Surface of Polycrystalline Copper. Poverkhn. Fiz. Khim. Mekh. **8-9**, 107-115 (1994).

236. *Zohm, H.:* The H-Mode: Current Understanding and Extrapolability. In: Proc. Workshop on Tokamak Concept Improvement, Varenna 1994, Eds. S. Bernabei, N. Sauthoff, E. Sindoni. Editrice Compositori, Bologna 1994, 149-162.

237. *Zohm, H., ASDEX-Upgrade-Team, NI-Group* and *ICRH-Group:* Dynamic Behaviour of the L-H Transition. Phys. Rev. Lett. **72**, 222-225 (1994).

238. *Zohm, H., K. Büchl, H.J. de Blank, A. Kallenbach, M. Kaufmann, F. Ryter, W. Suttrop, ASDEX-Upgrade-Team, ICRH-Group* and *NBI-Group:* Investigation of the Dynamics of the L-H Transition in ASDEX Upgrade. In: Proc. 21st EPS Conf. Control. Fusion and Plasma Phys., Montpellier 1994, Eds. E. Joffrin, P. Platz, P.E. Stott. ECA 18B. Europ. Phys. Soc., Geneva 1994, 850-853.

239. *Zohm, H., F. Ryter, A. Herrmann, M. Kaufmann, J. Neuhauser, N. Salmon, ASDEX-Upgrade-Team, ICRH-Group* and *NBI-Group:* Dynamic Behaviour of the H-Mode in ASDEX Upgrade. Plasma Phys. Control. Fusion **36**, A129-A134 (1994).

Diploma Theses

240. *Cramer, J.:* Die unbesetzte Bandstruktur von Ethylen auf Ni(110): Eine Studie mittels inverser Photoemission. Univ. München 1994.

241. *Häse, M.:* Elektron-Zyklotron-Emissionsspektroskopie am Stellarator Wendelstein 7-AS mit einem Michelson-Interferometer. Techn. Univ. München 1994.

242. *Hertle, R.:* Untersuchungen von transienten mechanischen Störungen in intern gekühlten Supraleiterkabeln. Techn. Univ. München 1994.

243. *Krumrey, J.:* Untersuchung zur spektroskopischen Bestimmung der Energieverteilung der Elektronen in einem ECR-Beschichtungsplasma. Techn. Univ. München 1994.

244. *Lange, K.:* Nutzung des optogalvanischen Effektes zur Wellenlängeneichung eines Farbstofflasers. Ingenieurhochschule Mittweida 1994.

245. *Reinmuth, J.:* Die Elektronen-Energieverteilung in Niederdruckplasmen. Techn. Univ. München 1994.

246. *Schömann, S.:* Ionenstreumessungen zur Sauerstoffadsorption an gestuften Kupfer-Oberflächen und zur Segregation bei Gold-Kupfer-Legierungseinkristallen. Univ. München 1994.

247. *Steltenpohl, A.:* Wachstum und Struktur ultradünner Goldfilme auf Ruthenium. Techn. Univ. München 1994.

Doctoral Theses

248. *Biener, J.:* Spektroskopische Untersuchungen von Reaktionen thermischer Wasserstoffatome an Oberflächen dünner C:H Filme. Univ. Bayreuth 1994.

249. *Bremer, U.:* Direkte und inverse Kaskadenprozesse in getriebener zweidimensionaler MHD-Turbulenz. Techn. Univ. München 1994.

250. *Detzel, Th.:* Epitaxy und Magnetismus dünner Schichten. Univ. Bayreuth 1994.

251. *Endler, M.:* Experimentelle Untersuchung und Modellierung elektrostatischer Fluktuationen in den Abschälschichten des Tokamak ASDEX und des Stellarators Wendelstein 7-AS. Techn. Univ. München 1994.

252. *Friedl, A.:* Aufbau eines in-situ IR-Spektralellipsometers zur Charakterisierung plasmadeponierter C:H-Schichten. Tech. Univ. München 1994.

253. *Linsmeier, Ch.:* Oberflächenanalytische Untersuchungen von getragenen Rhodium-Modellkatalysatoren. Univ. München 1994.

254. *Mayer, M.:* Reflexion von niederenergetischem Deuterium an Graphitoberflächen. Techn. Univ. München 1994.

255. *Passek, F.:* Untersuchungen zur Spinabhängigkeit der elektronischen Struktur von Eisen- und Nickel-Systemen mit reduzierter Dimension. Univ. Bayreuth 1994.

256. *Ramos Lopez, G.A.:* Strahlenschäden, Einfang, Desorption bei der Implantation von Helium und Deuterium in Graphit, Diamant und Siliziumkarbid. Univ. Bayreuth 1994.

257. *Sandl, P.:* Adsorbatinduzierte Veränderung von Oberflächenzuständen und Rekonstruktion an Metalloberflächen. Univ. Bayreuth 1994.

258. *Schenk, A.:* Struktur und chemische Erosion dünner C:H und C(B):H Filme. Univ. Bayreuth 1994.

259. *Schwörer, R.:* Einfluß von Bor auf die chemische Zerstäubung von Graphit mit Wasserstoffionen. Univ. Bayreuth 1994.

260. *Simmet, E.:* Ionenenergietransport in elektronengeheizten Entladungen am Tokamak ASDEX. Techn. Univ. München 1994.

261. *Suyter, A.:* Stabilität von Tokamaks bei endlichem Aspektverhältnis. Univ. München 1994

Patents

262. *Braun, F.:* "Breitbandige, ein- und ausschaltbare Koaxialleitungswiderstandsanordnung für hohe Leistungen". Deutschland 43 01 583, Patenterteilung: 28.7.1994.

263. *Fukarek, W.:* "Schnelles spektroskopisches Ellipsometer". Deutschland P 43 43 490.8, Auslandsanmeldung: 20.12.1994, PCT/EP 94/04235, PCT/USA.

264. *Haas, G.:* "Heißkathoden-Ionisationsmanometer II". USA-Patent 5,300,890, Patenterteilung: 5.4.1994.

265. *Haas, G.:* "Heißkathoden-Ionisationsmanometer II". Ausscheidung aus US-Patentanmeldung Ser. No. 07/866,869, USA-Patent 5,373,240, Patenterteilung: 13.12.1994.

266. *Koch, A.:* "Verfahren und Vorrichtung zur Temperaturmessung". Deutschland G 92 18 626.2., Gebrauchsmustereintragung. 1994.

267. *Koch, A., M. Langlotz, S. Marlier:* "Duales Mikrowelleninterferometer". Deutschland 43 00 949, Patenterteilung: 26.5.1994.

268. *Koch, A., O. Toedter:* "Vorrichtung und Verfahren zum Messen einer winkelabhängigen Größe". Deutschland P 44 27 724.5, Patentanmeldung 1994.

269. *Koch, A., K. Wiesemann:* "Vorrichtung und Verfahren zur Bestimmung von lokalen Eigenschaften eines teilweise ionisierten gasförmigen Mediums und von Schichtdicken." Deutschland P 44 00 689.6, Patentanmeldung 1994.

270. *Kraus, W.:* "Zur Anordnung in einem Vakuumgefäß geeignete selbsttragende isolierte Elektrodenanordnung, insb. Antennenspule für einen Hochfrequenz-Plasmagenerator". Deutschland 42 41 927, Patenterteilung: 22.9.1994.

271. *Liebl, H., B. Senftinger:* "Elektronenmikroskop". Deutschland Patent-Nr. 39 04 032, Freigabe: 11.1.1994, Großbritannien Patent-Nr. 2,230,643, Freigabe: 11.1.1994, Frankreich Anmeldenr. 9001551, Freigabe: 11.1.1994, USA-Patent Nr. 4,978,855, Freigabe: 7.3.1994.

272. *Mukherjee, S.B.:* "Wärmeschutzschild". USA-Patent 5,012,860, Freigabe: 7.9.1994.

273. *Richter, H.:* "Modulares Koppelnetz". Deutsches Gebrauchsmuster Nr. G 8900 757, Freigabe: 22.11.1994.

274. *Spensberger, W.:* "Hohlleiter für Mikrowellen". USA-Patent 4,646,040, Freigabe: 30.5.1994.

275. *Weichselgartner, H.:* "Abziehbare Beizfolie". Europapatent (DE, BE, FR, GB, IT, NL, AT, SE, CH) Nr. 0185393, Freigabe: 12.4.1994

Lectures

276. *Albrecht, M., A. Silva*, P. Varela*,* et al.*:* Einsatz von Mikrowellenreflektometrie als Randschichtdiagnostik an ASDEX Upgrade. Verhandl. DPG (VI) **29**, 280, P8.41 (1994).

277. *Asmussen, K., W. Engelhardt, A. Field, R. Radtke* and *ASDEX-Upgrade-Team:* Untersuchungen zum Verhalten schwerer Verunreinigungen in heißen Plasmen. Verhandl. DPG (VI) **29**, 316, P15.5 (1994).

278. *Behrisch, R.:* Die Plasma-Wand-Wechselwirkung bei den Versuchen zur kontrollierten thermonuklearen Fusion. Physik-Kolloquium, Univ. Leipzig 1994.

279. *Behrisch, R.:* Die Plasma-Wand-Wechselwirkung bei den Versuchen zur kontrollierten thermonuklearen Fusion. Forschungszentrum Rossendorf 1994.

280. *Behrisch, R.:* Erosion of Plasmafacing Materials. Int. Conf. on Effects of Irradiation on Materials in Fusion Reactors, St. Petersburg 1994.

281. *Behrisch, R.:* Plasma Surface Interaction in Controlled Thermonuclear Fusion. 20 Years of Progress in Fusion Materials Research, Ispra 1994.

282. *Behrisch, R.:* The Problem of Plasma Material Interaction in Controlled Thermonuclear Fusion Research. Univ. Kobe 1994.

283. *Behrisch, R., W. Bauer* and *R. Causey:* Plasmafacing Materials. 11th Int. Conf. on Plasma Surface Interactions in Control. Fusion Devices, Mito 1994.

284. *Behrisch, R., A.P. Martinelli, P. Grigull, D. Hildebrandt, W. Schneider,* et al.*:* Surface Layer Compositon of the JET Vessel Walls. 11th Int. Conf. on Plasma Surface Interactions in Control. Fusion Devices, Mito 1994.

285. *Bergmann, A.:* Hysteresis of HF Langmuir Probe Characteristics at Sweep Frequencies Well Below Ion Cylotron Frequency. Workshop on Electric Probes in Magnetized Plasmas, Berlin 1994.

286. *Bergmann, A.:* Two-Dimensional Particle Simulation of Langmuir Probe Sheaths with Oblique Magnetic Field. Workshop on Electric Probes in Magnetized Plasmas, Berlin 1994.

287. *Bertel, E.:* Adsorbatplatz-Bestimmung mit Hilfe von Oberflächenzustands-Spektroskopie. Seminar, Techn. Univ. München 1994.

288. *Bertel, E.:* Bestimmung von Adsorbatplätzen durch Spektroskopie von Oberflächenzuständen. Post-Deadline-Beitrag, DPG Frühjahrstagung, Münster 1994.

289. *Bertel, E.:* Der Einfluß von Oberflächenzuständen auf die Dynamik von Metalloberflächen. Seminar, Techn. Univ. Wien 1994.

290. *Bertel, E.:* Oberflächenzustände an Metallen. Seminar, Univ. München 1994.

291. *Bertel, E.:* Oberflächenzustände und die Physik und Chemie metallischer Oberflächen. Oberseminar, Univ. Düsseldorf 1994.

292. *Bertel, E.:* One- and Two-Dimensional Surface States on Metals. ECOSS 14, Leipzig 1994.

293. *Bertel, E.:* Surface Physics and Negative Ions. CE Cadarache, Cadarache 1994.

294. *Bertel, E.:* Surface States and Chemical Reactivity of Metals, Surface and Interface States on Metallic Systems. 134. WE-Heraeus-Seminar, Bad Honnef 1994.

295. *Bessenrodt-Weberpals, M.:* Diagnostik der Dynamik in Tokamakplasmen. Seminar für Atomphysik, Univ. Gießen 1994.

296. *Bessenrodt-Weberpals, M.:* Experimental Results in Tokamak Physics. IPP Summer Univ. for Plasma Physics, Garching 1994.

297. *Bessenrodt-Weberpals, M.:* Hochtemperatur-Plasmaphysik. Univ. Düsseldorf, WS 1994/95.

298. *Bessenrodt-Weberpals, M.:* Lasermeßtechniken in der Plasmaphysik. Univ. Düsseldorf, SS 1994.

299. *Bessenrodt-Weberpals, M.:* Lochkameras und parallele Datenverarbeitung zur Analyse schneller MHD-Phänomene. Informatik Workshop, Schloß Ringberg, Tegernsee 1994.

300. *Bessenrodt-Weberpals, M.:* Plasma-Material-Bearbeitung (Plasma Aided Manufacturing). Univ. Düsseldorf, WS 1993/94.

301. *Bessenrodt-Weberpals, M.:* Plasmadynamik und Instabilitäten in Tokamakentladungen. Phys. Kolloqium, Univ. Bochum 1994.

302. *Bessenrodt-Weberpals, M.:* Vom Sonnenfeuer zum Fusionsofen: von den Sternen auf die Erde, von der Theorie zum Experiment, von Göttingen nach Garching. 2 Schulvorträge, MPG Hauptversammlung, Göttingen 1994.

303. *Bessenrodt-Weberpals, M.:* Wechselwirkungen von heißem und kaltem Plasma in Tokamakentladungen. Phys. Kolloqium, Univ. Augsburg 1994.

304. *Bessenrodt-Weberpals, M., J.C. Fuchs, M. Kornherr, M. Schittenhelm, M. Zilker, H. Zohm* and *ASDEX-Upgrade-Team:* Aufnahmen schneller MHD-Ereignisse durch Lochkameras. Verhandl. DPG (VI) **29**, 241, P1.2 (1994).

305. *Bielmeier*, B., W. Schatz*, K.F. Renk*, K.-F. Mast* and *P.T. Lang:* Ein breitbandiges Bolometer-Detektorarray. Verhandl. DPG (VI) **29**, 729, Q9P.13 (1994).

306. *Biener, J., A. Schenk, C. Lutterloh, A. Horn* and *J. Küppers:* Ein detailliertes Modell der Wasserstoffreaktion auf Kohlenstoffilmen. Inst. für Plasmaphysik, KFA, Jülich 1994.

307. *Biener, J., A. Schenk, B. Winter, C. Lutterloh, A. Horn* and *J. Küppers:* Elementary Steps of the Interaction of C:H Film Surfaces with Thermal H/D Atoms. EVC-4, Uppsala 1994.

308. *Biener, J., A. Schenk, B. Winter, C. Lutterloh* and *J. Küppers:* A Surface Science Study on Elementary Steps in Low-Pressure Diamond Synthesis. ICNDST-4, Kobe 1994.

309. *Biener, J., A. Schenk, B. Winter, C. Lutterloh, U.A. Schubert* and *J. Küppers:* H/D Austausch an C:H-Filmen mit thermischen H (D) Atomen: Eine Eley-Rideal Reaktion. Verhandl. DPG (VI) **29**, 1456, O30.11 (1994).

310. *Biskamp, D.:* Collisionless Reconnection and the Behaviour of the Safety Factor in the Sawtooth Collapse. Seminar Talk, Courant Inst., New York 1994.

311. *Biskamp, D.:* Der Sägezahnabbruch: Ein Paradigma für magnetische Rekonnexion. Kolloquiumsvortrag, IPF, Stuttgart 1994.

312. *Biskamp, D.:* Dynamics of the Sawtooth Collapse in Tokamak Plasmas. 15th Int. Conf. on Plasma Phys. and Control. Nucl. Fusion Res., Seville 1994.

313. *Biskamp, D.:* Seven Lectures on Magnetic Reconnection. EADN Plasma Astrophysics School, S. Miniato 1994.

314. *Biskamp, D.:* Theory of the Sawtooth Collapse. Seminar Talk, PPPL, Princeton 1994.

315. *Bohmeyer, W., H. Behrendt, G. Fußmann, H. Grote, M. Kammeyer, P. Kornejew, E. Pasch* and *R. Radtke:* Planned Experimental Investigations in the PSI-1 Plasma Generator. Techn. Meeting and Workshop on ITER Divertor Physics and Design, Garching 1994.

316. *Bohmeyer, W., G. Fußmann* and *P. Kornejew:* Proposal for ITER Spectroscopy Diagnostics. ITER-Workshop, Moscow 1994.

317. *Bohmeyer, W., H. Grote, A. Herrmann, M. Kammeyer, P. Kornejew, E. Pasch, H.-D. Reiner, H. Behrendt, L. Dietrich* and *H. Greuner:* Parameterstudien am Plasmagenerator PSI-1. Verhandl. DPG (VI) **29**, 309, P13.46 (1994).

318. *Bosch, H.-S.:* Plasmaphysik und Fusionsforschung I. Univ. Augsburg, WS 1993/94.

319. *Bosch, H.-S.:* Plasmaphysik und Fusionsforschung II. Univ. Augsburg, SS 1994.

320. *Bosch, H.-S., J. Neuhauser, R. Schneider, A. Field, A. Herrmann, W. Junker, ASDEX-Upgrade-Team,* et al.: 2D Modelling of the ASDEX Upgrade Scrape-off Layer and Divertor Plasma. 11th Int. Conf. on Plasma Surface Interactions in Control. Fusion Devices , Mito 1994.

321. *Bosch, H.-S., R. Schneider, D. Coster, J. Neuhauser, A. Herrmann, A. Carlson, M. Weinlich, G. Lieder, A. Field,* et al.: 2D-Modelling of the ASDEX-Upgrade Srape-off Layer and Divertor Plasma. 11th Int. Conf. on Plasma Surface Interactions in Control. Fusion Devices, Mito 1994.

322. *Bosch, H.-S., R. Schneider, J. Neuhauser, A. Herrmann, ASDEX-Upgrade-Team,* et al.: Divertor- und Randschichtmodellierung an ASDEX Upgrade. Verhandl. DPG (VI) **29**, 296, P13.4 (1994).

323. *Brakel, R.:* Physics Contributions from IPP Garching to the Fusion Program. 5th Panhellenic Symp. on Nucl. Phys., Patras 1994

324. *Brakel, R., J. Baldzuhn, R. Burhenn, V. Erckmann, P. Grigull, H. Hacker, G. Kühner, H. Maaßberg, H. Ringler, F. Sardei, E. Unger* and *A. Weller:* Radial Transport of Bulk Particles and Impurities in the Core Plasma of Stellarators. 2nd Europ. Fusion Physics Workshop, Brussels 1994.

325. *Brosig, C.* and *M. Zilker:* Ein Transputer Multiprozessor System für Plasma Diagnostiken mit großen Datenmengen. 6. Parallelrechner-Anwender-Treffen TAT '94, Aachen 1994.

326. *Camargo, S.J.:* Electromagnetic Effects in Collisional Drift-Wave Turbulence. Workshop on Turbulent Transport in Tokamaks Plasmas, Garching 1994.

327. *Camargo, S.J.:* Resistive Drift-Wave Turbulence. Univ. Sao Paulo 1994.

328. *Carlson, A.:* Langmuir Probe Measurements and Theory on ASDEX Upgrade. Plasma Fusion Center, MIT, Cambridge 1994.

329. *Carlson, A.:* The Plasma-Wall Transition in an Oblique Magnetic Field. Workshop on Electric Probes in Magnetized Plasmas, Berlin 1994.

330. *Detzel, Th.:* Correlation of Growth, Structure and Magnetism in Ultrathin Transition Metal Films on Cu(001). Inst. de Physique et Chimie des Materiaux, Strasbourg 1994.

331. *Detzel, Th.:* Structure and Magnetism of Ultrathin Fe Films on Cu(001): A Multitechnique Study. 17th Int. Seminar on Surface Physics, Kudowa 1994.

332. *Detzel, Th.:* Structure and Magnetism of Ultrathin Metal Films. Centre d'Etudes de Chimie Metallurgique, Vitry-sur-Seine 1994.

333. *Detzel, Th.:* Structure and Magnetism of Ultrathin Metal Films. Univ. Neuchâtel 1994.

334. *Detzel, Th.:* Structure and Magnetism of Ultrathin Metal Films. Univ. Geneva 1994.

335. *Detzel, Th.:* Struktur und Magnetismus dünner Filme. Seminar über Photoemission, Univ. München 1994.

336. *Detzel, Th.:* Ultradünne Eisen-Filme auf Cu(001): Zusammenhang zwischen geometrischer und magnetischer Struktur. 134. WE-Heraeus-Seminar, Bad Honnef 1994.

337. *Detzel Th., M. Vonbank, K. Ertl, M. Donath* and *V. Dose:* Spin-Polarized Appearance-Potential Spectroscopy: A Powerful Tool to Study Surface and Thin-Film Magnetism. Int. Workshop on Auger Spectroscopy and Electronic Structure (IWASES III), Univ. Liverpool 1994.

338. *Donath, M.:* Earthquakes: Origins, Results and Benefits. 1994 Physics Seminar Series, Univ. of Western Australia, Perth 1994.

339. *Donath, M.:* Magnetic Coupling in Thin-Film Structures. Materials and Magnetics Group Seminar, Univ. of Western Australia, Perth 1994.

340. *Donath, M.:* Magnetic Surface States. 134. WE-Heraeus-Seminar, Bad Honnef 1994.

341. *Donath, M.:* Magnetismus an Oberflächen: Spinabhängige Elektronische Struktur. Verhandl. DPG (VI) **29**, 381, PV8 (1994).

342. *Donath, M.:* Magnetismus von Oberflächen. Seminar über laufende Forschungsarbeiten, Univ. Regensburg 1994.

343. *Donath, M.:* Spin-Dependent Electronic Structure at Magnetic Surfaces. Seminar, Centre of Atomic, Molecular and Surface Physics, Univ. of Western Australia, Perth 1994.

344. *Donath, M.:* Spinabhängige elektronische Struktur magnetischer Systeme mit reduzierter Dimension. Phys. Kolloquium, Univ. Regensburg 1994.

345. *Donath, M.:* Spinabhängige elektronische Struktur magnetischer Systeme mit reduzierter Dimension. Seminar, Fritz-Haber-Inst., Berlin 1994.

346. *Donath, M., F. Passek* and *V. Dose:* Spin-Dependent Electronic Structure at Magnetic Surfaces: Studies with Spin-Resolved Inverse Photoemission. 6th Asia Pacific Physics Conf. and 11th Australian Inst. of Physics Congress, Griffith Univ. Brisbane 1994.

347. *Dose, V.:* Inverse Photoemission. Forschungszentrum Rossendorf 1994.

348. *Dose, V.:* Inverse Photoemission. Humboldt-Univ. Berlin 1994.

349. *Dose, V.:* Maximum Entropy and Bayes' Theorem. Humboldt-Univ. Berlin 1994.

350. *Dose, V.:* Spin Resolved Soft X-Ray Appearance Potential Spectroscopy. Int. School of Solid State Physics: "Core Level Spectroscopies for Magnetic Phenomena" Theory and Experiment. E. Majorana Centre for Scientific Culture, Erice 1994.

351. *Drake, J.F.:* Magnetic Reconnection: in Kinetic Treatment. Chapman Conf. on the Physics of the Magnetopause, San Diego 1994.

352. *Drake, J.F.:* The L-H Transition: A Transition from Resistive Ballooning to Toroidal Drift Wave Transport. 15th Int. Conf. on Plasma Phys. and Control. Nucl. Fusion Res., Seville 1994.

353. *Drake, J.F.:* The Structure of Thin Current Layers: Implications for Magnetic Reconnection. Univ. Bochum 1994.

354. *Drake, J.F.:* Tokamak Edge Turbulence and the L-H Transition. Culham Lab. and JET, Culham 1994.

355. *Drake, J.F.:* Tokamak Edge Turbulence and the L-H Transition. Ecole Polytechnique, Palaiseau 1994.

356. *Drake, J.F.:* Tokamak Edge Turbulence and the L-H Transition. Forschungszentrum, Jülich 1994.

357. *Drake, J.F.:* Tokamak Edge Turbulence and the L-H Transition. Workshop on Transport in Fusion Plasmas, Göteborg 1994.

358. *Drake, J.F.:* Two Fluid Theory of Magnetic Reconnection. 2nd SNS Workshop on Magnetic Reconnection Processes, Pisa 1994.

359. *Drake, J.F, P.N. Guzdar*, A. Novakovski*, C.S. Liu*, A. Zeiler* and *D. Biskamp:* The L-H-Trigger: a Transition Resistive Ballooning to Toroidal Drift Wave Transport. 15th Int. Conf. on Plasma Phys. and Control. Nucl. Fusion Res., Seville 1994.

360. *Düchs, D.:* A Survey of Transport in Tokamak Plasmas. Univ. of Techn., Helsinki 1994.

361. *Düchs, D.:* Anomalous Transport for Large Ion Gyro-Radii. APS-Div. of Plasma Physics, Minneapolis 1994.

362. *Düchs, D.:* Behandlung von Stößen in der Theorie heißer Plasmen. Ruhr-Univ. Bochum, WS 1994/95.

363. *Düchs, D.:* Bemerkungen zum Transport in Tokamaks; Status und Entwicklungen. Plasmakolloquium, IPF, Stuttgart 1994.

364. *Düchs, D.:* Plasmainstabilitäten. Ruhr-Univ. Bochum, SS 1994.

365. *Düchs, D.:* Quantitative Modelling of Tokamak Plasmas with Computer Codes. Univ. of Techn., Helsinki 1994.

366. *Düchs, D.:* Transporteigenschaften magnetisierter Fusionsplasmen. Ruhr-Univ. Bochum, WS 1993/94.

367. *Eckstein, W.:* Backscattering of Low Energy Hydrogen from Carbon. Univ. of Mercantile Marine, Kobe 1994.

368. *Eckstein, W.:* Bombardment of Metals with Carbon Ions. Sandia Nat. Labs., Livermore 1994.

369. *Eckstein, W.:* Formation of Carbon Films Due to Paricle Bombardment. Nat. Res. Inst., Osaka 1994.

370. *Eckstein, W.:* Ionenbeschuß von Oberflächen. Univ. Bayreuth 1994.

371. *Eckstein, W.:* Plasma Wall Interaction and Sputtering. Univ. of Science, Okayama 1994.

372. *Eckstein, W.:* Reflection of Low Energy Hydrogen from Carbon. Tritium Workshop, Univ. Nagoya 1994.

373. *Eckstein, W.:* Sputtering of Metals with Carbon and Hydrogen. Lawrence Livermore Nat. Lab., Livermore 1994.

374. *Eckstein, W.:* Threshold Energy for Sputtering at Oblique Incidence. Univ. of Osaka Prefecture, Sakai 1994.

375. *Eckstein, W.:* Threshold Energy for Sputtering. RIKEN, Tokio 1994.

376. *Eckstein, W.:* Threshold Sputtering at Oblique Angles of Incidence. Univ. Nagoya 1994.

377. *Egorov*, S.M., K. Büchl, P. Cierpka, P.T. Lang, R.S. Lang, V. Mertens, G. Weber,* et al.: The New Diagnostic Pellet Injector for ASDEX Upgrade. Verhandl. DPG (VI) **29**, 296, P13.2 (1994).

378. *Endler, M., L. Giannone, K. McCormick, H. Niedermeyer, A. Rudyj, G. Theimer, ASDEX-Team, WVII-AS-Team,* et al.: Turbulent Fluctuations in the Scrape-off Layer of the ASDEX Tokamak and the W7-AS Stellarator. 11th Int. Conf. on Plasma Surface Interactions in Control. Fusion Devices, Mito 1994.

379. *Endler, M., L. Giannone, H. Niedermeyer, A. Rudyj* and *G. Theimer:* Fluktuationen in der Abschälschicht von Fusionsexperimenten – von der Beobachtung zur Kontrolle? SFB Kolloquium, Düsseldorf 1994.

380. *Endler, M., L. Giannone, H. Niedermeyer, A. Rudyj* and *G. Theimer:* Fluktuationen in der Abschälschicht des Tokamak ASDEX. Kolloquium, Inst. f¸r Plasmaphysik, KFA, Jülich 1994.

381. *Endler, M., H. Niedermeyer, L. Giannone, A. Rudyj* and *G. Theimer:* Fluctuations in the Scrape-off Layer of ASDEX and Wendelstein 7-AS. Inst. für Plasmaphysik, tschech. Akad. der Wissenschaften, Prag 1994.

382. *Engelhard, M., W. Jacob, W. Möller* and *A. Koch:* Absolute Dichtebestimmung von CH-Radikalen in einem Methan-ECR-Plasma. 6. Bundesdt. Fachtagung Plasmatechnologie, Wuppertal 1994.

383. *Erckmann, V.:* ECRH and ECCD with 70 and 140 GHz at the W7-AS Stellarator. 2nd Int. Workshop on Strong Microwaves in Plasmas, Nizhnij Novgorod 1994.

384. *Erckmann, V.:* Perturbative and Stationary ECRH and ECCD Experiments with 70 and 140 GHz at the W7-AS Stellarator. 15th Int. Conf. on Plasma Physics and Control. Nucl. Fusion Res., Seville 1994.

385. *Erckmann, V.:* Recent Results on Electron Cyclotron Heating and Current Drive at the W7-AS Stellarator. Inst. of Appl. Phys., Nizhnji Novgorod 1994.

386. *Erckmann, V.:* Status of the W7-X Stellarator. Inst. of Nuclear Fusion of Kurchatov Centre, Moscow 1994.

387. *Erckmann, V., U. Gasparino, H.-J. Hartfuß, H. Laqua, H. Maaßberg, H. Ringler, M. Romé, U. Stroth, WVII-AS-Team,* et al.: Perturbative and Stationary ECRH and ECCD Experiments with 70 and 140 GHz at the W7-AS Stellarator. 15th Int. Conf. Plasma Phys. and Control. Nucl. Fusion Res., Seville 1994

388. *Ertl, K.:* Spinaufgelöste Appearance-Potential-Spektroskopie an Eisen und Nickel. Kolloqium zur Festkörpertheorie, Humboldt-Univ. Berlin 1994.

389. *Estrada*, T, J. Sanchez*, H.-J. Hartfuß, M. Hirsch* and *T. Geist:* Density Fluctuations During the L-H Transition in W7-AS. IAEA Tech. Comm. Meeting on Microwave Reflectometry, Princeton 1994.

390. *Fauster, Th.:* Growth and Morphology of Ultrathin Metal Films Studied by the High-Resolution Spectroscopy of Image States through Two-Photon Photoemission. 134. WE-Heraeus-Seminar, Bad Honnef 1994.

391. *Fauster, Th.:* Lokalisation von Elektronen auf Metalloberflächen. Gesamthochschule Kassel 1994.

392. *Fauster, Th.:* Lokalisation von Elektronen auf Metalloberflächen. Univ. München 1994.

393. *Fauster, Th.:* Photoelektronenspektroskopie an epitaktischen Kobaltsilizidfilmen. Univ. Erlangen 1994.

394. *Fauster, Th.:* Photoelektronenspektroskopie an Oberflächen. Univ. Bonn 1994.

395. *Fauster, Th.:* Quantisierung elektronischer Zustände auf Metalloberflächen. Verhandl. DPG (VI) **29**, 1330, OII (1994).

396. *Feist, J.-H.:* Status of the RF-Source Development. Joint Development Comm. Meeting, Jülich 1994.

397. *Feist, J.-H., B. Heinemann, J. Sielanko** and *E. Speth:* Magnetic Shielding Considerations for the ITER Neutral Beam Injectors. 18th SOFT, Karlsruhe 1994.

398. *Feng, Y., F. Sardei* and *WVII-AS-Team:* Neutralgastransport in der Randschicht von W7-AS für Limiter- und Separatrix-dominierte Konfigurationen. Verhandl. DPG (VI) **29**, 296, P13.3 (1994).

399. *Fiedler, S., K. McCormick, P. Platzer** and *J. Schweinzer:* Bestimmung der Elektronendichte in der Plasmarandschicht von ASDEX Upgrade und W7-AS mittels Lithiumstrahl-aktivierter Spektroskopie. Verhandl. DPG (VI) **29**, 315, P15.3 (1994).

400. *Field, A., G. Fußmann, C. Garcia-Rosales, S. Hirsch, D. Naujoks, R. Neu, R. Radtke, U. Wenzel, ASDEX-Upgrade-Team,* et al.: Studies of Divertor Target Plate Erosion in the ASDEX Upgrade Tokamak. 11th Int. Conf. on Plasma Surface Interactions in Control. Fusion Devices, Mito 1994.

401. *Fischer, R.* and *Th. Fauster:* Alloying of Thin Ag and Au Films on Pd(111) Studied by High-Resolution Photoelectron Spectroscopy of Surface States. 125. WE-Heraeus-Seminar, Rathen 1994.

402. *Fuchs, J.C* and *R. Reichle*:* Twodimensional Reconstruction of the Radiation Power Density During Neon Puff Experiments at JET. JET ED2-Meeting, Culham 1994.

403. *Fußmann, G., W. Engelhardt, D. Naujoks, K. Asmussen, S. Deschka, A. Field, J.C. Fuchs, C. Garcia-Rosales, S. Hirsch, P. Ignacz, R. Neu, R. Radtke, J. Roth, U. Wenzel,* et al.: High-Z Elements as Target Materials in Fusion Devices. 15th Int. Conf. on Plasma Phys. and Control. Nucl. Fusion Res., Seville 1994.

404. *Garcia-Rosales, C.:* Wasserstoff in den Gefäßwänden von Fusionsexperimenten. Univ. Magdeburg 1994.

405. *Gentle*, K.W., G. Cima*, H. Gasquet*, O. Gehre* and *ASDEX-Upgrade-Team:* Characteristics of Equilibrium and Perturbed Transport Coefficients in Tokamaks. Workshop on Transport in Fusion Plasmas, Göteborg 1994.

406. *Greuner, H., W. Bitter, F. Kerl, J. Kisslinger* and *H. Renner:* Structure of Divertor for the Optimized Stellarator W7-X. 18th SOFT, Karlsruhe 1994.

407. *Grieger, G.:* Fusion Power Coordinating Committee - Report to CERT. IEA-OECD CERT 94, Paris 1994.

408. *Grieger, G.:* ITER und Wendelstein 7-X auf dem Weg zum Forschungsreaktor. Wissenschaftl. Tage, Greifswald 1994.

409. *Grieger, G.:* Status of Wendelstein 7-X. Nat. Inst. for Fusion Science, Nagoya 1994.

410. *Grieger, G.:* Teilinstitut des Max-Planck-Institutes für Plasmaphysik in Greifswald. Bürgerschaft Greifswald 1994.

411. *Grieger, G.:* Wendelstein 7-X - Phase II - Application for Preferential Support. First Presentation to the Ad Hoc Group for Examination of Wendelstein 7-X Phase II Proposal, Garching 1994.

412. *Grigull, P.:* Divertor Diagnostics for Wendelstein. AdHoc-Group, Schloß Ringberg, Tegernsee 1994.

413. *Grote, H., M. Behnke, H. Behrendt, W. Bohmeyer, L. Dietrich, M. Kammeyer, M. Laux* and *H.-D. Reiner:* Langmuir Probes at the PSI-1 Plasma Generator. 1st Workshop on Electrical Probes in Magnetized Plasmas, Berlin 1994.

414. *Grützmacher*, G., M.I. de la Rosa*, J. Seidel*, G. Fußmann, W. Bohmeyer,* et al.: ITER Plasma Measurement Requirements. ITER-Workshop, Moscow 1994.

415. *Häse, M.* and *H.-J. Hartfuß:* Fourierspektroskopie am Stellarator Wendelstein 7-AS. Verhandl. DPG (VI) **29**, 279, P8.39 (1994).

416. *Hartfuß, H.-J.:* Microwave Experiment for Plasma Diagnostic. Seminar Angewandte Physik, Univ. Regensburg 1994.

417. *Hartfuß, H.-J.:* Störexperiment zur Bestimmung der Elektronenwärmeleitung eines Fusionsplasmas. Phys. Kolloquium, Univ. Regensburg 1994.

418. *Hartfuß, H.-J., S. Sattler* and *WVII-AS-Team:* On Method and Results of Interior Temperature Fluctuation Measurements in the Stellarator W7-AS. 7th Transport Task Force Workshop, Dallas 1994.

419. *Hayashi*, T., T. Sato*, N. Nakajima*, P. Merkel, J. Nührenberg, U. Schwenn, et al.:* Behavior of Magnetic Islands in 3D MHD Equilibria of Helical Devices. 15th Int. Conf. Plasma Phys. and Control. Nucl. Fusion Res., Seville 1994.

420. *Heinrich, O., R. Schneider, H. Verbeek, J. Neuhauser, U. Stroth, H.-U. Fahrbach, W. Herrmann, ASDEX-Team, WVII-AS-Team,* et al.: CX-Ionentemperaturen in der Plasmarandschicht von ASDEX und W7-AS. Verhandl. DPG (VI) **29**, 315, P15.2 (1994).

421. *Herre, G., P. Grigull, F. Sardei* and *WVII-AS-Team:* Transportuntersuchung in der Plasmarandschicht am W7-AS. Verhandl. DPG (VI) **29**, 315, P15.1 (1994).

422. *Herrmann, A.:* Proposal for ITER Thermography Diagnostics. ITER-Workshop, Moscow 1994.

423. *Herrmann, A.* and *ASDEX-Upgrade-Team:* Charakterisierung der Leistungsdeposition auf die Prallplatten des Tokamaks ASDEX-Upgrade durch thermografische Messungen. Verhandl. DPG (VI) **29**, 286, P9.6 (1994).

424. *Herrmann, A., M. Laux, H. Kastelewicz, J. Neuhauser, H.-S. Bosch, A. Carlson, R. Schneider* and *M. Weinlich:* Energy Transport to the Divertor Plates of ASDEX-Upgrade During ELMs Edge Mode Phases. 11th Int. Conf. on Plasma Surface Interactions in Control. Fusion Devices, Mito 1994.

425. *Hildebrandt, D., P. Pech, W. Schneider* and *H. Wolff:* Auger-SIMS-Apparatur zur Materialanalyse in der Fusionsforschung. 4. Arbeitstagung des Dt. SIMS-Forums, Humboldt-Univ. Berlin 1994.

426. *Hildebrandt, D., P. Pech, H.-D. Reiner, W. Schneider, H. Wolff, R. Brakel, P. Grigull, J.V. Hofmann, J. Roth* and *WVII-AS-Team:* Studies on Plasma-Surface Interaction in the W7-AS Stellarator. 11th Int. Conf. on Plasma Surface Interactions in Control. Fusion Devices, Mito 1994.

427. *Hirsch, M., T. Geist, H.-J. Hartfuß,* et al.: Heterodyne Reflectometer for Phase and Time Delay Measurements in W7-AS. 10th Annual High-Temperature Plasma Diagnostics Meeting of the APS, 1994.

428. *Hofmann, J.V.:* Sichtbare Spektroskopie am Stellarator W7-AS. Kolloquium, IPF, Stuttgart 1994.

429. *Horn, A., J. Biener, A. Schenk, C. Lutterloh* and *J. Küppers:* H/D Exchange Reaction at Graphitic CH Groups by Thermal H(D) Atoms. ECOSS 14, Leipzig 1994.

430. *Hytry, R., W. Möller* and *R. Wilhelm:* Running Discharge for PECVD Inner Coating of Metal Tubes. 4th Int. Conf. on Plasma Surface Engineering, Garmisch-Partenkirchen 1994.

431. *Jaksic, N., J. Simon-Weidner* and *E. Harmeyer:* Mechanical Stresses of the W7-X Coil Set with Reduced Weight. 18th SOFT, Karlsruhe 1994.

432. *Junker, W., V. Mertens, K.-H. Steuer, H. Röhr, K. Büchl, O. Gruber, M. Kaufmann, K. Lackner, M. Laux, J. Neuhauser, R. Schneider, ASDEX-Upgrade-Team,* et al.: MARFE-Untersuchungen an ASDEX Upgrade. Verhandl. DPG (VI) **29**, 265, P6.4 (1994).

433. *Kallenbach, A.:* Das Verunreinigungsproblem im Tokamak-plasma. Phys. Kolloquium, Univ. Hannover 1994.

434. *Kallenbach, A.:* Impurity Puffing and Pumping. 2nd Europ. Fusion Physics Workshop, Brussels 1994.

435. *Kallenbach, A.:* Kohlenstoffchemie und Verunreinigungs-produktion in Fusionsplasmen. Plasmakolloquium, IPF, Univ. Stuttgart 1994.

436. *Kallenbach, A., A. Field, C. Garcia-Rosales* and *W. Poschenrieder:* Kohlenstoffchemie und Verunreinigungsproduktion in Fusionsplasmen. Verhandl. DPG (VI) **29**, 286, P9.5 (1994).

437. *Kallenbach, A., V. Mertens, M. Alexander, K. Behringer, M. Bessenrodt-Weberpals, H.-S. Bosch, K. Büchl, R. Dux, O. Gruber, J.C. Fuchs, G. Haas, A. Herrmann, W. Junker, M. Kaufmann, K. Lackner, K.-F. Mast, G. Neu, J. Neuhauser, S. de Pena Hempel, W. Poschenrieder, F. Ryter, K. Schönmann, A. Stäbler, K.-H. Steuer, W. Suttrop, O. Vollmer, T. Zehetbauer, H. Zohm, NI-Team, ASDEX-Upgrade-Team,* et al.: Radiative Boundary in ASDEX Upgrade Divertor Discharges. 15th Int. Conf. on Plasma Phys. and Control. Nucl. Fusion Res., Seville 1994.

438. *Kardon*, B., J.S. Bakos*, P. Ignacz,* et al.: Laser Accelerated Micro-Pellet (Granules of Materials) Injection into the MT-1M Tokamak Plasma. IAEA Technical Comm. Meeting on Research Using Small Tokamaks, Madrid 1994.

439. *Kass, T., H.-S. Bosch, F. Hoenen** and *ASDEX-Upgrade-Team:* Erste Ergebnisse aus schnellen Neutronenflußmessungen an ASDEX Upgrade. Verhandl. DPG (VI) **29**, 266, P6.7 (1994).

440. *Kaufmann, M.:* ASDEX Upgrade, a Poloidal Divertor Experiment. Kolloqium, Cadarache 1994.

441. *Kaufmann, M.:* ASDEX Upgrade: Future Investigations. ITER Workshop, Garching 1994.

442. *Kaufmann, M.:* ASDEX Upgrade: Programme, Results, Plans. Executive Comm. Meeting, GA, San Diego 1994.

443. *Kaufmann, M.:* ASDEX Upgrade: Programme, Results, Plans. Kolloquium, Frascati 1994.

444. *Kaufmann, M.:* Recent ASDEX Upgrade Results. ITER Kolloquium, Garching 1994.

445. *Kaufmann, M., K. Lackner, V. Mertens, J. Neuhauser, H. Zohm, M. Bessenrodt-Weberpals, K. Büchl, A. Field, J.C. Fuchs, C. Garcia-Rosales, O. Gruber, G. Haas, A. Herrmann, W., Herrmann, S. Hirsch, A. Kallenbach, P.T. Lang, K.-F. Mast, M. Schittenhelm, J. Stober, W. Suttrop, M. Troppmann, M. Weinlich, ASDEX-Upgrade-Team, NI-Team, ICRH-Team,* et al.: Divertor Characteristics During High-Density H-Mode Discharges in ASDEX Upgrade. 15th Int. Conf. on Plasma Phys. and Control. Nucl. Fusion Res., Seville 1994.

446. *Keudell, A. von:* Die Bedeutung der Ionen für das Aufwachsen von C:H-Filmen. Inst. für Laser und Plasmaphysik, Univ. Düsseldorf 1994.

447. *Keudell, A. von:* Welche Mechanismen sind für das Wachstum von wasserstoffhaltigen Kohlenstoffschichten bestimmend? 6. Bundesdt. Fachtagung Plasmatechnologie, Wuppertal 1994.

448. *Keudell, A. von* and *W. Fukarek:* In-situ-Ellipsometrie-Studie über die Oberflächenmechanismen während des Wachstums von Kohlenstoffilmen. Verhandl. DPG (VI) **29**, 904, DS1939 (1994).

449. *Klement, G., J. Engstler, D. Jacobi* and *B. Streibl:* OH Breaker of ASDEX Upgrade: Closing Switch without Ignitrons. 18th SOFT, Karlsruhe 1994.

450. *Konrad, C., H.-J. Hartfuß, E. Holzhauer** and *G. Siller:* Erste Ergebnisse der kohärenten Mikrowellenstreuung am Stellarator Wendelstein 7-AS. Verhandl. DPG (VI) **29**, 241, P1.3 (1994).

451. *Köppendörfer, W., F. Ryter, H. Zohm, M. Alexander, K. Büchl, D. Coster, J.C. Fuchs, O. Gehre, O. Gruber, A. Herrmann, A. Kallenbach, M. Kaufmann, K.-F. Mast, V. Mertens, R. Neu, J.-M. Noterdaeme, W. Suttrop, A. Stäbler, O. Vollmer, ASDEX-Upgrade-Team, NI-Team* and *ICRH-Team:* The H-Mode in ASDEX Upgrade: Physics and Operating Regimes. 15th Int. Conf. on Plasma Phys. and Control. Nucl. Fusion Res., Seville 1994.

452. *Kraus, W., J.-H. Feist, B. Heinemann, E. Speth* and *R. Wilhelm:* A High Power RF Plasma Source for ASDEX Upgrade NBI. 18th SOFT, Karlsruhe 1994.

453. *Krieger, K., W. Eckstein, J.D. Elder*, A. Field, M. Laux, G. Lieder, R. Radtke, J. Roth,* et al.: Modelling of the ASDEX-Upgrade Divertor Plasma with DIVIMP. 11th Int. Conf. on Plasma Surface Interactions in Control. Fusion Devices, Mito 1994.

454. *Kühner, G., J. Baldzuhn, R. Brakel, R. Burhenn, J. Das, A. Elsner, Y. Feng, U. Gasparino, P. Grigull, H. Hacker, O. Heinrich, H.-J. Hartfuß, M. Hirsch, J.V. Hofmann, M. Kick, H. Maaßberg, W. Mandl, W. Ohlendorf, F.-P. Penningsfeld, M. Romé, H. Ringler, F. Sardei, U. Stroth, H. Verbeek, A. Weller, WVII-AS-Team, ECRH-Group* and *NBI-Group:* Transport Investigations in the Wendelstein 7-AS Stellarator. 15th Int. Conf. Plasma Phys. and Control. Nucl. Fusion Res., Seville 1994.

455. *Kühner, G., U. Gasparino* and *H. Ringler:* Nichtmaxwellsche Elektronenenergieverteilungen und Temperaturrelaxationen ECR geheizter Plasmen im W7-AS Stellarator. Verhandl. DPG (VI) **29**, 292, P11.10 (1994).

456. *Küppers, J.:* H Atom Impact Induced Reactions at C:H Film Surfaces and Physisorbed Hydrocarbons. Stanford Univ. 1994.

457. *Küppers, J.:* H Atom Impact Induced Reactions at C:H Film Surfaces and Physisorbed Hydrocarbons. Univ. of California, Riverside 1994.

458. *Küppers, J.:* H Atom Impact Induced Reactions at C:H Film Surfaces and Physisorbed Hydrocarbons. Univ. of California, Santa Barbara 1994.

459. *Küppers, J.:* H Atom Impact Induced Reactions at Hydrogenated Surfaces and Physisorbed Hydrocarbons. Univ. of California, Berkeley 1994.

460. *Küppers, J.:* Model Studies on Chemical Erosion of C Based Materials and B Doping Effects. Sandia Nat. Labs., Livermore 1994.

461. *Küppers, J.:* Thermally and H Atom Impact Induced Reactions at C:H Surfaces. Stanford Univ. 1994.

462. *Küppers, J.:* Wechselwirkung von H Atomen mit C:H Oberflächen und adsorbierten Kohlenwasserstoffen. Phys. Kolloquium, Univ. Kassel 1994.

463. *Kurzan, B., K.-H. Steuer, G. Fußmann, H. Murmann, H. Röhr, H. Salzmann* and *U. Schumacher:* Untersuchung von Runaway-elektronen durch relativistische Thomsonstreuung an ASDEX Upgrade. Verhandl. DPG (VI) **29**, 265, P6.5 (1994).

464. *Labich, S., Ch. Linsmeier, E. Taglauer* and *H. Knözinger*:* Untersuchungen von Rh/TiO_2 Modellkatalysatoren mit AES, ISS und TDS. Verhandl. DPG (VI) **29**, 1389, O14.2 (1994).

465. *Lackner, K., H.-S. Bosch, D. Coster, O. Gruber, G. Haas, A. Herrmann, A. Kallenbach, M. Kaufmann, V. Mertens, J. Neuhauser, F. Ryter, M. Weinlich, H. Zohm, M. Albrecht, M. Alexander, K. Asmussen, M. Ballico, K. Behler, K. Behringer, M. Bessenrodt-Weberpals, M. Brambilla, K. Büchl, A. Carlson, H.J. de Blank, S. de Pena Hempel, S. Deschka, C. Dorn, R. Drube, R. Dux, A. Eberhagen, W. Engelhardt, C. Garcia-Rosales, O. Gehre, J. Gernhardt, W. Herrmann, S. Hirsch, P. Ignacz, B. Jüttner, W. Junker, T. Kass, K. Kiemer, W. Köppendörfer, H. Kollotzek, M. Kornherr, K. Krieger, B. Kurzan, P.T. Lang, R.S. Lang, M. Laux, M. Maraschek, K.-F. Mast, H.-M. Mayer, D. Meisel, R. Merkel, H. Murmann. B. Napiontek, D. Naujoks, G. Neu, R. Neu, J.-M. Noterdaeme, G. Pautasso, W. Poschenrieder, G. Raupp, H. Richter, T. Richter, H. Röhr, J. Roth, N. Salmon, H. Salzmann, W. Sandmann, H.-B. Schilling, M. Schittenhelm, H. Schneider, R. Schneider, W. Schneider, K. Schönmann, G. Schramm, J. Schweinzer, U. Seidel, M. Sokoll, E. Speth, A. Stäbler, K.-H. Steuer, J. Stober, B. Streibl, W. Suttrop, W. Treutterer, M. Troppmann, M. Ulrich, H. Vernickel, O. Vollmer, H. Wedler, U. Wenzel, F. Wesner, R. Wunderlich, D. Zasche, H.-P. Zehrfeld,* et al.: Recent Results from Divertor Operation in ASDEX Upgrade. 15th Int. Conf. on Plasma Phys. and Control. Nucl. Fusion Res., Seville 1994.

466. *Lang, P.T.:* Pellet Fuelling Experiments on ASDEX Upgrade. Statusseminar des russ.-deut. WTZ-Abkommens Pelletinjektion, St. Petersburg 1994.

467. *Lang, P.T.:* Pellet-Injektion als Werkzeug der Fusionsforschung. Fraunhofer-Inst. für Kurzzeitdynamik/Ernst-Mach-Inst., Freiburg 1994.

468. *Lang, P.T., C. Andelfinger, P. Cierpka, R.S. Lang* and *V. Mertens:* A Centrifuge for High-Speed Pellet Injection. 18th SOFT, Karlsruhe 1994.

469. *Lang, P.T., K. Büchl, B.V. Kuteev*, R.S. Lang, V. Mertens, ASDEX-Upgrade-Team,* et al.: Plasmanachfüllung mittels Pelletinjektion an ASDEX Upgrade. Verhandl. DPG (VI) **29**, 295-296, P13.1 (1994).

470. *Lang, P.T., S.M. Egorov*, B.V. Kuteev*, R.S. Lang, L.L. Lengyel, V. Mertens,* et al.: A Compact Gas Gun Injection System for Diagnostic Pellets with Variable Size and First Applications in ASDEX Upgrade. 18th SOFT, Karlsruhe 1994.

471. *Lange, K.* and *W. Möller:* Die Rolle von Ionen und Radikalen bei der plasmagestützten Abscheidung amorpher Kohlenstoffschichten. Verhandl. DPG (VI) **29**, 866, DS5.9 (1994).

472. *Lange, K.* and *W. Möller:* Ratenbestimmende Teilchenflüsse aus Methan-Gleichspannungsentladungen zur Deposition dünner a-C:H-Schichten. 6. Bundesdt. Fachtagung Plasmatechnologie, Wuppertal 1994.

473. *Langhoff, M.* and *B.M.U. Scherzer:* In-situ Messungen von Wasserstoff-Inventar in Graphit unter RF-Plasma-Exposition. Verhandl. DPG (VI) **29**, 249, P4.2 (1994).

474. *Laux, M.* and *K. Günther:* Remarks to the Probe in the Most Simple Environment: the Cylindrical Case. 1st Workshop on Electrical Probes in Magnetized Plasmas, Berlin 1994.

475. *Leuterer, F.* and *M. Münich:* Status of the ASDEX Upgrade ECRH-System. 6th Russian-German Meeting on ECRH and Gyrotron, IAP Nizhny Novgorod; KIAE, Moscow 1994.

476. *Lieder, G.* and *K. Behringer:* Spectroscopic Diagnostic Requirements for the ITER Divertor (Proposal). Progress Meeting on Spectroscopic Systems for ITER, Moscow 1994.

477. *Lieder, G., K. Behringer, A. Field, A. Kallenbach, B. Napiontek, D. Naujoks* and *R. Radtke:* Spektroskopische Untersuchungen zur chemischen Erosion im Divertor von ASDEX Upgrade. Verhandl. DPG (VI) **29**, 249, P4.4 (1994).

478. *Linden, W. von der:* Applications of the Concept of Maximum Entropy. Kolloquium, Univ. Lausanne 1994.

479. *Linden, W. von der:* Bayesian Consideration of the Tomography Problem. 14th Int. Maximum Entropy Workshop, Cambridge 1994.

480. *Linden, W. von der:* Coulomb Interaction in Electron-Phonon-Driven Superconductors. Int. Conf. Cross-Over Phenomena in Solid State Physics, Turin 1994.

481. *Linden, W. von der:* Das Holstein-Hubbard Model. Theorie-Seminar, Univ. Karlsruhe 1994.

482. *Linden, W. von der:* Die Maximum-Entropie Methode: Theorie und Anwendungen. Kolloquium, Freie Univ. Berlin 1994.

483. *Linden, W. von der:* Einsatz der Maximum-Entropie-Methode bei der Datenanalyse. Verhandl. DPG (VI) **29**, 1334, OXIII (1994).

484. *Linden, W. von der:* Numerische Simulationen zur Physik kondensierter Materie. Kolloquium, Univ. Greifswald 1994.

485. *Linden, W. von der:* QMC Simulationen zu aktuellen Fragen in der Festkörperphysik. Kolloquium, Univ. Kassel 1994.

486. *Linden, W. von der:* Verwendung der MaxEnt-Methode in der theoretischen und experimentellen Physik. Kolloquium, Univ. Regensburg 1994.

487. *Linden, W. von der:* Weakly Coupled One- and Two-Dimensional Strongly Correlated Fermion Systems. Int. Conf. on Surface Magnetism and Strong Correlations, Turin 1994.

488. *Linsmeier, Ch.:* Strong Metal-Support Interactions on Rh/TiO_2 Model Catalysts. 2nd German-Australian Workshop on Surface Science, Schloß Ringberg, Tegernsee 1994.

489. *Linsmeier, Ch., E. Taglauer* and *H. Knözinger*:* Characterization of SMSI Effects on Rh/TiO_2 Model Catalysts. Symp. on Surf. Sci., Les Arcs 1994.

490. *Lortz, D.:* Thermodynamik TL IV. Univ. München, SS 1994.

491. *Lutterloh, C., J. Biener, A. Schenk* and *J. Küppers:* Deuteration of Physisorbed Xylene with Thermal D Atoms. ECOSS 14, Leipzig 1994.

492. *Lutterloh, C., A. Schenk, J. Biener, U.A. Schubert, B. Winter* and *J. Küppers:* Wechselwirkung von Wasserstoff- und Edelgasionen mit dünnen C:H Filmen.Verhandl. DPG (VI) **29**, 1363, O11.4 (1994).

493. *Mandl, W.:* Edge Ion Temperature Behaviour at DIII-D. Tore Supra, Cadarache 1994.

494. *McCormick, K.:* Modellierung der Plasmarandschicht von Tokamaks. Seminar, Techn. Univ. Wien 1994.

495. *McCormick, K.:* Scaling of SOL Widths (European Overview - invited). 2nd Europ. Fusion Phys. Workshop, Brussels 1994.

496. *McCormick, K.:* The SOL Power and Density Widths in ASDEX: Theory and Experiment. JET Divertor Task Force Seminar, Abingdon 1994.

497. *Memmel, N.:* Growth and Stability of Ultrathin Iron and Cobalt Films on Copper Surfaces. 2nd German-Australian Workshop on Surface Science, Schloß Ringberg, Tegernsee 1994.

498. *Memmel, N.:* Structural and Magnetic Properties of Ultrathin Iron Films on a Copper Surface. CAMP-Kolloquium, Univ. Aarhus 1994.

499. *Memmel, N.:* Structural and Magnetic Properties of Ultrathin Iron Films on a Copper Surface. Phys. Kolloquium, Univ. Odense 1994.

500. *Merkel, P.:* Coil and Equilibrium Studies for Stellarators. Colloquium Nat. Inst. Fusion Science (NIFS), Nagoya 1994.

501. *Merkel, P., J.L. Johnson*, D.A. Monticello*, et al.:* Stellarator Equilibrium Studies with the PIES Code. 15th Int. Conf. Plasma Phys. and Control. Nucl. Fusion Res., Seville 1994.

502. *Meyer-Spasche, R.:* Chaotische dynamische Systeme: Konzepte, Sätze, Beweise, Beispiele und Anwendungen. Ferienakademie über komplexe Systeme und nichtlineare Dynamik, Tutzing 1994.

503. *Meyer-Spasche, R.:* Dynamische Systeme. Ferienakademie über komplexe Systeme und nichtlineare Dynamik, Tutzing 1994.

504. *Meyer-Spasche, R.:* Gleichgewichte und Stabilität: nichtlineare Fluiddynamik. Techn. Univ. München, SS 1994.

505. *Meyer-Spasche, R.:* Gleichgewichte und Stabilität bei Plasmen. Techn. Univ. München, WS 1994/95.

506. *Meyer-Spasche, R.:* Hilda Geiringer (1893-1973), Frauen in der Mathematik. Oberwolfach 1994.

507. *Meyer-Spasche, R.:* Vom Gleichgewicht zum Chaos: nichtlineare Dynamik. Techn. Univ. München, WS 1993/94.

508. *Milch, I.:* Energie aus dem Sternenfeuer. Kernfusionsforschung. Vortragsreihe: Frauen führen Frauen. Dt. Museum, München 1993.

509. *Möller, W., W. Fukarek, A. von Keudell* and *K. Lange:* Mechanisms of the Deposition of Hydrogenated Carbon Films. Symp. on Dry Process, Tokio 1994.

510. *Napiontek, B., G. Fußmann, G. Lieder* and *R. Radtke:* CX-induzierte Strahlung im Divertor von ASDEX-Upgrade. Verhandl. DPG (VI) **29**, 317, P15.7 (1994).

511. *Naujoks, D.:* Messungen der Erosion und Redeponierung in Fusionsexperimenten. Verhandl. DPG (VI) **29**, 285, P9.3 (1994).

512. *Naujoks, D.:* Plasmainduzierte Erosion und Redeponierung in Fusionsanlagen. Institutskolloquium, KFA, Jülich 1994.

513. *Naujoks, D.* and *R. Behrisch:* Erosion and Redeposition at the Vessel Walls in Fusion Devices. 11th Int. Conf. on Plasma Surface Interactions in Control. Fusion Devices, Mito 1994.

514. *Naujoks, D.* and *W. Eckstein:* Sputtering of Plasma Facing Material by Simultaneous Bombardment with Carbon and Deuterium Ions. 11th Int. Conf. on Plasma Surface Interactions in Control. Fusion Devices, Mito 1994.

515. *Neu, G., C. Aubanel, V. Mertens, G. Raupp, H. Richter, D. Zasche* and *T. Zehetbauer:* An Enhanced Plasma Control for ASDEX Upgrade. 18th SOFT, Karlsruhe 1994.

516. *Neu, R., A. Kallenbach, J.C. Fuchs, K.-F. Mast* and *ASDEX-Upgrade-Team:* Einfluß der C- und O-Konzentration auf das Dichtelimit in ASDEX Upgrade. Verhandl. DPG (VI) **29**, 280, P8.40 (1994).

517. *Noterdaeme, J.-M.:* Comments on the ICRF System for ITER as Presented on the TAC4 Report. 8th Coord. Comm. Meeting on Fast Wave Current Drive and Heating, JET, Culham 1994.

518. *Noterdaeme, J.-M.:* Experience with ELMs with Respect to ICRF in ASDEX Upgrade. JET-ICRF Assessment Comm., JET, Culham 1994.

519. *Noterdaeme, J.-M.:* Overview of Past Experiments and Future Plans for ICRF on W7-AS and Details of the Next Step. W7-X Ad-hoc Group Meeting, Schloß Ringberg, Tegernsee 1994.

520. *Noterdaeme, J.-M.:* Recent Results of ICRF on ASDEX Upgrade. 9th Coord. Comm. Meeting on Fast Wave Current Drive and Heating, Jülich 1994.

521. *Noterdaeme, J.-M.:* Report on the Working Group on Faradayscreen-Less Antenna Operation. 11th Coord. Comm. Meeting on Fast Wave Current Drive and Heating, Cadarache 1994.

522. *Noterdaeme, J.-M.:* Results, Status and Plans for ICRF on ASDEX Upgrade. 8th Boulder Int. Workshop on RF Current Drive and Profile Control for Advanced Tokamaks, Boulder 1994.

523. *Nührenberg, J., W. Lotz, P. Merkel, C. Nührenberg, U. Schwenn* and *E. Strumberger:* Overview on Wendelstein 7-X Theory. 6th Int. Toki Conf. (ITC-6), Toki 1994.

524. *Pamela*, J., J. Feist, M. Fumelli*, B. Heinemann, E. Speth,* et al.*:* Outline Design of a Neutral Beam Injector for ITER EDA. 18th SOFT, Karlsruhe 1994.

525. *Pasch, E., W. Bohmeyer* and *H. Grote:* Thomson-Streuung am Plasmagenerator PSI-1. Verhandl. DPG (VI) **29**, 243, P1.9 (1994).

526. *Passek, F.:* Magnetismus-spinabhängige elektronische Struktur. Seminar, Inst. für Werkstoffkunde, Univ. Erlangen-Nürnberg 1994.

527. *Passek, F.:* Spinabhängigkeiten von elektronischen Zuständen an Fe(110). Seminar, Univ. München 1994.

528. *Passek, F., M. Donath* and *V. Dose:* Thickness Dependence of the Spin-Polarized Electronic Structure of Iron Films on W(110). Europ. Res. Conf. on Fundamental Aspects of Surface Science: Surface and Thin Film Magnetism, Port d' Albert 1994.

529. *Pecher, P., W. Jacob* and *K. Lange:* Massenselektierte Ionenenergieverteilung aus Methan-ECR-Plasmen. 6. Bundesdt. Fachtagung Plasmatechnologie, Wuppertal 1994.

530. *Pereverzev, G.:* First Results of LH Modelling with a Beam Tracing Code. JET, Culham 1994.

531. *Pereverzev, G.:* Influence of Wave Phenomena on LH Wave Propagation and Absorption. Plasma Fusion Center, MIT, Cambridge 1994.

532. *Pereverzev, G.:* New Fast Lower Hybrid Deposition Code for Profile Control Modelling with a Transport Code. JET, Culham 1994

533. *Pereverzev, G.:* Transport Code Modelling of LHC. CCFM, Montreal 1994.

534. *Pfirsch, D.:* Einführung in die Theoret. Plasmaphysik 1 (Mikroskopische Theorie). Techn. Univ. München, SS 1994.

535. *Pfirsch, D.:* Einführung in die Theoret. Plasmaphysik 2 (Makroskopische Theorie). Techn. Univ. München, WS 1994/95.

536. *Pfirsch, D.* and *R.N. Sudan*:* Small Scale Magnetic Flux-Averaged Magnetohydrodynamics. Int. Sherwood Fusion Theory Conf., Dallas 1994.

537. *Pfirsch, D.* and *R.N. Sudan*:* Small Scale Magnetic Flux-Averaged Magnetohydrodynamics. Meeting of the Plasma Phys. Div. of the APS, Minneapolis 1994.

538. *Pinkau, K.:* Fusionsforschung und Vorsorge für die Energieversorgung von morgen. Eröffnung der Fusionsausstellung im Dt. Museum, München 1994.

539. *Pinkau, K.:* Internationalität der Forschung und ihre nationale Organisation. Villa Hügel-Gespräch des Stifterverbandes, Essen 1994.

540. *Pinkau, K.:* The Role of the Associations in the European Fusion Programme. 18th SOFT, Karlsruhe 1994.

541. *Pinkau, K.:* Welche Ziele soll sich die Forschung stellen und welche Wege soll sie beschreiten, um angemessene Freiräume zu sichern? MPG-Symposium: Der schrumpfende Freiraum der Forschung, Schloß Ringberg, Tegernsee 1994.

542. *Pinkau, K.:* Wissensfolgenabschätzung und Risiko. VDE Baden-Württemberg, Stuttgart 1994.

543. *Pitcher*, C.S., H.-S. Bosch, A. Field, A. Herrmann* and *ASDEX-Upgrade-Team:* The Effect of Density on Divertor Conditions in ASDEX-Upgrade. 11th Int. Conf. on Plasma Surface Interactions in Control. Fusion Devices, Mito 1994.

544. *Poschenrieder, W., K. Behringer, H.-S. Bosch, A. Field, A. Kallenbach, M. Kaufmann, J. Küppers, K. Krieger, G. Lieder, J. Neuhauser, D. Naujoks, C. Garcia-Rosales, J. Roth* and *ASDEX-Upgrade-Team:* Molecular Impurities in the ASDEX-Upgrade Plasma Discharges. 11th Int. Conf. on Plasma Surface Interactions in Control. Fusion Devices, Mito 1994.

545. *Rangelov, G., Th. Fauster, U. Strüber** and *J. Küppers:* Stacking of Ag Layers on Pt(111). ECOSS 14, Leipzig 1994.

546. *Rangelov, G., U. Thomann** and *Th. Fauster:* Growth of Ultrathin Si Films on fcc Co(100) Surfaces. ECOSS 14, Leipzig 1994.

547. *Raupp, G., O. Gruber, V. Mertens, G. Neu, H. Richter, B. Streibl, W. Treutterer, D. Zasche, T. Zehetbauer,* et al.: Protection Strategy in the ASDEX Upgrade Control System. 18th SOFT, Karlsruhe 1994.

548. *Reiter, S., P. Roos, P. Sandl, S. Schömann* and *E. Taglauer:* Ion Scattering and STM Studies of Stepped Cu(115) Surfaces. Symp. on Surf. Sci., Les Arcs 1994.

549. *Reiter, S., E. Taglauer* and *I.S.T. Tsong*:* Untersuchung der Cu(115)-Oberfläche mit Rastertunnelmikroskopie. Verhandl. DPG (VI) **29**, 1468, O34.7 (1994).

550. *Richter, H.:* Der Einsatz paralleler Rechentechnik in der Hochenergiephysik am Beispiel des Fusionsexperiments ASDEX-Upgrade. GMD FIRST, Berlin 1994.

551. *Richter, H.:* Neuere Entwicklungen bei den transputerbasierten Parallelrechnern von ASDEX-Upgrade. Lehrstuhl Prof. Färber, Techn. Univ. München 1994.

552. *Richter, H.:* Verbindungsnetzwerke für Parallelrechner - Einführung, Klassifikation und Vergleich. SFB-Kolloquium, Techn. Univ. München 1994.

553. *Roth, J., D. Naujoks* and *K. Krieger:* Erosion and Redeposition in the ASDEX-Upgrade Divertor. 11th Int. Conf. on Plasma Surface Interactions in Control. Fusion Devices, Mito 1994.

554. *Roth, J., D. Naujoks, K. Krieger, A. Field, G. Lieder* and *S. Hirsch:* Experimental Investigations of High-Z Materials in the ASDEX-Upgrade Divertor. 11th Int. Conf. on Plasma Surface Interactions in Control. Fusion Devices, Mito 1994.

555. *Ryter, F.:* First ASDEX Upgrade Contribution to the ITER Threshold Database. ITER Expert Group Meeting, Seville 1994.

556. *Ryter, F.:* ITER H-Mode Threshold Database. ITER Expert Group Meeting, Seville 1994.

557. *Ryter, F.:* Status of the ITER H-Mode Threshold Database. H-Mode-Database-Working-Group Meeting, JET, Culham 1994.

558. *Ryter, F., M. Alexander, J.C. Fuchs, O. Gruber, A. Kallenbach, M. Kaufmann, W. Köppendörfer, V. Mertens, W. Poschenrieder, W. Schneider, A. Stäbler, O. Vollmer, H. Zohm, ASDEX-Upgrade-Team, NI-Team* and *ICRH-Team:* H-Mode Operating Regimes and Confinement in ASDEX Upgrade. Workshop on Transport in Fusion Plasmas, Göteborg 1994.

559. *Ryter, F., O. Gruber, A. Kallenbach, M. Kaufmann, W. Köppendörfer, V. Mertens, A. Stäbler, O. Vollmer, H. Zohm, ASDEX-Upgrade-Team, NI-Team* and *ICRH-Team:* H-Mode Operation in ASDEX Upgrade. H-Mode and Boundary/Divertor Physics Workshop, Culham 1994.

560. *Ryter, F.* and *H. Zohm:* ELMs, and the ITER H-Mode Confinement Database. ITER Expert Group Meeting, Seville 1994.

561. *Sandl, P.:* Qualitative Beschreibung elektronischer Oberflächenzustände von Metalloberflächen: Anwendung am System Na/Cu(110). Univ. München 1994.

562. *Sandl, P.:* Qualitative Beschreibung elektronischer Oberflächenzustände von Metalloberflächen: Anwendung am System Na/Cu(110). Univ. Saarbrücken 1994.

563. *Sandl, P.:* Surface States on Metals and the Interaction with Alkali Metal Adsorbates. 17th Int. Seminar on Surface Physics, Kudowa 1994.

564. *Sardei, F., P. Grigull, Y. Feng, G. Herre, D. Hildebrandt, J. Kisslinger, F. Wagner, H. Wolff* and *WVII-AS-Team:* Boundary Layer Study on the Wendelstein 7-AS Stellarator. 11th Int. Conf. on Plasma Surface Interactions in Control. Fusion Devices, Mito 1994.

565. *Schauer, F., W. Bitter, R. Holzthüm, S. Huber, N. Jaksic, S. Kamm, F. Kerl, H. Münch, J. Simon-Weidner, B. Sombach* and *J. Tretter:* Demonstration Cryostat Sector for Wendelstein 7-X. 18th SOFT, Karlsruhe 1994.

566. *Schenk, A., B. Winter, C. Lutterloh, J. Biener, U.A. Schubert* and *J. Küppers:* Einfluß von Bor auf die Struktur und chemische Erosion von dünnen C/B:H-Filmen. Verhandl. DPG (VI) **29**, 1456, O30.9 (1994).

567. *Schenk, A., B. Winter, C. Lutterloh, J. Biener, U.A. Schubert* and *J. Küppers:* The Origin of Reduced Chemical Erosion of Graphite Based Materials Induced by Boron Doping. 11th Int. Conf. on Plasma Surface Interactions in Control. Fusion Devices, Mito 1994.

568. *Schimmel*, Th., R. Kemnitzer*, J. Küppers,* et al.: Giant Atomic Corrugations on Layered Dichalcogenides Investigated by AFM/LFM. NATO-Workshop Forces in Scanning Probe Methods, Schluchsee 1994.

569. *Schimmel*, Th., R. Kemnitzer*, J. Küppers,* et al.: Nanometer Scale Machining of Covalent Monolayers Investigated by Combined AFM/LFM. NATO-Workshop Forces in Scanning Probe Methods, Schluchsee 1994.

570. *Schimmel*, Th., Th. Koch*, J. Küppers,* et al.: True Atom-by-Atom Resolution Obtained by AFM at Ambient Conditions. Park Europ. User Meeting, Genf 1994.

571. *Schimmel*, Th., J. Küppers* and *M. Lux-Steiner*:* Reibung auf atomarer Skala. Workshop über methodische Entwicklungen und industrielle Anwendungen der Nahfeld-Rastersondentechniken, SXM 1, Münster 1994.

572. *Schönmann, K., W. Engelhardt* and *G. Fußmann:* Ein Bragg-spektrometer zur Verunreinigungsdiagnostik an ASDEX Upgrade. Verh. DPG (VI) **29**, 307, P13.39 (1994).

573. *Schweinzer, J.:* Aktueller Stand der Garchinger Lithiumstrahl-Diagnostiken (Quelle, Optik, Codes). Workshop Lithium-Betaeukriptid-Ionenquellen, KFA, Jülich 1994.

574. *Schweinzer, J.:* Übungen zur Vorlesung PHYSIK III (Atom- und Molekülphysik). Univ. Augsburg, WS 1993/94.

575. *Schweinzer, J.:* Übungen zur Vorlesung PHYSIK IV (Atom-, Kern- und Elementarteilchenphysik). Univ. Augsburg, SS 1994.

576. *Speth, E.:* Progress on the Second Injector for ASDEX Upgrade. Joint Development Comm. Meeting, Cadarache 1994.

577. *Speth, E., J.-H. Feist* and *J. Sielanko*:* Space Charge Effects in the Ion Removal System of the ASDEX Upgrade Injector. 18th SOFT, Karlsruhe 1994.

578. *Spong*, D.A., B.A. Carreras*, C.L. Hedrick*, A. Weller,* et al.: Energetic Particle Destabilization of Shear Alfvén Waves in Stellarators and Tokamaks. 15th Int. Conf. Plasma Phys. and Control. Nucl. Fusion Res., Seville 1994.

579. *Stäbler, A.:* D^0 Injection into ASDEX Upgrade. Joint Development Comm. Meeting, Jülich 1994.

580. *Stäbler, A.:* Progress of NBI into ASDEX Upgrade. Joint Development Comm. Meeting, Cadarache 1994.

581. *Stäbler, A.:* Review on Neutral Beam Injection Achievements. ITER Technical Meeting and Workshop on Heating and Current Drive, Cadarache 1994.

582. *Stäbler, A.:* Survey of Tokamak Results with Neutral Beam Injection. Joint Development Comm. Meeting, Cadarache 1994.

583. *Stäbler, A., O. Vollmer, J.-H. Feist, E. Speth, B. Heinemann, W. Melkus, S. Obermayer, R. Riedl, W. Schärich* and *K. Wittenbecher:* Performance of the First ASDEX Upgrade Neutral Beam Injector. 18th SOFT, Karlsruhe 1994.

584. *Steltenpohl, A.:* Wachstum und Struktur ultradünner Goldfilme auf Ruthenium. Seminar Photoemission, Univ. München 1994.

585. *Steuer, K.-H.:* Energie aus Kernfusion. Europ. Woche der Wissenschaft, Hausenstein Gymnasium, München 1994.

586. *Steuer, K.-H.:* Fusionsreaktoren, schnelle Brüter und Sonnenkraftwerke - Stand und Perspektiven bei der Erschließung neuer Energiequellen. 3 Schulvorträge, MPG Hauptversammlung, Göttingen 1994.

587. *Steuer, K.-H.:* Kernfusion, 'Lüscher-Lectures'. Akad. für Lehrerfortbildung, Dillingen 1994.

588. *Steuer, K.-H.:* Stand der Kernfusionsforschung. VDI, Trier 1994.

589. *Stroth, U.:* ASDEX and W7-AS Contributions to the Profile Database. ITER Confinement Database and Modelling Workshop, Seville 1994.

590. *Stroth, U.:* ASDEX L-Me Confinement and its Contribution to the Database. ITER Confinement Database and Modelling Workshop, Seville 1994.

591. *Stroth, U.:* Durch Vergleich von Stellarator und Tokamak den Transport enträtseln. Verhandl. DPG (VI) **29**, 238, PII (1994).

592. *Stroth, U.:* Recent Transport Experiments in W7-AS. CHS-Seminar, Nat. Inst. Fusion Science, Nagoya 1994.

593. *Stroth, U.:* Recent Transport Experiments in W7-AS. Heliotron E-Seminar, Univ. Kyoto 1994.

594. *Stroth, U.:* Recent Transport Experiments in W7-AS. Poster, 6th Int. Conf. on Plasma Phys. and Control. Nucl. Fusion, Toki 1994.

595. *Stroth, U.:* Recent Transport Experiments on the Stellarator Tokamak Comparison. Local Transport Workshop, Göteborg 1994.

596. *Stroth, U.:* Transient Transport Phenomena in W7-AS Plasmas. Kolloquium, FOM Inst., Rijnhuizen 1994.

597. *Stroth, U.:* Vergleichende Transportstudien in Stellaratoren und Tokamaks. Seminarvortrag, Univ. Heidelberg 1994.

598. *Stroth, U., J. Baldzuhn, R. Brakel, V. Erckmann, L. Giannone, M. Hirsch, H.-J. Hartfuß, M. Kick, G. Kühner, H. Ringler, F. Wagner, ECRH-Group, WVII-AS-Team,* et al.: Recent Transport Experiments in W7-AS. 15th Int. Conf. Plasma Phys. and Contr. Nucl. Fusion Res., Seville 1994.

599. *Stroth, U., B. Branas*, T. Estrada*, L. Giannone, H.-J. Hartfuß, M. Hirsch, M. Kick, G. Kühner, S. Sattler, J. Baldzuhn, R. Brakel, V. Erckmann, R. Jänicke, H. Ringler* and *F. Wagner:* Recent Transport Experiments in W7-AS on the Stellarator-Tokamak Comparison. Meeting on Local Transport, Göteborg 1994.

600. *Taglauer, E.:* Niederenergetische Ionen als Sonden zur Untersuchung von Oberflächen. Hahn-Meitner-Inst., Berlin 1994.

601. *Taglauer, E.:* Particle-Surface Interactions in Fusion Devices. Gordon Res. Conf. on Particle-Solid Interactions, Plymouth 1994.

602. *Taglauer, E.:* Probing Surfaces with Low-

603. *Taglauer, E.:* Segregation bei binären Energy Ions. 7th Int. Conf. of Highly Charged Ions, Wien 1994.Legierungen - Untersuchungen mit Ionenstreuung. Univ. Osnabrück 1994.

604. *Taglauer, E.:* Segregation on Single Crystal Surfaces of Ordered Alloys. 125. WE-Heraeus-Seminar, Rathen 1994.

605. *Taglauer, E.:* Surface Segregation and Preferential Sputtering of Binary Alloys. 2nd German-Australian Workshop on Surface Science, Schloß Ringberg, Tegernsee 1994.

606. *Taglauer, E.:* Untersuchungen des Oberflächenaufbaus von Modell- und Realkatalysatoren mittels Ionenstreuung. Analytica Conf., München 1994.

607. *Tasso, H.:* Energy Methods in Magnetohydrodynamics. Workshop on Energy Methods in Continuum Mechanics, Oviedo 1994.

608. *Theimer, G., M. Endler, L. Giannone* and *H. Niedermeyer:* Modellierung elektrostatischer Fluktuationen in der Abschälschicht des Tokamaks ASDEX. Verhandl. DPG (VI) **29**, 246, P3.2 (1994)

609. *Thomann*, U., G. Rangelov* and *Th. Fauster:* Angular Distributions of VUV Photoelectrons from Cu Surfaces. ECOSS 14, Leipzig 1994.

610. *Unger, E., H. Hacker, R. Burhenn* and *A. Weller:* Transportuntersuchungen an Niedrig-Z-Verunreinigungen am Stellarator W7-AS. Verhandl. DPG (VI) **29**, 316, P15.4 (1994).

611. *Valásék, P., W. von der Linden* and *V. Dose:* Two-Particle Spectra of Heavy Fermion Systems. 3rd Int. Workshop on Auger Spectroscopy and Electronic Structure, Liverpool 1994.

612. *Verplancke, P.:* Changes of the Langmuir Characteristic at Frequencies up to the Ion Cyclotron Resonance. Fusion Research Center, Univ. Texas, Austin 1994.

613. *Vonbank, M., Th. Detzel, M. Donath* and *V. Dose:* Strukturelle und magnetische Eigenschaften von Fe/Cu(001) untersucht mit spinpolarisierter APS. Dreikönigstreffen: "Grenzflächenmagnetismus und Zwischenschicht-Austauschkopplungseffekte", Bad Honnef 1994.

614. *Wagner, F.:* Aktuelle physikalische Fragestellungen der Fusionsforschung. Univ. Saarbrücken 1994.

615. *Wagner, F.:* Boundary Layer and H-Mode Studies in W7-AS. 15th IAEA Int. Conf. Plasma Phys. and Control. Nucl. Fusion Res., Seville 1994.

616. *Wagner, F.:* Energie aus Kernfusion - Wo steht die Forschung? Wissenschaft für Jedermann, Dt. Museum, München 1994.

617. *Wagner, F.:* Physik des "Advanced Stellarators". Kolloquium, Univ. Düsseldorf 1994.

618. *Wagner, F.:* Some Physics Aspects of Advanced Stellarators. Stockholm 1994.

619. *Wagner, F.:* Status of Fusion Research - Fusion Research at the IPP. 5th Europ. Conf. on Science and Techn., Freising/Garching 1994.

620. *Wagner, F.:* Stellarator und Tokamakforschung im IPP. Wissenschaftl. Tage in der Ernst-Moritz-Arndt Univ., Greifswald 1994.

621. *Wagner, F.:* Studies in Transports of Toroidal Plasmas. 6th Int. Toki Conf. on Plasma Phys. and Control. Nucl. Fusion, Toki 1994.

622. *Wagner, F.:* The H-Mode of Wendelstein 7-AS. Workshop on Transport in Fusion Plasmas, Göteborg 1994.

623. *Wagner, F., J. Baldzuhn, V. Erckmann, Y. Feng, P. Grigull, J.V. Hofmann, C. Konrad, F. Sardei, R. Brakel, S. Fiedler, L. Giannone, H.-J. Hartfuß, G. Herre, D. Hildebrandt, M. Hirsch, R. Jänicke, W. Ohlendorf, P. Pech, E. Würsching* and *WVII-AS-Team:* Boundary Layer and H-Mode Studies in W7-AS. 15th Int. Conf. Plasma Phys. and Control. Nucl. Fusion Res., Seville 1994.

624. *Wagner, F.* and *R. Brakel:* Physics Contribution from IPP Garching to the Fusion Programme. 5th Panhellic Symp. of Nucl. Phys., Patras 1994.

625. *Wallauer, W., Th. Fauster* and *W. Steinmann*:* Growth of Ag, Au, and Co on Cu(111) Studied by High-Resolution Spectroscopy of Image States. Discussion Meeting Structural and Functional Modification of Metal Surfaces by Thin Film Epitaxy, Ascona 1994.

626. *Wallauer, W., Th. Fauster* and *W. Steinmann*:* Growth of Ag, Au and Co on Cu(111) Studied by High-Resolution Spectroscopy of Image States. ECOSS 14, Leipzig 1994.

627. *Wallauer, W., Th. Fauster* and *W. Steinmann*:* Zweiphotonen-Photoemission an dünnen Ag-Schichten auf Cu(111). Verhandl. DPG (VI) **29**, 1335, O1.1 (1994).

628. *Weinlich, M., A. Carlson, A. Bergmann* and *M. Laux:* Flush Mounted Probes at Grazing Incidence of a Strong Magnetic Field. 1st Workshop on Electrical Probes in Magnetized Plasmas, Berlin 1994.

629. *Weinlich, M., A. Carlson* and *M. Laux:* Langmuirsonden bei streifendem Einfall eines starken Magnetfeldes. Verhandl. DPG (VI) **29**, 214, P1.1 (1994).

630. *Weller, A., J. Geiger, D.A. Spong*, H.-J. Hartfuß, M. Hirsch, R. Jänicke, C. Konrad, F.-P. Penningsfeld, S. Sattler, WVII-AS-Team* and *NBI-Group:* Pressure and Energetic Particle Destabilized Global MHD Modes in the Stellarator W7-AS. 15th Int. Conf. Plasma Phys. and Control. Nucl. Fusion Res., Seville 1994.

631. *Wesner, F., F. Braun, F. Hofmeister, C. Hoffmann, J.-M. Noterdaeme* and *T. Sperger:* ICRF Heating and H-Mode: Operational Experience and Results at ASDEX Upgrade. 18th SOFT, Karlsruhe 1994.

632. *Wieczorek, A.* and *J. Sapper:* Simulation Studies of the Power Supply and the Protection System for the Wendelstein 7-X Stellarator. 18th SOFT, Karlsruhe 1994.

633. *Wilhelm, R.:* Plasmaverfahren - Grundlagen, Anwendungsgebiete und Grenzen. Wirtschaftliche Beschichtung von Kunststoffen, Dt. Forschungsges. für Oberflächenbehandlung e.V., Münster 1994.

634. *Winter, B., C. Lutterloh, A. Schenk, J. Biener, U.A. Schubert* and *J. Küppers:* Wechselwirkung von atomarem thermischen Wasserstoff mit C:H Filmen: Eley-Rideal-induzierte C-Erosion. Verhandl. DPG (VI) **29**, 1456, O30.10 (1994).

635. *Wobig, H.:* Plasma Confinement in Toroidal Systems. 36ème Cours de perfectionnement de l'Assoc. Vaudoise des chercheurs en physique, Grimentz 1994.

636. *Wobig, H.:* The Helias Reactor. 36ème Cours de perfectionnement de l'Assoc. Vaudoise des chercheurs en physique, Grimentz 1994.

637. *Wolff, H., P. Pech, D. Hildebrandt* and *H.-D. Reiner:* Langmuir Probe Measurements in the W7-AS Stellarator. 1st Workshop on Electrical Probes in Magnetized Plasmas, Berlin 1994.

638. *Zeiler, A.:* 3-D Collisional Drift-Wave Turbulence. Workshop on Turbulent Transport in Tokamak Plasmas, Garching 1994.

639. *Zeiler, A.:* Tokamak-Randschicht-Turbulenz. Schloß Ringberg, Tegernsee 1994.

640. *Zohm, H.:* Dynamic Behaviour of the L-H Transition. 7th Transport Task Force Meeting, Dallas 1994.

641. *Zohm, H.:* Dynamisches Verhalten von Zuständen verbesserten Plasmaeinschlusses. Univ. Augsburg 1994.

642. *Zohm, H.:* ELM Effects on Transport under Varying Edge Conditions. Joint JET/Culham/IPP Workshop on H-Mode and Edge Physics, Culham 1994.

643. *Zohm, H.:* Kern- und Elementarteilchenphysik (Physik IV). Univ. Augsburg, SS 1994.

644. *Zohm, H.:* Plasmaphysik und Fusionsforschung. Univ. Augsburg, WS 1994/95.

645. *Zohm, H.:* Seminar zur MHD heißer Plasmen. Seminar, Univ. Augsburg, WS 1994/95.

646. *Zohm, H.:* Statistical Analysis of Disruptions in ASDEX. ASDEX-DoE Meeting, Boston 1994.

647. *Zohm, H.:* The Effect of the H-Mode Transport Barrier and ELMs on Transport. 2nd Europ. Fusion Physics Workshop, Brussels 1994.

648. *Zotova*, S., W. Jacob, A. von Keudell* and *N. Zotov*:* Secondary Electron Emission Coefficient Investigation of C:H Thin Films Deposited by ECR-Plasma Deposition and SiC Thin Films Deposited by DC Magnetron Sputtering. 14th General Conf. on Condensed Matter Div., Madrid 1994.

Internal Laboratory Reports

IPP 1/278 ASDEX Upgrade Results Publications and Conference Contributions Period 10/93 to 7/94.

IPP 1/280 *Lang, P.T., P. Cierpka, S.M. Egorov*, T. Kass, H. Vetter, G. Weber*, et al.: Pellet Injector for Diagnostics Purposes.

IPP 1/281 *Bosch, H.-S., D. Coster, S. Deschka, W. Engelhardt, C. Garcia-Rosales, O. Gruber, M. Kaufmann, W. Köppendörfer, K. Lackner, J. Neuhauser, H. Salzmann, H. Schneider, R. Schneider, S. Schweizer, B. Streibl* and *M. Troppmann:* Extension of the ASDEX Upgrade Programme: Divertor II and Tungsten Target Plate Experiment.

IPP 1/282 *Gentle*, K.W., O. Gehre* and *P.T. Lang:* Particle Transport in ASDEX Upgrade.

IPP 2/322 *Wobig, H.:* Stationary Equilibrium and Rotation of a Collisional Plasma in a Torus.

IPP 2/323 *Junker, J.:* The FORMEX Plasma Formulary.

IPP 2/324 *Hertle, R.:* Untersuchungen von transienten mechanischen Störungen in intern gekühlten Supraleiterkabeln.

IPP 2/325 *Schauer, F.:* Optimierung eines verstärkten Supraleiterkabels für W7-X.

IPP 2/326 *Karulin, N.* and *H. Wobig:* Resonant Interaction of Energetic Ions with Alfvén-like Perturbations in Stellarators.

IPP 2/327 *Beidler, C.D.* and *W.D. D'Haeseleer:* A General Solution of the Ripple-Averaged Kinetic Equation (GSRAKE).

IPP III/194 *Yamada*, H., J. Geiger, U. Stroth, A. Weller*, et al.: Remarks on Application of VMEC and PROCTR to the W7-AS Experiments.

IPP III/195 *Stroth, U., M. Murakami*, G. Kühner, H. Maaßberg*, et al.: A First Step to a Joint Stellarator Database.

IPP III/196 W7-AS Contributions to 10th Topical Conf. on Radio Frequency Power in Plasmas, Boston 1993; Local Transport Studies on Fusion Plasmas, Varenna 1993; 5th Europ. Theory Conf., El Escorial 1993; 4th Int. Workshop on Plasma Edge Theory in Fusion Devices, Varenna 1993; 5th Int. Toki Conf. on Plasma Phys. and Control. Nuclear Fusion, Phys. and Technology of Plasma Heating and Current Drive, Toki 1993; 4th H-Mode Workshop, IAEA Tech. Comm. Meeting on H-Mode Physics, Naka 1993; IAEA Tech. Comm. Meeting on Radio-Frequency Launchers for Plasma Heating and Current Drive, Naka 1993.

IPP III/197 *Endler, M.:* Experimentelle Untersuchung und Modellierung elektrostatischer Fluktuationen in den Abschälschichten des Tokamak ASDEX und des Stellarators W7-AS.

IPP III/198 *Simmet, E.:* Ionenenergietransport in elektronengeheizten Entladungen am Tokamak ASDEX.

IPP III/199 *Morita*, S.* and *J. Baldzuhn:* Z_{eff} Measurement and Analysis of Reheat-Mode Discharges in W7-AS.

IPP III/200 W7-AS Contributions to 11th Conf. on Plasma Surface Interactions in Control. Fusion Devices, Mito 1994; 21st EPS Conf. on Control. Fusion and Plasma Phys., Montpellier 1994; 15th Int. Conf. on Plasma Phys. and Control. Nucl. Fusion Research, Sevilla 1994.

IPP 4/266 *Teubel, A.:* FAFNER 2: 3-D "Flux Coordinate" Neutral Beam Injection Code Using Monte Carlo Methods.

IPP 4/267 *Friedl, A.:* Aufbau eines in-situ-IR-Spektralellipsometers zur Charakterisierung plasmadeponierter C:H-Schichten = Design of an in-situ Spectroscopic IR Ellipsometer for Characterization of Plasma-Deposited C:H Films.

IPP 4/268 *Teubel, A., J. Guasp** and *M. Liniers*:* Monte Carlo Simulations of Neutral Beam Injection into the TJ-II Helical-Axis Stellarator.

IPP 5/48 *Ludescher*, C., J. Gernhardt, K. Lackner, F. Schneider* and *ASDEX-Team:* A Data Bank of Disruptive Discharges in ASDEX.

IPP 5/55 *Richter, T.:* Betrachtungen über die chemische Erosion von Graphit in Wasserstoffplasmen.

IPP 5/57 *Richter, T.:* Cooling Water Calorimetry Measuring Results from the First Years of ASDEX Upgrade Operation.

IPP 5/58 *Werthmann, H.:* Zur Effizienz der Ionen-Bernstein-Wellen-Heizung von Fusionsplasmen.

IPP 5/59 ASDEX Upgrade Results Publications and Conference Contributions Period 10/93 to 7/94.

IPP 5/60 *Callaghan*, H.P.* and *P.J. McCarthy*:* Sensitivity Study of a Proposed Polarimetry Diagnostic on ASDEX Upgrade.

IPP 6/319 *Tasso, H.:* Two Stability Problems Related to Resistive Magnetohydrodynamics.

IPP 6/320 *Biskamp, D.* and *U. Bremer:* Dynamics and Statistics of Inverse Cascade Processes in 2D Magnetohydrodynamic Turbulence.

IPP 6/321 *Tasso, H.:* Energy Methods in Dissipative Magnetohydrodynamics.

IPP 6/322 *Biskamp, D.* and *A. Zeiler:* Nonlinear Instability Mechanism in 3-D Collisional Driftwave Turbulence.

IPP 6/323 *Salat, A.:* Nonexistence of MHD Equilibria with Poloidally Closed Field Lines in the Case of Violated Axisymmetry.

IPP 6/324 *Salat, A.:* Exact Three-Dimensional MHD Equilibria without Continuous Symmetries.

IPP 8/3 *Kastelewicz, H., R. Schneider, J. Neuhauser, D. Reiter*, B. Braams*, K. Büchl* and *U. Wenzel:* Numerical Marfe Studies at ASDEX Upgrade.

IPP 8/4 *Bachmann, P.* and *D. Sünder:* Radiative Thermal Instability and Bifurcation.

IPP 9/99 *Passek, F.:* Untersuchung zur Spinabhängigkeit der elektronischen Struktur von Eisen- und Nickel-Systemen mit reduzierter Dimension.

IPP 9/100 *Linsmeier, Ch.:* Oberflächenanalytische Untersuchungen von getragenen Rhodium-Modellkatalysatoren = Surface-Analytical Investigations of Supported Rhodium Model Catalysts.

IPP 9/101 *Detzel, Th.:* Epitaxie und Magnetismus dünner Schichten.

IPP 9/102 *Schwörer, R.:* Einfluß von Bor auf die chemische Zerstäubung von Graphit mit Wasserstoffionen.

IPP 9/103 *Verbeek, H.* and *A. Schiavi:* The Low Energy Neutral Particle Analyzer (LENA) at W7-AS.

IPP 9/104 *Mayer, M.:* Reflexion von niederenergetischen Deuterium an Graphitoberflächen.

IPP Z/1 *Jandl, O., J. Sapper* and *J. Simon-Weidner:* FE-Untersuchungen für den Modulspulensatz von W7-AS.

External Laboratory Reports

GA-A21302 *Zohm, H., T.H. Osborne*, K.H. Burrell*,* et al.: ELM Studies on DIII-D and a Comparison to ASDEX Results. General Atomics, San Diego.

GA-A21685 *Mandl, W., K. H. Burrell*, R. J. Groebner*,* et al.: Investigation into Ion Edge Temperature Behavior Using CER Spectroscopy at DIII-D. General Atomics, San Diego.

IPF 94-1 *Behringer, K.* and *U. Fantz*:* Spectroscopic Diagnostics of Glow Discharge Plasmas with Non-Maxwellian Electron Energy Distributions. Stuttgart Univ.. Inst. für Plasmaforschung.

NIFS-269 *Hayashi*, T., T. Sato*, P. Merkel, J. Nührenberg* and *U. Schwenn:* Formation and 'Self-Healing' of Magnetic Islands in Finite-β Helias Equilibria. Nat. Inst. for Fusion Science, Nagoya.

NIFS-305 *Hayashi*, T., T. Sato*, N. Nakajima*, P. Merkel, J. Nührenberg, U. Schwenn, et al.:* Behavior of Magnetic Islands in 3D MHD Equilibria of Helical Devices, Nat. Inst. for Fusion Science, Nagoya.

Author Index

* No Member of the IPP

Teams

ASDEX-Team: R.Aratari, G.Becker, M.Bessenrodt-Weberpals, B.Bomba, H.-S.Bosch, K.Büchl, R.Büchse, A.Carlson, G.Dodel, A.Eberhagen, M.Endler, W.Engelhardt, H.-U.Fahrbach, G.Fußmann, O.Gehre, J.Gernhardt, L.Giannone, O.Gruber, G.Haas, T.Hartinger, W.Herrmann, J.V.Hofmann, H.Hohenöcker, E.Holzhauer, K.Hübner, G.Janeschitz, A.Kallenbach, O.Kardaun, F.Karger, M.Kaufmann, O.Klüber, M.Kornherr, K.Krieger, J.Kucinski, K.Lackner, R.S.Lang, F.Leuterer, R.Loch, G.Lisitano, H.-M.Mayer, K.McCormick, D.Meisel, V.Mertens, E.R.Müller, H.Murmann, J.Neuhauser, H.Niedermeyer, J.-M.Noterdaeme, W.Poschenrieder, H.Röhr, J.Roth, A.Rudyj, N.Ruhs, F.Ryter, W.Sandmann, F.Schneider, U.Schneider, R.Schubert, G.Siller, E.Simmet, F.X.Söldner*, E.Speth, A.Stäbler, K.-H.Steuer, U.Stroth, E.Taglauer, N.Tsois*, H.Verbeek, O.Vollmer, F.Wagner, K.Wira, F.Wesner, D.Zimmermann, H.Zohm.

ASDEX-Upgrade-Team: W.Köppendörfer, M.Albrecht, M.Alexander, K.Asmussen, G.Becker, K.Behler, A.Bergmann, M.Bessenrodt-Weberpals, H.-S.Bosch, M.Brambilla, F.Braun, K.Büchl, A.Carlson, R.Chodura, D.Coster, H.J.De Blank, S.De Pena Hempel, S.Deschka, C.Dorn, R.Drube, R.Dux, A.Eberhagen, B.Ebersberger, W.Engelhardt, J.Engstler, H.-U.Fahrbach, H.-U.Feist, W.Feneberg, S.Fiedler, D.Fieg, A.Field, J.C.Fuchs, G.Fußmann, C.Garcia-Rosales, O.Gehre, J.Gernhardt, J.Gruber, O.Gruber, K.Günther, G.Haas, B.Heinemann, G.Herppich, A.Herrmann, W.Herrmann, F.Hofmeister, H.Hohenöcker, H.Hupfloher, Yu.Igitkhanov, D.Jacobi, B.Jüttner, W.Junker, A.Kallenbach, O.Kardaun, T.Kass, M.Kaufmann, H.Kollotzek, M.Kornherr, K.Krieger, B.Kurzan, K.Lackner, P.T.Lang, R.S.Lang, M.Laux, L.L.Lengyel, F.Leuterer, G.Lieder, M.Maraschek, K.-F.Mast, H.-M.Mayer, P.McCarthy, D.Meisel, R.Merkel, V.Mertens, M.Münich, H.Murmann, B.Napiontek, D.Naujoks, G.Neu, R.Neu, J.Neuhauser, J.-M.Noterdaeme, J.Oswald, G.Pautasso, S.Pitcher, W.Poschenrieder, G.Raupp, K.Reinmüller, H.Richter, T.Richter, H.Röhr, J.Roth, F.Ryter, N.Salmon, H.Salzmann, W.Sandmann, H.-B.Schilling, M.Schittenhelm, H.Schneider, R.Schneider, W.Schneider, K.Schönmann, G.Schramm, J.Schweinzer, S.Schweizer, B.D.Scott, U.Seidel, M.Sokoll, E.Speth, A.Stäbler, K.-H.Steuer, J.Stober, B.Streibl, W.Suttrop, W.Teutterer, M.Troppmann, M.Ulrich, G.Venus, H.Verbeek, H.Vernickel, O.Vollmer, H.Wedler, M.Weinlich, U.Wenzel, H.Werthmann, F.Wesner, A.Wieczorek, R.Wilhelm, K.Wolf, R.Wunderlich, R.Zanino, D.Zasche, H.-P.Zehrfeld, H.Zohm.

ECRH-AUG-Team: H. Brinkschulte, F. Leuterer, F. Monaco, M. Münich, F. Ryter, M. Zouhar.

Gyrotron-Group: H.U.Nickel, M.Thumm.

ITER H-Mode Database-Working Group: J.A. Snipes*, R.S. Granetz*, M. Greenwald*, F. Ryter, O.Kardaun, U.Stroth, A.Kus, P.G. Carolan*, S.J. Fielding*, M. Valovic*, J.C. DeBoo*, T. Carlstrom*, D.P. Schissel, K. Thompson*, D.J. Campbell*, J.P. Christiansen*, J.G. Cordey*, Y.Miura*, N. Suzuki*, M. Mori*, T. Matsuda*, H. Tamai*, T. Takizuka*, S.-I. Itoh*, K. Itoh*, S.M. Kaye*.

ICRH-Team: W.Becker, F.Braun, R.Fritsch, F.Hofmeister, C.Hoffmann, J.-M.Noterdaeme, S.Puri, P.Verplancke, H.Wedler, F.Wesner.

IPF ECRH-Group: W.Kasparek, G.Müller, P.G.Schüller, M.Thumm.

NI-Group: M.Ciric, J.-H.Feist, K.Freudenberger, B.Heinemann, W.Kraus, W.Melkus, S.Obermayer; W.Ott, F.-P.Penningsfeld, F.Probst, R.Riedl, W.Schärich, E.Speth, A.Stäbler, R.Süß, A.Teubel, O.Vollmer, K.Wittenbecher.

NI-Team(ASDEX): E.Speth, A.Stäbler, O.Vollmer.

NI-Team(WVII-AS): K.Freudenberger, W.Melkus, W.Ott, F.-P.Penningsfeld, F.Probst, E.Speth, R.Süß, A.Teubel.

PSI-Group: R.Behrisch, A.P.Martinelli, V.Prozesky, J.Roth, E.Taglauer.

WVII-AS-Team: R.Balbin, J.Baldzuhn, K.Behringer, B.Bomba, R.Brakel, R.Büchse, R.Burhenn, G.Cattanei, A.Dodhy, D.Dorst, K.Dyabilin, A.Eslner, M.Endler, K.Engelhardt, V.Erckmann, U.Gasparino, J.Geiger, T.Geist, S.Geissler, L.Giannone, P.Grigull, G.Grünwald, H.Hacker, H.-J.Hartfuß, O.Heinrich, G.Herre, C.Hidalgo, M.Hirsch, J.V.Hofmann, J.Hofner, E.Holzhauer, R.Isler, R.Jänicke, J.Junker, F.Karger, M.Kick, A.Kislyakov, J.Kisslinger, C.Konrad, H.Kroiss, G.Kühner, N.F.Larinova, A.Lazaros, T.Luce, P.Luttner, H.Maaßberg, C.Mahn, W.Mandl, K.McCormick, H.Niedermeyer, W.Ohlendorf, F.Rau, H.Renner, H.Ringler, A.Rudyj, N.Ruhs, J.Saffert, J.Sapper, F.Sardei, S.Sattler, F.Schneider, U.Schneider, G.Siller, U.Stroth, G.Theimer, M.Tutter, E.Unger, F.Wagner, R.Waltz, U.Weber, A.Weller, H.Wobig, E.Würsching, S.Wurdack, D.Zimmermann, M.Zippe, S.Zöpfel.

WVII-X-Team: C.D.Beidler, W.Dommaschk, H.Greuner, G.Grieger, E.Harmeyer, F.Herrnegger, J.Junker, N.Karulin, J.Kisslinger, W.Lotz, P.Merkel, H.Münch, C.Nührenberg, J.Nührenberg, M.Pillsticker, F.Rau, H.Renner, J.Sapper, F.Schauer, A.Schlüter, I.Schönewolf, U.Schwenn, M.Spada, E.Strumberger, D.Sünder, A.Wieczorek, H.Wobig, L.-J.Zheng.

WVII-X-Technical-Group: W.Bitter, H.Greuner, E.Harmeyer, R.Holzthüm, S.Huber, N.Jaksic, S.Kamm, F.Kerl, H.Münch, M.Pillsticker, J.Sapper, F.Schauer, I.Schoenewolf, J.Simon-Weidner, B.Somach, J.Tretter, F.Werner, A.Wieczorek.

University Contributions to IPP Programme

LEHRSTUHL FÜR EXPERIMENTALPHYSIK VI
DER UNIVERSITÄT BAYREUTH

(Prof. Dr. Jürgen Küppers)

Elementary steps of chemical erosion of graphite based materials by hydrogen. Modelling of chemical erosion. Physico-chemical classification of reaction steps.

(J. Biener, C. Lutterloh, A. Horn, R. Kemnitzer, A. Schenk, M. Wittmann)

The cooperation activities of IPP and the University of Bayreuth are concentrated on investigating fusion relevant plasma-wall interaction processes. Accordingly, the surface chemistry of hydrogen on possible reactor wall materials (Be, C, C/B) is the primary research topic.

At H atom exposed C:H surfaces the following reactions were identified:

$$H \rightarrow (network)\text{-}CH_3 \rightarrow H_2\,(gas) + (network^*)\text{-}CH_3 \quad (1)$$

$$(network^*)\text{-}CH_3 \rightarrow (network) + CH_3\,(gas) \quad (2)$$

$$(network^*)\text{-}CH_3 \rightarrow (network)\text{-}CH_3 + H\,(gas) \quad (3)$$

Reaction (1) is an Eley-Rideal type hydrogen abstraction reaction and exhibits therefore only a small activation barrier. Reaction (2) consists of a split-off of a surface methyl group which is driven by the energy gain obtained by the network by de-exciting from the (*) excited state. Therefore, the activation barrier of this step is much smaller than the dissociation energy of a methyl group from a saturated hydrocarbon species. Reaction (3) is a thermally activated step. The combination of steps (1) to (3) leads to H atom impact induced erosion.

The temperature dependence of the erosion yield was found to exhibit a maximum of 0.01 C/H around 600 K. Below 400 K and above 700 K the yield was negligible. Between 400 K and 700 K the dominant contribution of the surface hybridization states switches from sp^3 to sp^2. In accordance with step (3) the erosion yield was found to exhibit an isotope effect, i.e. D etches more effectively at temperatures above 600 K as D dissociates from the network less easily than H.

Calculations were performed to model the H impact induced erosion yield using activation energies and network hydrogenation/H abstraction cross-sections which had been determined at the present model systems. The results of these calculations showed good correlations with experiments if one adjustable energy parameter was set at a physically reasonable value.

Scanning Tunnelling Microscopy (STM) measurements revealed that etching of graphite by H atoms proceeds at the terrace edges.

The reactions observed upon impact of H on physisorbed hydrocarbon molecules confirm that hydrogenation and H abstraction at C:H film surfaces belong to a general class of H atom induced processes.

Publications and Conference Reports

Biener, J., A. Schenk, B. Winter, U.A. Schubert, C. Lutterloh, J. Küppers: Hydrogenation of Amorphous C:H Surfaces by Thermal H(D) Atoms. Surf. Sci. 307-309, 228-234 (1994).

Biener, J., A. Schenk, B. Winter, U.A. Schubert, C. Lutterloh, J. Küppers: Spectroscopic Investigation of Electronic and Vibronic Properties of Ion Beam Deposited and Thermally Treated Ultrathin C:H Films. Phys. Rev. B 49, 17307-17318 (1994).

Küppers, J., J. Biener, A. Schenk, B. Winter, C. Lutterloh: Elementary Reactions at Carbon Surfaces under Impact of H. In: Proc. 21st EPS Conf. on Control. Fusion and Plasma Phys., Montpellier 1994, Eds. E. Joffrin, P. Platz, P.E. Stott, ECA 18B. Europ. Phys. Soc., Geneva 1994, 1524-1527.

Lutterloh, C., A. Schenk, B. Winter, J. Biener, U.A. Schubert, J. Küppers: D(H) Atom Impact Induced Eley-Rideal Abstraction Reaction Toward HD at Fully Hydrogenated C:H(D) Surfaces. Surf. Sci. 316, 1039-1043 (1994).

Strüber*, U., A. Kastner*, J. Küppers: Growth and Properties of Thin Ag Films on Pt(100) Surfaces. Thin Solid Films 250, 101-110 (1994).

Oral Presentations

Biener, J., A. Schenk, B. Winter, C. Lutterloh, A. Horn, J. Küppers: Elementary Steps of the Interaction of C:H Film Surfaces with Thermal H/D Atoms. EVC-4, Uppsala, Schweden (1994).

Biener, J., A. Schenk, B. Winter, C. Lutterloh, J. Küppers: A Surface Science Study on Elementary Steps in Low-Pressure Diamond Synthesis. ICNDST- 4, Kobe, Japan 1994.

Biener, J., A. Schenk, B. Winter, C. Lutterloh, U.A. Schubert, J. Küppers: H/D Austausch an C:H-Filmen mit thermischen H(D) Atomen: Eine Eley-Rideal Reaktion. Verhandl. DPG (VI) 29, 1456, O 30.11 (1994).

Biener, J.: Ein detailliertes Modell der Wasserstoffreaktion auf Kohlenstoffilmen. Institut für Plasmaphysik, Forschungsanlage Jülich, 1994.

Horn, A., J. Biener, A. Schenk, C. Lutterloh, J. Küppers: H/D Exchange Reaction at Graphitic CH Groups by Thermal H(D) Atoms. ECOSS 14, Leipzig 1994.

Kemnitzer, R., Th. Schimmel*, J. Küppers, Ch. Kloc, M. Lux- Steiner*: Mechanisch induzierter Abbau kovalenter Schichten auf $NbSe_2$ mit AFM/LFM. Frühjahrstagung Arbeitskreis Oberflächenphysik d. Deutschen Physikalischen Gesellschaft, Münster 1994.

Koch*, Th., Th. Schimmel*, Th. Winzer*, J. Küppers, M. Schwoerer*: In situ-Polymerisation von Diacetylen-Einkristallen unter dem Rasterkraftmikroskop. Verhandl. DPG (VI) 29, 1402, O 19.2 (1994).

Küppers, J., J. Biener, A. Schenk, B. Winter, C. Lutterloh: Elementary Reactions at Carbon Surfaces under Impact of H. EPS Conference on Controlled Fusion and Plasma Physics, Montpellier 1994.

Küppers, J.: H Atom Impact Induced Reactions at C:H Film Surfaces and Physisorbed Hydrocarbons. Stanford University, USA 1994.

Küppers, J.: H Atom Impact Induced Reactions at C:H Film Surfaces and Physisorbed Hydrocarbons. University of California, Riverside, USA 1994.

Küppers, J.: H Atom Impact Induced Reactions at Hydrogenated Surfaces and Physisorbed Hydrocarbons. University of California, Berkeley, USA 1994.

Küppers, J.: Model Studies on Chemical Erosion of C Based Materials and B Doping Effects. Sandia Laboratories, Livermore, USA 1994.

Küppers, J.: Thermally and H Atom Impact Induced Reactions at C:H Surfaces. Stanford University, USA 1994.

Küppers, J.: Wechselwirkung von H Atomen mit C:H Oberflächen und adsorbierten Kohlenwasserstoffen. Physikalisches Kolloquium, Universität Kassel 1994.

Küppers, J: H Atom Impact Induced Reactions at C:H Film Surfaces and Physisorbed Hydrocarbons. University of California, Santa Barbara, USA 1994.

Lutterloh, C., A. Schenk, J. Biener, U.A. Schuber, B. Winter, J. Küppers: Wechselwirkung von Wasserstoff- und Edelgasionen mit dünnen C:H Filmen. Verhandl. DPG (VI) 29, 1363, O 11.4 (1994).

Lutterloh, C., J. Biener, A. Schenk, J. Küppers: Deuteration of Physisorbed Xylene with Thermal D Atoms. ECOSS 14, Leipzig 1994.

Schenk, A., B. Winter, C. Lutterloh, J. Biener, U.A. Schubert, J. Küppers: The Origin of Reduced Chemical Erosion of Graphite Based Materials Induced by Boron Doping. PSI, Mito, Japan 1994.

Schenk, A., B. Winter, C. Lutterloh, J. Biener, U.A. Schubert, J. Küppers: Einfluß von Bor auf die Struktur und chemische Erosion von dünnen C/B:H-Filmen. Verhandl. DPG (VI) 29, 1456, O 30.9 (1994).

Schimmel*, Th., R. Kemnitzer, J. Küppers, Ch. Kloc*, M. Lux-Steiner*: Giant Atomic Corrugations on Layered Dichalcogenides Investigated by AFM/LMF. NATO Workshop "Forces in Scanning Probe Methods", Schluchsee 1994.

Schimmel* Th., J. Küppers, M. Lux-Steiner*: Reibung auf atomarer Skala. Workshop über methodische Entwicklungen und industrielle Anwendungen der Nahfeld Rastersondentechniken, SXM 1., Münster 1994.

Schimmel*, Th., R. Kemnitzer, Th. Koch*, J. Küppers, M. Lux-Steiner*: "Giant Atomic Corrugations" per AFM auf Schichtgitterverbindungen. Frühjahrstagung Arbeitskreis Oberflächenphysik d. Deutschen Physikalischen Gesellschaft, Münster 1994.

Schimmel*, Th., Th. Koch*, J. Küppers, M. Lux-Steiner*: True Atom-by-Atom Resolution Obtained by AFM at Ambient Conditions. Park European User Meeting, Genf 1994.

Schimmel*, Th, Th. Koch*, J. Küppers, Ch. Kloc*, M. Lux-Steiner*: Nanometer Scale Machining of Covalent Monolayers Investigated by Combined AFM/LFM. NATO Workshop "Forces in Scanning Probe Methods", Schluchsee 1994.

Doctoral Theses

Schenk, A.: Struktur und chemische Erosion dünner C:H und C(B):H Filme. Universität Bayreuth 1994.

Biener, J.: Spektroskopische Untersuchungen von Reaktionen thermischer Wasserstoffatome an Oberflächen dünner C:H Filme. Universität Bayreuth 1994.

LEHRSTUHL FÜR MESSTECHNIK (LMT) DER UNIVERSITÄT DES SAARLANDES

(Prof. Dr. Alexander W. Koch)

1. LASER SPECKLE TECHNIQUES FOR INNER WALL EROSION/REDEPOSITION MONITORING

W. Kirchner, M. Ruprecht, F. Salazar[1], and A. Trunzler

[1] Universidad Politécnica de Madrid

1.1 Introduction

The cooperation of IPP and the University of Saarland was focused on the development of long-range laser speckle techniques for measurement of surface changes of target plates. In order to obtain information on the surface structure and its change, the surface is illuminated with coherent light. The roughness of the surfaces under investigation (graphite tiles, divertor plates) results in a reflected speckle pattern. In 1994 measurements were performed with three principal aims: (i) to investigate the surface roughness and its change, (ii) to create contour line plots of specific surface areas with variable fringe resolution, and (iii) to address the problem of superposed deformation and vibration. In all cases the resulting images are detected by a standard CCD camera. The data are stored by a computer using a frame-grabber.

1.2 Surface Roughness Measurement

One application of the speckle technique is measurement of the surface roughness. This application requires no interferometer, but the correlation of different images of the surface[1)]. The difference between the images, according to the different speckle interferometer techniques, is the illumination angle (ASC: angular speckle correlation) or the wavelength (SSC: spectral speckle correlation). The method mainly focused on was the ASC with a single-line laser as light source (Fig. 1). For the SSC a tunable multi-wavelength argon-ion laser was used.

First measurements of graphite tiles of ASDEX show that these techniques are applicable to the material. The next steps are reference measurements on tiles with different roughnesses in order to calibrate the measurement system. It will then be possible to detect the roughness from large distances and the change of roughness during plasma exposure.

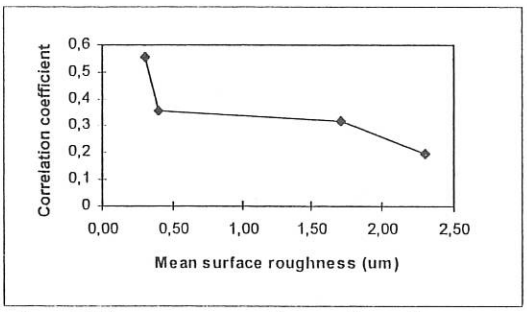

FIG. 1: ASC measurement of a rough surface

1.3 Contour Line Plots

A project which started two years ago is contour line measurement of rough surfaces. The principle of this measurement is based on the two-wavelength technique. The basic setup consists of a modified Mach-Zehnder interferometer. The adjustable fringe sensitivity is given by the synthetic wavelength Λ, depending on both illumination wavelengths.

1.4 Erosion and Deformation: Qualitative Measurement

For measurements in experimental fusion devices the discrimination between deformation and erosion/redeposition is of major concern. Figure 2 shows the qualitative result of the superposition of two images before and after erosion (scratch on the surface) in the presence of a deformation. Quantitative measurement of the erosion is not yet possible with this method, but this may be achieved by combining this measurement and the aforementioned two-wavelength technique.

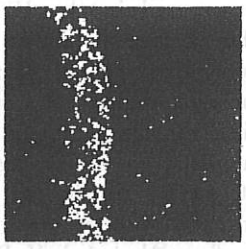

FIG. 2: Qualitative erosion measurement

---

1) W. Kirchner: Opt. Rauheitsmessung an techn. Oberflächen mittels Speckle-Korrelation, LMT, Univ. d. Saarl., 1994

ISOTOPE SEPARATOR LABORATORY, PHYSICS DEPARTMENT, TECHNICAL UNIVERSITY OF MUNICH

(Dr. E. Hechtl)

The self–sputtering yield of the low–Z material Be was measured as a function of the angle of ion incidence. The measured data are compared with those of the TRIM.SP (version TRVMC) computer simulation.

SPUTTERING OF SOLID SURFACES WITH HEAVY IONS

(E. Hechtl, R. Obermaier)

Experiments on Be self–sputtering were performed with our Harwell–type isotope separator. The targets were untreated, sintered Be samples with a technical surface, provided by JET. The experimental sputtering yields of Be as a function of the angle of ion incidence for an ion energy of 1 keV is shown in Fig. 1; TRIM.SP calculated data for Be self–sputtering are also shown. The curves drawn in Fig. 1 for both cases are Yamamura fits. Comparison of the experimental and calculated data shows a growing discrepancy with increasing angle of incidence. An important difference between experiment and simulation is certainly the surface structure. The target surface assumed for the calculation is completely smooth. In such a case there is typically a steep increase in the sputtering yield with increasing angles of incidence. However, the target used for the experiment was an unpolished and completely untreated sample as used in the JET machine. A micrograph of the surface is shown as insert in Fig. 1. This moon–like surface topography does not allow glancing angles of incidence and therefore the yield increase should be strongly reduced. In principle, this is in agreement with computer simulations by Ruzic in which it was attempted to include surface roughness effects. The present data show that 1 keV Be ions exceed a self–sputtering yield of unity at angles of incidence between 60° and 75°. Consequently, in the light of the present data, earlier estimates of the range of energies and angles of incidence showing self–sputtering yields larger than unity have to be corrected. Clearly, for a typical technical surface used in fusion applications, the range where self–sputtering reaches or exceeds unity is strongly reduced. Consequently, self–sputtering yields larger than unity will not occur if the plasma boundary temperature does not exceed about 80 eV, assuming the incidence of Be^{3+} ions accelerated in the surface sheath potential to energies of about 10 kT_e.

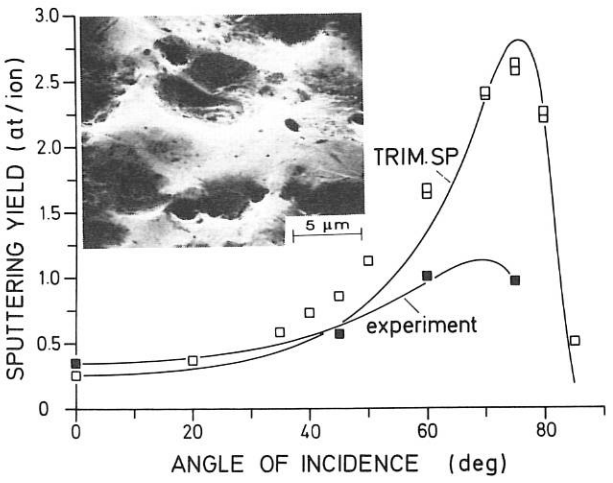

FIG.1: Self–sputtering yield of Be versus the angle of ion incidence for 1 keV. The insert shows the Be surface before irradiation.

Conference contribution

Hechtl, E., Roth, J., Eckstein, W., and Wu, C.H.: Experimental investigation of the angular dependence of Be self–sputtering, 11th PSI, Mito, Japan, May 23–27, 1994.

INSTITUT FÜR PLASMAFORSCHUNG (IPF) DER UNIVERSITÄT STUTTGART

(Prof. Dr. U. Schumacher)

The close collaboration of Institute for Plasma Research (IPF) at Stuttgart University with Max Planck Institute of Plasma Physics at Garching is based on developing and supplying measurements and interpretations in connection with electron cyclotron resonance heating (ECRH) systems as well as microwave and spectroscopic diagnostic systems for the stellarator and tokamak. The successful application of ECRH using 70 GHz and 140 GHz gyrotrons and transmission line systems on W7-AS and ASDEX Upgrade, respectively, favours the development and design of ECRH systems for future devices like W7-X and ITER. Moreover, a new collective Thomson scattering diagnostic for ion temperature determination with microwave generators is being developed. Basic spectroscopic investigations are being performed for plasma edge diagnostics and to understand the interaction of the divertor plasma with the walls.

1. ELECTRON CYCLOTRON RESONANCE HEATING (ECRH)

(U. S c h u m a c h e r, L. Empacher*), V. Erckmann**), W. Förster, G. Gantenbein, W. Kasparek, H. Kumrić, G. A. Müller, P. G. Schüller, J. Schwarz, K. Schwörer, D. Wagner)

1.1 Millimeter Wave Technology for ECRH at 140 GHz

1.1.1 ECRH system for W7-AS

In 1994 construction of the 2 MW, 140 GHz ECRH system was continued. Two of the 70 GHz, 200 kW gyrotrons and their associated transmission lines were dismantled and replaced by two 140 GHz, 500 kW modules. For plasma experiments the two remaining 70 GHz units stayed operational together with the quasi-optical 140 GHz prototype system. These experiments are described in the stellarator section of this report. Additionally, the 140 GHz prototype system was used for experiments on collective Thomson scattering (see Sec. 1.2).
The two new 140 GHz 500 kW gyrotrons were inserted into new superconducting magnets which have very low liquid helium consumption. Heating supplies, protection units and other auxiliary systems were adapted to these diode-type gyrotrons.
The gyrotrons had demonstrated the full specified performance (output power 500 kW with pulse length 3 s) in tests at the manufacturer's in Moscow. At IPP, however, only short-pulse operation could be carried out due to imperfections of the superconducting magnets. After repair, which is expected in early 1995, the acceptance tests at IPP will be resumed.
The matching optics between the gyrotron and the corrugated waveguide, the waveguide section of about 25 m length, and the mirror box containing the polarizer were installed and aligned for two new transmission lines. Mitre bend switches are integrated in the waveguide part of the transmission line, which allow a calorimetric or dummy load to be connected for quick control of the gyrotron operation. First low-power measurements of the whole waveguide part yielded a transmission efficiency of about 95 % which may be slightly increased by improved adjustment.
The components for the remaining optical part of the transmission line are under construction and are expected to be set up in spring 1995.

1.1.2 ECRH system for ASDEX Upgrade

The implementation of ECRH on ASDEX Upgrade started with the construction of a first 140 GHz module equipped with a Russian gyrotron (output power 0.5 MW, pulse length 0.5 s) previously operated on W7-AS. In its final stage the ECRH system consists of four 140 GHz, 0.5 MW gyrotrons with transmission lines which are, as on W7-AS, a combination of beam waveguide and corrugated HE_{11} waveguide sections. Components developed for W7-AS were modified and adapted to the different geometrical arrangement at ASDEX Upgrade.
In the gyrotron hall a fully quasi-optical transmission is used. Two mirrors transform the astigmatic gyrotron output beam into a stigmatic fundamental gaussian beam. Along the beam path a combination of two grooved mirrors allows one to adjust any polarization of the beam between linear and circular to obtain optimum accessibility to the plasma.
In the torus hall parts of the corrugated HE_{11} waveguide were installed, aligned, and tested at low power together with the launching mirrors inside the vacuum vessel and the pick-up waveguide monitor system on the inner torus wall.
High power tests were performed in the gyrotron hall up to the full performance of the installed gyrotron (0.5 MW, 0.5 s). For these tests a mobile absorber load built for high-power applications was successfully used.

1.1.3 Development of special components

1.1.3.1 Beam-forming techniques

For several applications it is necessary to shape the power distribution of a beam according to specific requirements. An example is the flattening of the power distribution to reduce the peak thermal load due to microwave dissipation in vacuum windows; other examples are beam splitters or synthesis of

*) since 1.11.94
**) IPP Garching

antenna beams. To produce such patterns, beams are reflected from special mirrors which introduce a phase variation over the beam cross-section such that higher-order free-space modes are excited, which establish the wanted pattern after some distance. An example is shown in Fig. 1.1 where a gaussian beam is transformed into a flattened beam profile with a peak power reduction of 60 %. Up to now, the beam patterns have been analyzed using two-dimensional Kirchhoff diffraction integrals. Work was started to develop codes to synthesize such patterns, and first results were obtained.

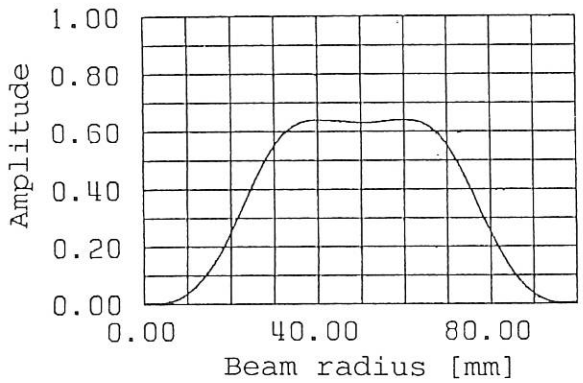

FIG. 1.1: Flattened beam (amplitude) profile obtained by phase modification of a gaussian beam.

1.1.3.2 *Synthesis and applications of special power distributions by HE_{1n} mode mixtures*

Megawatt microwave power transmission systems for ECRH on nuclear fusion experiments often use a combination of quasi-optical mirror lines and overmoded, corrugated, circular waveguides (W7-AS, W7-X, ASDEX Upgrade, ITER). In this context, several problems arise: the optimum coupling of a free-space gaussian beam into a corrugated waveguide, generation of antenna patterns, generation of special, nearly rectangular power distributions to reduce the heat load in vacuum barrier windows. The power distributions appropriate to these problems can be produced by mode mixtures of hybrid modes.

a) Synthesis of gaussian beam

The wanted amount of the HE_{12} can be generated from the HE_{11} in corrugated mode converters with periodic diameter variation or in corrugated horns with nonlinear diameter distribution. Very good agreement of low-power measurements with theoretical predictions, described in the Annual Report 1993, was achieved. The design and production of corrugated horns for application in transmission lines of W7-AS as well as ASDEX Upgrade was finished in 1994. Far-field low-power measurements of the optimized horns for 140 GHz were made. Figure 1.2 shows the measured far field of the optimized corrugated horn (L = 545.6 mm, I.D. = 43.5 mm, aperture radius 61.8 mm). There are no significant side lobes in the pattern. The analysis of the far-field measurements yields a beam waist to aperture radius ratio of 0.47, which corresponds to the theoretical value. The location of the beam waist is nearly 5000 mm behind the aperture.

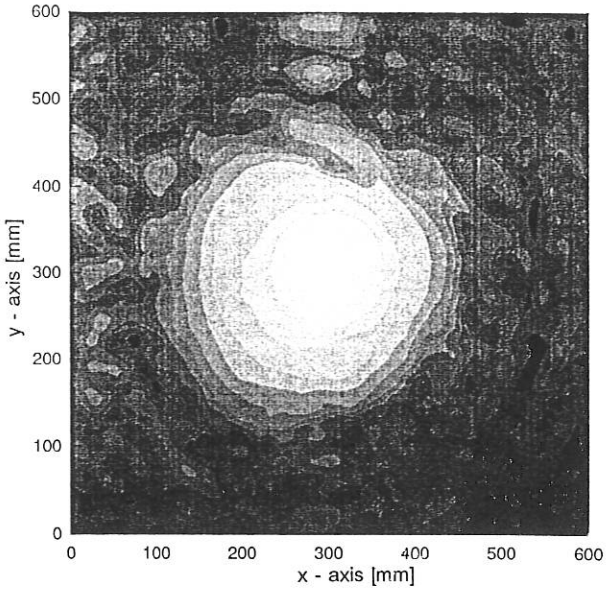

FIG. 1.2: Far-field pattern of an optimized corrugated horn at 140 GHz.

b) Window applications

Mode mixtures with optimized relative phase have a flattened power distribution in the waveguide, which is an important issue for use with vacuum barrier windows for CW operation of gyrotrons. The mode composition and the phase between the modes was varied. The calculated power distribution of a mixture with only 5% HE_{12} (z-component of Poynting vector), given in Fig. 1.3, shows the reduction of the peak power in the waveguide by more than 2 dB compared with a pure HE_{11} mode. The mode mixture can be generated in a short nonlinear taper, followed by a straight corrugated waveguide with a particular length.

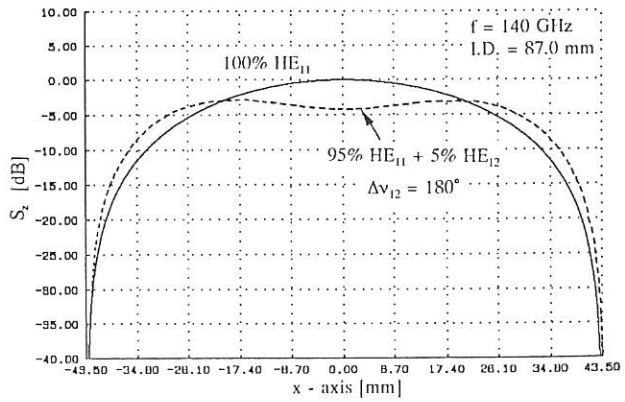

FIG. 1.3: Power distribution (S_z of Poynting vector) in corrugated waveguide of a pure HE_{11} mode and a 95 % HE_{11} + 5 % HE_{12} mode mixture with 180° relative phase difference.

1.1.3.3 *Waveguide components for ECE diagnostics*

a) HE11 waveguide with optimized corrugation

Corrugated waveguides suitable for transport of microwave radiation in the fundamental HE_{11} hybrid mode can be used in ECE transmission lines. A scattering matrix code is used in

order to optimize the corrugation depth and period. The losses of the HE_{11} mode in the corrugated waveguide are significantly lower compared with the TE_{11} mode in the smooth waveguide. Another main advantage is the reduced mode conversion and reflection at various waveguide transitions. Such mode conversions and reflections can lead to significantly higher losses and standing waves in the transmission line and therefore reduce the dynamic range of the measurement. Due to the excellent coupling of the HE_{11} mode to the fundamental gaussian free-space mode (98.5 %) it is ideal for use in quasi-optical mitre bends, where a phase correction of the mirror surface can further reduce the losses by half. The required length of taper sections avoiding the excitation of parasitic modes is also shorter compared with the smooth TE_{11} waveguide.

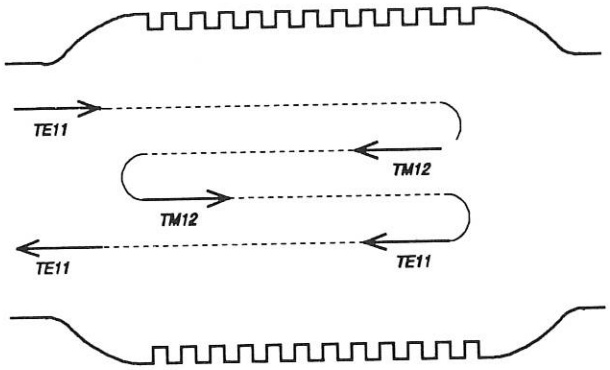

FIG. 1.4: Waveguide notch filter with Bragg corrugation.

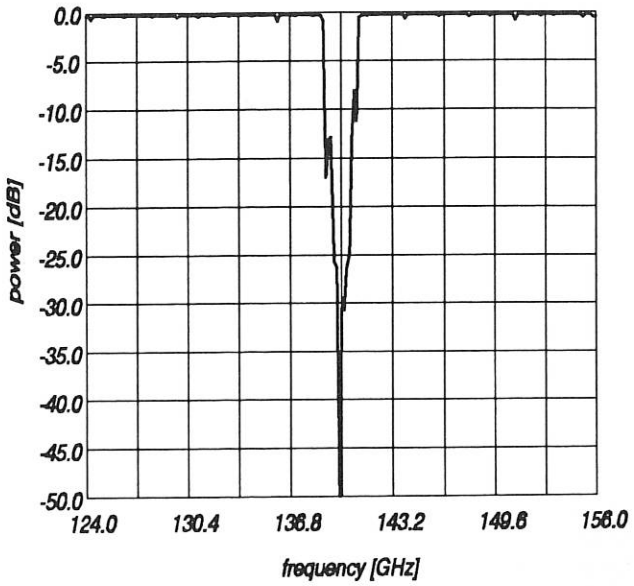

FIG. 1.5: Calculated transmitted power.

b) Waveguide notch filter using a Bragg reflection structure

The principle of a filter design consisting of a Bragg reflector and two nonlinear tapers to be inserted in a monomode transmission line (d = 1.85 mm) is shown in Fig. 1.4. At the Bragg resonance the incoming TE_{11} mode from the monomode waveguide is reflected into the TM_{12} mode close to cutoff in the larger cross-section (d = 5.6 mm) by the Bragg reflector. In this example the Bragg corrugation consists of 200 periods with an overall length of 285 mm and a corrugation amplitude of 0.04 mm. The TM_{12} mode is totally reflected by the left taper and then converted back into the TE_{11} mode, which can pass nearly undisturbed through the left taper. Choosing a mode close to cutoff for the Bragg resonance in the larger cross-section affords the advantage that the Bragg resonance is well separated from other ones over a wide frequency range, which can be seen in Fig. 1.5. Window tapering of the Bragg corrugation leads to high mode purity and therefore a smooth frequency dependence of the Bragg reflection. The filter is tunable by means of thermal expansion.

1.1.4 Development of electronic equipment

1.1.4.1 Cathode heater supply for 140 GHz gyrotron

The Russian 140 GHz gyrotrons use cathodes which need heating powers of up to 1.5 kW AC. Therefore, a modified version of the supply used for 70 GHz Varian gyrotrons was developed.
Using an electronically variable inductance as tuning element allowed regulation of the heating power of up to 1.5 kW 50 Hz AC with a stability of 10^{-3}.

1.1.4.2 Sawtooth current generator for gyrotron collector sweeping coil

The newly developed 140 GHz long pulse gyrotrons from TORIY require steering of the electron beam across the collector electrode surface to prevent local overheating. For this purpose a coil for modulating the magnetic field at the collector surface has to be powered by a current with sawtooth behaviour in time. A programmable DC-to-DC converter using switched power technique was developed for driving this coil. IGBT semiconductor switches operating at 40 kHz together with ferrite cores for transformers were used as main elements. These supplies can drive a 150 mH inductance with a sawtooth current of up to 70 A peak value.

1.1.4.3 Servo-drives and control system for the transmission line components.

For the upgraded 140 GHz ECR heating system at W7-AS all the adjustable components of the microwave power beam lines, i.e. the polarizer mirrors as well as the launching and deflecting mirrors, shall be controlled and monitored by a dedicated personal computer in order to save time and minimize errors when setting up and surveying the beam lines between experiment shots. This system shall accept control data and return status information in local stand-alone operation, and also be able to exchange these data with the higher level experiment control and data acquisition system. To this end, all the servo-drives of the adjustable microwave mirrors will be connected to a personal computer by a CAN bus, a serial data bus for control systems (ISO 11898).
For this reason, new, compact drive-controller modules were designed with intelligence of their own due to a powerful

Siemens SAB 80C166 microcontroller with integrated 10-bit ADC and pulse width modulation unit.
This microcontroller receives the position signal, performs the control algorithm, and controls the positioner motor by a pulse-width-modulated signal. It also scans the keys on the module's front panel for off-line manual control, and, in on-line mode, it exchanges data messages with the personal computer via a Philips PCA82C200 CAN controller and the CAN bus.
On the personal computer the user interface for manual control data entry and status display as well as the corresponding dialogue with the positioners connected to the CAN bus will be implemented, and also data exchange with the experiment data acquisiton system. This software is under development.

1.1.5 Design work for WENDELSTEIN 7-X (W7-X)

For the planned 10 MW CW ECRH/ECCD system on W7-X, a conceptual design was elaborated (ECCD - Electron Cyclotron Current Drive). It consists of a generator including ten 140 GHz gyrotrons, a fully optical transmission system running in an underground duct, and plug-in launchers with independently movable mirrors to guarantee high experimental flexibility. The system is characterized by simple, modular design, which promises reliable and cost-effective operation. Based on this work, the ECRH part of the Phase II Application for Preferential Support was written in collaboration with IPP Garching.
In this context, detailed studies were started or continued on various aspects of CW ECRH systems:

- Power supply concepts using vacuum-tube and solid-state technology for gyrotrons with and without depressed collector.
- System control and data acquisition for larger installations.
- Transmission of several beams over a common mirror system (multi-beam waveguide).
- Beam shaping and beam dividing to reduce thermal loads and stresses, e.g. in vacuum windows (see Sec. 1.1.3.1)
- Development of a CW dummy load.

1.1.6 Conceptual design of a 50 MW ECRH/ECCD system for ITER

At the end of 1993, a concept of an optical launcher for a 50 MW ECRH/ECCD system on the ITER international reactor project had been elaborated. On the basis of this concept, a more detailed design study was undertaken. Optimization of the system with respect to high beam quality, shielding of sensitive components, reasonable thermal loading of mirrors, and easy maintenance was done. Especially, beam-forming techniques to minimize the beam divergence and simultaneously reduce the peak power were investigated. Among the different methods under study, namely the use of HE_{1n} mode mixtures in the feed, integration of phase-modifying reflecting surfaces into the beam path, and shaping of the total beam profile by optimizing size, location, and direction of the individual beams on the common antenna mirror, the latter method has proven to be best adapted for ITER.
This led to an antenna which can be switched between perpendicular launch for heating and fixed oblique launch for current drive, which is characterized by good localization of the power in the centre of the plasma (FWHM of the total beam < 0.5 m), a relatively small aperture in the first wall of 0.14 m^2 (average power density in the port 360 MW/m^2), and a tolerable microwave dissipation on the deflecting mirror near the first wall (<370 W/cm^2, if a beryllium-coated mirror at 200 C is assumed).
In parallel to these investigations, the work on a launcher which allows continuous change of the injection angle between 20° and 35° continued. Depending on the space available between the magnetic field coils, it was shown that it may be possible to inject 50 MW with a single launcher also in this case. Division of the power into two launchers can be envisaged if the available space is not sufficient for a 50 MW launcher.
The work was performed in the frame of the ITER tasks IVA-EC and G 51 TD 04, D15. The results obtained up to now were summarized in the final report for the first and two intermediate reports for the latter task.

1.2 Collective Thomson Scattering Diagnostic

(in collaboration with G.G. Denisov*), V. Erckmann**), S. Filchenkov*), T. Geist**), E. Holzhauer, A. Kostrov*), L. Kukin*), L.V. Lubyako*), O.B. Smolyakova*), A. Stanjuk*), E. Suvorov*))

The aim of these experiments is to measure the ion temperature or, more generally, the energy distribution of the different ion species in the plasma. This diagnostic method could ultimately be used to get information on the energy spectrum of alpha particles generated in fusion reactions. The present experiments were performed on the W7-AS stellarator at IPP Garching.
In 1994 the gyrotron originally envisaged primarily for ECRH at 140 GHz was used. The quasi-optical ECRH heating system was used as the scattering source. A separate receiver antenna was installed. On the basis of the experimental phase in 1993, the complex and very sensitive receiver system (quasi-optical notch filter, heterodyne receiver, 32-channel filter bank and A/D converters) was optimized at IAP in Nizhni Novgorod and re-installed on the W7-AS stellarator. In addition, a second receiver system with 4 channels and a high dynamic range was built at IPF Stuttgart to provide a monitor for non-thermal effects.
Frequency spectra of the thermal ion feature with a typical width of 0.5 GHz were measured in agreement with theoretical models. This is the first time that the ion feature has been measured in a fusion device using a gyrotron source. It is remarkable that the thermal level of density fluctuations exists in spite of the presence of auxiliary heating. If a perpendicular 30 keV diagnostic neutral beam is injected close to the scattering volume, a lower hybrid resonance is excited in the frequency range of the ion feature. The instability produces a corresponding line in the frequency spectra which is considerably above the thermal ion feature. The dependence of the lower hybrid frequency on electron density was demonstrated.

It is planned to perform a systematic investigation of the scattering spectra over a wide range of operating parameters of

*) Institute of Applied Physics, Nizhni Novgorod
**) IPP Garching

the stellarator experiment using a 140 GHz gyrotron. A new receiver antenna will allow adjustment and thus optimization of the scattering volume during the next experimental phase. In addition, experiments at 70 GHz in discharges with NI heating will allow scattering experiments in optimized magnetic field configurations between 1.4 - 2.2 T. Under these conditions, the ECR layer is outside the scattering volume, thus eliminating possible complications due to resonant absorption of radiation.

2. PLASMA EDGE DIAGNOSTICS

(K. B e h r i n g e r , M. Bross, U. Fantz, H. Jentschke, K. Hirsch, E. Holzhauer, G. Lieder, N. Mommer, M. Niethammer, T. Schütte, G. Volk)

2.1 Erosion Measurements

The interaction of materials with plasmas is being investigated within the framework of "Sonderforschungsbereich 259", a project dealing with the material and heat load problems of thermal protection systems during re-entry of spacecraft into the earth's atmosphere. For these studies, arc jets are operated in an air-like mixture at Institut für Raumfahrtsysteme, IRS. The IPF contribution to this project consists of plasma diagnostics and erosion measurements by means of emission spectroscopy and laser scattering. Due to the requirement of low weight, but high mechanical strength and high thermal conductivity, carbon fibre compound materials (C/C-SiC) are the candidates favoured at present, showing far smaller erosion than pure carbon fibre materials (C/C). When exposed to the arc jet plasma ($T_e \geq 10\ 000\ K \geq T_G$, $n_e \approx 10^{20}\ m^{-3}$, $n_{gas} \approx 10^{21}\ m^{-3}$), the C/C-SiC materials reach surface temperatures of 1900 K. Even under these conditions, the sublimation rates of carbon and SiC are still small and the erosion is mainly due to chemical reactions with oxygen and nitrogen molecules, atoms, and ions.

The integral erosion rates of these materials can be obtained in the usual way from weight loss (C/C .80 mg/cm^{2}s, C/C-SiC .03 mg/cm^{2}s at 1900 K). Spectroscopic measurements of particle fluxes from the surface of the heated probes must be based on measurements of the respective particle densities in the plasma, derived from their line emission, and on their thermal velocities away from the surface. The so-called S/XB ratios, used for particle flux measurements in fusion research, cannot be applied here, because the plasmas in front of the C/C-SiC probes are not fully ionized and even have a high molecular fraction due to a turbulent gas mixing in the arc jet. However, both methods of flux measurements require knowledge of the excitation rate coefficients of the elements under investigation and, at least at higher densities, also collisional radiative population calculations. It is a distinct advantage of the air jet experiment that the spectroscopic technique can be calibrated and verified by the weight loss results. Any conclusions on basic atomic data obtained in this way are also of interest for similar investigations in fusion research.

As an example, the spectrum in Fig. 2.1 shows some SiI lines at 251 nm ($3p^2\ ^3P$ - $3p4s\ ^3P$) emitted in front of the probes in the case of a C/C-SiC probe exposed to an air-like plasma (surface temperature 1900 K). The net erosion is small and

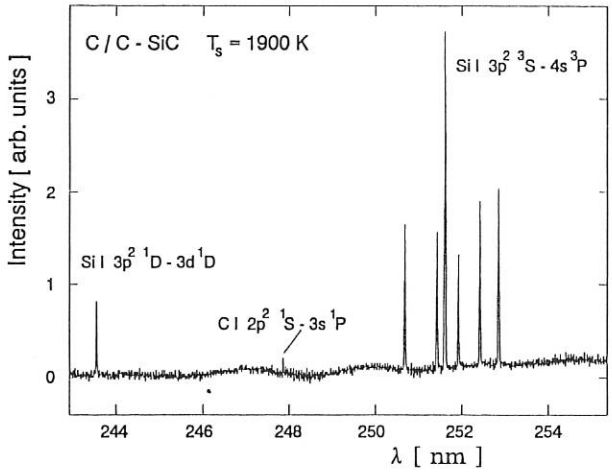

FIG. 2.1: Si I line emission for C/C-SiC material at a surface temperature of 1900 K in an air-like re-entry plasma.

would even be about one order of magnitude smaller in experiments with pure nitrogen only. Therefore, only a very weak indication of the carbon line CI at 247.8 nm can be seen, while this line is much stronger in the case of pure C/C fibre or graphite (see Annual Report 1993). The SiI lines are very sensitive indicators of the Si flux, and their analysis is in agreement with weight loss results.

The 1994 erosion studies of C/C-SiC are also of importance for future application of these materials in the W7-AS stellarator. Since new types of wall materials may be required in order to withstand the high thermal load of future fusion plasma reactors, the C/C-SiC material with high thermal conductivity ($\varkappa_\parallel \approx$ 10-15 W/K m, $\varkappa_\perp \approx$ 6-8 W/K m) and specific heat capacity (C ≈ 1150-1800 J/kg K) [1], combined with very low erosion rates at high surface temperatures, will be examined in this experiment as a prospective candidate. Even if the erosion mechanisms are different (chemical effects and evaporation in the arc jet, sputtering in fusion experiments), the spectroscopic analysis technique can be transferred and details of the appearance of SiI and CI lines and molecular bands (e.g. CN), as measured by a high-resolution Echelle spectrometer, can be used for comparison.

2.2 Molecular Spectra of H_2

H_2 and D_2 molecular bands have been observed in hydrogen laboratory plasmas and equally in the edge regions of fusion experiments like TEXTOR and W7-AS, usually with much lower spectral resolution. By means of the absolute intensities of these bands, and knowing the excitation and ionization rate coefficients, the local H_2 influx density could be determined, a method which is well established in the case of impurity atom and ion fluxes. However, the appearance of the H_2 molecular bands had been found to vary considerably with the type and the plasma parameters of the individual discharges. Therefore, further investigations were carried out, mainly in glow discharges (100 - 1000 Pa) but also in microwave plasmas (2 - 20 Pa), in a wide range of temperatures and densities (T_e = 2 - 4 eV, $n_e = 2 \cdot 10^{16}$ - $2 \cdot 10^{17}\ m^{-3}$, T_G = 350 - 700 K) in order to shed some light on the interrelation of plasma parameters and the population of rotational and vibrational levels.

Various H_2 molecular bands ($3p^3\Pi_u \rightarrow 2s^3\Sigma^+_g$ Fulcher band, $3d^1\Sigma^+_g \rightarrow 2p^1\Sigma^+_u$, $3d^1\Pi_g \rightarrow 2p^1\Sigma^+_u$, vibrational levels 0-5) were investigated in detail [2]. It should be pointed out that, in the case of glow discharges, a non-Maxwellian electron energy distribution was used for the analysis [3] because electron-electron collisions are not frequent enough to compensate for the inelastic collision processes at higher energies, and the tail of the distribution function is therefore depleted and falls off more steeply with energy than a Maxwellian distribution. The mean electron energies were determined on the basis of the absolute line intensities of neutral helium and argon lines.

The appearance of the H_2 molecular bands can be summarized as follows: The rotational temperatures of the above-mentioned electronic states are quite different and range from below room temperature to about 700 K (gas temperature ≈ 400 K). For larger rotational quantum numbers (K > 4) the populations are non-thermal. This behaviour is a consequence of the fact that there is no strict selection rule for collisional excitation. The rotational temperatures are independent of the electron densities, but increase significantly with the neutral particle densities. The population of the vibrational levels is completely non-thermal. At the lowest pressures investigated, it probably just reflects the Franck-Condon factors for excitation from the H_2 ground state in the lowest vibrational level v=0. This means that the highest population, e.g. in the upper state of the Fulcher system $3p^3\Pi_u$, is found in v = 2. At higher pressures, the distribution changes in favour of the v = 0 state in $3p^3\Pi_u$. The relative intensities of the various electronic transitions investigated also change with pressure. All these observations can be explained by a redistribution of the population amongst the electronically excited states by neutral particle collisions. The Fulcher transition, which was investigated most extensively [2], shows a particularly strong dependence of the rotational temperature and the distribution over the vibrational states on the plasma parameters. In the case of glow discharges, collisions with neutrals are clearly of high importance, whereas in microwave discharges at lower pressures electron collisions play the dominant role. As expected, the latter low-pressure spectra agree best with hydrogen molecular bands observed in fusion plasmas. Another important result of the above investigation was that the ground state vibrational distribution can be derived from the spectra at low neutral pressure.

The investigation of H_2 molecular bands was also extended to the region from 455 nm to 463 nm, where two singlet transitions can be observed ($3d^1\Sigma^+_g \rightarrow 2p^1\Sigma^+_u$ 456 - 463 nm; $3d^1\Pi_g \rightarrow 2p^1\Sigma^+_u$ 454 - 458 nm). Singlet transitions are usually more suitable for diagnostics because they are more closely connected to the ground state, which is also a singlet state. The R-branch of the first transition is a conspicuous feature in the spectra and consists of only a few well-separated rotational lines (see Fig. 2.2), facilitating identification and analysis even when measured with limited spectral resolution. For the transition shown in Fig. 2.2, the rate coefficient is known from experimental investigations [4], thus allowing measurements of the H_2 influx density by means of the absolute intensity of this band.

In the above investigation, the rate coefficient for the Fulcher transition was found to be significantly higher than expected. Part of the explanation may again be the excitation transfer from $3p^3\Pi_u$ to $3d^3\Sigma_g$ by neutral collisions. In contrast, the rate

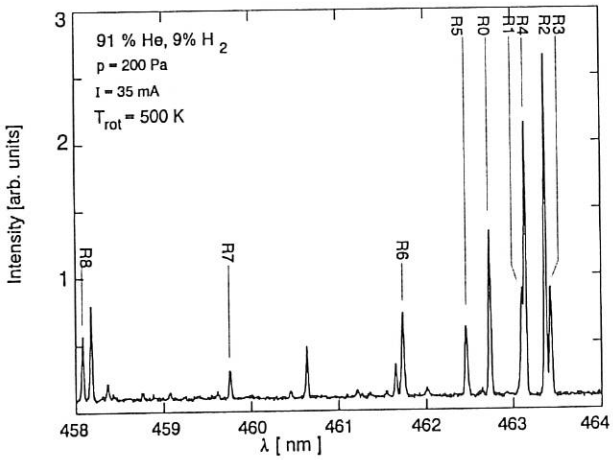

FIG 2.2: R-branch of the 0-0 transition $3d^1\Sigma^+_g \rightarrow 2p^1\Sigma^+_u$.

coefficient for the singlet transition ($3d^1\Sigma^+_g \rightarrow 2p^1\Sigma^+_u$) appears to be too small. Another explanation for these discrepancies is the fact that there is usually a substantial population in higher vibrational levels of the electronic ground state in these plasmas, which could increase or reduce the effective rate coefficients to the upper electronic states.

The described investigations will be continued in microwave plasmas, the conditions of which are closer to fusion edge plasmas and where collisions with neutral particles can be neglected.

2.3 CH/CD A-X Emission Rate Coefficient

Investigations of microwave discharges in methane (CH_4 and CD_4) and in methane noble gas mixtures were performed by means of optical emission spectroscopy and active laser techniques. Emission spectra of the $A^2\Delta$ -$X^2\Pi$ electronic transition have already been presented (see Annual Report 1993) and CH/CD number densities obtained by laser-induced fluorescence (LiF). By combining the LiF measurements, which determine the CH/CD molecular ground state densities, with the information on the excited state population from the intensities of emission bands, it is possible to calculate the emission rate coefficient X_{EM} of the ground state excitation for the CH/CD A-X transition. The required plasma parameters were determined by microwave interferometry (n_e) and measurements of the absolute intensities of He lines (T_e). In Fig. 2.3, results for the emission rate coefficient of the CH/CD A-X transition are shown for microwave plasmas in CH_4 and CD_4, in comparison with calculations based on the impact parameter method (IPProg [5], using the optical f-value).

The accuracy of the experimental emission rate coefficient is mainly limited by a competing excitation mechanism, namely, the dissociative excitation of CH_4, which is much more abundant in the plasma than CH. The influence of this second excitation path increases with electron temperature and the results are therefore most uncertain at higher T_e values, where the error bars may approach a factor of two. Nevertheless, the results in Fig. 2.3 are the first experimental data for the excitation of CH/CD A from the CH/CD ground state by electron collisions and they confirm, at least within the error limits, the theoretical calculations, particularly at low electron temperatures.

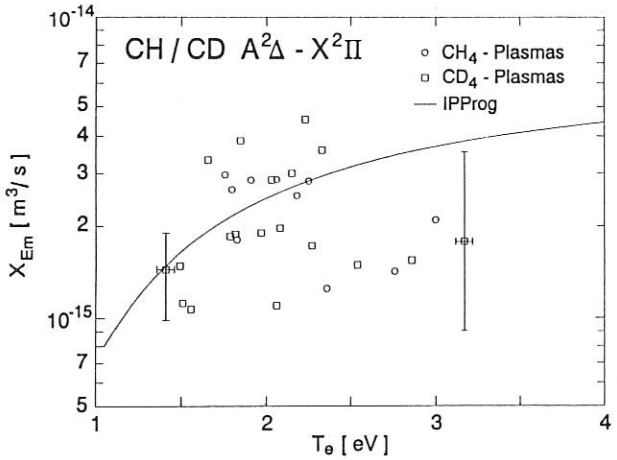

FIG. 2.3: Measured emission coefficient for the CH/CD A-X transition for ground state excitation and comparison with calculation from IPProg [5].

2.4 Spectroscopic Investigation of Molecular Impurities in the ASDEX Upgrade Divertor

Emission spectroscopic studies of molecules close to the target plates performed with the divertor spectrometer on ASDEX Upgrade, show strong emission bands of CH/CD, C_2, and BH/BD at high densities. They indicate the importance of hydrocarbons for the carbon impurity source. The absence of carbon oxides (CO) or hydroxides (OD) is due to the reduction of oxygen by boronization.

The emission profiles of the BD bands peak near the divertor plate of ASDEX Upgrade [6]. The penetration depth is about 1.8 cm. The B I line has its maximum about 0.5 cm from the plate, while C I peaks very near the plate, which supports the dissociation of the BD molecules being the dominant source of the observed B I.

The molecular influxes as obtained from the measured line intensities give an estimate of the chemical sputtering yield for methane and higher hydrocarbons of about 0.03 and 0.06, respectively. While the chemical sputtering yield of methane CD_1 is in good agreement with the result of mass spectroscopy measurements, the higher value of the C_2D_x sputtering yield may reflect the increasing production rate of heavier hydrocarbons under low-energy bombardment. The molecular influxes and the local plasma electron density n_e depend on the average electron density $\bar{n}_e$ in a similar way.

The measured emission profiles are simulated by an interpretative model which takes many reaction paths of the molecules into account.

2.5 Development of High-resolution Divertor Spectroscopy on ASDEX Upgrade

For detailed spectroscopic investigations of the divertor action of ASDEX Upgrade measurements of the ion temperature T_i, flow velocities V_i along the magnetic field lines, erosion mechanisms, and impurity transport in the divertor region have to be made. These data are obtained by high-resolution spectroscopy in the visible and ultraviolet spectral ranges from measurements of Doppler broadening and shifts of spectral lines, from analysis of molecular band structures, and from absolutely calibrated radiation profiles.

The high-resolution divertor spectrometer on ASDEX Upgrade consists of 32 radial lines of sight which are oriented parallel to the outer divertor plate at a distance of 0.1 cm to 10 cm and a spatial resolution of 0.1 cm. Moreover, 2 times 25 lines of sight in the toroidal direction will be installed.

There are two detection systems simultaneously available, two 16-channel photomultiplier arrays and a 1.5 m echelle spectrometer with a prism predisperser fitted with a 2D CCD camera. This allows observation of 32 channels simultaneously with a spectral resolution of about 1 pm at a wavelength of 300 nm.

References:

[1] W. Krenkel, P. Schanz, DLR Stuttgart, private communication (1994)
[2] N. Mommer, Diploma Thesis, IPF, Universität Stuttgart, 1994
[3] K. Behringer, U. Fantz, J. Phys. D: Appl. Phys. **27** (1994) 2128-2135
[4] R.L. Day, R.J. Anderson, J. Chem. Phys. **71** (1979) 3683
[5] IPProg: A. Burgess, H.P. Summers, Mon. Not. R. astr. Soc. **174** (1976) 345
[6] G. Lieder, K. Behringer, et al., Europhys. Conf. Abstr. **18B** Part II (1994) 722-725

PUBLICATIONS, CONFERENCE REPORTS, DIPLOMA THESIS, AND SEMINAR TALKS

PUBLICATIONS

Alius, H., and G. Dodel:
"Far-infrared modulation techniques based on optical excitation of semiconductors".
Infrared Phys. Technol. 35 (1994) 73-78.

Behringer, K., and U. Fantz:
"Spectroscopic diagnostics of glow discharge plasmas with non-Maxwellian electron energy distribution".
J. Phys. D: Appl. Phys. 27 (1994) 2128-2135.

Holzhauer, E., G. Dodel, M. Endler, J. Gernhardt, L. Giannone, M. Manso, K. McCormick, V. Mertens, H. Niedermeyer, A. Rudyj, F. Serra, A. Silva, G. Theimer, P. Varela, F. Wagner, H. Zohm, and ASDEX Team:
"The H-mode in the ASDEX tokamak".
Plasma Phys. Control. Fusion 36 (1994) A3-A11.

Ogawa, I., T. Idehara, H. Ibe, K. Kawahata, and W. Kasparek:
"A transmission line for plasma scattering measurements with a submillimeter wave gyrotron".
Int. J. of Infrared and Millimeter Waves 15 (1994) 1587-1602.

CONFERENCE REPORTS

Frühjahrstagung der Deutschen Physikalischen Gesellschaft, Fachausschuß Plasmaphysik, Erlangen (Germany), March 7 - 10, 1994.

Behringer, K. und U. Fantz:
"Spektroskopische Diagnostik von Niederdruckentladungen mit speziellen Verteilungsfunktionen".
Verhandl. DPG (VI) 29 (1994) P 14.1 (Fachvortrag).

Lieder, G., K. Behringer, A Field, A. Kallenbach, B. Napiontek, D. Naujoks und R. Radtke:
"Spektroskopische Untersuchungen zur chemischen Erosion im Divertor von ASDEX Upgrade".
Verhandl. DPG (VI) 29 (1994) P 4.40.

Napiontek, B., G. Fussmann, G. Lieder und R. Radtke:
"CX-induzierte Strahlung im Divertor von ASDEX Upgrade".
Verhandl. DPG (VI) 29 (1994) P 15.7.

6th Russian-German Meeting on ECRH and Gyrotrons, KIAE, Moscow, June 13-14, 1994 and IAP Nizhni Novgorod, June 15 - 18, 1994.

Erckmann, V., T. Geist, E. Holzhauer, W. Kasparek, and E. Suvorov:
"New development for collective Thomson scattering experiments with gyrotron at W7-AS".

Erckmann, V., G. Gantenbein, T. Graubner, W. Kasparek, H. Kumrić, G.A. Müller, and P.G. Schüller:
"First tests of the new 140 GHz transmission lines for ECRH on W7-AS".

Wagner, D., and G.A. Müller:
"Application of a scattering matrix code for the design of millimeter wave and gyrotron components".

12th European Sectional Conference on the Atomic and Molecular Physics of Ionized Gases, Noordwijkerhout (Netherlands), August 23 - 26, 1994.

Behringer, K., and U. Fantz:
"Spectroscopic diagnostics of glow discharge plasmas with non-Maxwellian electron energy distributions".
EPS 18E (1994) 302-303.

21st EPS Conf. on Controlled Fusion and Plasma Physics, Montpellier (France), June 27 - July 1st, 1994.

Lieder, G., K. Behringer, A. Field, C. Garcia-Rosales, S. Hirsch, B. Napiontek, D. Naujoks, C.S. Picker, R. Radtke, J. Roth, M. Weinlich, and the ASDEX Upgrade Team:
"Spectroscopic investigation of molecular impurities in the ASDEX Upgrade divertor".
Proc. ECA 18B Part II, (1994) 722-725.

19th Int. Conf. on Infrared and Millimeter Waves, Sendai (Japan), October 17 - 20, 1994.

Erckmann, V., G. Gantenbein, T. Graubner, W.Kasparek, H. Kumrić, G.A. Müller, P.G. Schüller, and D.Wagner:
"Transmission lines for the 140 GHz ECRH system on the stellarator W7-AS".
Conf. Digest, p. 236-237.

Wagner, D., G. Gantenbein, W. Kasparek, J. Petterebner, and M. Thumm:
"Improved gyrotron cavities with high quality factors".
Conf. Digest, p. 289-290.

Int. Conf. on Plasma Physics, Foz do Iguaçu (Brazil), October 31 - November 5, 1994.

Moser, F.:
"Propagation of electron-Bernstein-waves in non-Maxwellian, weakly relativistic Vlasov-plasmas with temperature anisotropy".
Proc. Vol. I, p. 361-364.

Progress Meeting on Spectroscopic Systems for ITER, Moscow, November 29 - December 1st, 1994.

Lieder, G., and K. Behringer:
"Spectroscopic diagnostic requirements for the ITER divertor".

DIPLOMA THESIS

Mommer, N.:
"Spektroskopische Untersuchung der H_2-Molekülstrahlung einer Glimmentladung".

SEMINAR TALKS:

Fantz, U.:
"Spektroskopische Diagnostik von Niederdruckentladungen mit speziellen Verteilungsfunktionen".
Ruhr-Universität Bochum, Arbeitsgruppe für Grundlagen der Elektrotechnik, SFB 191, April 14, 1994.

Kumrić, H.:
"Overmoded waveguides - Transmission of microwaves between gyrotron and fusion plasma".
Zavod za visokofrekventnu tehniku, Elektrotehnički fakultet, University of Zagreb, March 31, 1994.

Schütte, T.:
"Laser-induzierte Fluoreszenzmessungen und Emissionsspektroskopie am ECR-Methanplasma".
Technische Universität München, Lehrstuhl für Technische Elektrophysik, June 24, 1994.

How to reach
Max-Planck-Institut für Plasmaphysik (IPP)

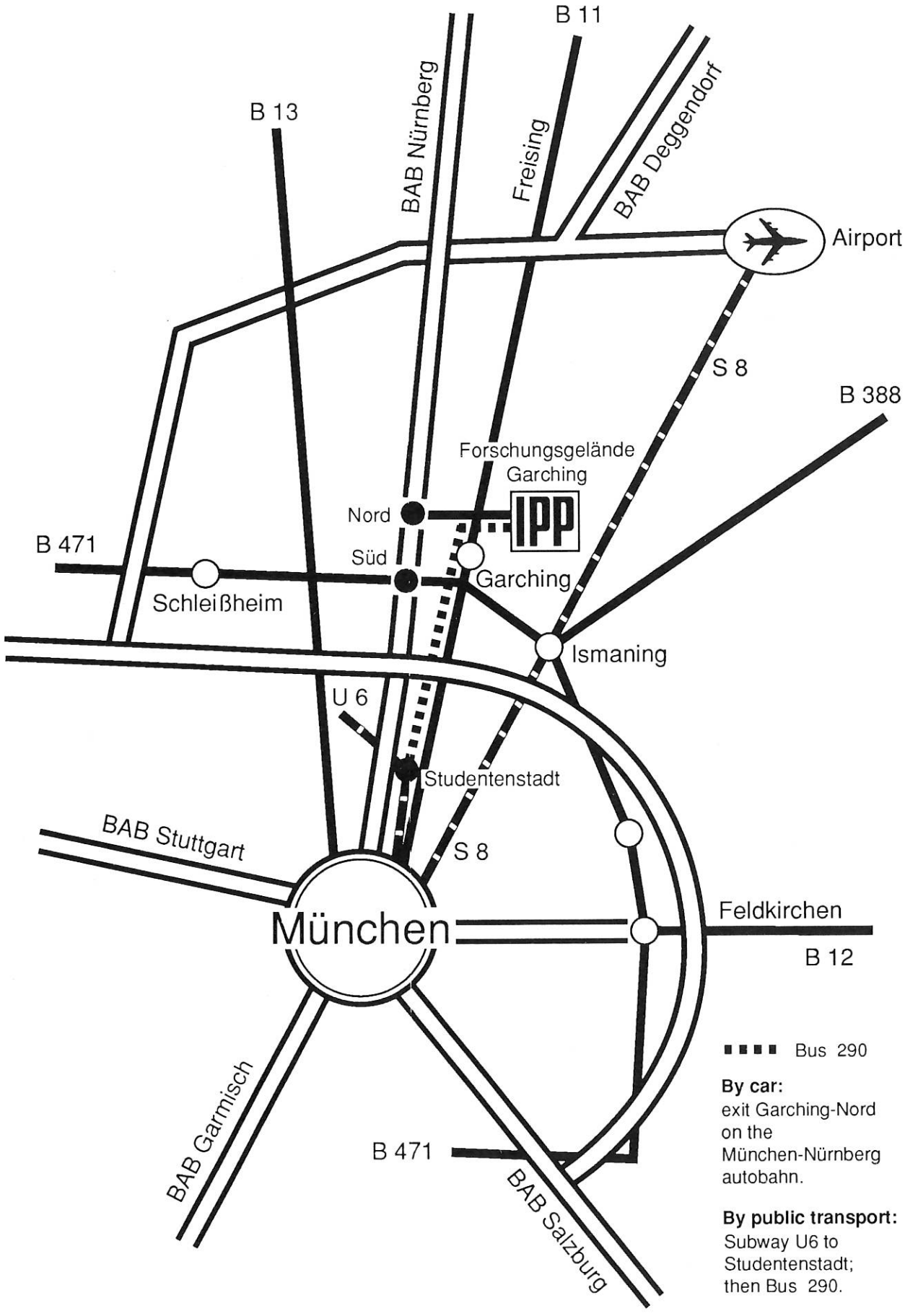

ANNUAL REPORT 1994

Max-Planck-Institut für Plasmaphysik (IPP) · 85748 Garching bei München
Telephone (0 89) 32 99-01 · Telefax (0 89) 32 99-22 00

Printing: SV-Kommunalschriften-Druckerei, München

Printed in Germany
ISSN 0179-9347

This work was performed under the terms of the agreement between Max-Planck-Institut für Plasmaphysik and the European Atomic Energy Community to conduct joint research in the field of plasma physics.

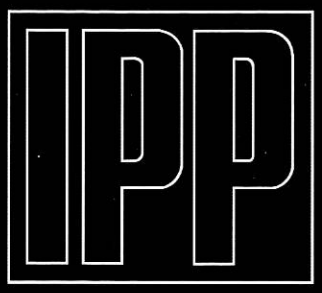
IPP